DC GLOW DISCHARGE ELECTRON GUNS FOR THE EXCITATION OF RARE GASES

R.J. Carman

A Thesis Submitted for the Degree of PhD
at the
University of St Andrews

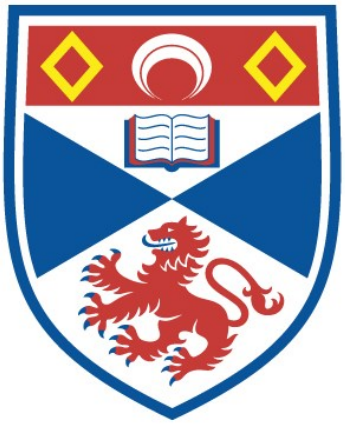

1986

DC GLOW DISCHARGE ELECTRON GUNS FOR THE EXCITATION OF RARE GASES

A thesis presented by

R J Carman, BSc

to the

University of St Andrews

in application for the degree of

Doctor of Philosophy

May 1986

ProQuest LLC.
789 East Eisenhower Parkway
P.O. Box 1346
Ann Arbor, MI 48106 – 1346

UNIVERSITY OF ST. ANDREWS

Thesis Copyright Declaration Form.

A UNRESTRICTED

"In submitting this thesis to the University of St. Andrews I understand that I am giving permission for it to be made available for public use in accordance with the regulations of the University Library for the time being in force, subject to any copyright vested in the work not being affected thereby. I also understand that the title and abstract will be published, and that a copy of the work may be made and supplied to any bona fide library or research worker."

B RESTRICTED

"In submitting this thesis to the University of St. Andrews I wish access to it to be subject to the following conditions:

for a period of 5 years [maximum 5] from the date of submission the thesis shall be

a) withheld from public use.

b) made available for public use only with consent of the head or chairman of the department in which the work was carried out.

I understand, however, that the title and abstract of the thesis will be published during this period of restricted access; and that after the expiry of this period the thesis will be made available for public use in accordance with the regulations of the University Library for the time being in force, subject to any copyright in the work not being affected thereby, and a copy of the work may be made and supplied to any bona fide library or research worker."

Declaration

I wish to exercise option Bb [i.e. A, Ba or Bb] of the above options.

Signature pp. R. Carman Date 1/7/86

DECLARATION

I hereby certify that this thesis has been composed by me, and is a record of work done by me, and has not previously been presented for a higher degree.

This research was carried out in the Physical Sciences Laboratory of St Salvator's college, in the University of St Andrews, under the supervision of Dr A Maitland.

R J Carman

CERTIFICATE

I certify that R J Carman has spent nine terms at research work in the Physical Sciences Laboratory at St Salvator's College, in the University of St Andrews, under my direction, that he has fulfilled the conditions of Ordinance No 16 (St Andrews) and that he is qualified to submit the following thesis in application for the degree of Doctor of Philosophy.

A Maitland.

A Maitland

Research Supervisor

AUTHOR'S CAREER

The author was born in Kingston-upon-Thames in 1959. Primary and Secondary education were in Kingston-upon-Thames at Latchmere school, and at Rivermead Secondary Boy's School. A BSc in Physics was obtained from the University of Manchester (1978-1981). From 1982, the author has been at the University of St Andrews as a postgraduate student studying Gas Discharges for applications to Gas Lasers.

ACKNOWLEDGEMENTS

I would like to thank Arthur Maitland for his support, guidance and most of all, his enthusiasm at all stages of this project. I would also like to thank my colleagues in the laser 1 group; Unny, Ben, Ian, Janet, Graeme and Roger for valuable discussions, and other social events. I am grateful to Mr.Ron McRaw and his collegues in the mechanical workshops for their skills and advice in the construction of the experimental apparatus. I am grateful also to members of the electronic workshop, the teaching laboratories, the administrative staff, and to Mr.Fritz Akerboom the glassblower, for his skills and advice in the fabrication of the discharge tubes. I am grateful to the staff of the computing laboratory and in particular, John Henderson and Malcolm Bain.

I would like to thank Mr.Hugh Menown and his collegues at the English Electric Valve Company in Chelmsford for their interest in this work, and the subsequent publication of a patent.

Finally, I would like to thank my parents for their unwavering support and encouragement during the course of this work. My thanks to my wife, Deborah, for her help in proof reading the text of this thesis, for valuable discussions, and lighter moments of humour.

Dedicated to my Parents

ABSTRACT

Glow discharge electron guns are used to generate continuous electron beams at 0.5keV-3.0keV in the intermediate range of gas pressures (0.1mb-10.0mb). Cathodes incorporating internal cavities are used to generate distinct electron beam filaments in both Helium and Argon. The formation of such beam filaments has been investigated using a number of different cathode types, and criteria for the production of stable electron beams are established.

The production of an electron beam in a glow discharge is largely determined by the motion of electrons in the Cathode dark space sheath region next to the cathode, and other discharge processes in this region. A theoretical model has been developed to simulate electron motion in the sheath region, and in the Negative glow plasma region, of a Helium discharge with a Cathode fall of between 150V and 1000V. It is shown that the electron flux at the sheath/Negative glow boundary becomes increasingly monoenergetic as the Cathode fall rises to 1000V. The results are also compared with experimental spatial emission profiles of the glow in the Cathode dark space and Negative glow regions of a helium discharge. In particular, properties of the Cathode glow region in the sheath are discussed. Aspects of the theoretical model and results from the experimental measurements are also used to discuss discharge processes in the sheath region of cathodes incorporating internal cavities, and mechanisms leading to the formation of the electron beam filaments.

The production of fast electrons in a glow discharge has a number of applications, including the excitation of gases leading to laser action. Aspects relating to the excitation of high lying energy states in gases, corresponding to known laser transitions, are

discussed. It is shown that the production of helium ions, which are responsible for the excitation of metal atoms via asymmetric charge transfer in metal ion lasers, is theoretically more efficient in an electron beam discharge. The results are compared with the theoretical ion production rates in Hollow cathode discharges, and high-voltage Hollow cathode devices. Several electrode geometries using multiple arrays of electron gun cathodes have been developed.

Investigations of an electron beam excited argon plasma suggest that Ar II excited states are pumped directly by single electron impacts, even at very low current densities ($\sim 10^{-3}$ A cm^{-2}). From previous calculations using the 'sudden perturbation' approximation, those ion states known to have large cross-sections for direct electron impact excitation ($3p^4 4p\ ^2P$) appear to be favourably pumped in the electron beam plasma.

PUBLICATIONS LIST

Carman R.J. and Maitland A., Proceedings of the XVII International Conference on Phenomena in Ionised Gases, Contributed papers vol II, J-5, 652, Budapest (1985)

Maitland A., Menown H., Strudwick I.A., Weatherup C.R. and Carman R.J., UK. Patent application G.B. 2153140A, "Apparatus for forming electron beams".

"The phenomena in these exhausted tubes reveals to physical science a new world, a world where matter may exist in a fourth state..."

W. Crookes (1879)

CONTENTS

1 Introduction 1

1.1 The Importance of Fast Electrons in Ion Gas Lasers 1

1.1.1 Metal Ion Vapour/Rare Gas Systems 1

1.1.2 Rare Gas Ion Lasers 5

1.2 Electron Beam Pumping of Gas Lasers 7

1.2.1 Electron Energies 7

1.2.2 Techniques for Producing Electron Beams 8

1.3 Pumping Geometries for Glow Discharge Guns 12

1.3.1 Longitudinal Pumping 12

1.3.2 Transverse and Coaxial Pumping 14

References 16

CONTENTS

2 Glow Discharge Electron Guns 18

2.1 Review of Glow Discharge Theory 18

2.1.1 The Abnormal Glow Discharge 19

2.1.1.1 The Cathode Region and Negative Glow 20

2.1.1.2 The Anode Region and Positive Column 23

2.1.1.3 Negative Glow Discharges 24

2.1.2 Electron Beam Production from Glow Discharges 26

2.1.2.1 Discharges using Shaped Cathodes 26

2.1.2.2 Discharges using Perforated Cathodes 27

2.1.2.3 Electrostatic and Magnetic Focussing 31

References 34

CONTENTS

3 Experimental Investigation of Glow Discharge Electron Guns 36

3.1 Preliminary Studies of e-guns in Helium and Deuterium 36

3.2 Diagnostic Techniques in the Cathode Region 39

3.3 Electrical Characteristics of Perforated Cathode Electron guns 42

3.3.1 Experimental Arrangement 42

3.3.2 Results of Comparative Studies 45

3.3.2.1 Single Aperture e-guns 45

3.3.2.2 Multiple Aperture e-guns 46

3.3.3 Transition Points 47

3.4 Spectroscopic Observations of Discharges in Helium 52

3.4.1 Experimental Arrangement 53

3.4.2 Results 54

3.5 Observations of an e-beam Discharge in Argon 58

3.5.1 Experimental Arrangement 58

3.5.2 Results 59

References 63

CONTENTS

4 Electron Motion in the Cathode Region of a Helium Discharge 65

4.1 Introduction 65

4.2 The Propagation of Fast Electrons in Helium 69

4.2.1 Preliminary Assumptions 69

4.2.2 The Collision Cross-sections 72

4.2.2.1 Ionisation and Excitation Cross-Sections 72

4.2.2.2 Differential Cross-Sections 73

4.2.2.3 Secondary Ionisation 73

4.2.3 The Computer Simulation 79

4.3 Electron Motion in the CDS 86

4.3.1 Electron Energy Distribution Functions 86

4.3.2 Ionisation and Excitation Rates in the CDS 88

4.3.3 Excitation Profiles in the CDS 91

4.4 Electron Motion in the NG 93

4.4.1 Electron Energy Distribution Functions 93

4.4.2 Ionisation and Excitation Rates in the NG 94

4.4.3 Electron Ranges and the Length of the NG 95

4.5 Efficiency of Ion Production in a Helium Discharge 98

4.6 Plasma Processes in a Perforated Cathode 102

References 105

CONTENTS

Electron Gun Configurations for Laser Plasmas 107

5.1 Electron Gun Cathode Geometries 108

5.1.1 Experimental Arrangement 108

5.1.2 Results 109

5.2 A Multiple e-beam Discharge using Argon 114

5.2.1 Experimental Arrangement 114

5.2.2 Results 115

5.3 References 121

Appendix I 122

Appendix II.1 127

Appendix II.2 131

Appendix III 132

Chapter 1

1 Introduction

1.1 The Importance of Fast Electrons in Ion Gas Lasers

Energetic electrons can provide an important source of excitation in argon ion and krypton ion rare gas lasers and also in metal ion vapour/rare gas lasers. Fast electrons can directly populate high lying energy states corresponding to the laser transitions and this is especially important in ion lasers since the upper laser levels may lie many 10's of eV above the ground state. The precise role of fast electrons in the metal vapour lasers is different to that found in the argon and krypton types, and it is convenient to discuss the metal vapour lasers separately.

1.1.1 Metal Ion Vapour/Rare Gas Systems

Laser action in metal vapour/rare gas mixtures has been observed with the radiation derived from both atomic transitions (M I) [1] and ionic transitions (M II) [2] as depicted in fig 1.1 and fig 1.2, respectively. However, the diagnostics of the two systems are quite different. In both types, the active medium consists of an ionised rare gas plasma at 1-100 mb, usually of helium or neon, which is seeded with the metal vapour at a relatively low partial pressure.

Lasing action between atomic levels (M I) in the neon/copper vapour laser for example, has a high quantum efficiency since the upper laser level is only a few eV above ground state. The lasing action in copper is self-terminating due to a build-up of atoms in the lower laser level which is metastable, and also energetically close to the ground level. Therefore, these lasers can only operate in a pulsed mode. Metal ion lasers (M II), however, can operate continuously since the lower laser level is well above ground state and pumping by direct electron impact is comparatively small. A population inversion can be created by preferential pumping of the upper laser level via collisions of the second kind (eg. charge transfer) in addition to direct electron impact. Metal ion lasers have a low quantum efficiency since the laser levels are high lying ionic states. Typical electron energy distributions found in the rare gas plasmas used with each type of laser are shown in fig 1.3. In the atomic copper laser, electrons derived from the pulsed discharge distribution shown in fig 1.3a with energies greater than ~4 eV are able to pump the upper laser level, and a significant fraction of the electrons in the distribution can be used [3]. In contrast, only electrons with energies greater than 24.6eV, the first ionisation potential of helium, can be used to excite certain high lying levels by charge transfer in the helium/Zinc ion laser [4] as shown in fig 1.3b. Nevertheless, metal ion lasers are able to operate continuously and many more metal vapour/rare gas combinations have shown lasing action in the visible region from ionic levels than from atomic levels. The total number of distinct lines seen to date covers a wide range of wavelengths from 2500Å in the ultra-violet to 9000Å in the near infra-red [5]. Continuous output in the near UV is particularly useful in a number of applications including atomic spectroscopy for

pumping laser dyes and in UV photo-lithography. Aspects relating the overall efficiency of the metal ion lasers are of interest here, and atomic metal lasers are not discussed further.

Metal ion lasers can be subdivided into to two classes depending upon the electrode geometry used, which in turn determines the type of plasma employed as the active medium. The lasers use either a Positive column discharge (PC) as illustrated in fig 1.4a, or a Negative glow discharge (NG). The latter type of plasma is usually generated inside a tubular cathode as a Hollow cathode discharge (HCD) as shown in fig 1.4b. Here, advantage is taken of the 'Hollow cathode effect' (HCE) to create a high electron density [1]. Typical electron energy distributions for PC and NG plasmas are shown in fig 1.5. The electron energy distribution in the Positive column plasma is usually characterised by a Druyvesteyn profile and has fewer high energy electrons than the typical Maxwell-Boltzmann distribution. The NG plasma has an energy distribution that contains a relatively large number of low energy electrons, and also a 'tail' of high energy electrons, as shown in fig 1.3b. These fast electrons bring about more efficient pumping of high lying metal ion states in NG plasmas through two main processes. Firstly, M II states (M^{+*}) can be populated via asymmetric charge transfer in collisions between ground state rare gas ions (R^+) and ground state metal atoms (M)

$$e_1 + R \geqslant R^+ + e_1 + e_2$$

$$R^+ + M \geqslant R + M^{+*} + \Delta E_1 \qquad (1.1)$$

where e_1 is the primary electron (fast), e_2 is the secondary electron (slow) and ΔE_1 is the kinetic energy carried away by the products of

the collision. Secondly, direct electron impact between fast electrons and ground state metal atoms produces M^{+*} states via

$$e_1 + M \geqslant M^{+*} + e_1 + e_2 + \Delta E_2 \qquad (1.2)$$

A third type of reaction is found to occur frequently in both NG and PC plasmas. Ground state metal atoms are excited through impact with rare gas metastables (R^*) (Penning ionisation)

$$e_1 + R \geqslant R^* + e_1$$

$$R^* + M \geqslant R + M^{+*} + e_2 + \Delta E_3 \qquad (1.3)$$

The charge transfer reaction is particularly effective as an efficient pumping mechanism since it is a two body process, and is therefore selective and resonant over a narrow range of positive energies (ΔE_1) of only a few tenths of an eV. The cross-sections are usually high and are typically of order $10^{-15}cm^2$ [1]. Selective excitation of a specific metal ion state is possible if the energy level can be correctly matched with the rare gas ionisation potential (I_o) (fig 1.2). Helium ions (I_o=24.6eV) and neon ions (I_o=21.5eV) are usually used for charge transfer reactions in metal vapour lasers since the other rare gases have ionisation potentials generally too low to excite the relevant metal ion states.

Owing to the presence of these energetic electrons in NG plasmas, Hollow cathode discharges are able to produce ground state helium ions more effectively than are Positive column devices. This is reflected in the relative number of metastables (R^*) and ground state ions (R^+) in the two types of plasma. The ion density is typically an order of

magnitude larger than the metastable density in a Hollow cathode plasma as reported by Iijima and Takahashi [6]. In a Positive column plasma, the ratio is reversed and there are approximately ten times as many metastables as ions [7]. Further, Borodin and Kagan [8] observe that in PC and HCD plasmas of the same physical dimensions operating under identical discharge conditions, the electron densities are 2-5 times higher in the Hollow cathode. It is found that the charge transfer reaction is the principal pumping mechanism for many metal ion states which show laser action in HCD plasmas [9]. In most cases, the same levels do not lase in PC plasmas. A few high lying states also are pumped partly by direct electron impact in collisions with fast electrons but this mechanism is almost always observed only in HCD plasmas [10]. Finally, the production of fast electrons in NG plasmas is not greatly affected by the presence of metal vapour which has a low ionisation potential. Hollow cathode discharges can tolerate higher metal vapour densities than Positive column discharges before instabilities arise. The availability of a high density of ground state metal atoms for pumping to M^{+*} states is clearly desirable.

1.1.2 Rare Gas Ion Lasers

Laser action in the rare gases argon and krypton is generated from transitions between excited ionic states ($3p^4$ 4p-4s in Ar II) (fig 1.6) and like the metal ion lasers, the rare gas lasers have a low quantum efficiency but can be run continuously. Direct electron impact of the upper laser level in Ar II does not, by itself, generally produce a population inversion between the 4p-4s states. At

the electron temperatures of 2-6eV observed in DC arc discharges [11], only a small proportion of the electrons possess sufficient energy for the single step process to occur. Cascading from higher energy states accounts for a small percentage of the total pumping. The most important process is stepwise excitation via the atomic and ionic metastables and ground state ion levels. A population inversion is achieved as a result of favourable transition probabilities of the substates in the 4p and 4s levels. The argon plasma has to be run at high current levels in order to ensure that sufficient numbers of argon atoms are pumped to the upper laser level by stepwise excitation. Typically, overall efficiencies of around 0.1% are achieved.

In high voltage pulsed discharges in argon, the electron energy distribution contains greater numbers of rast electrons and a number of states within the 4p level, which have large individual cross-sections for single-step electron-impact, give rise to laser action [11]. Such states have very small populations in DC discharges through the usual stepwise excitation routes. Hollow cathode discharges also have been employed to generate laser action in Ar II, and single step electron impact excitation of the upper laser levels also is found to be one of the important pumping mechanisms [12].

Transitions between excited states in Ar III and Ar IV can be used to generate laser action in the UV. When run continuously, however, the plasma must be run at very high current levels ($\sim$700A.cm^{-2}) [13] to generate a high electron density to promote adequate stepwise excitation of the states involved. In the case of Ar III, these are 70-75eV above the ground level. The overall efficiency of such devices is predictably quite low (<0.01%). Single step electron impact excitation may improve the overall efficiency of

generating laser action in the UV from such high lying levels.

1.2 Electron Beam Pumping of Gas Lasers

1.2.1 Electron Energies

In summary, energetic electrons can be used to pump atoms to the upper laser level directly (Ar^{+*} states) or generate helium or neon ions which subsequently take part in the charge transfer reaction (producing M^{+*} states). To improve the overall efficiency of the ion lasers discussed in section (1.1), it is necessary to generate the energetic electrons directly with energies well above the thresholds for the relevant collision processes. The ionisation potential of helium is 24.6eV, whereas the ionisation cross-section varies with electron energy and peaks around 130eV as shown in fig 1.7 [14],[15]. To calculate the optimum energy for the fast electrons however, other inelastic collisions, in addition to ionisation, must be taken into account. The relative amount of excitation and ionisation in helium produced by a single fast electron propagating through the gas has been calculated by Miller [16]. The energy required to produce a single electron/ion pair, averaged over the entire path of the electron can be defined as:

$$W(E) = E / N_i \qquad (1.4)$$

where N_i is the total number of electron/ion pairs created and E is

the initial energy of the electron. The form of W (E) is shown in fig 1.8. At low energies (<100eV), a large fraction of the initial electron energy is used in pumping atoms to excited states. It is shown that electrons with energies over 1keV are the most suitable for efficiently creating electron/ion pairs in helium, and the average energy then lost for each ionising collision is approximately twice that of the ionisation potential.

The Ar II 4p states lie approximately 35eV above the atomic ground state, and the cross-sections for single electron impact peak around 60-70eV. A similar calculation to that for helium to estimate the optimum energy to excite these Ar II levels has not been carried out by Miller, but it is again likely that the electrons must have energies several times that of the ionisation potential. Electron energies of perhaps a few hundred eV are required. To reduce the proportion of collisions pumping atomic levels in favour of collisions producing excited ionic states, it is likely that the optimum electron energy is also in the keV range.

These fast electrons may be generated ideally in the form of a monoenergetic beam directed into the gas volume containing the rare gas or metal vapour/rare gas mixture, which then acts as the active medium of the laser.

1.2.2 Techniques for Producing Electron Beams

There are a number of methods available for producing high energy electron beams, and these have been applied to Carbon-dioxide or Excimer laser systems to provide the entire pump power or pre-ionisation prior to the main discharge pulse [17],[18]. For pre-ionisation, fast electrons with energies of a few hundred keV can provide uniform pumping of the gain volume. The electrons can be generated via three main processes:

(i) field emission from a thin razor edged cold cathode;

(ii) thermionic emission using a heated cathode;

(iii) secondary emission through ion impact on a cathode surface.

The first two methods can only be operated in a hard vacuum environment (10^{-5}-10^{-4} mb), whereas a low pressure gas (0.001-1.0 mb) is employed to provide the necessary flux of ions which collide with the cathode to induce secondary emission. The electrons are then accelerated to high energies (10keV-1MeV) by a large electric field and finally pass through a thin metal foil which separates the acceleration region from the laser medium. The laser gas is typically held at 1-2 atmospheres pressure. Almost without exception, e-beam devices are operated in a pulsed mode owing to the high voltages and high power levels employed. Those guns relying on field emission (i) or thermionic emission (ii) under hard vacuum are easily damaged by vacuum failure. Low pressure glow discharge guns (iii) can, however, produce collimated pulsed beams of electrons between 10keV and 200keV [19] and have been thoroughly investigated in connection with electron beam welding and the heat treatment of metals. They are generally the

most versatile and robust type of electron gun. Energetic ions, metastables and neutrals which collide with the cathode face to induce secondary emission also act to remove surface impurity layers through the sputtering mechanism. Glow discharge e-guns are less susceptible to 'poisoning' of the cathode surface caused by impurity gases than e-guns relying on processes (i) or (ii). Continuous operation is possible if the power levels employed are not prohibitively high, and the cathode and foil elements are adequately cooled. The e-beam current is often limited by the glow-arc transition caused by overheating of the cathode face. The use of electrons of intermediate energies (5-100keV) derived from a continuous glow discharge gun and used in conjunction with a thin foil window in a transversly pumped laser system has been suggested [20], and a feasibility study of such a scheme is reported in Appendix (I) of this thesis. From the results of this study, it becomes apparent that foil type systems have a number of drawbacks and a significant fraction of the beam energy may be lost in the foil element, or lost in collisions with the walls of the containment vessel.

A longitudinal pumping scheme also has been proposed where the active medium and the electron gun regions are maintained at different pressures by differential pumping of the two regions [21]. The single electron gun is set at a small angle to the optic axis and the beam is steered into the active region by a combination of magnets. However, there are serious difficulties in coupling the e-beam through an aperture, which by necessity must have a small diameter for differential pumping, and into the active medium.

Improved coupling efficiency of the e-beam energy to the active medium may be achieved by operating the electron gun at the same pressure as the laser gas enabling the beam to be passed directly into

the active medium. Therefore, glow discharge guns which have the capability of producing continuous beams of electrons in helium in the relatively high pressure range 0.1-10.0 mb are of interest.

The characteristics of a typical high voltage continuous glow discharge in this pressure range have been discussed previously [22]. At somewhat lower helium pressure (0.01-0.1 mb), which is the pressure region normally associated with e-beam production, the beam collimation is good, the gun impedance high and the electrons suffer relatively few collisions in the gas. Nearly monoenergetic electrons with energies close to the applied potential (10-100keV) are generated. The e-beam current is maintained by secondary emission as ions, generated in a plasma region (NG) in front of the cathode, collide with the cathode face (fig 1.9). Between the NG and the cathode, a sheath region is observed which carries across it most of the applied cathode/anode potential. The purpose of the sheath region is twofold; firstly, it draws ions out of the plasma region to maintain secondary emission at the cathode face, and secondly, it accelerates electrons generated at the cathode face to form the e-beam. As the pressure is increased, more elastic and inelastic collisions occur in the NG plasma region which lead to an increase in the gas conductivity and a drop in the discharge impedance. In addition, a greater spread of electron energies is observed in the energy distribution of beam electrons in the plasma. As the pressure is raised further, a larger proportion of electrons possess energies that are only a fraction of the applied potential. The energetic electrons also steadily lose energy through multiple collisions as they propagate away from the cathode. Each one has a characteristic range which is dependent on the initial energy, on the background gas pressure, and on the number of collisions that take place. Above a

pressure of about 1 mb in helium, few electrons have energies close to the applied potential and at pressures more than a few mb, it becomes difficult to identify a collimated electron beam. Thus, there is a trade-off between operating pressure and beam quality. Electron guns which operate in 0.1-2.5 mb helium producing continuous e-beams up to 6keV have been reported [23],[24] and in this pressure range, it is observed that the beam contains significant numbers of fast electrons as shown in rig 1.10.

1.3 Pumping Geometries for Glow Discharge Guns

It is important to ensure that there is efficient coupling of the beam energy to the active medium of the laser, and this is achieved by matching the penetration depths of the fast electrons with the dimensions of the gas volume. The electron ranges must be chosen to be compatible with the pumping geometry employed.

1.3.1 Longitudinal Pumping

To pump the active medium longitudinally, the electron gun must be placed clear of the optic axis and the beam steered into the active medium by additional magnets. Alternatively, the electrons can be generated by an annular shaped glow discharge gun to allow a clear path along the main optic axis (fig 1.11). The fast electrons are guided into the main tube by a magnetic field whose H_z axis is coaxial with the axis of the tube. They are drawn together after leaving the electron gun by spiralling around the converging magnetic field lines

and after the beam enters the main tube, the magnetic field confines it to a small region around the main axis. Beam divergence is caused principally by scattering in collisions with gas atoms and, to a lesser extent, by space charge repulsion. The confining action of the magnetic field also helps to increase the ranges of the electrons in the gas. The energy required to penetrate the full length of the tube depends on the gas type, the gas density, the magnetic field strength and on the total tube length. Dual gun systems, which use a gun placed at each end of the magnet can improve the uniformity of the pumping [25]. Energies of a few keV are typically required to penetrate helium at a few mb to a depth of about 1 metre using a magnetic field of 0.3-0.4T. Longitudinal pumping allows the functions of the electron gun and those of the main active medium containing the rare gas/metal vapour mixture to be separated, thus, simplifying the construction and operation. The main tube contains no internal electrodes and the inclusion of additional heaters or a cooling jacket around it allows the temperature to be controlled independently of the e-beam current, an important factor in metal vapour systems.

Laser action has been observed in a number of helium/metal vapour systems by Rocca et-al [26]. A separate oven in a side-arm is used to generate the metal vapour. A total beam power of 1.2W CW has been reported from the combined lines at 4912Å and 4924Å using a helium/Zinc mixture in a dual gun system [25]. This power is over an order of magnitude higher than that obtained previously from a helium/Zinc Hollow cathode device [2]. The overall efficiency of the laser, without including the power used in the large magnet, is about 0.034% for an active medium of length 100cm.

In another longitudinal scheme, laser action has been observed in low pressure argon using a low energy electron beam (up to 300eV)

which is generated by a multi-stage glow discharge gun [27]. The optimum pressure is 0.07mb (53mtorr) and an output of 30mW is reported (an efficiency of 0.0025%) on the 4880Å line from an 80cm long active medium using a 0.06T magnetic field.

1.3.2 Transverse and Coaxial Pumping

The electron energies required to penetrate rare gas volumes transversly are significantly lower than those discussed for the longitudinal scheme because the requisite electron ranges are a few cm, corresponding to the width of the active medium. Low energy electrons of about 100-200eV are needed to penetrate helium at 1 mb by a few cm, but these potentials are too low to maintain a glow discharge in helium at the current levels required. The same penetration depths can be realised by operating at higher electron energies with higher gas pressures. Indeed, Hollow cathode discharges begin to operate at a few mb in Helium, and it is probable that the ranges of the fast electrons present in the glow are integrally related to the onset (and ultimately the cessation at higher pressure) of the Hollow cathode effect. The cylindrical Hollow cathode discharge thus may be loosely described as a coaxially pumped e-beam discharge, whilst the slotted Hollow cathode types with parallel cathodes [28] can be described as transversly pumped discharges. However, the helium pressures employed in Hollow cathode discharges are typically 5-20 mb and in this range, there is a considerable spread of the energies in the electron energy distribution of the NG plasma. It is perhaps more correct in this context to view the NG plasma as containing only a relatively small proportion of energetic

beam electrons, particularly since the applied potential is almost always in the region of only a few hundred volts. The electron energy distribution in Hollow cathode discharges is more usually described as having a 'beam component' of fast electrons at the applied Cathode fall potential and a high energy 'tail' of fast electrons [1],[4]. In an effort to increase the proportion of high energy 'tail' electrons in Hollow cathode discharges and in particular the number of 'beam' electrons, recent studies have centred on HCD's operating at voltages around 1-2kV to generate beam electrons with energies around 1-2keV [29],[30]. These high voltage HCD's appear to show improved pumping of the upper laser levels in both metal ions and in rare gas ions.

References

1. Willett C.S., 'Introduction to Gas Lasers', Permagon Press, (1974)
2. Piper J.A. and Gill P., J.Phys.D., 8, 127 (1975)
3. Mnatsakanyan A.K.. Naidis G.V. and Shternov N.P., Sov. J.Q.E., 8, 343 (1978)
4. Gill P. and Webb C.E., J.Phys.D., 10, 299 (1977)
5. Schuebel W.K., Proc.Int.Conf.Lasers, Orlando USA, 431-9 (1979)
6. Iijima T. and Takahashi T., Jpn.J.Appl.Phys., 20, 2267 (1981)
7. Mori M., Takasu K., Goto. and Hattori S., J.Appl.Phys., 48,
6. Borodin V.S. and Kagan Y.M., Sov.Phys-Tech.Phys., 11, 131 (1966) 2226 (1977)
9. Green J.M. and Webb C.E., J.Phys.B., 7, 1698 (1974)
10. McIntosh A.I. and Grace J.R., Austr.J.Phys., 32, 561 (1979)
11. King T.A. and Davis C.C., 'Advances in Quantum Electronics', ed. D.W. Goodwin, Academic Press, (1975)
12. Pacheva Y.. Pramatarov P. and Stefanova M., Opt.Comm., 31, 203 (1979)
13. Maitland A., Private Communication.
14. Rapp D. and Englander-Golden P., J.Chem.Phys., 43, 1464 (1965)
15. Schram B.L., De Heer F.J., Van der Wiel M.J. and Kistemaker J., Physica, 31, 94 (1965)
16. Miller W.F.. Dissertation thesis, Purdue University USA, (1956)
17. Garnsworthy R.K., Mathias L.E.S. and Carmichael C.H.H., Appl.Phys.Lett., 19, 506 (1971)
18. Shaw M.J., 'Progress in Quantum Electronics', 6, 3 (1979)
19. Dugdale R.A., 'Glow Discharge Material Processing', Mills & Boon, (1971)
20. Bayless J.R. and Knechtli R.C., IEEE. J.Q.E. QE-10, 213 (1974)

21. Tkach Y.V., Fainberg B., Bolotin L.I. Bessarab Y.Y., Gadetskii N.P., Chernenkii Y.N. and Berezin A.K. (1968)

22. von-Engel A., 'Ionised Gases', Oxford University Press, (1965)

23. Rocca J.J., Meyer J.D.. Yu Z., Farrell M. and Collins G.J., Appl.Phys.Lett., 41, 811 (1982)

24. Yu Z., Rocca J.J. and Collins G.J., J.Appl.Phys., 5, 131 (1983)

25. Rocca J.J., Meyer J.D. and Collins G.J., Appl.Phys.Lett., 43, 37 (1983)

26. Rocca J.J., Meyer J.D., Yu Z. and Collins G.J., Appl.Phys., B 28 2/3, 239 (1982)

27. Hara T., Sadamoto Y., Hamagaki M., Ohgo T. and Dote T., Jpn.J.Appl.Phys., 22, L379 (1983)

28. Schuebel W.K., Appl.Phys.Lett., 30, 516 (1977)

29. Rozsa K., Z. Naturforsh. 35a, 649 (1980)

30. Iijima T., Jap.Jour.Appl.Phys., 21, 1732 (1982)

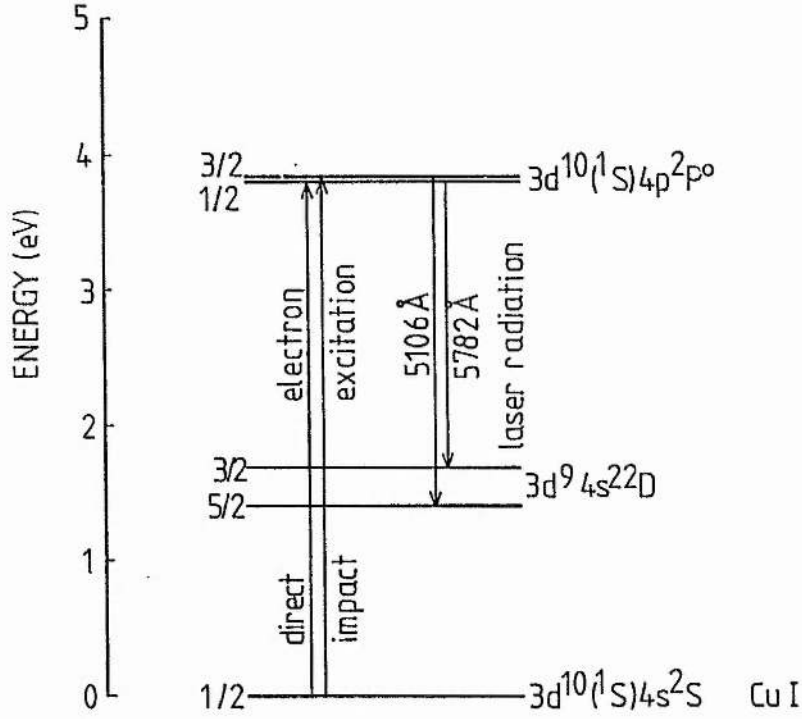

Fig 1.1. Energy level diagram showing the laser transitions and excitation routes in the atomic copper vapour laser [1].

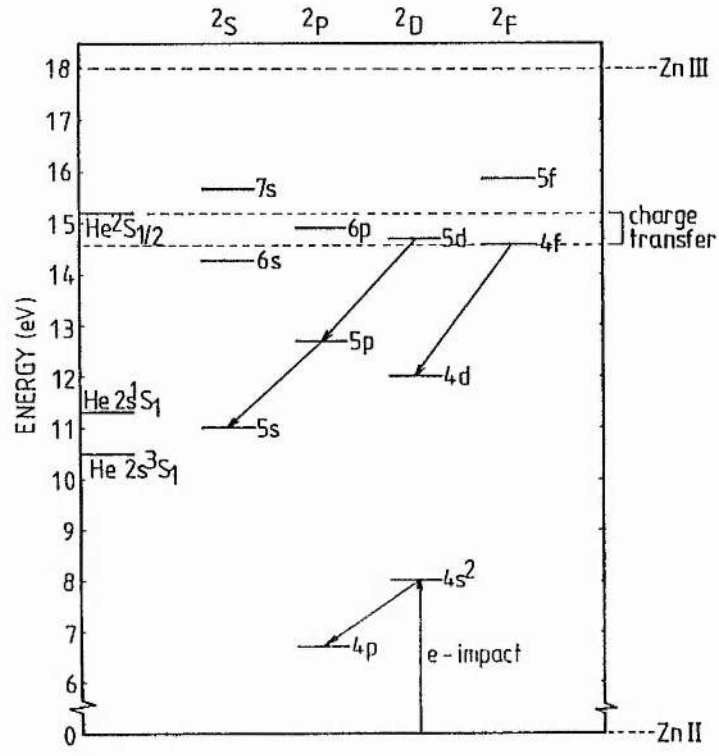

Fig 1.2. Energy level diagram showing the states in singly ionised zinc (Zn II), excited via charge transfer or direct electron impact, which give rise to laser action. The arrows denote laser transitions. The energy levels of the neutral helium singlet and triplet metastables, and the ground state helium ion are included also.

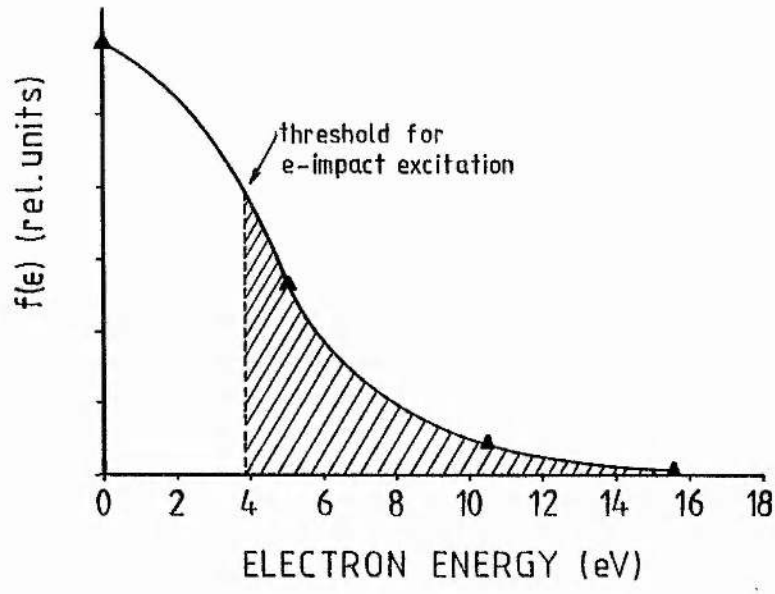

Fig 1.3a. Calculated electron energy distribution in an atomic copper/neon laser for a pulsed discharge (density ratio [Cu]/[Ne] = 0.01). (The data points are taken from [3] and the curve is fitted here as an approximation.) The shaded area refers to electrons which have sufficient energy to excite the upper laser levels.

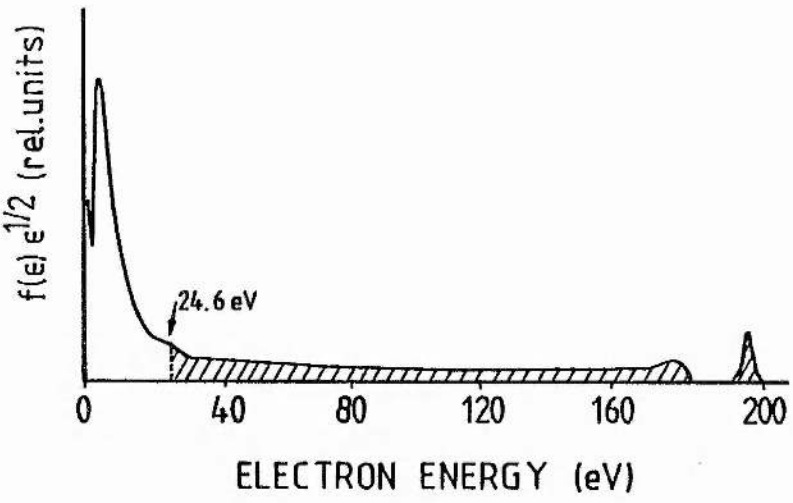

Fig 1.3b. A measured electron energy distribution in the NG of a helium discharge at 13mb with a Cathode fall of ~200V [4]. The shaded area refers to electrons which are above threshold for single step ionisation of helium.

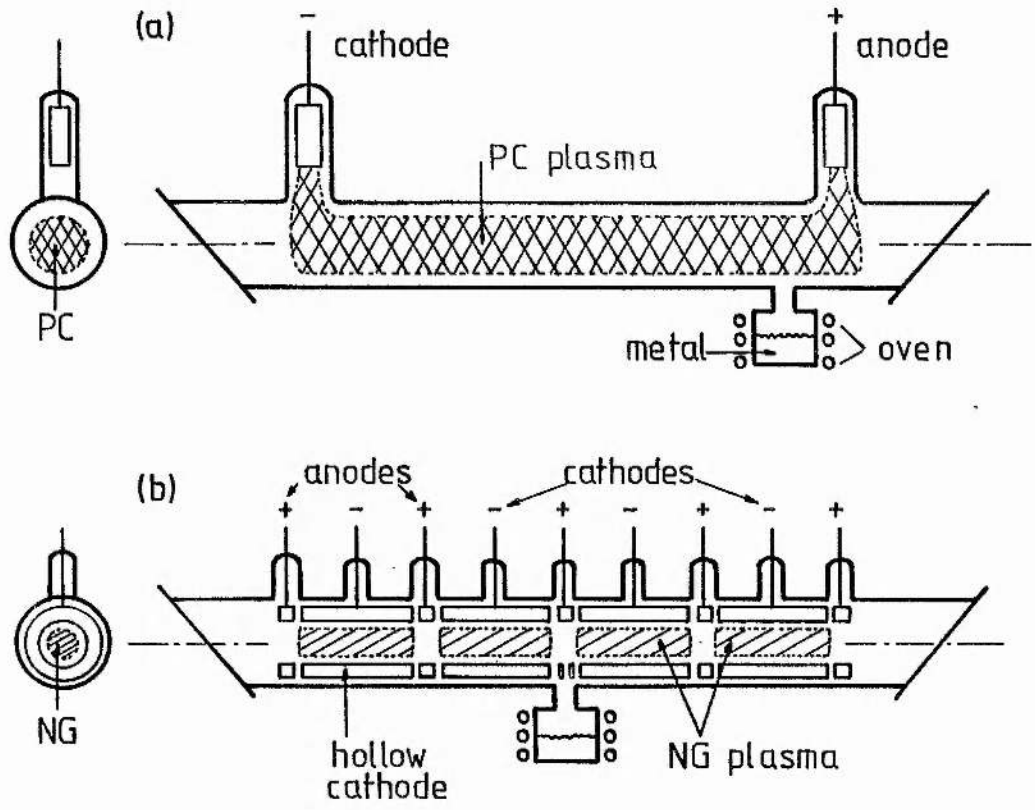

Fig 1.4. Two types of electrode geometry utilizing different plasma regions, the Positive column (a) and the Negative glow (b), of a glow discharge are used to excite metal vapour ion/rare gas lasers.

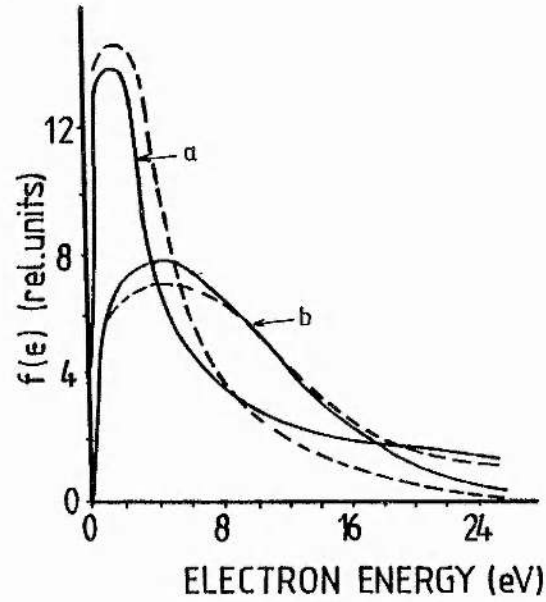

Fig 1.5. Measured electron energy distributions for comparable Hollow cathode (a) and Positive column (b) discharges in a helium discharge at 1.6mb [6]. The dashed curves are of Maxwellian profile and matched to the experimental curves at low energy.

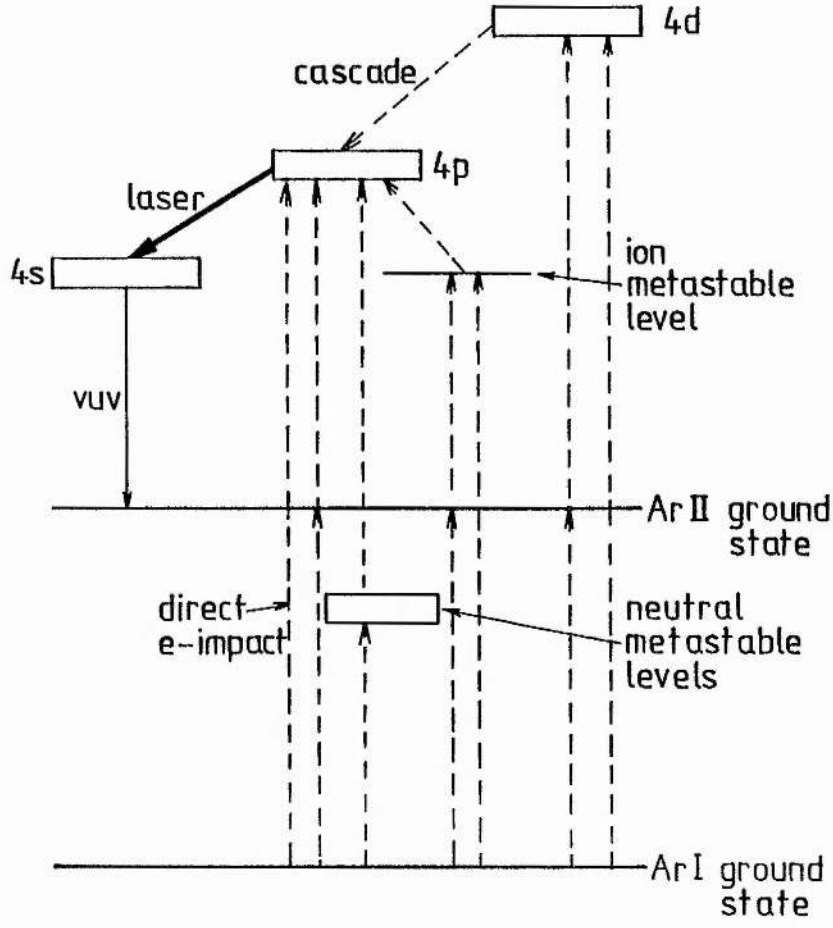

Fig 1.6. Schematic energy level diagram showing the laser levels in Ar II and the different excitation mechanisms populating the Ar II 3p 4p levels, adapted from [11].

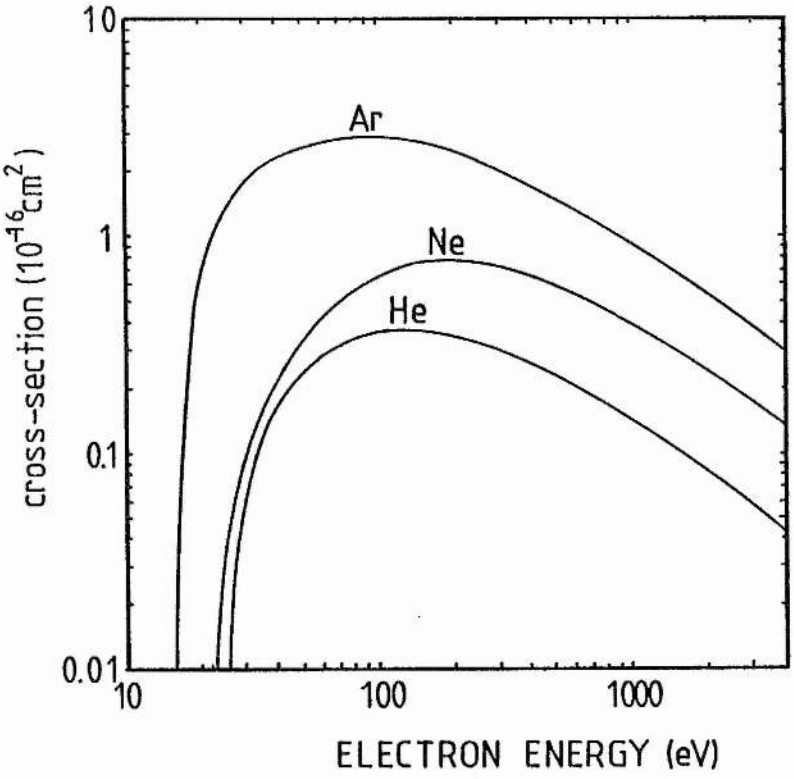

Fig 1.7. The ionisation cross-section of the rare gases He, Ne and Ar for single electron impact [13],[14].

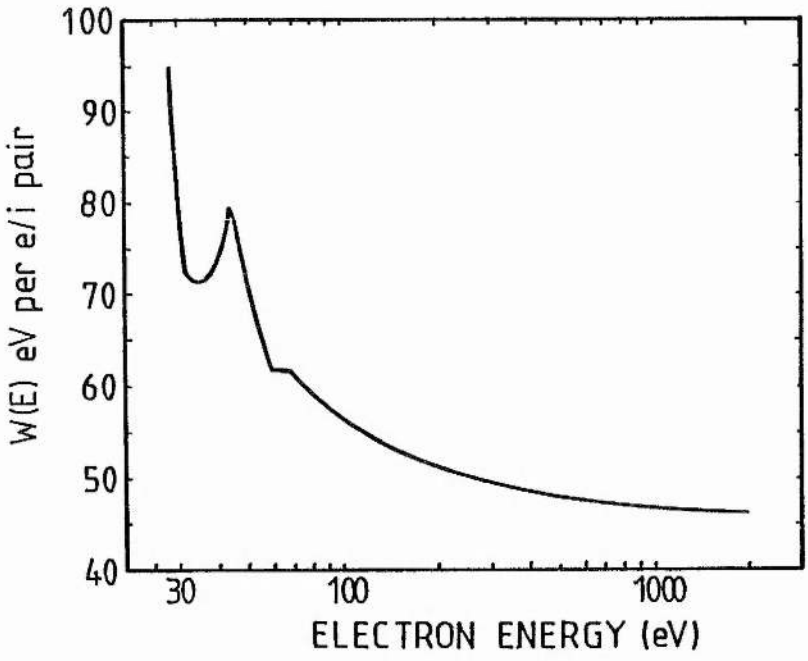

Fig 1.8. The average energy loss W(E) per ionising collision in helium for electrons of initial energy E, after Miller [16].

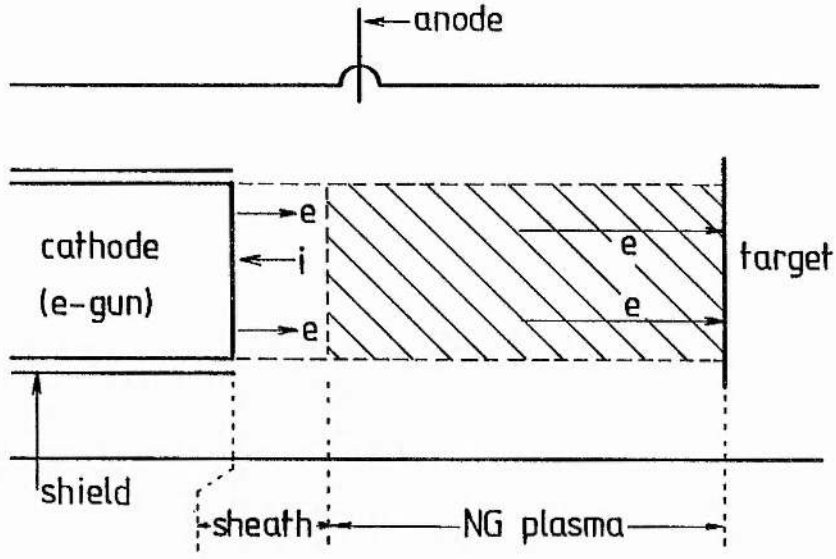

Fig 1.9. Schematic diagram showing a typical low pressure glow discharge electron gun used in material processing. Electron emission is confined to the cathode face by a close fitting ceramic shield around the body of the electron gun.

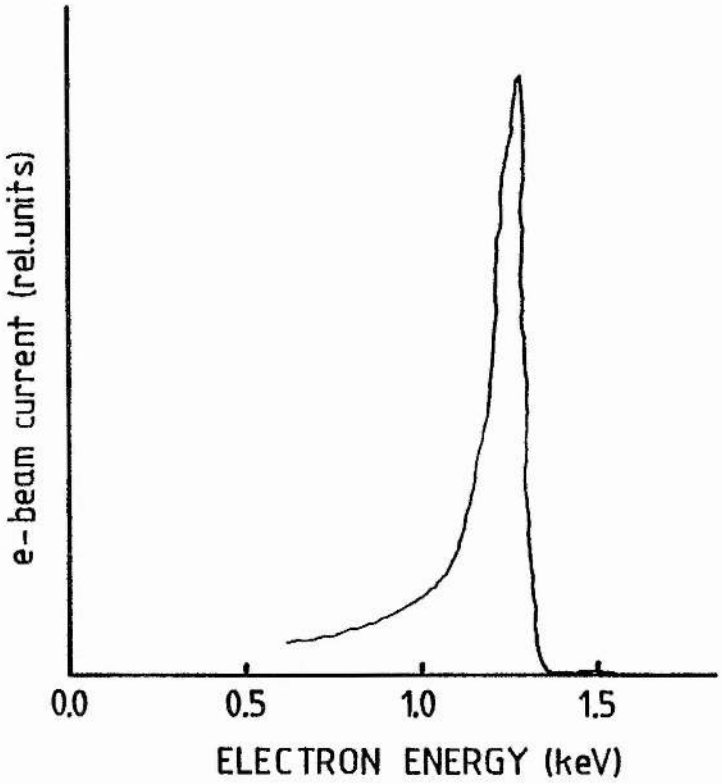

Fig 1.10. Electron energy distribution in the NG of a helium discharge at 0.8mb with a discharge voltage at 1.31kV and discharge current at 400mA [24].

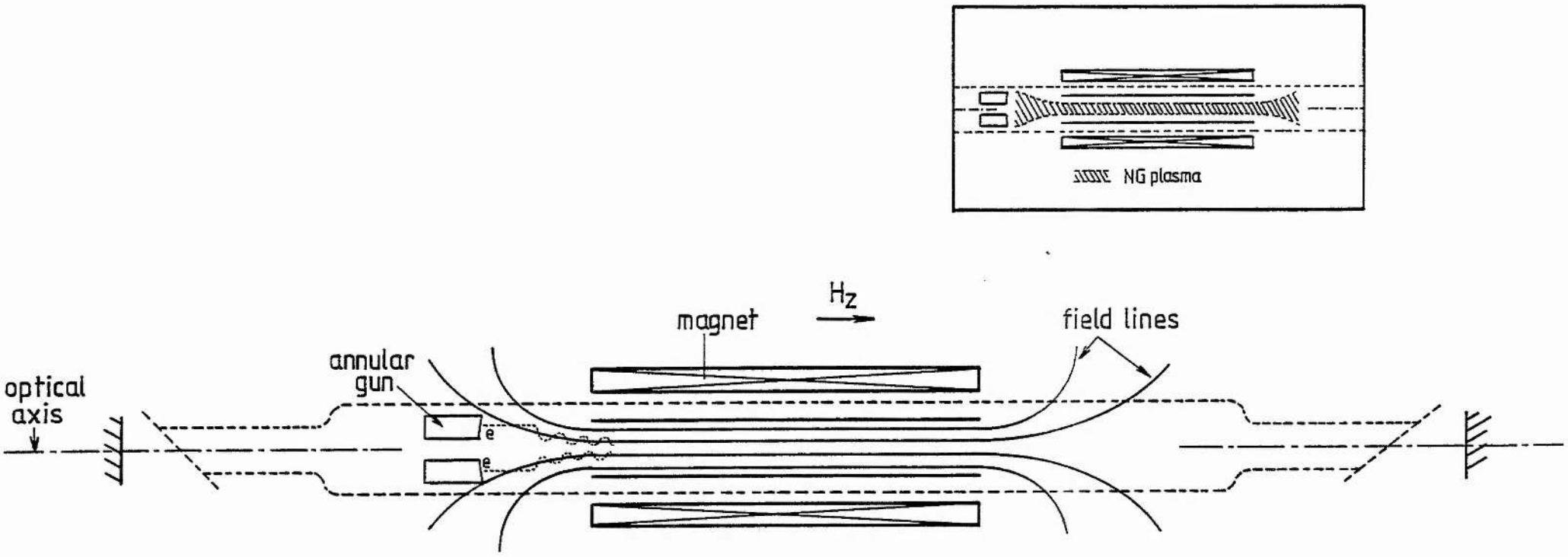

Fig 1.11. Schematic diagram for longitudinal pumping by an electron beam of a rare gas or metal vapour/rare gas ion laser. Inset: the shape of the NG plasma which acts as the active medium.

Chapter 2

2 Glow Discharge Electron Guns

As discussed in chapter 1, most types of glow discharge electron guns operate at ambient pressures of around 0.001-1.0 mb. In this chapter, the properties of glow discharge guns operating at pressures in the region of a few mb, which are needed for direct e-beam pumping of a gas laser, are discussed.

2.1 Review of Glow Discharge Theory

An ordinary self-sustaining glow discharge in helium at low current and low pressure (a few mb) is depicted in fig 2.1(i) and the principal glow regions observed are shown shaded [1]. The roles of the different glow regions in maintaining the discharge current are reflected in the voltage (ii) and electric field (iii) distributions between the electrodes. The voltage does not vary linearly across the tube due to the presence of positive and negative space charges, and a significant proportion of the tube voltage may be dropped across a narrow sheath region immediately in front of the cathode. This voltage drop (V_c) is known as the Cathode fall. The properties of the various glow regions depend to some extent on the discharge current and therefore, it is necessary to distinguish between two operating regimes. At low current, only part of the cathode appears to be covered by glow. As the current is raised, the Cathode fall stays more or less constant, at a value around 150V in helium, and the glow

spreads over the cathode face to keep the current density (j) at the cathode constant. This is the 'normal' glow regime. Once the cathode face is completely covered by glow, further increases of the current are accompanied by a rise in the Cathode fall. This is known as the 'abnormal' regime and the relative lengths of the glow regions then change as the current is raised. Glow discharge electron guns usually operate with a Cathode rall of several kV, well into the abnormal regime.

2.1.1 The Abnormal Glow Discharge

The morphology of abnormal glow discharges has been investigated and reviewed extensively in recent years [2]-[5]. Certain aspects of abnormal discharges in the rare gases however, are not fully understood. Conditions at the cathode are especially difficult to investigate experimentally due to the large space charge densities found in this region. Furthermore, relatively few studies have been carried out with highly abnormal discharges where the Cathode fall may be several kV. In this section and in (2.1.2), the principal features of abnormal discharges in helium, with a Cathode fall of several hundred volts, are presented. The discussion is also applicable to discharges of neon or argon.

2.1.1.1 The Cathode Region and Negative Glow

The region of positive space charge near the cathode (fig 2.1(iv)) is caused by a build up of slow ions drifting toward the cathode from the Negative glow region (NG). A region of high electric field is produced by the build-up of positive space charge and this coincides with the sheath region of the Cathode dark space (CDS). The electric field across the CDS region decreases approximately linearly with distance from the cathode face, from a typical value of a few thousand volts per centimetre at the cathode face to almost zero at the CDS/NG boundary. The ions which drift into the CDS from the NG are accelerated by the field and when they collide with the cathode face, electrons with energies of a few eV are released by secondary emission. Metastable atoms and UV photons from the NG also produce electrons via secondary emission. The overall efficiency of electron production is denoted by the total secondary emission coefficient (γ), a quantity dependent on the cathode material, the gas type and the kinetic energy of the particles hitting the cathode. In the abnormal glow regime, the voltage rise required for any current increase is ultimately related to the efficiency of the secondary emission processes. A rise in the tube voltage produces an increase in the Cathode fall and particles may collide with the cathode with greater energy, releasing more electrons per collision. In a highly abnormal discharge, where the Cathode fall is large and sputtering of the cathode surface occurs. a thin surface glow immediately in front of the cathode may be observed. and the light emission from this glow may contain lines characteristic of the cathode metal.

The slow electrons produced from secondary emission are quickly accelerated away from the cathode and pass through the Aston dark

space (ADS), a narrow region next to the cathode where they have insufficient energy for excitation of the gas. On reaching energies around 40-50eV, which correspond to the peaks of the excitation cross-sections in helium, a few electrons collide with He atoms to produce the thin Cathode glow layer. This is a narrow region because the high electric field produces rapid acceleration and the electrons quickly gain enough momentum to reach energies well past the maxima of the excitation cross-sections. A small proportion of the electrons, on reaching energies in the region of 100-150eV lose energy through ionising collisions (fig 1.7) and the secondary electrons produced are themselves accelerated and join the main flux of electrons. They may, in turn, suffer inelastic collisions and give rise to further excitation and ionisation. The amount of ionisation in the CDS is, however, insufficient to maintain the discharge.

At the boundary of the CDS and NG regions where the electric field approaches zero, the electrons reach a terminal velocity and the overall electron energy distribution in this region has a large number of high energy electrons. A few electrons from the cathode reach this boundary without suffering collisions in the CDS and have energies comparable to the Cathode fall (eV_c). The electron energy distribution at the CDS/NG boundary has been measured experimentally by Gill and Webb [6] using a differentially pumped retarding field analyser which sampled electrons through a hole in the anode. An energy distribution taken at a helium pressure of 20mb with a Cathode fall of 270V is reproduced in fig 2.2a. Yu et-al have used an electro-static electron energy analyser to sample fast beam-like electrons from the cathode at a position some way into the NG [7]. Two distributions are shown in figs 2.2b,c. The electron energy distribution at the CDS/NG boundary in a highly abnormal discharge

using several different gases has been investigated by Chaudhri and Chaudhri [8]. They observe a sharp peak of electrons with energies corresponding to the Cathode fall, which is typically several kilovolts (fig 2.2d).

These observations indicate that the proportion of fast electrons in the energy distribution at the CDS/NG boundary increases as the pressure is reduced, and as the Cathode fall is raised. As the electrons pass through the 'head' of the NG and into the relatively field-free region beyond which constitutes the main body of the NG, they are effectively in free flight and their energy gradually diminishes due to multiple inelastic collisions. The secondary electrons produced are no longer accelerated and therefore do not possess an average drift velocity in any preferred direction as in the PC, and instead move by diffusion. As the beam-like electrons propagate through the gas in the NG, the overall energy distribution changes, with the proportion of lower energy electrons, generated via ionising collisions, increasing with distance into the glow. The NG is almost always the most luminous part of the discharge, and the ionisation produced by the fast electrons is a critical factor in maintaining the discharge. The slow moving ions generated in ionising collisions are eventually lost by diffusion to the walls of the discharge vessel, by volume recombination with the group of low energy electrons in the NG, and by collisions with the cathode face where they may produce further electrons. When metal vapour is added to the discharge, ions are also lost in asymmetric charge transfer reactions. The discharge current is carried mainly by the fast electrons in the NG whereas in the CDS close to the cathode, the current is carried by fast ions (fig 2.1(v)). The length of the NG is determined by the penetrating power of the electrons, a factor

dependent on their initial energy at the CDS/NG boundary, and the gas density in the NG.

2.1.1.2 The Anode Region and Positive Column

As the energy of the electrons is attenuated by the gas in the NG, they eventually slow to energies below the threshold for excitation, and drift towards the anode experiencing only elastic collisions. This region is the Faraday dark space (FDS). The boundary region between the NG and the FDS is diffuse in appearance and it is often difficult to estimate the actual length of the NG. The diffuse boundary results from both the spread in energy of the electrons at the CDS/NG boundary and the statistical nature of multiple collisions in the NG. The electric field in the FDS is often found to be slightly reversed, decelerating the electrons further. However, the numerous slow electrons form a density gradient of sufficient magnitude that they maintain the flow of electrons, via diffusion, towards the anode. A point along the tube is reached, however, when a small longitudinal field must be applied to accelerate the electrons and make up for charge losses through recombination and diffusion to the walls. This occurs at the start of the Positive column (PC) which has a constant low electric field throughout its length to compensate for charge loss through ambipolar diffusion. The net space charge is zero throughout the PC and the positive and negative charge densities are identical. At the anode, a charge sheath is built-up to repel positive ions and attract the slow electrons, thus completing the circuit. The electrons usually produce a narrow band of glow next to the anode, not shown in fig 2.1(i),

which is known as the anode glow. The potential drop across this sheath, the Anode fall, is about the same as the ionisation potential of the gas used.

2.1.1.3 Negative Glow Discharges

It is clear that the properties of the NG and PC regions are quite different. Whilst the PC behaves like a homogenous plasma throughout its length, the NG is highly anisotropic with markedly dissimilar electron energy distributions at the CDS/NG boundary and the NG/FDS boundary. The principal function of the PC is to form a conducting bridge between the FDS and the anode to maintain current flow between the electrodes. This can be demonstrated by reducing the electrode spacing (fig 2.1(vi)) whilst keeping the discharge current constant. Both the CDS and the NG regions are unaffected by the change, the PC is shortened, whilst the tube voltage drops to a value (V'). Ultimately, the anode may be pushed into the FDS without affecting the CDS or NG. The stability of the discharge is only affected when the anode is pushed into the NG so that a substantial proportion of the glow is missing. A glow discharge in helium, or indeed any of the rare gases, thus can be maintained with only the CDS and NG regions present. Under such circumstances, the tube voltage is equal to the Cathode fall (V_c), possibly with a small correction for the Anode rall. The anode can therefore be placed in the FDS and its position within the FDS, with respect to the NG, is not critical. It does not affect the properties of the CDS or NG provided it is placed well clear of the CDS and away from the main body of the NG.

Modelling the CDS and NG regions of an abnormal glow discharge on

a theoretical basis has received much attention in the past because of the key role the two regions play in the maintenance of the discharge [9],[10]. Considerable difficulties are encountered, however, resulting from the non-uniform, high electric field in the CDS. The electrons derived from the cathode are rapidly accelerated in the CDS and within this region, the electron energy distribution is nighly non-Maxwellian because the electrons are not in equilibrium with the electric field. The whole energy distribution therefore must be considered in calculations, and the macroscopic quantities such as the Townsend first ionisation coefficient (α_t/p) and the average electron temperature (T_e) measured under conditions of equilibrium (in the PC for example) are not applicable. Models based on the concept of electron avalanches using these average quantities can provide some insight into the general properties of the CDS, but are unable to explain the presence of groups of fast electrons identified experimentally by Gill and Webb [6] amongst others. The availability of fast computers in the past ten years or so has made it possible for the first time to deal directly with microscopic quantities in the discharge, namely, collisions between individual particles. The trajectories of individual electrons in the CDS have been tracked through successive collisions using random number, 'Monte-Carlo' type simulations and only the relevant elastic and inelastic impact cross-sections are required initially. By repeating the calculations to chart the case histories of a few thousand electrons, averaged quantities can be obtained which can be used to re-define the macroscopic quantities. Excellent agreement is observed between the Monte-Carlo calculations of Tran-Noc [11] and Boeuf et-al [12] in helium glow discharges and the experimental observations of Gill and Webb [6], with Cathode falls of a few hundred volts.

2.1.2 Electron Beam Production from Glow Discharges

2.1.2.1 Discharges using Shaped Cathodes

To Summarise, a plane cathode operating in the abnormal regime with a Cathode fall of several hundred volts can produce a significant proportion of fast electrons and their energy is imparted to the gas in the field-free region which is the NG (fig 2.3). Experimentally, it appears that the proportion of fast electrons at the head of the NG may be increased by reducing the pressure to around 1mb, and raising the Cathode fall to several kV. At helium pressures of about 1-2mb, the ranges of such electrons can produce a NG region which may be several 10's of cm in length. Broadly speaking, the electrons may be considered to constitute a beam, although the beam diameter is large (approximately equal to the cathode diameter). The beam becomes also progressively less well defined further from the cathode as the cumulative effects of elastic and inelastic collisions become important. In addition, the initial trajectories of the electrons are determined by the shape of the CDS and the associated electric equipotentials. An electron released from the cathode is accelerated in a direction perpendicular to the local equipotentials. These equipotentials follow the profile of the cathode face and unless the diameter of the cathode (D) is much larger than the thickness of the CDS (d_c), edge effects give rise to slightly outwardly curving equipotentials which produces a diverging beam. Beam spread can therefore be reduced by adopting a concave geometry as shown in fig 2.4 with the radius of curvature chosen to be comparable to the

length of the NG. The electron gun proposed by Rocca et-al [13] for pumping gas lasers longitudinally is constructed along these lines and this is shown schematically in fig 2.5. The focusing action of the curved profile nelps to keep the electron beam collimated before it reaches the confining magnet (fig 1.9). The gun is made annular by drilling out the centre part of the cathode and inserting a ceramic shield. With water cooling of the cathode body, electron beams are reported to be generated to give beam currents of up to 1 amp using a Cathode fall between 1-6kV, helium pressures in the range 0.1-3mb.

2.1.2.2 Discharges using Perforated Cathodes

The electron gun shown in rig 2.3 produces a beam with a diameter which is determined essentially by the cathode diameter. A more distinct electron beam may be generated, however, from a cathode that contains an internal cavity. This has been been suggested by van Paassen et-al [14]. Using such a cathode, a low impedance discharge relying on the well known 'Hollow cathode effect' may be maintained between the internal surfaces of the cathode cavity and an external anode, as shown in fig 2.6. The NG regions of the discharge, resulting from excitation of the gas by electrons from opposing sides of the cavity, coalesce in the centre to form a region of intense glow. When attempting to run the HCD in the lower pressure ranges however, van Paassen et-al identified a second stable mode of operation with high impedance in which a well defined electron beam is produced coaxially with the axis of the hole aperture. This is shown in fig 2.7. In this e-beam mode, the CDS and NG regions are located across the front face of the cathode as observed in the case of a

discharge using a simple plane cathode (fig 2.3). The operational pressure range of this second, e-beam mode is observed to increase with decreasing size of the hole aperture, and the e-beam current may be increased by raising either the gas pressure or the Cathode fall. When increasing the beam current however, a transition point may be reached when the current rises rapidly (on a timescale less than ~0.1sec), and the discharge switches to the low impedance HCD mode. The e-beam mode may be re-established by extinguishing the HCD and then restarting the discharge at low current. It has been demonstrated by van-Paassen that e-beam discharges can be produced from a range of cathode sizes using argon at pressures between 0.001-1.0 mb.

In addition to the e-gun shown in fig 2.7 (to be referred to here as type I), an e-beam discharge may be established using a cathode in which a simple hole is drilled (to be referred to as type II) as shown in fig 2.8. The hole diameter is chosen to be comparable to the aperture size of the type I e-gun. When either type of e-gun is operated at low pressure (0.01-0.1 mb in helium for example), the CDS region in front of the cathode may have a width comparable to the dimensions of the e-gun and containment vessel, and the filament of the e-beam discharge is observed as shown in fig 2.9.

The operation of perforated cathodes in the high impedance e-beam mode may have been unintentionally employed in early studies of glow discharges to generate 'cathode rays' and 'canal rays' [15],[16]. Cathode rays (electrons) and canal rays (ions, metastables and neutrals) have been observed simultaneously by Goldstein in the discharge tube reproduced in fig 2.10. The hole in the cathode (or 'canal') is included to observe the paths of the canal rays, which are otherwise incident on the cathode face, as they pass through the hole

and excite the gas in the lower part of the vessel. Fast electrons derived from the cathode face and in the e-beam filament excite the gas in the upper chamber. In another experiment, Goldstein describes the deflection of an e-beam, produced by a hollow metal cylindrical cathode, by a separate wire cathode (fig 2.11). More recently, Boring and Stauffer [17] have investigated e-beam production in argon at 0.002-0.013mb, and in helium at 0.07-0.13 mb with energies up to 100keV using a type (I) e-gun. The beam is generated using a hole aperture of about 6mm diameter and an internal cavity of about 25mm diameter. The beam is sufficiently collimated to carry out heat treatment and welding of metals at a target area about 100mm away from the cathode face. Popa et-al have investigated the electrical characteristics of a type (II) e-gun using low pressure hydrogen (0.03-0.1mb) [18]. The gun design allows the overall depth of the hole to be adjusted. They observe a correspondence between the hole depth and the beam current, with deeper holes producing more intense e-beams. Beam-like plasma generated by an HCD operating in a high voltage mode, using low pressure neon, argon or hydrogen, has been reported also [19],[20].

Recently, a type (II) e-gun with a hole diameter of 4.7mm has been used by Rocca et-al [21] to generate an e-beam at the relatively high pressures of 0.4-2.0mb in helium, and 0.1-0.5mb in argon. The body of the gun is water cooled allowing continuous operation with a Cathode fall of 1-10kV at currents up to 100mA. The hole in the cathode is open-ended and allows a clear optical path through the cathode body. This type of e-gun is therefore especially well suited for longitudinal pumping of gas lasers since the e-beam can be produced collinearly with the optic axis, and with the axis of the gain medium. In contrast, the e-gun shown in fig 2.5 generates

electrons essentially off-axis. Those electrons produced by the outer regions of the gun face may travel some distance longitudinally before intersecting the gain volume, a cylindrical volume, whose outer diameter is equal to the diameter of the shielded hole. A proportion of the beam energy is undoubtedly wasted in exciting the outer regions of the gas which cannot contribute to lasing action.

The discharge mechanisms which govern the production of an e-beam from a perforated cathode have been the subject of relatively few investigations. Information concerning the particle densities and ion and electron energies in different regions of the beam discharge is lacking. A knowledge of these would enable a rough assessment of the importance of space charge effects. More importantly, only a few measurements of the electric field distribution around the e-beam filament and inside the cathode cavity have been reported. Boring and Stauffer, however, have identified an internal plasma in the hole cavity and, with the aid of a sampling probe of tungsten wire, established that the plasma has a positive potential with respect to the cathode. This is observed to be a few hundred volts in argon when the tube voltage is around 10kV. This internal plasma is thought to act as a source of slow electrons for the e-beam. Control of the e-beam current has been achieved by incorporating a third grid electrode close to the walls inside the cavity, which can be separately biased with a low DC potential. Beam cut-off is observed when the grid is negatively biased by about 10 volts. Therefore, it is suggested that the electrons are probably derived from the cavity walls initially, and released by secondary emission following bombardment by energetic ions and UV photons. Mention is also made of the importance of the electric fields in the region of the hole aperture in determining the quality of the e-beam, although the actual

form of the electric field distribution around the hole aperture and inside the cavity is not reported.

The transition of the e-beam discharge to the HCD mode, which limits the beam current obtainable from this type of electron gun, has been investigated by van Paassen et-al. They suggest that the transition is brought about by the build-up of a conducting bridge caused by the high current e-beam originating at the hole aperture, and the flux of ions travelling along the central axis in the opposite direction to pass into the cavity. They demonstrate that the operational range of the electron gun may be extended by altering the shape of the electric field distribution around the hole aperture by using a concave shaped cathode. This acts to defocus the ion flux incident on the cathode aperture.

In conclusion, electron beams derived from perforated cathodes using open-ended holes can be used as a novel and efficient method of pumping rare gas lasers using energetic electrons. The e-beam can be generated along the central axis of the electron gun, which can be used also as the optic axis of the laser.

2.1.2.3 Electrostatic and Magnetic Focussing

An essential feature of the glow discharge e-guns discussed in the previous sections is that the anode is placed in the FDS region, well clear of the CDS and NG. Its position within the FDS does not affect the properties of the CDS and NG since the electron trajectories from a cathode running at several kV are highly directional. The electrons move according to the shape of the electric field within the CDS which is determined by the profile of

the cathode. Furthermore, since the electric field decreases linearly across the CDS, most of the electron acceleration takes place over the first part of the CDS, close to the cathode face.

If the anode is placed very close to the cathode with a separation less than the thickness of the CDS, however, a discharge cannot be established across the narrow gap because the electrons cannot cascade to initiate breakdown of the gas before hitting the anode. Breakdown can only occur if the Paschen criterion for electron avalanche is satisfied [5]. If a gap is left in the anode of width G which is large compared to the CDS thickness d_c ($G>>d_c$), an e-beam discharge can be established with a beam diameter comparable to G as suggested by Dugdale [22] and shown in fig 2.12. If a narrower gap of width g is left in the anode (where $g<d_c$) however, the edge effects can be used to radically alter the profiles of the equipotential surfaces as shown in fig 2.13. The resulting electric field around the aperture draws the ion flux incident on the cathode toward the centre of the cathode face where most of the secondary electrons are then generated. The electrons appear to originate from the centre part of the cathode and form a thin, slightly diverging beam. By including a second anode or grid element between the anode and cathode, with a diameter the same as that of the original anode, the equipotentials can be shaped further by applying a suitable bias potential to the grid as shown in fig 2.14 [23]. The electric field between the grid and cathode acts as an electron lens to produce a converging effect on the beam when the spacings (d) between the elements are equal. The grid is biased at a potential approximately midway between the anode/cathode potential.

Magnetic focussing of an e-beam generated by a perforated e-gun has been employed by Rocca et-al [21] as illustrated in fig 1.11 and

fig 2.15. The e-gun itself is placed at one end of the magnet with electrons being drawn into a thin column by the 'funnel' of the magnetic field. Magnetic confinement of the electrons is thus used to maintain beam collimation throughout the length of the NG.

References

1. Chapman B., 'Glow Discharge Processes', Wiley, pp77-138 (1980)
2. Emeleus K.G., J.Phys.D., 14, 2179 (1981)
3. Francis G., 'Handbuch Der Physik', XXII, Springer-Verlag, pp53-203, (1956)
4. Warren R., Phys.Rev., 98, 1650 (1955) and 98, 1658 (1955)
5. von-Engel A., 'Ionised Gases', Oxford University Press', (1965)
6. Gill P. and Webb C.E., J.Phys.D., 10, 299 (1977)
7. Yu Z., Rocca J.J. and Collins G.J., J.Appl.Phys., 54, 131 (1983)
8. Chaudhri R.M. and Chaudhri M.M., Int.Conf.Phenom.Ion.Gases., vol I, Belgrade, 392 (1965)
9. Ward A.L., J.Appl.Phys., 33, 2789 (1962)
10. Segur P., Yousfi M., Boeuf J.P., Marode E., Davies A.J. and Evans J.G., 'Electrical Breakdown in Gases', Part A, ed. Kunhardt E.E. and Luessen L.H., Plenum Press, (1983)
11. Tran Ngoc An.. Marode E. and Johnson P.C., J.Phys.D., 10, 2317 (1977)
12. Boeuf J.P. and Marode E., J.Phys.D., 15, 2169 (1982)
13. Rocca J.J., Meyer J.D.. Yu Z., Farrell M. and Collins G.J., Appl.Phys.Lett., 41, 811 (1982)
14. van Paassen H.L.L., Muly E.C. and Allen R.J., Proc.Nat.Electronics. Conference., 590 (Oct 1962)
15. Goldstein E. see Thomson J.J. 'Rays of Positive Electricity', Longmans, (1921)
16. Thomson J.J., 'Conduction of Electricity Through Gases', Cambridge University Press, (1906)
17. Boring K.L. and Stauffer L.A., Proc.Nat.Electr.Conf. 19, 535 (1963)

18. Popa G., Sandulovicіu M., Croitoru P. and Moldovan C., J.de.Phys., coll. C7-187 (1979)

19. Mateescu I., Avram E. and Popovici C.. Eleventh Int.Conf.Phenom Ionis.Gases., p123, Prague (1973)

20. Zamfir O. and Popovici C., Eleventh Int.Conf.Phenom.Ion.Gases., p122, Prague (1973)

21. Rocca J.J., Meyer J. and Collins G.J., Phys.Lett., 87A, 237 (1982)

22. Dugdale R.A., 'Glow Discharge Materials Processing', Mills & Boon, (1971)

23. Issacs G.G., IEE. Gas Discharge Conf., 53 (1972)

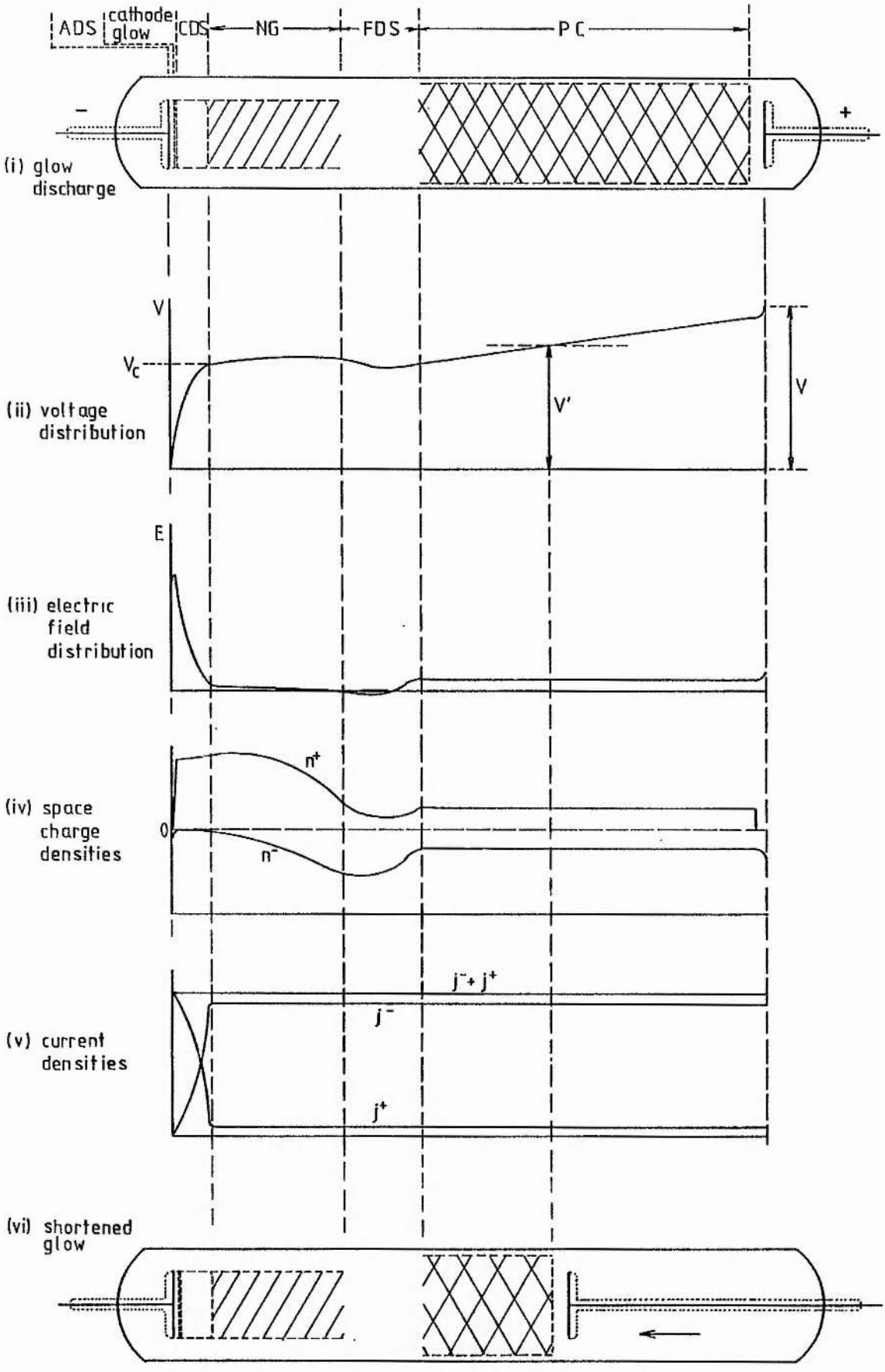

Fig 2.1. Discharge parameters of an abnormal glow discharge in helium at a few mb, with a tube voltage (V) of around 200-300V (adapted from [1]).

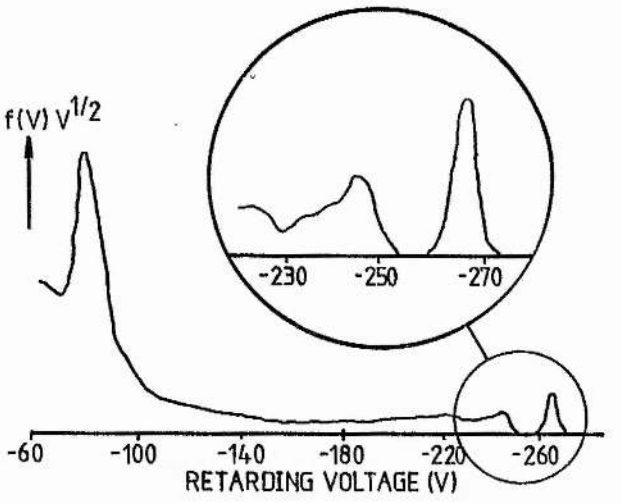

Fig 2.2a. An electron energy distribution in the NG near the CDS/NG boundary of a helium discharge at 20mb, with a cathode fall of 270V [6]. The horizontal voltage scale refers to the grid potential of the electrostatic analyser used.

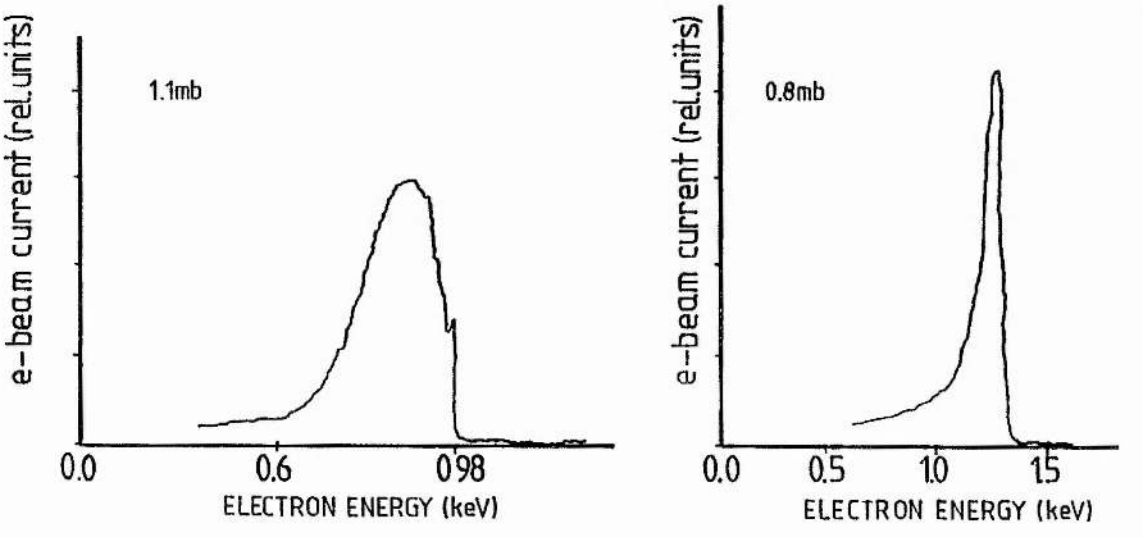

Fig 2.2b,c. Electron energy distributions in the NG of a low pressure helium discharge [7].

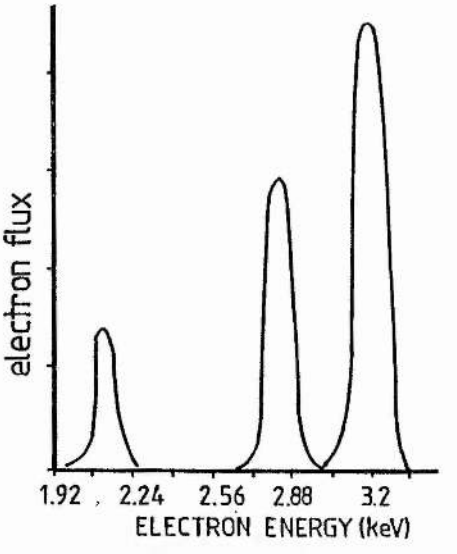

Fig 2.2d. Electron energy distributions at the CDS/NG boundary for three values of the Cathode fall [8].

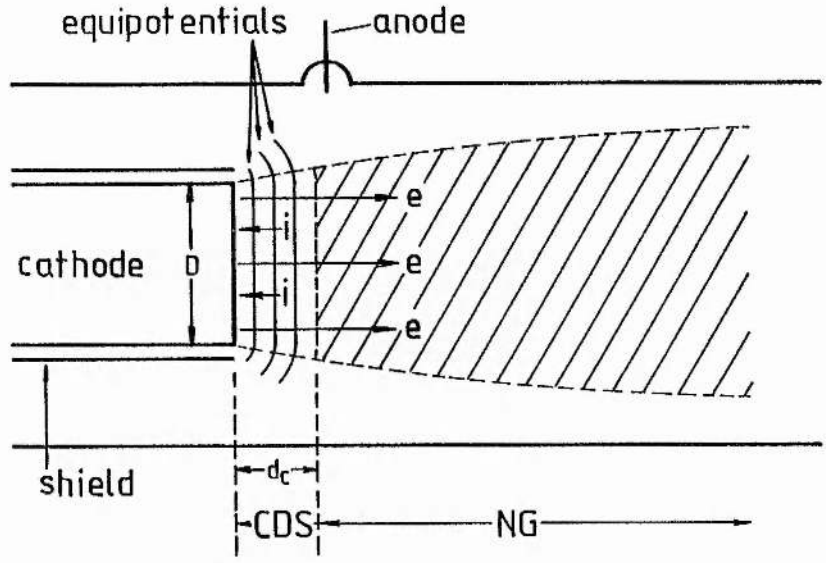

Fig 2.3. Production of fast electrons in the cathode region of an abnormal glow discharge in helium at 1-2mb; the Cathode glow region is not shown. The anode is located in the FDS which is adjacent to the NG.

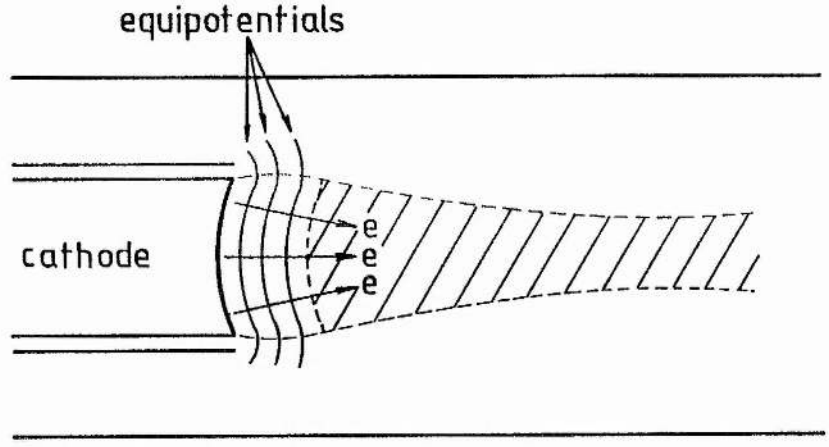

Fig 2.4. Focussing action of a curved cathode in an abnormal glow discharge with a focal length comparable with the radius of curvature of the cathode surface.

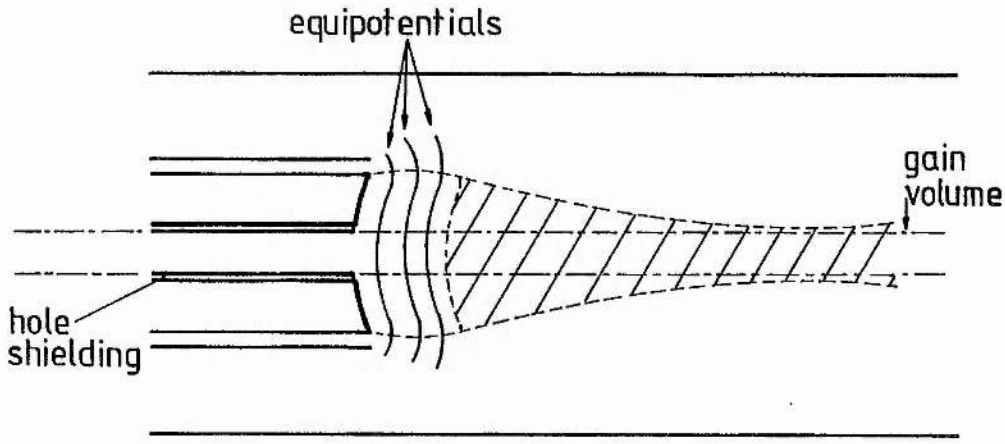

Fig 2.5. Annular electron gun of the same type used for longitudinal pumping of gas lasers [13]. The magnetic field used in [13] is not shown.

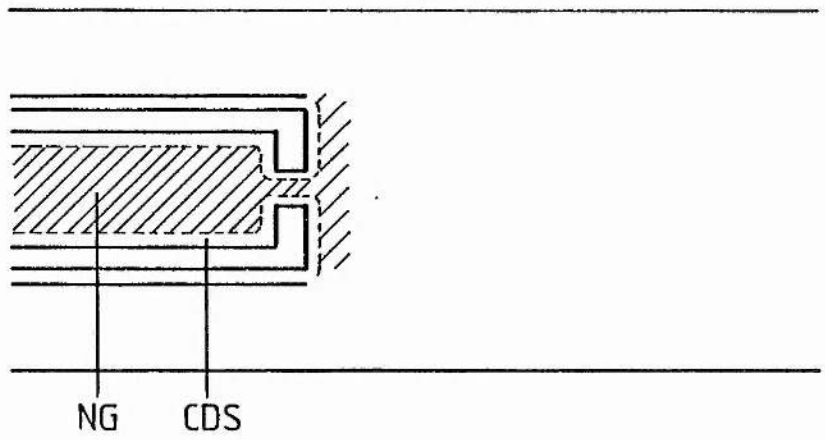

Fig 2.6. A hollow cathode discharge in which an intense NG region occupies the interior of the cathode. The anode (not shown) is located outside the cavity and is connected to the internal plasma by a plasma filament passing through the hole aperture.

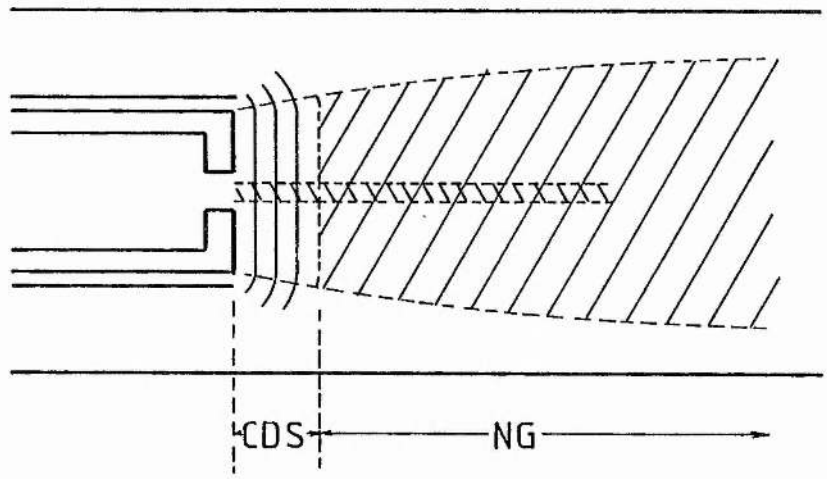

Fig 2.7. Production of an electron beam from a cathode with an internal cavity operating in the high impedance, electron beam mode (type I).

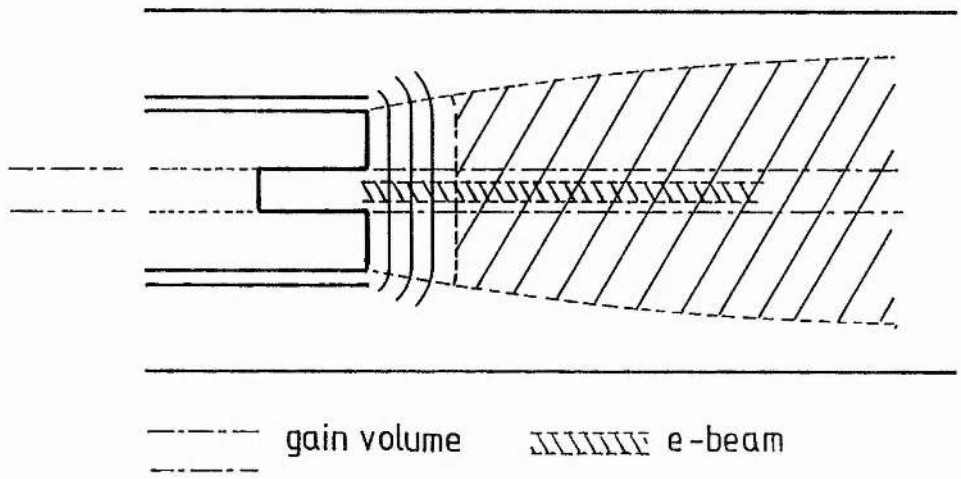

Fig 2.8. Production of an electron beam from a drilled cathode operating in the high impedance mode (type II). When the hole is open-ended and the gun is set coaxially with the optic axis of a laser, the width of the active medium is limited by the hole diameter.

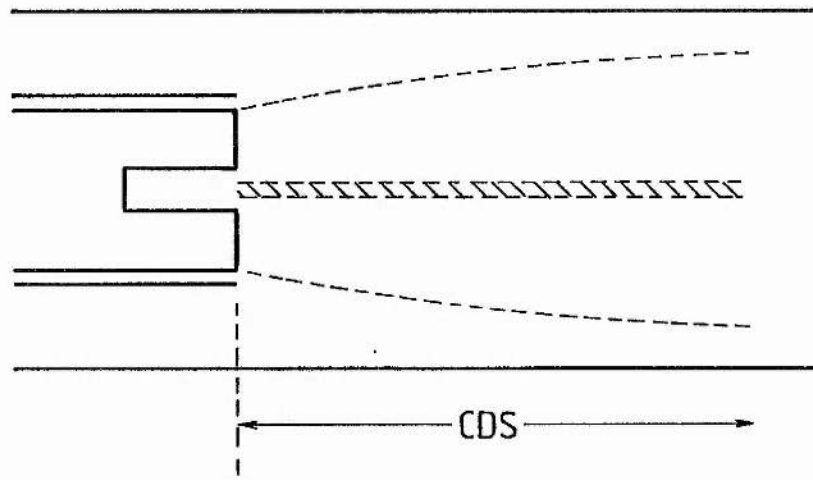

Fig 2.9. Production of an electron beam in helium at low pressure (<0.1mb).

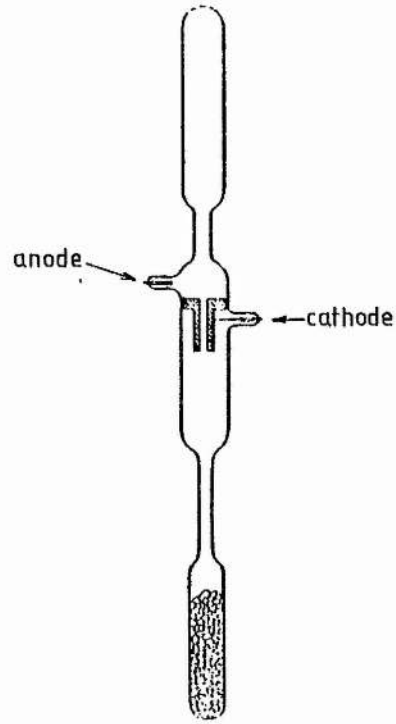

Fig 2.10. Discharge tube used to investigate 'cathode rays' and 'canal rays' in various gases [15].

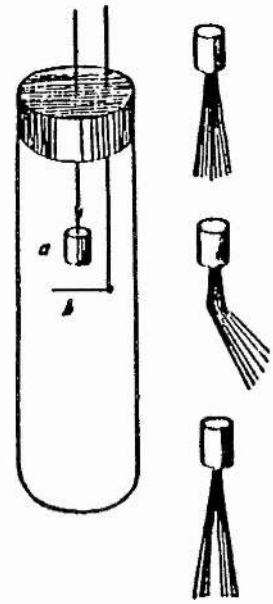

Fig 2.11. An investigation into the behaviour of an electron beam produced by a hollow metal cylinder (a) [16].

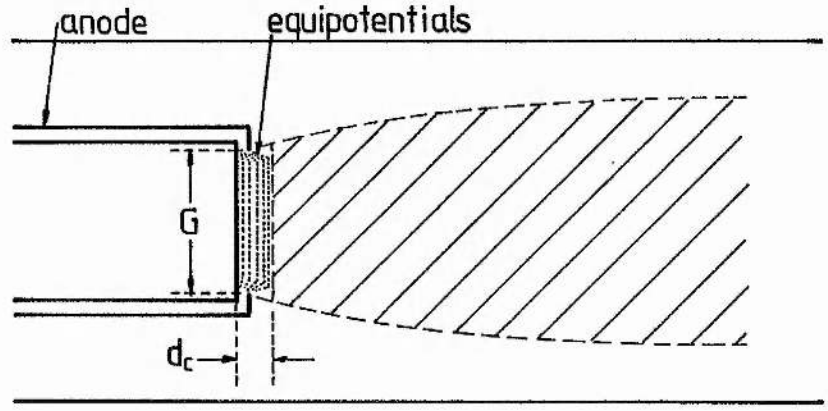

Fig 2.12a. Production of fast electrons by a plane cathode surrounded by a closely spaced anode [20].

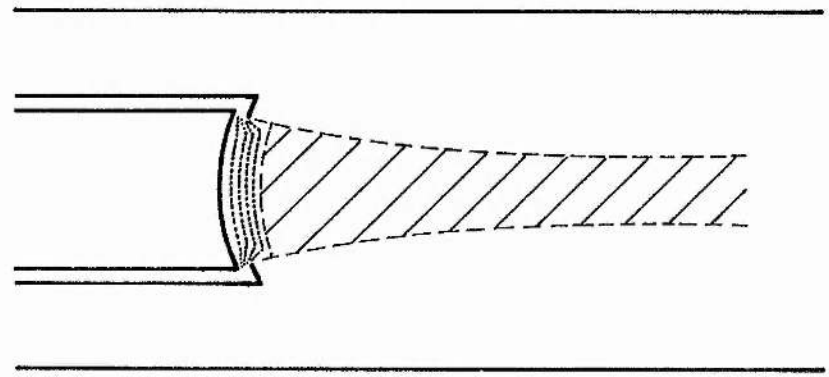

Fig 2.12b. Production of a converging beam of fast electrons using a closely spaced anode/cathode [20].

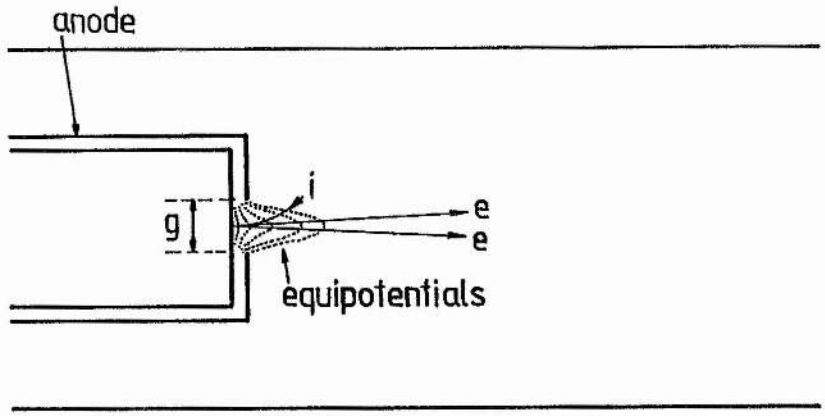

Fig 2.13. Production of a thin diverging electron beam from a narrow aperture electron gun [20].

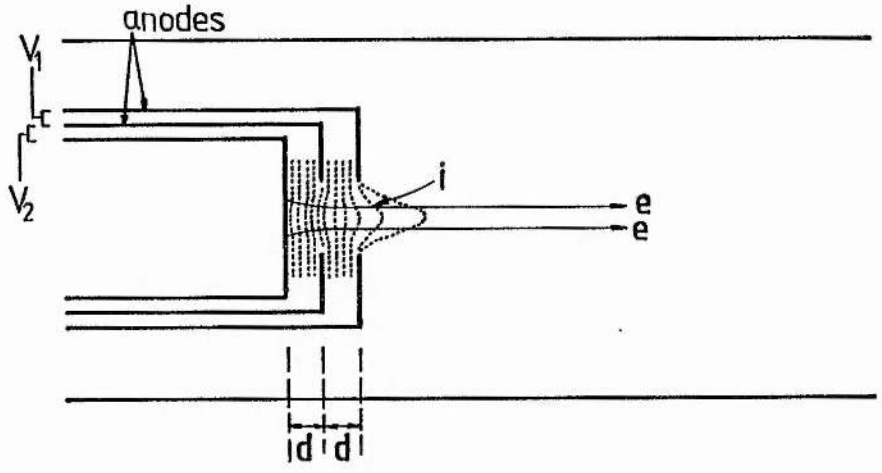

Fig 2.14. Electrostatic focussing of a thin electron beam by a twin anode electron gun. The beam is made to converge or diverge by adjusting the anode potential V_2 [21].

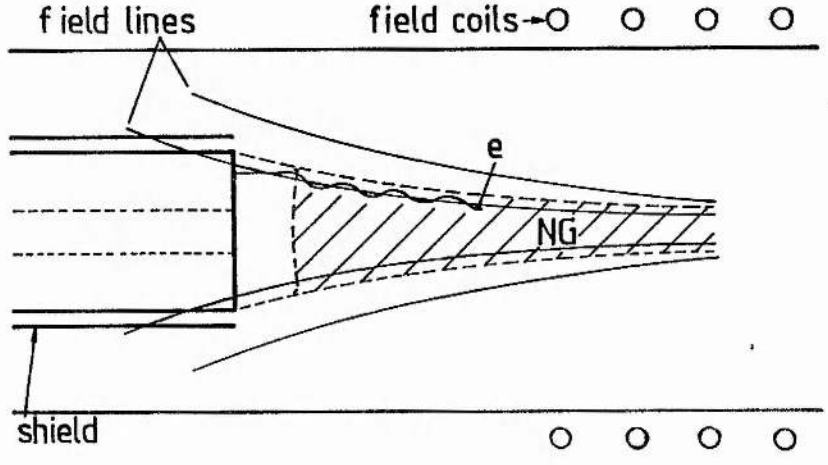

Fig 2.15. Magnetic focussing of fast electrons generated by a simple planar cathode.

Chapter 3

3 Experimental Investigation of Glow Discharge Electron Guns

3.1 Preliminary Studies of e-guns in Helium and Deuterium

An electron gun of similar design to that used by Boring and Stauffer has been constructed to investigate the characteristics of an e-beam discharge operating in helium in the pressure regime of 1-10 mb [1]. The circular stainless steel cathode, which is shown in fig 3.1a, is machined to achieve a close fit inside a quartz jacket of diameter 2cm. This confines the discharge to the front face of the cathode. The electron beam is produced from a hole of diameter 2mm drilled in the centre of the cathode face. The cathode also incorporates an internal cavity to act as a source of electrons for the beam. Electron emission from the front face of the cathode is prevented. however, by the inclusion of a quartz shield placed close to the cathode face with a gap of about 0.5mm. A 2mm hole at the centre of this shield allows the e-beam discharge to be established so that the discharge current can be attributed specifically to the flow of charged particles at the cathode aperture. A number of small holes of diameter 1mm are also drilled in the side wall of the cathode to observe the internal plasma in the cathode cavity. A tungsten pin anode is located in a side limb in the vacuum vessel about 20cm away from the cathode face. The electrodes are connected to a DC power supply in series with a ballast resistor of 20kΩ to prevent arcing

(fig 3.1b).

The system is pumped down to around 10^{-4} mb using an oil diffusion pump and U.H.P. grade helium (99.995%) is then backfilled into the system, via a needle valve, to provide gas pressures between 1-10 mb. The interior surfaces of the discharge tube are cleaned by running a discharge for a period of several hours with several new fills of gas. Reproducibility of the V-I characteristics of the discharge. which are shown in fig 3.2a, is achieved by recording each curve quickly (~1sec) to overcome heating and sputtering effects. Each curve is also recorded after a fresh fill of helium, and after running the discharge for a period of several minutes at low current (<0.5mA). At high helium pressures, or at low tube voltages, the NG does not extend to the anode and a length of PC fills the remaining space between the end of the NG and the anode (fig 3.1c). The small voltage drop across the PC has been calculated from values of E/p ($V.cm^{-1}.mb^{-1}$) given by von-Engel [2], in order to calculate the Cathode fall from the overall tube voltage. A further small correction is made to allow for the Anode fall potential which is approximately 25V.

The positive V-I characteristics of the discharge demonstrate that e-beam production is only possible for a limited range of discharge parameters. The transition points on the individual V-I curves mark points at which the discharge current rises rapidly on a timescale less than ~0.1sec, and the discharge is observed to switch from a high impedance e-beam mode to an HCD mode. Several sets of transition points have been recorded on subsequent runs, and are illustrated collectively in fig 3.2b. The discharge can thus operate in an e-beam mode over the pressure range 1.0-10.5 mb with the discharge current reaching a maximum of 14 mA at 7.5 mb. These

transition points are observed to occur at lower values of discharge current during the 'running in' period, and this suggests that impurities in the gas may act to reduce the range of operation of the discharge in the e-beam mode.

When the discharge operates in the e-beam mode, an internal plasma is observed inside the cavity which is considerably less intense than either the NG or PC, in contrast to the observations of Boring and Stauffer. It has a colour similar to that of the PC and Anode glow, and may therefore represent a weak plasma region. It is noted also that the electron beam flux from the hole aperture is not well collimated compared with the observations of Boring and Stauffer, and this may be due to operating the discharge in the high pressure regime. At high pressure, increased scattering of the beam electrons is to be expected. It is possible, however, that the quartz cover placed immediately in front of the aperture may accumulate a static charge when the discharge is running, and affect the electric field distribution in the CDS.

Several e-beam discharge tubes have been operated in Deuterium gas in the pressure range ~0.7-1.3 mb. These studies have been carried out in collaboration with the English Electric Valve Co. [3]. The discharge tube shown in fig 3.3 consists of a Kovar cathode with a ~1.5mm diameter cavity, and is sealed into a glass envelope together with a Tungsten pin acting as the anode. The e-beam is used to excite a fluorescent layer deposited on the inside of the glass tube (see Appendix III). The discharge is observed to operate with a Cathode fall of up to 4kV, and with a beam current of up to ~6mA, and collimation of the beam is observed to be better than seen with the tube in fig 3.2a. This demonstrates the importance of the equipotentials around the hole aperture in the formation of a

collimated e-beam. Obstacles placed in this region, whether insulators or conductors, appear to affect these equipotentials. The importance of the external CDS in the formation of the beam is illustrated further by the discharge generated by the cathode shown in fig 3.4. The e-beam is produced perpendicular to the front face in this case, and not in a direction collinear with the hole. This confirms, therefore, that the bulk of the Cathode fall is normally located in front of the hole cavity, when the discharge operates in the e-beam mode.

3.2 Diagnostic Techniques in the Cathode Region

Electron beam production from perforated cathodes has been the subject of relatively few investigations. Known characteristics of the plasma in the cathode regions of such discharges have been summarised in the previous chapter. From the results of several preliminary experiments with e-beam discharges in helium and in deuterium, aspects of the behaviour of these cathodes can be identified for further investigation:

1. The factors which determine the operating regime of the discharge in the e-beam mode, and conditions under which the discharge switches to a low impedance mode;
2. Possible extension of the transition points to allow the discharge to operate stably in the e-beam mode at higher current levels;
3. The role of the internal plasma in the formation of the e-beam.

Plasma diagnostics carried out in the CDS and NG regions are notoriously difficult to perform due to the non-Maxwellian distribution of electron energies in both regions. There are a number of diagnostic methods used to examine these regions for discharges with simple plane cathodes. These methods may be applied to investigate e-beam discharges. Langmuir probes cannot be used easily in the CDS region because the electric field is large and non-uniform. More importantly, objects placed in the CDS interrupt part of the ion flux to the cathode, and part of the electron flux in the opposite direction, thereby increasing the discharge impedance. To a lesser extent, probes placed in the NG affect the ionisation balance by blocking part of the flux of fast electrons. This is probably less important at sampling points in the glow further from the CDS/NG boundary. Popa et-al also express doubts about the suitability of Langmuir probes for use in the cathode regions because fast beam electrons collide with the probe to generate slow secondary electrons [4]. Similar problems are likely to be encountered by placing small orifices in these regions to act as electron or ion samplers. Distortion of the low energy region of the electron energy spectrum is reported by Gill and Webb when the sampling orifice (in this case a hole drilled in the anode) is placed near to the CDS/NG boundary [5].

Particles incident on the cathode face may be sampled through a small hole drilled in the cathode as demonstrated by Davis and Vanderslice [6]. The perturbation of the discharge current is negligible if the hole size is small compared with the cathode area. Although this type of experiment yields important information about the flux and energies of particles incident on the cathode face, it cannot be used to examine the flux of electrons travelling in the

opposite direction. Fluorescence spectroscopy can be used to investigate the population of excited atomic and ionic states. With proper allowance being made for cascade pumping from higher states, measurements of line intensities can be used to predict the form of the electron energy distribution function. Unlike fluorescence spectroscopy, absorption and optogalvanic spectroscopy both represent a source of perturbation to the discharge and furthermore, they can usually be used to measure metastable populations only.

The observations of the internal plasma in a perforated cathode by Boring and Stauffer indicate that the electric fields in the plasma are low compared with those in the CDS. If this is also the case at higher pressure, the internal glow may be amenable to probe analysis to investigate field strengths at points inside the cavity. However, since the cavity dimensions must be reduced at higher pressure to operate within the e-beam regime, the probe size has to be reduced. It is necessary also to ensure that the thickness of the probe sheath is small compared with the dimensions of the hole. Furthermore, this sheath is likely to be asymmetric due to the directionality of the ions and the electrons in the discharge glow near the cathode. Fitting small biasing grids into the cavity is more difficult at high pressure for a similar reason. The current flux at the hole aperture is also of prime interest and can be compared with the current flux derived from the same area of a flat cathode. Overall, much information can be gleaned from the electrical characteristics of perforated cathodes when compared with the characteristics of simple plane cathodes operating under otherwise identical discharge conditions.

3.3 Electrical Characteristics of Perforated Cathode Electron guns

Perforated cathodes operate in the e-beam mode over a limited range of discharge parameters. This e-beam regime has been investigated for e-gun cathodes using a wide range of aperture sizes, as shown in fig 3.5. These cathodes are mounted in the discharge cell shown in fig 3.6, and are interchangeable, allowing characteristics of each one to be investigated in the same experimental environment. A plane 'control' cathode is also characterised to act as a baseline for comparison with all the e-beam cathodes. Edge effects around the cathode perimeter, resulting in a reduced current flux at the cathode perimeter, have been investigated by Chaudhri and Baqui [7]. These are likely to be significant when the cathode diameter is comparable to the CDS width d_c. However, by comparing the characteristics of the e-gun cathodes with those of the 'control' cathode, differences that arise can be attributed to the presence of the aperture and e-beam filament. Beam production from larger cathodes with multiple apertures has been investigated also.

3.3.1 Experimental Arrangement

The discharge cell shown in fig 3.6 (and plate 1) consists of a quartz tube 300mm in length, 65mm I.D.. held between two stainless steel end flanges with 'o' ring seals. Helium gas (U.H.P. grade 99.995%) enters the cell through one end flange, and the cell is evacuated through a port in the opposite flange. The e-gun cathodes are held in a removable mount which is seated centrally on one end flange by an 'o' ring seal and a perspex clamping plate. The mount is

conveniently withdrawn from the rear of the flange to change cathodes without disturbing the main flange seals. All parts of the cathode except the front face are shielded from the discharge. This is achieved by using a closely fitting quartz jacket around the cathode mount, and an electrically isolated metal end cap which is set close to the cathode body. The cathode assembly is held at negative potential whilst the anode and end flanges are all earthed. A ballast resistance of 20kΩ is used between the power supply and cathode as a current limiter to prevent arcing. The vacuum system used to pump the discharge cell is shown in fig 3.7. All surfaces in the discharge cell in contact with the vacuum have been degreased using acetone, and the cathodes are cleaned with acetone more thoroughly in an ultrasonic bath. The discharge tube has been heated to ~80 °C using heating tapes for about 24 hours. All vacuum seals in the system have been tested using a commercial helium leak detector unit. The system is pumped by an oil diffusion pump to reach a pressure of 4×10^{-5} mb routinely, as shown on the ionisation gauge. The base pressure in the discharge cell may be slightly higher due to a loss of pumping speed through the bellows connectors. During preliminary experiments with the discharge cell, it has been found that reproducible electrical characteristics of the cathode can only be recorded if a flow of helium through the discharge cell is maintained. For a sealed off system, operation of the e-gun cathodes in the e-beam mode is found to be unstable, and severely restricted. Similar unfavourable characteristics are observed if the cathode is not cleaned. Scintillations, or micro-arc discharges, are observed on the cathode face and are accompanied by bursts of current, when the discharge is run continuously.

For the cathodes investigated. a 'running in' procedure has been adopted. After setting the gas pressure to 1mb initially, the

discharge is run at 0.12mA (single aperture cathodes) or 0.4mA (multiple aperture cathodes) for 20 minutes. Then, a number of V-I curves are recorded at 1mb, one every 5 minutes, until good reproducibility is observed between successive curves. Between 5 and 10 V-I curves are recorded finally, and an average is taken of the group. The scatter between curves in this final group is observed to be ~5%. Several preliminary curves, and between 5 and 10 final V-I curves, are recorded for each subsequent pressure. For curves terminating at transition points marking the transfer to the HCD mode, the transition points are observed to occur at values of the discharge current which increase steadily during the running-in stage. Eventually, the transitions points themselves become reproducible, and the final set of curves are then recorded. Overall reproducibility is observed only if the V-I curves are recorded quickly (~1 sec), and if the discharge is left running at very low current (~0.1mA) between taking curves. The V-I characteristics of the plane cathode have been recorded on two different days to test reproducibility, and agreement to within 5% is obtained between the two sets of curves.

3.3.2 Results of Comparative Studies

3.3.2.1 Single Aperture e-guns

The V-I characteristics of e-gun cathodes with hole diameters between 1mm-5mm operating in the e-beam mode are shown in fig 3.8. The characteristics of a plane cathode are included for comparison. The V-I curves for a 1mm aperture are almost identical to those of the plane cathode but for larger apertures, the V-I curves rise more steeply. However, the pressure range over which the cathode operates in the e-beam mode is reduced for larger apertures. For hole diameters of 4mm and 5mm, e-beam production is restricted to 1mb-3mb.

The V-I characteristics of the plane cathode are used as a baseline to overcome systematic errors in measuring the current density at the cathode face. These errors are caused mainly by edge effects around the cathode perimeter. A ratio η_j of the discharge current derived from the e-gun cathodes and from the plane cathode is calculated at identical values of pressure and Cathode fall. A set of current ratios are shown in fig 3.9 for aperture sizes 2mm-5mm. No discernable variation of η_j with Cathode rall is observed for a 1mm aperture, but for larger sizes, the current density from e-gun cathodes is larger than from an equivalent area of plane cathode. For larger apertures or higher gas pressures, the current ratios are larger but are found at lower values of Cathode fall. For aperture sizes 2mm-4mm operating at pressures between 1mb-3mb, the ratios are similar and appear constant up to $V_c \sim 1.4$kV, and then increase sharply for nigher values of V_c. For higher pressures, this sharp increase of

η_j occurs at progressively lower values of V_c.

A further set of current ratios have been calculated for apertures of diameter 3mm with different overall depths, as shown in fig 3.10. A shallow hole of depth 1.5mm does not exhibit beaming characteristics (fig 3.10a) whereas there is a marked increase in η_j with rising V_c for an aperture of depth 21mm (fig 3.10b). Current ratios for different gas pressures between 1mb-4mb, with hole depth as a parameter, are shown in fig 3.10c-f. The current ratios for all depths are similar in size at low Cathode fall, but again increase sharply at around 1.4kV. In addition, a saturation effect is clearly identified with the shallower holes saturating first. The e-gun of depth 10mm is beginning to saturate at about 3kV. These observations imply that discharge processes in the e-gun cavity, which are responsible for the formation of the e-beam filament, are confined to the front region of the holes at low Cathode fall. At higher values of V_c, the deeper regions in the holes also participate in the beam discharge. Similar effects showing saturation of beam current have been reported by Popa et-al for an e-beam discharge in Hydrogen [8].

3.3.2.2 Multiple Aperture e-guns

Several types of e-gun cathodes incorporating multiple apertures have been investigated. In all cases, the e-beam filaments from the separate cavities are produced simultaneously and with good stability. The individual beam filaments are observed to have equal glow intensities and do not require individual ballasting of the separate beam channels. The V-I characteristics of these e-guns are broadly similar to those of single aperture cathodes, and are shown in

fig 3.11a-c. The current ratios η_j (fig 3.11d-f) increase with Cathode fall altnough a sharp rise in η_j at 1.4kV, observed previously for pressures between 1mb-3mb, is not seen. Production of an e-beam from the cathode shown in fig 3.5k is found to be particularly unstable, and the discharge switches to an HCD mode at very low values of discharge current or Cathode fall. This is is contrast to the behaviour of the e-gun cathode shown in fig 3.5i which does operate stably in the e-beam mode over a wider range of discharge conditions (fig 3.11f).

3.3.3 Transition Points

The operation of an e-gun cathode in one of two stable modes is closely related to the properties of a discharge generated by a dual cathode consisting of two opposing electrodes (fig 3.12). When the ambient pressure is low, or if the cathode separation D is small, electrons from the cathode faces are unable to initiate breakdown of the gas in the gap. This is similar to an Obstructed glow discharge [2] and the discharge forms only at the cathode edges, with the CDS filling the interelectrode gap (fig 3.12a). As the width of the CDS is reduced (by raising the pressure, or by increasing the Cathode fall). a point is reached when the glow suddenly transfers to the region between the electrodes (fig 3.12b). The discharge impedance drops markedly, and the superposition of electron avalanches from each cathode face contributes to the Hollow cathode effect [9]. In this HCD mode, clearly the width of the CDS (d_c') must be less than half the plate separation D for NG to form in the central region. Undoubtedly, e-gun cathodes operating in the e-beam regime are a type of Obstructed

glow discharge. Indeed, distinct e-beam filaments have been generated using dual cathodes operated in an Obstructed mode as reported by Kunz [10] (fig 3.12c). Using a dual cathode geometry, Badareu et-al have investigated the electrical characteristics of the discharge operating in the Obstructed and HCD modes, and in the transition phase [11]. Dual cathode discharges exhibit a negative resistance characteristic during the transition phase but by regulating the discharge current, Badareu et-al have determined the V-I characteristics during the transition phase. They concluded that there is a simple criterion for the transfer from the Obstructed mode to the HCD mode relating to the relative sizes of d_c and D, namely,

$$D = K \times d_c \qquad (3.1)$$

where K is a constant of the gas used.

For a plane cathode, the width of the CDS (d_c) is known to obey the similarity relationship ($p.d_c=f(V_c)$ as shown in fig 3.13 [2]. The product $p.d_c$ decreases with increasing V_c and levels off at about 0.7 mb.cm for $V_c>1.5$kV. This similarity criterion may not apply in the HCD discharge, however, since d_c and d_c' are not necessarily equal. The ionisation balance in the HCD is likely to be markedly different to that for a plane cathode. However, it is expected that there is an equivalent relationship linking p,D and V_c at the transition points from the e-beam mode to the HCD mode. The transition points on the V-I curves from all e-gun cathodes investigated here, including those with multiple apertures, are plotted in fig 3.14 with $p^m.D$ as a parameter against V_c. The optimum fit for the data points is found for a index value m=1/2. For larger settings of V_c, which are needed to produce more energetic electrons,

it is therefore necessary to operate at lower settings of $p^{1/2}.D$ to remain within the e-beam mode. To produce e-beams with energies in the keV range, it is necessary to operate with $p^{1/2}.D<0.5$. The discharge current at each of the transition points for the single aperture cathodes is shown in fig 3.15. It is clear that there is a further disadvantage in operating with a low Cathode rall. For the e-guns to remain in the e-beam mode, the discharge current is limited to a few mA. From the electrical characteristics observed here, the following mechanisms are proposed as being responsible for the production of e-beams from perforated cathodes.

If the CDS width at the cathode face is much larger than the hole diameter D, few equipotentials from the CDS penetrate the hole region, as shown in fig 3.16a. This is illustrated by the results shown in fig 3.10c. The current ratio η_j is the same for all hole depths at low values of V_c. As the Cathode fall is increased, more equipotentials are forced into the hole since the CDS width is then reduced, and because there are more equipotentials for higher values of V_c (fig 3.16b). Electrons are released from the cavity walls by secondary emission as ions and metastables from the NG pass through the CDS and into hole cavity. These electrons are accelerated by the perturbed equipotentials, and may generate further ions and metastables inside the hole cavity, through collisions with helium atoms. If the production rates of these species in the cavity are significant compared with the rates in the main NG region, the cavity begins to assume the characteristics of an HCD discharge, since the newly created species are trapped within the cavity. This is illustrated by the general rise of η_j with increasing Cathode fall as shown in fig 3.9. As the CDS width is reduced further, the degree of perturbation of the equipotentials around the hole entrance is such

that electrons within the cavity are accelerated with larger radial components of velocity. Ionisation produced by such electrons leads to a build up of the ion density in the central region of the hole, and the resulting positive space charge perturbs the equipotential distribution further. Eventually. the build up of positive space charge in the central region is sufficient to allow the discharge to be sustained by ionisation within the cavity, and the discharge switches to an HCD mode (fig 3.16c). The increase of the gradient of the V-I characteristics just before the transition point is reached may reflect the onset of the Hollow Cathode effect in the hole cavity (fig 3.8). The ratio η_j also increases for higher values of p or D, for a given Cathode fall. By increasing these parameters, greater penetration of the equipotentials into the cavity is expected, giving rise to more internal ionisation.

Operating the the discharge in the e-beam mode near a transition point on a V-I curve may not result in the production of a collimated e-beam, however, aside from the instability expected in this region. A large number of equipotentials are expected to penetrate the hole cavity in this case, and the exterior CDS is left with few unperturbed equipotentials at the hole entrance. These must be present to accelerate the cavity electrons to form the collimated e-beam filament. For optimum e-beam production, only a slight perturbation of the equipotential distribution is necessary. In this case, the resulting electric fields act as an electron lens to focus electrons generated within the cavity into a narrow beam (fig 3.16b).

Those e-gun cathodes operating at V_c>1.5kV and with low values of $p^{1/2}.D$ (eg. 3mm cathode at 1mb-3mb, and 2mm cathode at 1mb-4mb), do not transfer to the HCD mode within the voltage range investigated. Indeed, an upturn in the current ratios η_j for large V_c settings,

signifying the onset of the HCE, is not observed (fig 3.9a,b). For a plane cathode, the parameter $p.d_c$ does not vary appreciably with increasing Cathode fall (V_c) for voltages of a few kV, as shown in fig 3.13. For a fixed pressure, the CDS width therefore remains relatively constant, and this behaviour is also expected for the external CDS of the e-beam discharge when V_c>1-2kV. If an e-gun cathode is operated in this regime, with the parameter $p^{1/2}.D$ selected so that the discharge is operating well away rrom a transition point, the bulk of the Cathode fall is located across the exterior CDS, as is necessary for good beam collimation. As V_c is increased further, the CDS width does not vary appreciably, and the most of the equipotentials in the exterior CDS remain unperturbed. Most of the Cathode fall is then still dropped across the exterior CDS, thus maintaining beam good collimation. In this case, a transition to the HCD mode is likely to be innibited since the electrons generated within the cavity are extracted by the larger field in the exterior CDS.

Finally, for continuous operation of the e-gun cathodes, a degree of gas heating is expected, reducing the effective gas pressure in the discharge. Therefore, it is necessary to select slightly higher values of $p^{1/2}.D$ than suggested by the results in fig 3.14.

3.4 Spectroscopic Observations of Discharges in Helium

Observations of the cathode regions in a glow discharge using a plane cathode reveal that the intensities of the Cathode glow and NG are comparable, when the discharge operates well into the abnormal regime. For an e-gun cathode operating in the abnormal regime, an intense Cathode glow is seen also. In addition, an e-beam filament is observed in the CDS which originates at the aperture entrance, and can be followed some way into the NG. The filament has a diameter between 1mm-2mm for the range of hole sizes investigated (2mm-5mm), and has a colour similar to that of the NG, but different from that of the Cathode glow. Although it appears in the CDS, the filament may therefore possess properties similar to that of the NG plasma.

Spectroscopic analysis of the Cathode glow regions using a plane cathode with finite dimensions presents difficulties because the emission profiles are two dimensional (fig 2.3). Measurements in the PC glow are easier since the emission profiles are radially dependent only. However, if the diameter of the cathode is large compared with the dimensions of the Cathode glow regions, the emission profiles are approximately one dimensional. When running a discharge continuously up to 0.5mA-1.0mA using a plane cathode of diameter 14mm, however, it is found that the discharge impedance slowly rises over a period of about twenty minutes. This effect is probably due to gas heating, or sputtering of material from the cathode face. It is not possible to make reproducible measurements of glow intensities under these conditions. All spectroscopic measurements have therefore been recorded using 6mm diameter cathodes which are found to operate up to 1kV and 1mA before similar effects are encountered. Measurements of the glow intensity have been taken in the CDS and in the first stages

of the NG using a plane cathode, and using an e-gun cathode of dimensions 3mm×21mm.

3.4.1 Experimental Arrangement

The experimental arrangement is shown in fig 3.17 and the apparatus is placed on a rigid steel table to maintain the alignment of the optics. The discharge cell is mounted on a movable table to enable the entire discharge tube to be scanned across the field of view of the optical arrangement, which remains stationary. The discharge cell is decoupled from the vacuum system by two flexible bellows connectors. Optical layouts for carrying out spatial sampling of glow discharges have been discussed extensively by Webb [12]. Here, the problem is relatively simple because the plasma thickness for sampling of the sidelight emission is relatively thin (<1cm). A single slit of width 0.02cm and height 0.3cm is placed close to the discharge cell to form an aperture, with the slit set parallel with the cathode face. A lens placed close to the monochromator (Carl Zeiss SPII) collects a narrow cone of light passing through the aperture and chopper, and brings it to a focus at the monochromator entrance slits (fig 3.18). Ray tracing reveals that light rays emerging from the front slit are transmitted through the monochromator slits only if they pass through a virtual slit of width b' located at the lens element. The thin slice of plasma glow sampled by the monochromator is calculated to have a width of 0.026cm for the dimensions and slit widths used. There is negligible divergence of the field of view over the width of the plasma (<1cm). A He-Ne laser is used to align the optical system initially. The position of the

cathode with respect to the sampling aperture is deduced from the resistance of a 1kΩ, ten-turn precision potentiometer which allows a translational movement of 0-2cm. This is connected to a stabilised DC power supply giving +2V output, and the ramp output from the potentiometer (0-2V) is fed to the X-axis of an X-Y recorder. The monochromator is fitted with a diffraction grating (6000 lines cm^{-1}) and a photomultiplier tube (type EMI 9558B). The output from the PM tube is fed to a low noise pre-amplifier to allow different sensitivity settings, and then to a lock-in amplifier which amplifies the chopped signal. An optimum chopping frequency of 1500Hz is found to give the maximum signal level. Finally, the signal from the lock-in amplifier is fed to the Y-axis of the X-Y recorder. Calibration of the system to determine the instrumental response has not been carried out. The spectra recorded have been corrected for the response of the PM tube only [13], which is the principal source of error. The transmission of the quartz lens [14] and the response of the diffraction grating [15] over the visible range 4000Å-7000Å are both almost constant. A running-in procedure for the cathodes, as described in section 3.3.1, has been followed before recording the emission profiles.

3.4.2 Results

Emission profiles in the cathode region, for a number of HeI transitions, are depicted in figs 3.19-3.22. Profiles for gas pressures between 1mb-4mb have been recorded using the plane cathode, and at 1mb for the e-beam cathode (fig 3.22). The cathode face is located at a position +0.15cm on the horizontal scale for all

measurements taken with the plane cathode, and at +0.18cm for those with the e-gun cathode. The discharge current can be raised to about 1.0mA before gas heating effects are observed, as shown in fig 3.23.

Emission profiles at 1mb are shown in fig 3.19 for the four most prominent lines in the observed spectrum. The profiles for 5016Å ($3p^1P$-$2s^1S$) have a peak close to the cathode which becomes more prominent as the Cathode fall is increased. It corresponds to the Cathode glow region. A second peak is observed at the CDS/NG boundary. Two peaks are observed for 5876Å ($3d^3D$-$2p^3P$) also, and the first peak is more pronounced than at 5016Å, and increases rapidly as V_c is raised. The emission profiles for the remaining two lines at 6678Å ($3d^1D$-$2p^1P$) and 4922Å ($4d^1D$-$2p^1P$) are somewhat similar to the first two sets. It has been reported that the Cathode glow is the most intense region of the discharge in other gases for strongly abnormal discharges [16]. At a pressure of 2mb, the intensity of the first peak, which is the Cathode glow, as a ratio of the height of the second peak, generally decreases slightly (fig 3.20). However, a third broad peak begins to appear in the NG for the profiles at 5876Å, as the discharge current reaches 0.5mA. This peak in the NG is observed also for the other triplet transition at 4471Å ($4d^3D$-$2p^3P$), but is absent from the profiles of the singlet transitions. At 4mb, the Cathode glow is generally not observed but in this case, the Cathode fall is not increased beyond ~0.5kV (fig 3.21). At 5876Å, the third peak in the NG is more pronounced than at 2mb, and begins to form at 0.3mA. Similar broad peaks in the spatial emission profiles of triplet transitions, but not singlet transitions, have been observed by Soldatov [17].

The intensity of the third peak in the NG at 5876Å increases with both pressure and discharge current. It is known that its presence is

due to cascade pumping of the upper triplet states following volume recombination in the NG between He^+ ions and slow electrons [18]. The rate of recombination in the NG of an HCD discharge is proportional to the gas pressure and the discharge current also, as reported by Kuen et-al [19]. They suggest that the likely mechanism in the NG is dielectronic recombination:

$$He^+ + e(slow) \geqslant He^{**}$$

followed by

$$He^{**} + He \geqslant He^{*} + He\ (+K.E.) \qquad (3.2)$$

$$\text{or} \qquad He^{**} \geqslant He^{*} + h\nu\ (\text{photon})$$

It is found to be important for p>5.0mb at a current density of $j=0.8mA.cm^{-2}$, with triplet levels pumped by recombination more than singlets. Here, the third peak appears in the profiles of 5876Å line at 4mb when $j=1.06mA.cm^{-2}$ and at 2mb when $j=1.8mA.cm^{-2}$ (fig 3.20a and fig 3.21). Ultimately, the majority of the atoms in excited triplet states will decay to the $2s^3S$ metastable state, as suggested by Kuen et-al, and the density of these metastables may be relatively high in the recombination zone. Therefore, it may be a suitable plasma region for metal vapour lasers relying on Penning collisions between metal atoms and He^* ($2s^3S$) states (eq 1.3).

It is possible that the intense Cathode glow region seen at 1mb for the emission line at 5876Å is also due to recombination. However, this seems unlikely since the intensity of this peak, compared with the second at the CDS/NG boundary, decreases with increasing gas pressure. In addition, the region in the CDS near the cathode is not likely to have a high concentration of very slow electrons. unlike the NG, since the electric field here is $\sim 2.0kV.cm^{-1}$. The Cathode glow is

probably generated by collisions between fast moving electrons from the cathode and He atoms, or by the flux of ions, metastables and neutrals from the NG moving towards the cathode. The impact cross-sections for the excitation of helium atoms by helium ions and excited species (He^+, He^{++}, He^*, He_2^+) are not well known. Cross-sections of between 10^{-20}-10^{-19} cm^2 have been reported for excitation by fast moving neutrals with energies of around 1keV [20]. These cross-sections are two or three orders of magnitude smaller than those for electron impact excitation. It seems likely, therefore, that the the Cathode glow is generated by the passage of fast electrons from the cathode through the CDS. The properties of the Cathode glow are of interest here since the internal glow in the cavity of an e-gun cathode has a similar physical appearance. Furthermore, it is in this region close to the cathode where perturbation of the equipotentials is expected for the e-gun cathode (fig 3.16b). The production of excited species in the CDS by the electron swarm from the cathode is calculated in Chapter 4, where the properties of the Cathode glow are further discussed.

The emission profiles of the e-gun cathode are shown in fig 3.22. They appear to be very similar to the profiles recorded for the plane cathode operating at the same pressure. The Cathode glow peak for 5876Å is found to be slightly less pronounced than for the plane cathode. In retrospect, it is probable that the e-gun is not operating far enough into the e-beam regime for differences in the emission profiles to show up clearly. The current ratios Π_j at 1mb increase sharply only when V_c>1.4kV as shown in fig 3.10c. Operating the e-gun cathode at this voltage continuously leads to serious gas heating effects.

3.5 Observations of an e-beam Discharge in Argon

3.5.1 Experimental Arrangement

An e-beam plasma generated in pure argon has been investigated using the discharge tube shown in fig 3.24. The stainless steel cathode is drilled with a 1.5mm hole from which the e-beam is generated, and the beam passes into a hollow anode tube which has a number of observation ports drilled along the side. The discharge tube is mounted on the scanning table described in section 3.4.1 to enable the NG sidelight spectral emission to be detected by the monochromator and photomultiplier. Spectra have been recorded using the same experimental procedure as outlined previously in section 3.4.1. The glow intensity has been sampled from the region between the electrodes, and from the anode ports. The tube is evacuated by a rotary pump to around 0.03mb and U.H.P grade argon is flowed continuously through the tube, via a needle valve, in order to purge impurities. The tube has been also subjected to a brief 'running in' period of several hours during which the discharge current is held at ~0.05-0.1 mA.

In terms of the tube technology, attempting to generate laser action in argon is perhaps easier in some respects than in an helium/metal vapour mixture. In the latter case, the requisite partial pressure of metal vapour must be maintained in the lasing volume, and the metal vapour tends to diffuse out of the discharge region over long periods of operation. It is fortunate that argon can simultaneously act as a buffer gas to establish a discharge, and as a

lasing medium.

3.5.2 Results

The V-I characteristics of the argon discharge shown in fig 3.25 demonstrate that e-beam production occurs over a lower range of gas pressures than in helium. This is to be expected since the gas similarity laws indicate that the discharge parameter $p.d_c$ (mb.cm) decreases for heavier molecules or atoms [2], as shown in fig 3.13. Additional transition points from several subsequent runs are also plotted. Sidelight emission from the glow region between the electrodes has been examined, and a spectrum of the principal emission lines is depicted in fig 3.26. In the region of the spectrum between 5000Å-5500Å, only a few very weak lines are observed. Beyond 5500Å, the spectrum contains a small number of ArI lines. Despite the very low current level of ~0.1mA ($<5\ 10^{-3}$ A.cm^{-2}). it is interesting to note that the spectrum shown contains a large number of emission lines corresponding to transitions within the ion state (Ar II), including several known laser lines. This is in marked contrast to the spectrum of lines observed from an RF excited argon plasma where ArI emission lines are observed mainly and few, if any, ArII lines are seen [14]. The ten most prominent lines in this part of the spectrum are listed in table 3.1.

Simultaneous ionisation and excitation of argon neutrals by electron impact leading to direct excitation of the upper laser levels is represented by:

$$e_1 + Ar \Rightarrow Ar^{+*}(4p) + 2e \qquad (3.3)$$

	Wavelength (A)	Transition		Intensity(arb.units)
1.	4198.3	ArI*		13.91
2.	4259.4	ArI		12.23
3.	4158.6	ArI		9.70
4.	4277.2	ArII	$4p^2P_{3/2}$-$4s^2D_{5/2}$	9.16
5.	4764.9	ArII L	$4p^2P_{3/2}$-$4s^2P_{1/2}$	9.11
6.	4609.6	ArII L	$4p^2F_{7/2}$-$4s^2D_{5/2}$	8.54
7.	4545.1	ArII L	$4p^2P_{3/2}$-$4s^2P_{3/2}$	7.53
8.	4879.9	ArII L	$4p^2D_{5/2}$-$4s^2P_{3/2}$	7.52
9.	4657.9	ArII L	$4p^2P_{1/2}$-$4s^2P_{3/2}$	5.37
10.	4726.9	ArII L	$4p^2D_{3/2}$-$4s^2P_{3/2}$	5.25

Table 3.1. The ten most prominent emission lines in the NG. '*' denotes a doublet line, and 'L' is a known laser transition.

This is known to be a predominant pumping mechanism in pulsed argon discharges, where the electron temperature is generally higher than in a CW discharge [21]. Furthermore, in applying the 'sudden perturbation' approximation to collisions of this type, it is calculated that preferential pumping of the upper laser levels $3p^4 4p$ over the lower levels $3p^4 4s$ occurs [22]. Sub-levels within the $3p^4 4p$ configuration have different cross-sections for direct electron impact. The results of the 'sudden perturbation' calculations on the excitation of these sub-levels suggest that the $4p^2P_{3/2}$ and $4p^2P_{1/2}$ states in particular are pumped preferentially by single electron impacts [23]. The cross-sections of the $3p^4 4p$ levels for such collisions have been investigated experimentally by Latimer and

St John [24]. The cross-sections of the $4p^2P_{1/2}$ and $4p^2P_{3/2}$ states are found to be similar in profile to the first ionisation cross-section curve (fig 1.7), whereas the quartet levels have cross-sections which peak at around ~50eV, and then fall away more rapidly with increasing electron energy. The other doublet states ($4p^2D_J$ and $4p^2S_J$) are found to have cross-section curve profiles between these two extremes [25]. Individual levels within the $3p^4 4p$ and $3p^4 4s$ configurations are shown in fig 3.27, together with the known laser transitions [26]. The cross-sections of these levels near threshold electron energies have been investigated by Bennet et-al [27]. They also conclude that the levels $4p^2P_{3/2}$ and $4p^2P_{1/2}$ are pumped by direct electron impact. The emission line intensities from transitions originating from these levels show a linear dependence with increasing electron current. Line emission from the quartet states, however, is observed to have a quadratic or cubic dependence on current, suggesting stepwise excitation of these states. Strong emission at 4765Å from an argon NG plasma in a slotted HCD tube has been reported by Schuebel [28]. He also reports moderate spontaneous emission at 4880Å and weak emission at 5145Å, and concludes that direct electron impact of the $3p^4 4p$ levels is an important pumping mechanism in the HCD.

In the spectra recorded of the e-beam discharge shown in fig 3.24. the emission line at 5145Å is weak, and indeed is not observed at low current (fig 3.26), whereas the line at 4765Å is one of the most prominent. The intensities of four ArII lines (4765Å,4880Å,4806Å and 5145Å) have been monitored as the discharge current and Cathode fall are increased. Sample points near the CDS/NG boundary and in the body of the NG have been selected. A ratio of the line intensities (4765Å)/(4806Å) is expected to decrease with rising

discharge current, since the doublet state population is proportional to the current (I) and the quartet population to I^2 or I^3. Cascading from higher states $3p^4 5d$ or $3p^4 5s$ is assumed to be negligible since the respective populations are expected to be small. Pumping of Ar neutrals to these higher states by direct electron impact is less probable than to $3p^4 4p$ states, when the electrons have high energies (E>100eV). Several intensity ratios are depicted in fig 3.28 and are seen to be practically constant over the current range investigated. As the current is raised, the Cathode fall rises introducing more energetic 'beam' electrons into the NG from the CDS. The validity of the 'sudden perturbation' approximation improves for higher energy electrons, and this may result in a higher probability of pumping the $4p^2P_J$ states. Therefore, level populations are likely to be dependent on both the discharge current and the Cathode fall.

In conclusion, it appears that the emission line at 4765Å remains prominent throughout the current range investigated, with the emission line at 5145Å remaining weak. It is suggested, therefore, that those lines corresponding to ArII transitions in table 3.1 are pumped mainly by direct electron impact in the e-beam discharge. Discharge currents larger than 1-2mA cannot be used in the present tube because sputtering of the stainless steel cathode face causes a layer of sputtered material to be deposited on the walls of the tube. When this occurs, the intensities of all emission lines are observed to diminish, preventing further spectral analysis.

References

1. Boring K.L. and Stauffer L.A., Proc.Nat.Electr.Conf., 19,535 (1963)
2. von-Engel A., 'Ionised Gases', Oxford University Press', (1965)
3. Strudwick I., English Electric Valve Co.Ltd., Chelmsford, U.K.
4. Popa G., Toma M. and Sandulovicіu M., Tenth Int.Conf.Phenom.Ion.Gases., p100, Oxford (1973)
5. Gill P. and Webb C.E., J.Phys.D., 10, 299 (1977)
6. Davis W.D. and Vanderslice T.A., Phys.Rev., 131, 219 (1963)
7. Chaudhri R.M. and Baqui M.A., Proc.Phys.Lon., B65, 324 (1952)
8. Popa G.. Sandulovicіu M., Croitoru P. and Moldovan C., J.de.Phys.. coll. C7-187 (1979)
9. Little P.F. and von Engel A., Proc.Roy.Soc., 224, 209 (1954)
10. Kunz J., Philosophical Magazine, 16, 161 (1908)
11. Badareu E., Popovici C. and Somesan M., Z.Phys.Chemie, 230, 90 (1965)
12. Webb C.E., J.Appl.Phys., 39, 5441 (1968)
13. EMI Electronics Ltd.. data sheet 'Photomultiplier tubes Selection Chart'
14. American Institute of Physics Handbook, ed. D.E.Gray (6-67 and 7-52) (1972)
15. Carl Zeiss SPII monochromator (manual)
16. Emeleus K.G. and Coulter J.R.M., J.Phys.D., 16, 2181 (1983)
17. Soldatov A.N., Muravev I.I.. Karimov R.G. and Evtushenko G.S., Opt. Spectroscopy, 39, 594 (1975)
18. Persson K.G., J.Appl.Phys., 36, 386 (1965)
19. Kuen I., Howorka F. and Stori H., Phys.Rev.A., 23, 829 (1981)
20. Massey H.S.W. and Burhop E.H.S., 'Electronic and Ionic Impact Phenomena', O.U.P., (1952)

21. King T.A. and Davis C.C., 'Advances in Quantum Electronics', ed. D.W.Goodwin, Academic Press (1975)

22. Bennet W.R., Knutson J.W., Mercer G.N. and Betch J.L., Appl.Phys.Lett., 4, 180 (1964)

23. Koozekanani S., J.Quant.Electr., 2, 14 (1966)

24. Latimer I.D. and St John R.M., Phys.Rev.A., 1, 1612 (1970)

25. Felstan P.V. and Povch M.M., Optics and Spectroscopy, 28, 119 (1970)

26. Bashkin S. and Stoner J.O., Atomic Energy-Level and Grotrian Diagrams, II, pub. North Holland, (1978)

27. Bennet W.R., Mercer G.N., Kindlemann P.J., Wexler B. and Hyman H., Phys.Rev.Lett., 17, 987 (1966)

28. Schuebel W., Eleventh Int.Conf.Phenom.Ionis.Gases, p174 Prague (1973)

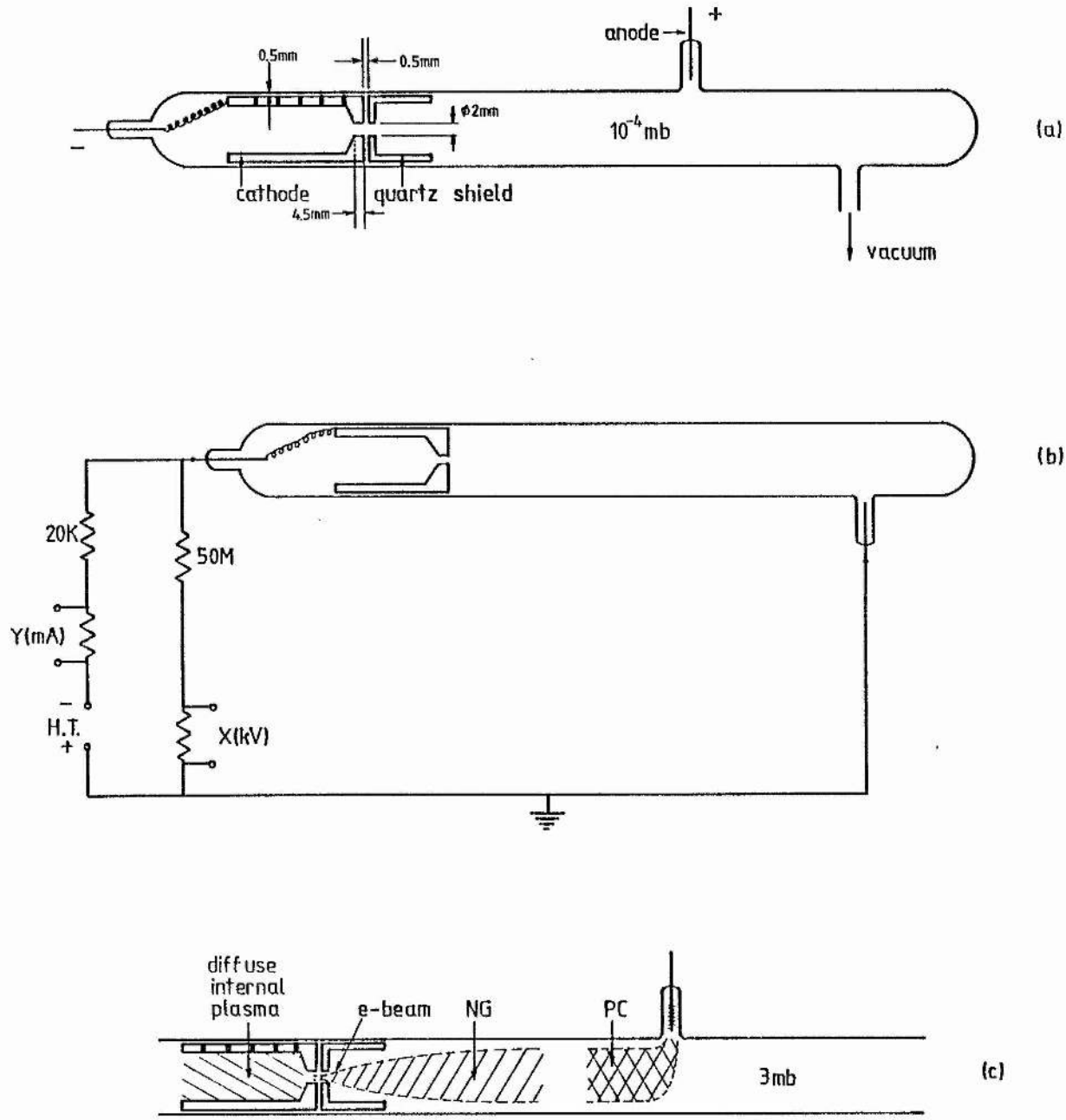

Fig 3.1. A preliminary investigation of an electron beam discharge in helium.

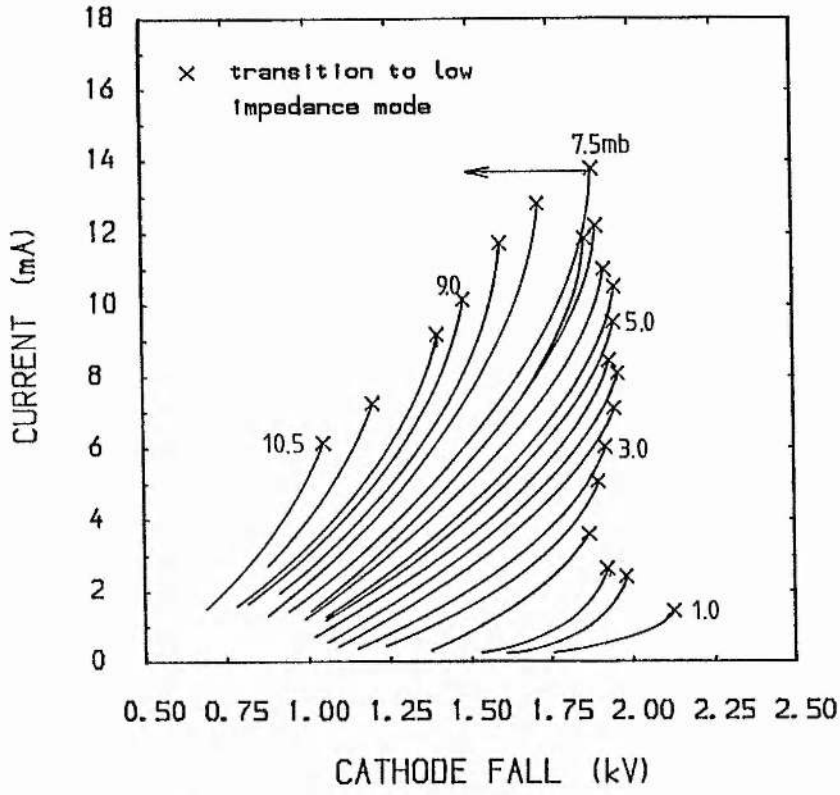

Fig 3.2a. The V-I characteristics of an electron beam discharge in helium, with pressure as a parameter. The transition from the e-beam mode to the HCD mode is shown for a pressure of 7.5mb only.

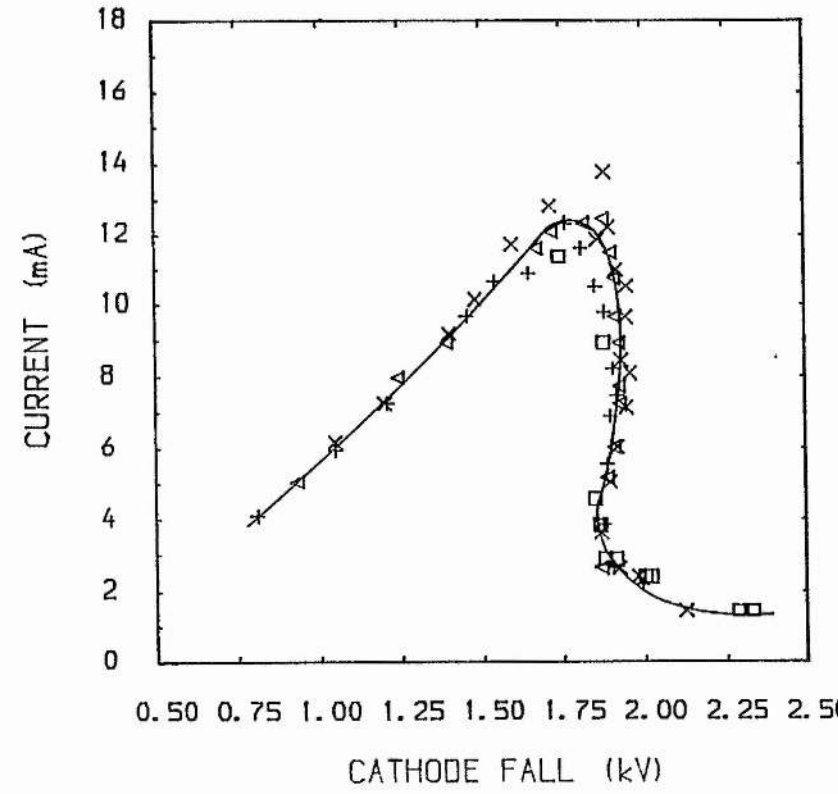

Fig 3.2b. Transition points for the electron beam discharge.

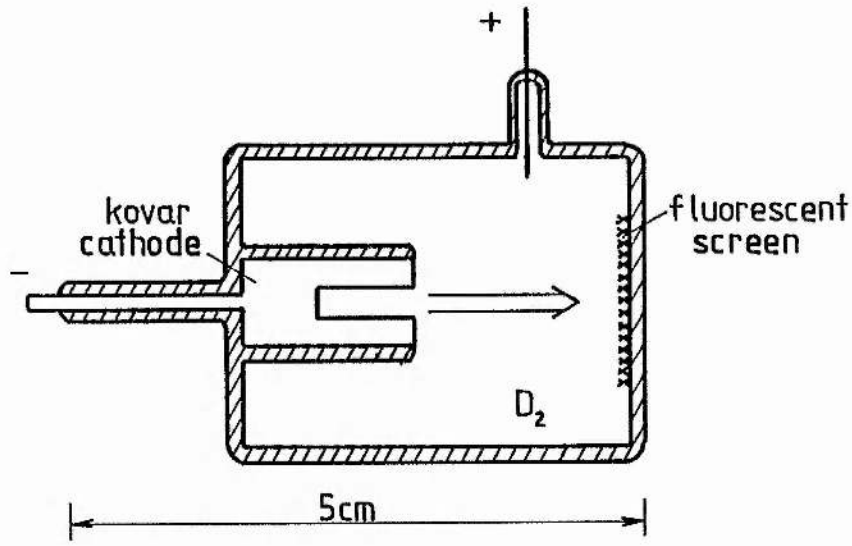

Fig 3.3. Electron beam production in a sealed off discharge cell containing low pressure deuterium.

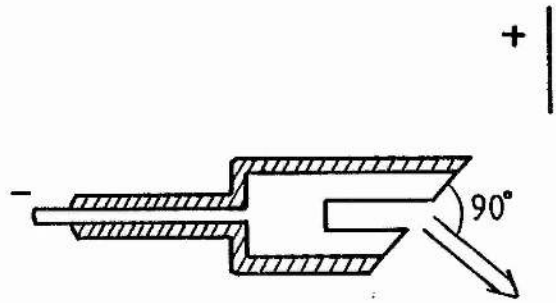

Fig 3.4. An electron gun cathode used to illustrate the importance of the external Cathode dark space in the formation of the electron beam.

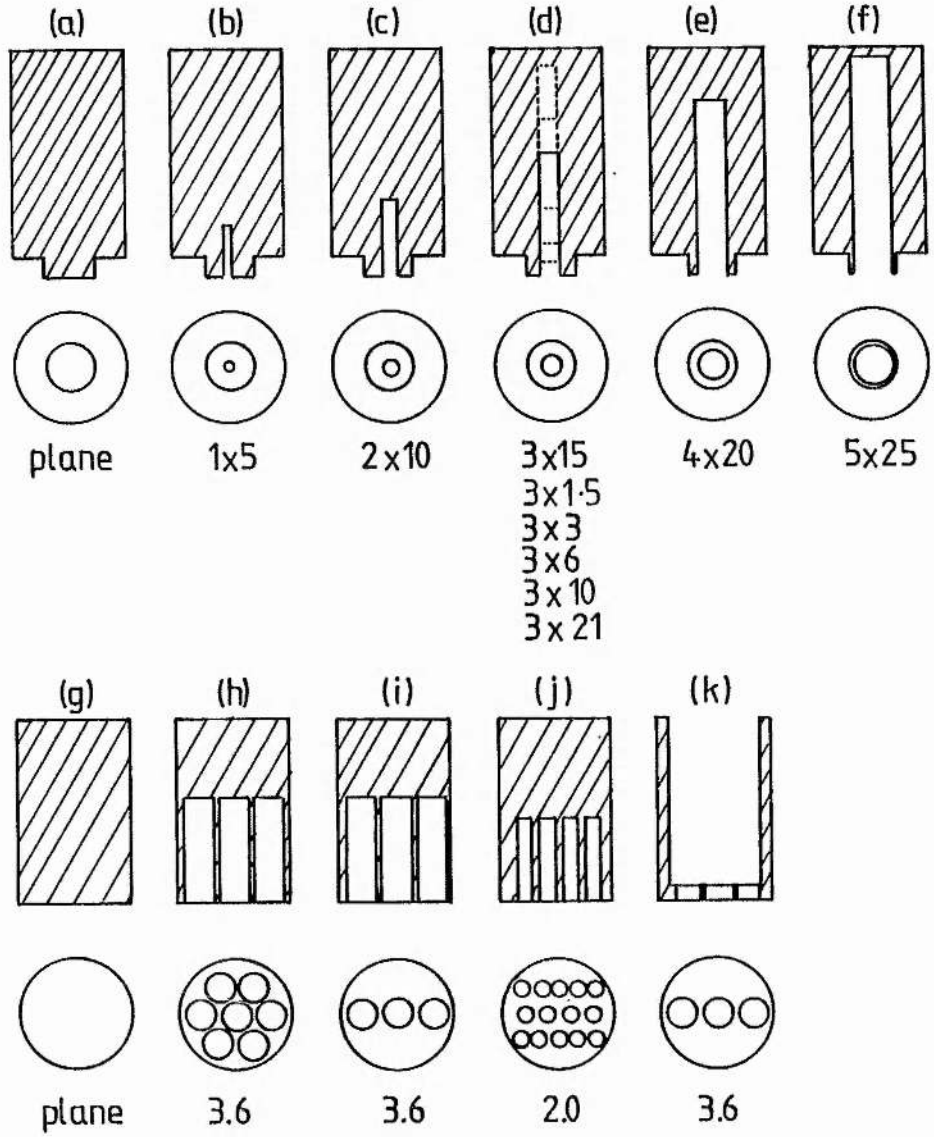

Fig 3.5. The various sizes and types of electron gun cathodes which have been investigated.

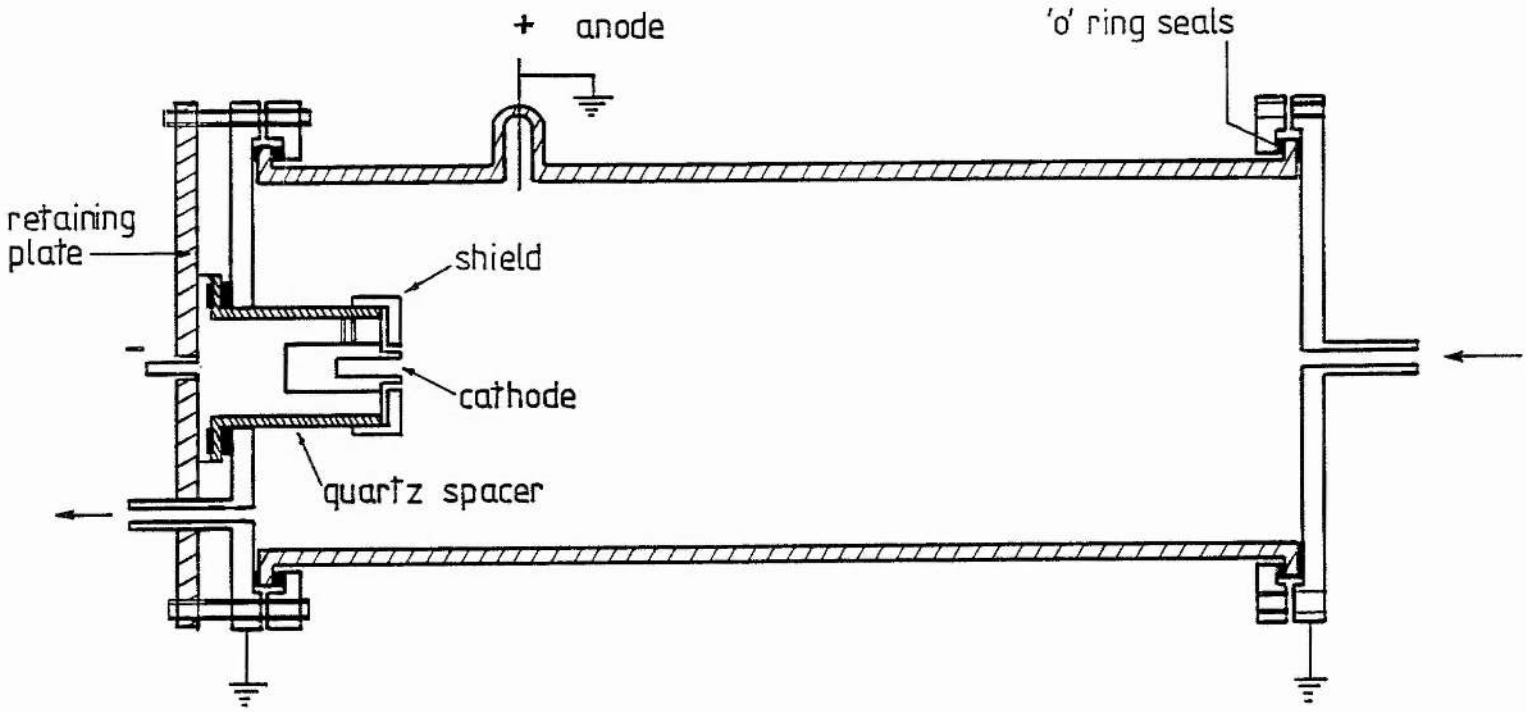

Fig 3.6. The discharge cell used with the interchangeable electron gun cathodes.

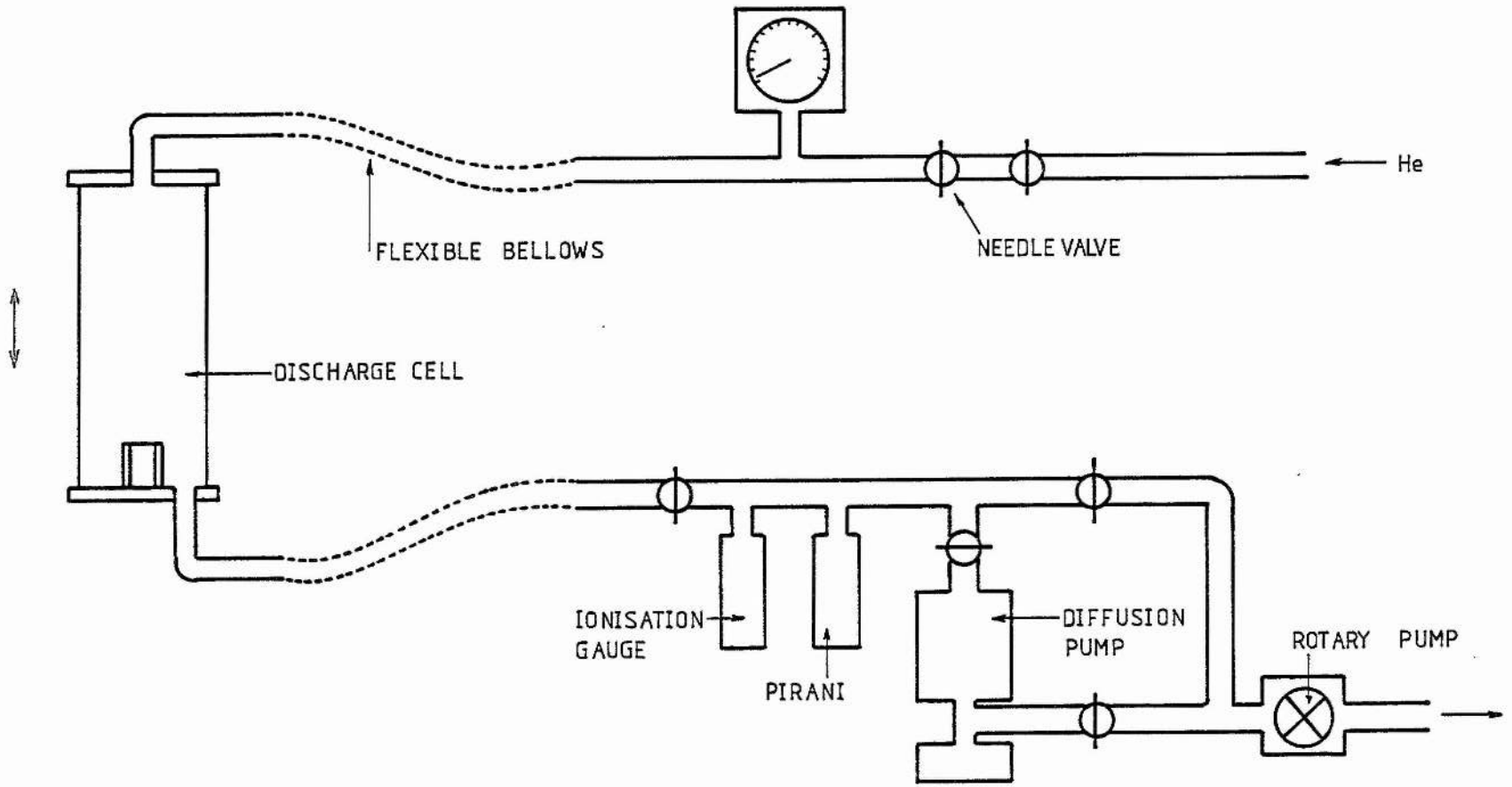

Fig 3.7. The vacuum system used with the discharge cell.

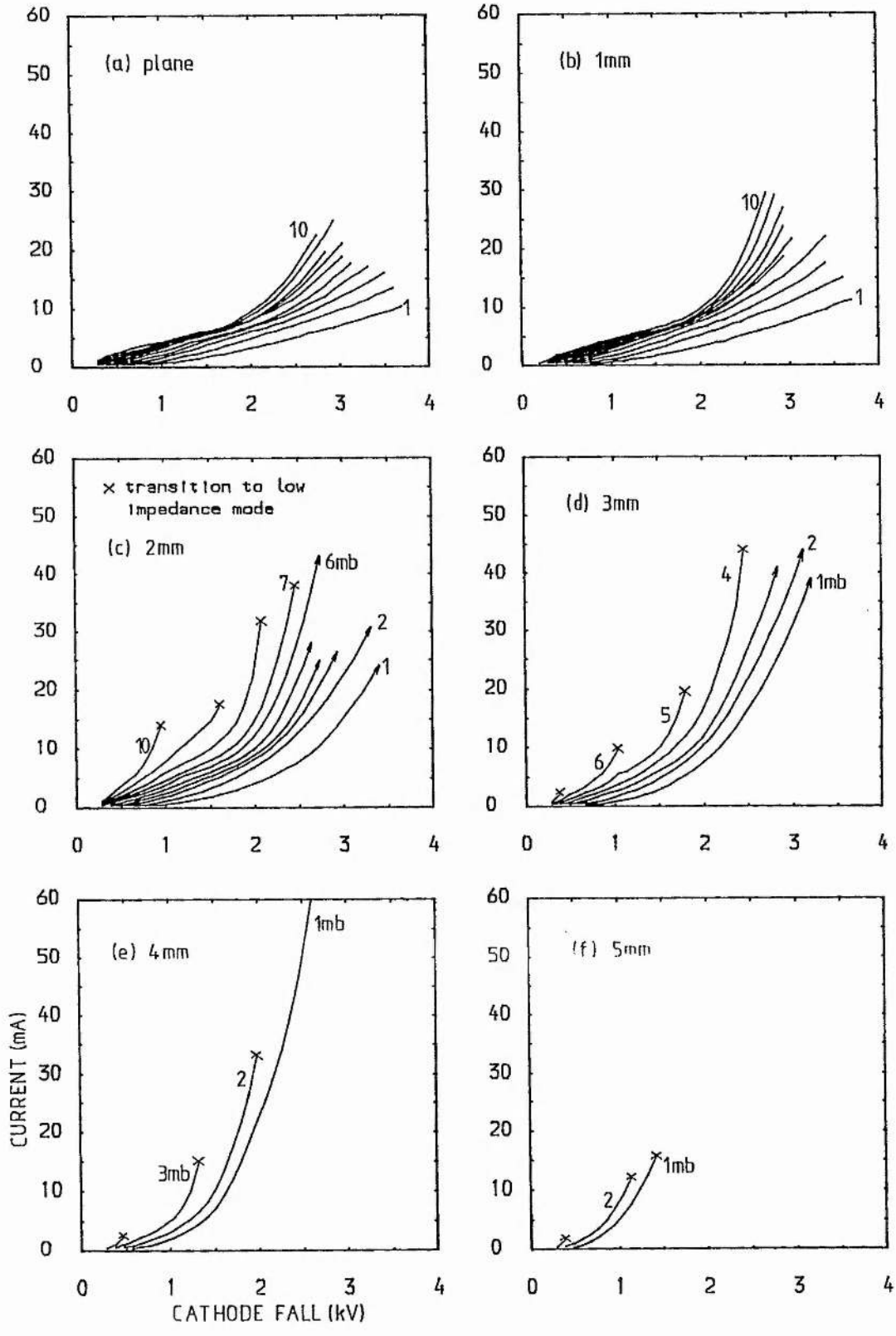

Fig 3.8. The V-I characteristics of a plane cathode, and five sizes of electron-gun cathode, with pressure as a parameter. Transition points are observed for aperture sizes greater than 1mm.

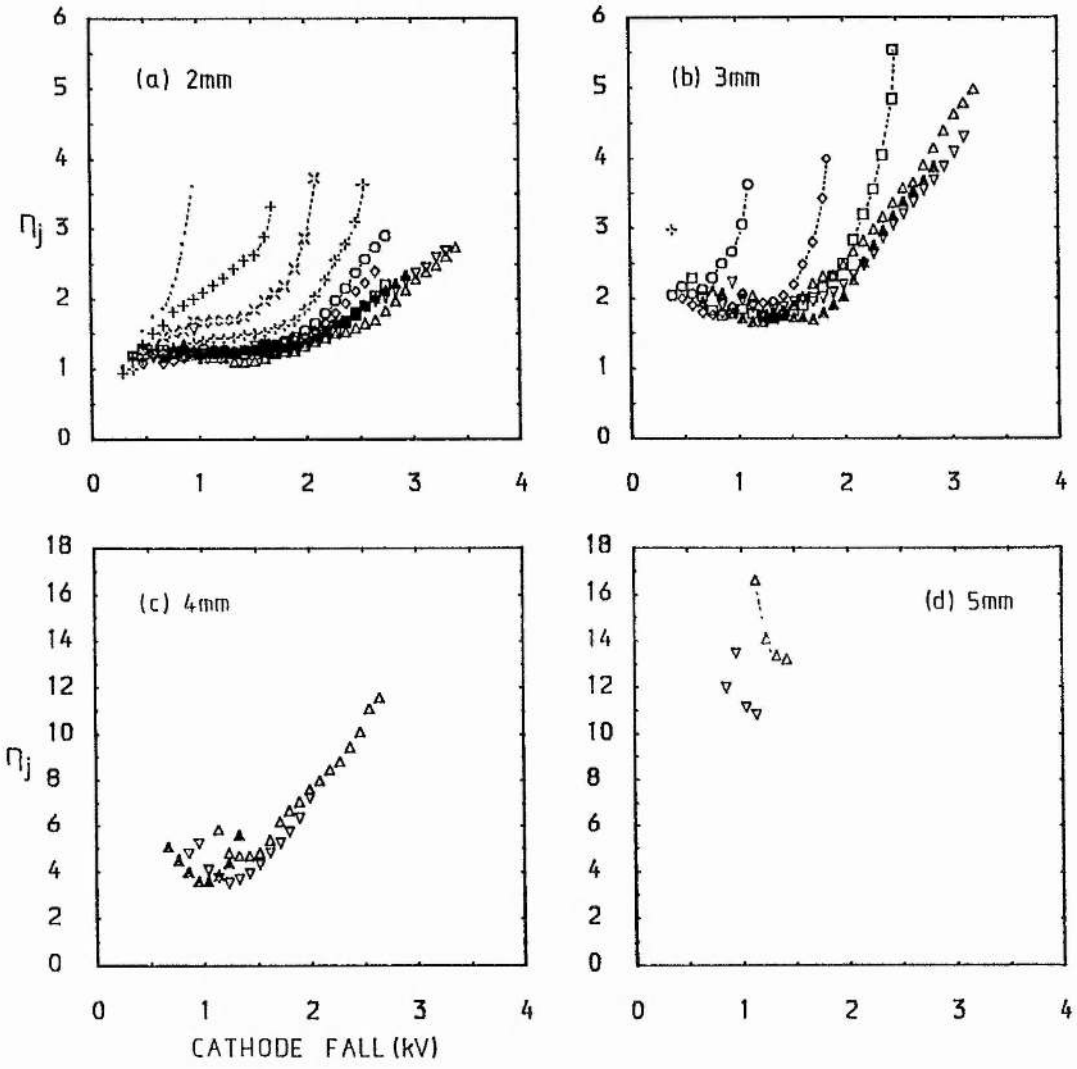

Fig 3.9. Current ratios for electron gun cathodes with hole diameters of between 2mm-5mm, with pressure as a parameter. △ 1mb, ▽ 2mb, ▲ 3mb, □ 4mb, ◇ 5mb, ○ 6mb, ⊹ 7mb, × 8mb, + 9mb, • 10mb.

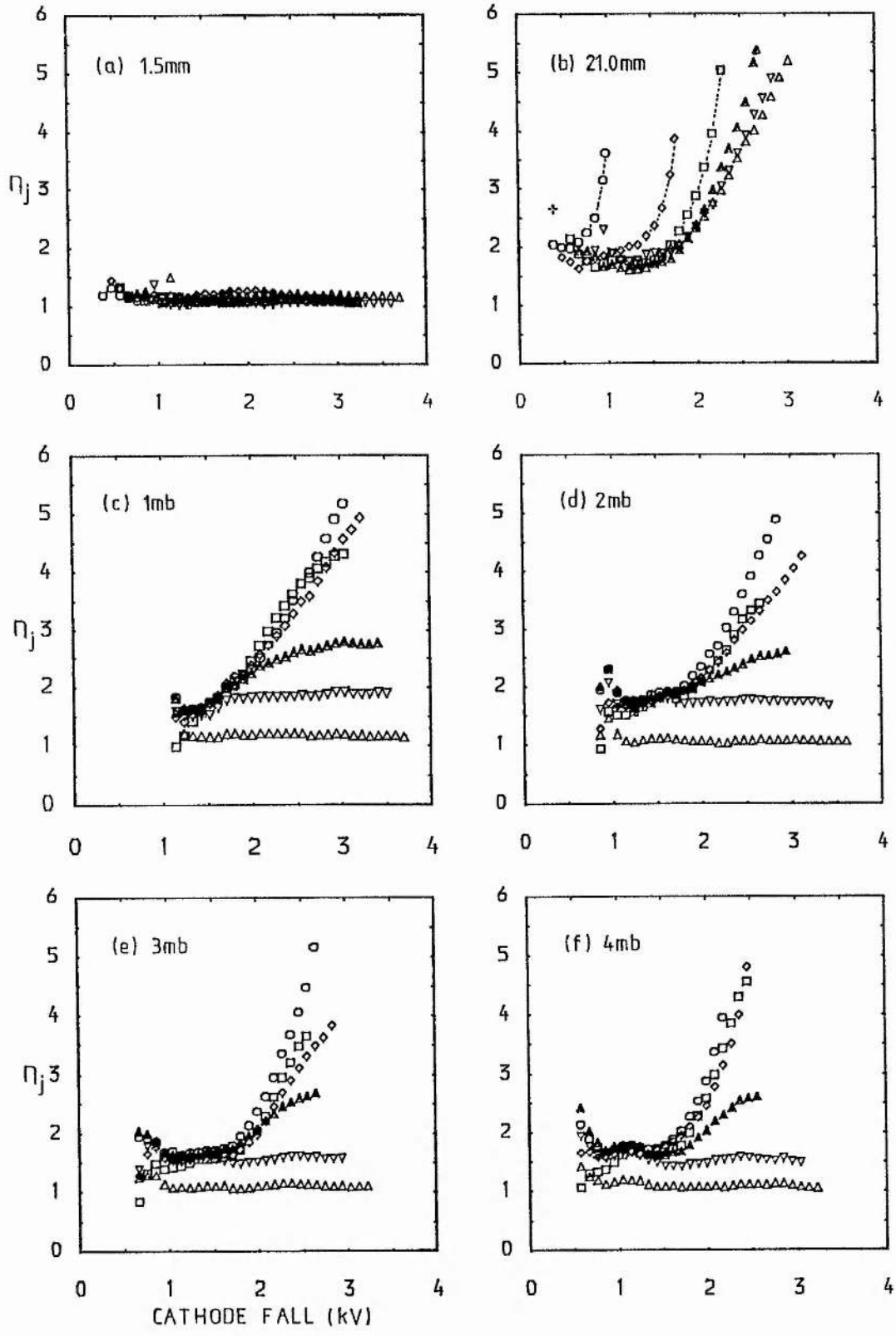

Fig 3.10. Current ratios for 3mm electron gun cathodes of different hole depth. (a) & (b): △ 1mb, ▽ 2mb, ▲ 3mb, □ 4mb, ◇ 5mb, ○ 6mb, ⊹ 7mb. (c) - (f): △ 1.5mm, ▽ 3.0mm, ▲ 6.0mm, □ 10.0mm, ◇ 15mm, ○ 21mm.

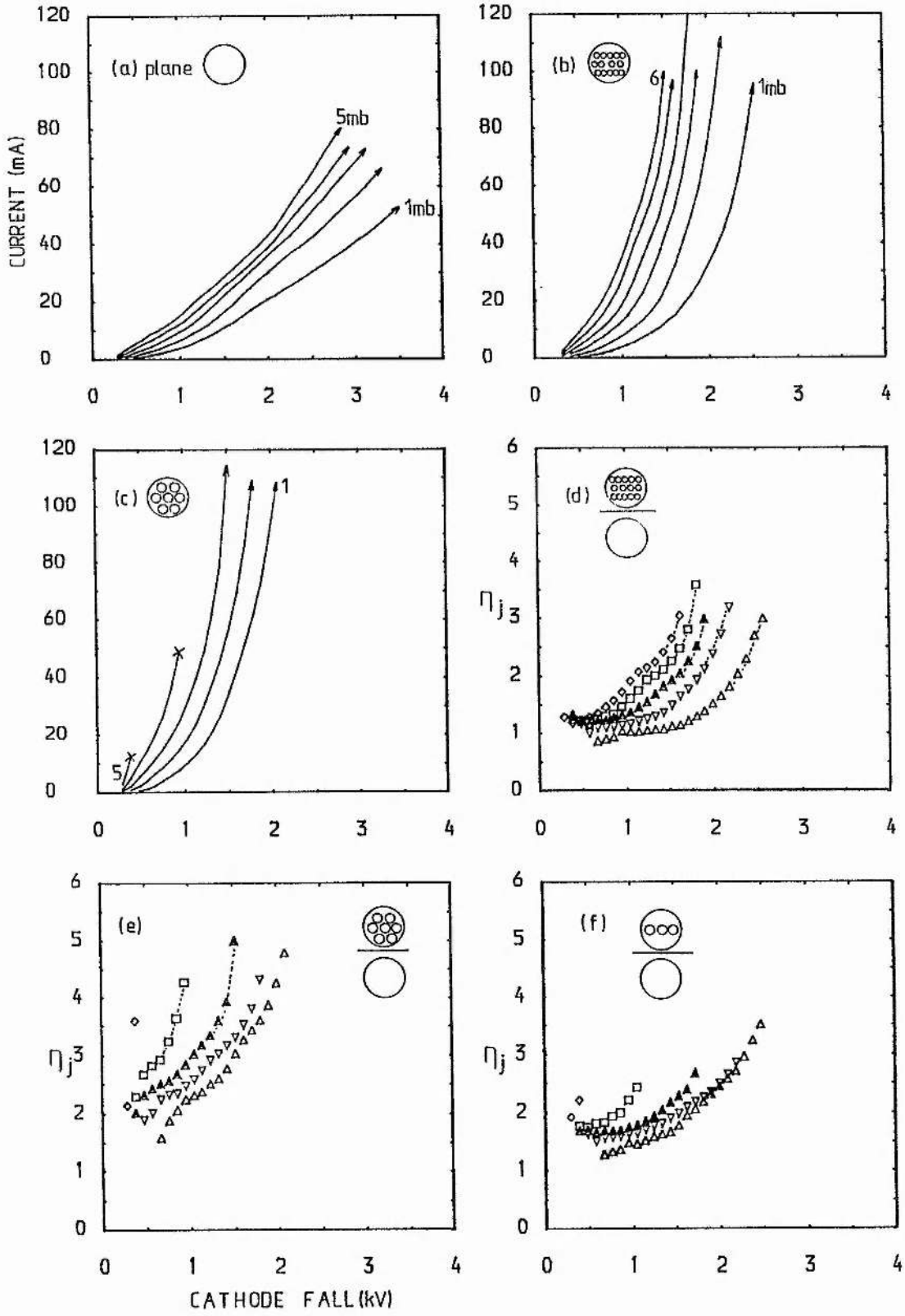

Fig 3.11. V-I characteristics (a) - (c), and current ratios (d) - (f), for multiple aperture electron guns, with pressure as a parameter. (d) - (f): △ 1mb, ▽ 2mb, ▲ 3mb, □ 4mb, ◇ 5mb.

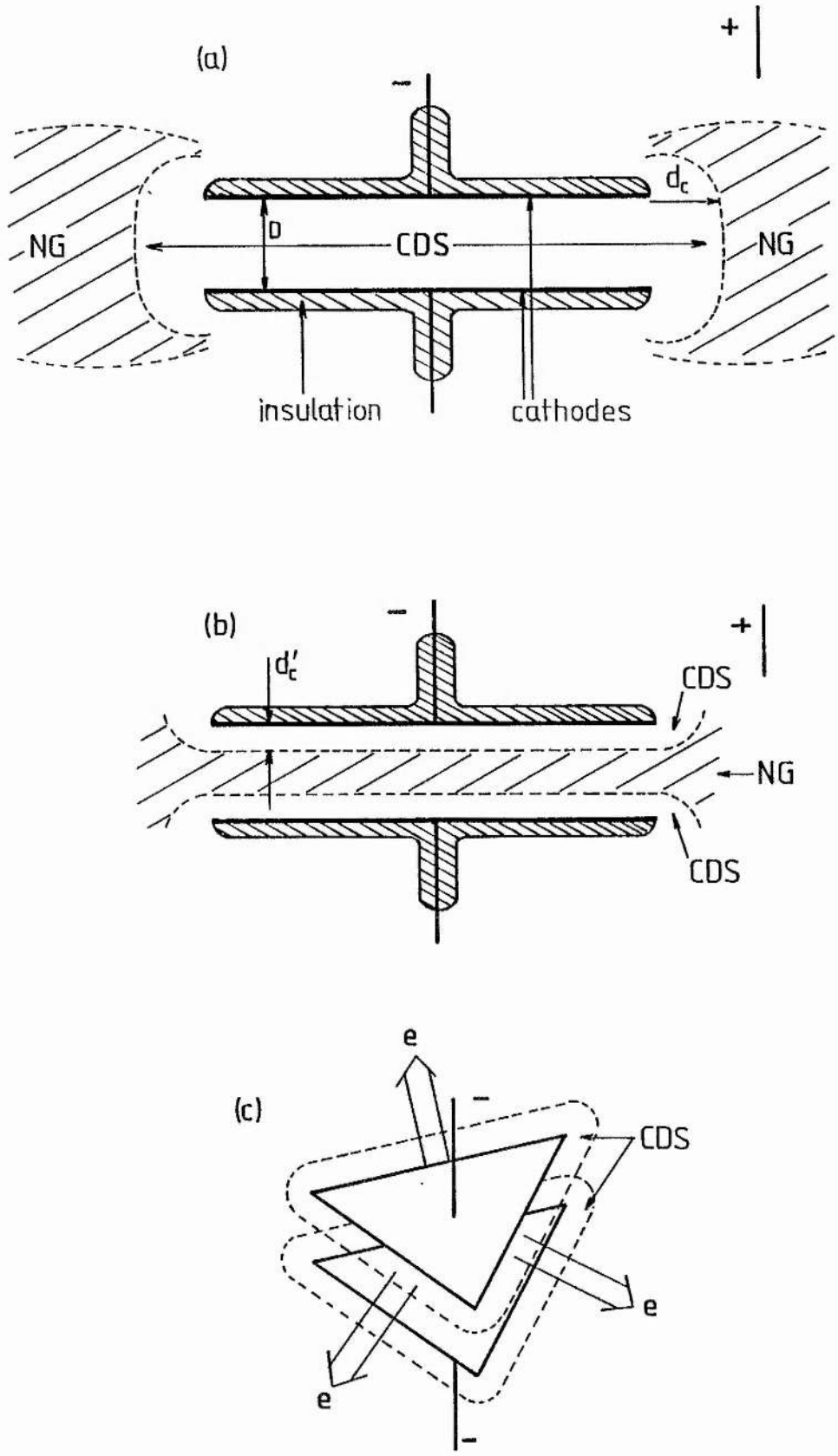

Fig 3.12. The discharge regions of dual cathode geometries.

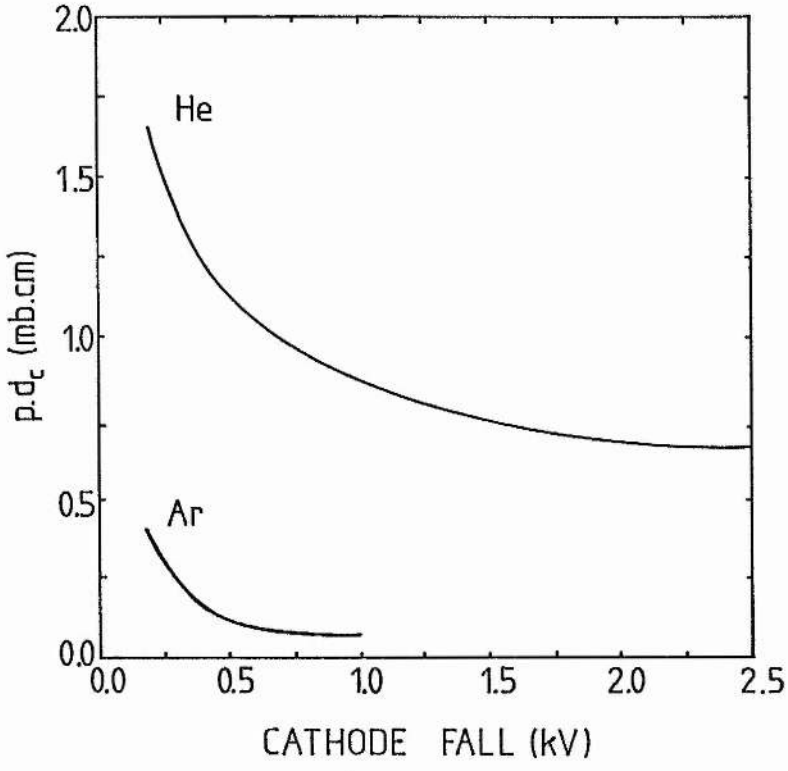

Fig 3.13. The similarity parameter (p.d_c) as a function of the Cathode fall V_c for helium and argon glow discharges.

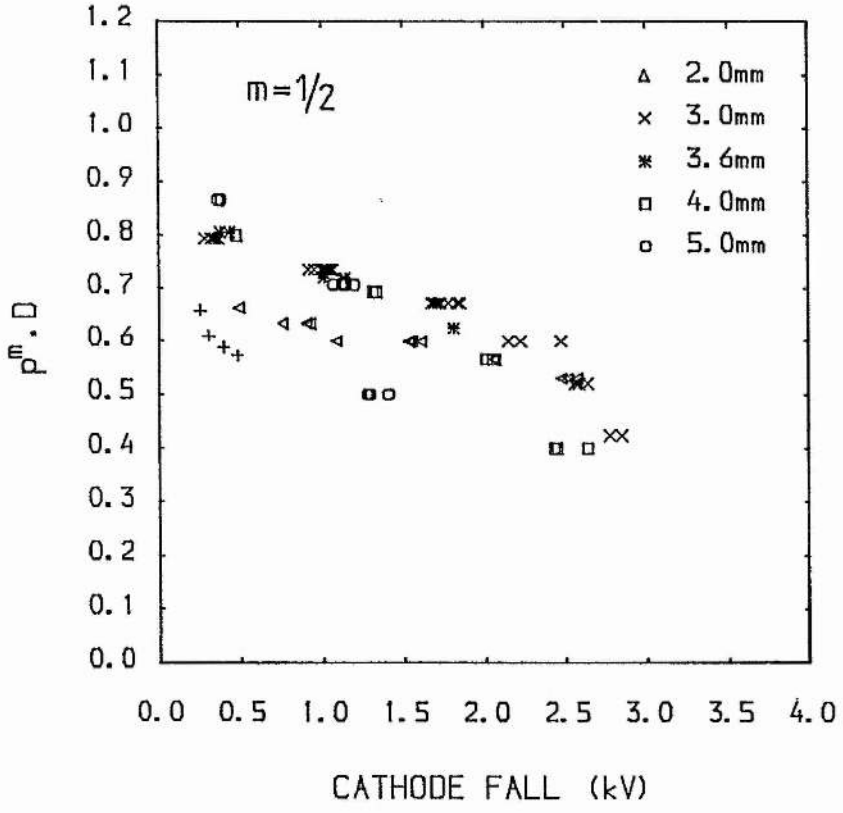

Fig 3.14. Transition points for the electron beam discharge as a function of the Cathode fall. '+' : transition points from the results of Badareu for a dual cathode geometry [11].

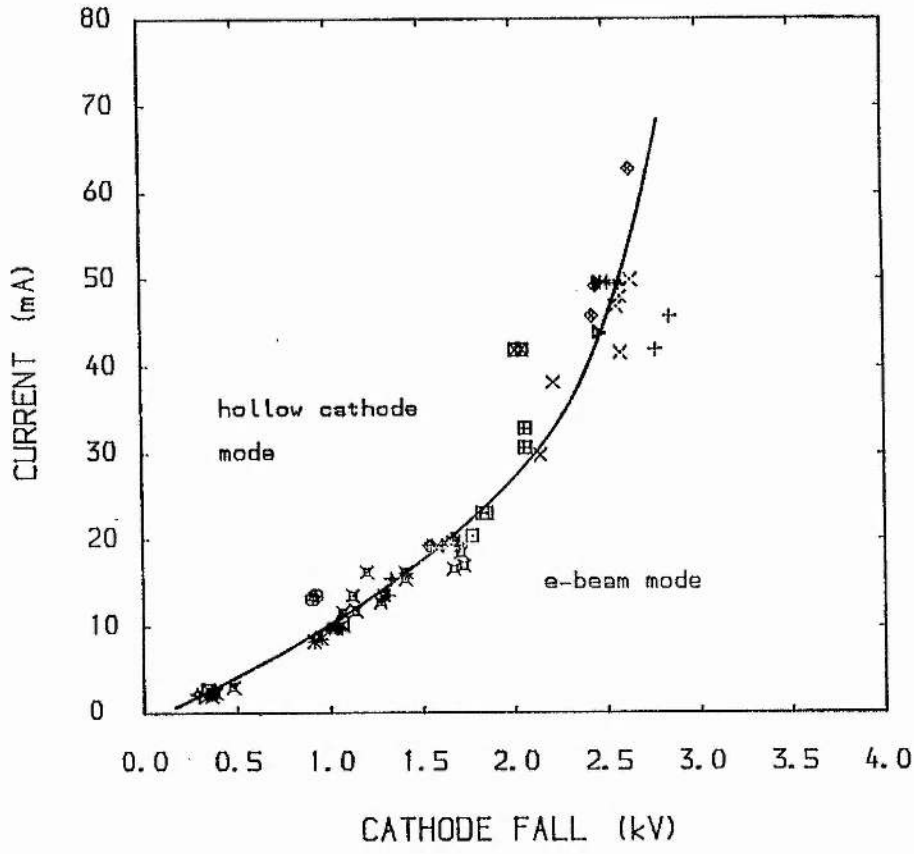

Fig 3.15. Transition points for electron beam discharges using the single aperture electron guns.

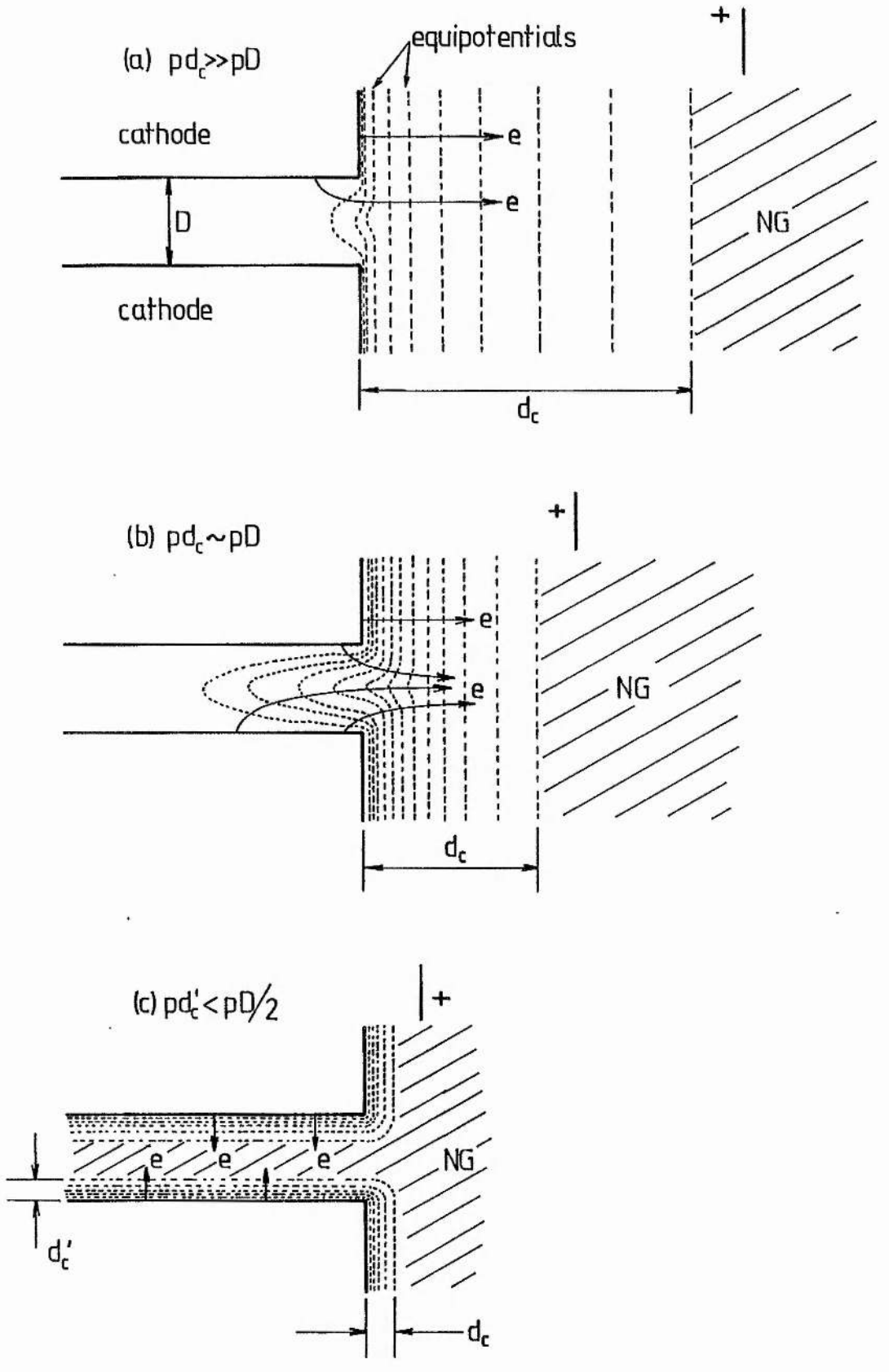

Fig 3.16. Expected distribution of voltage equipotentials in the CDS around the aperture of an electron gun cathode.

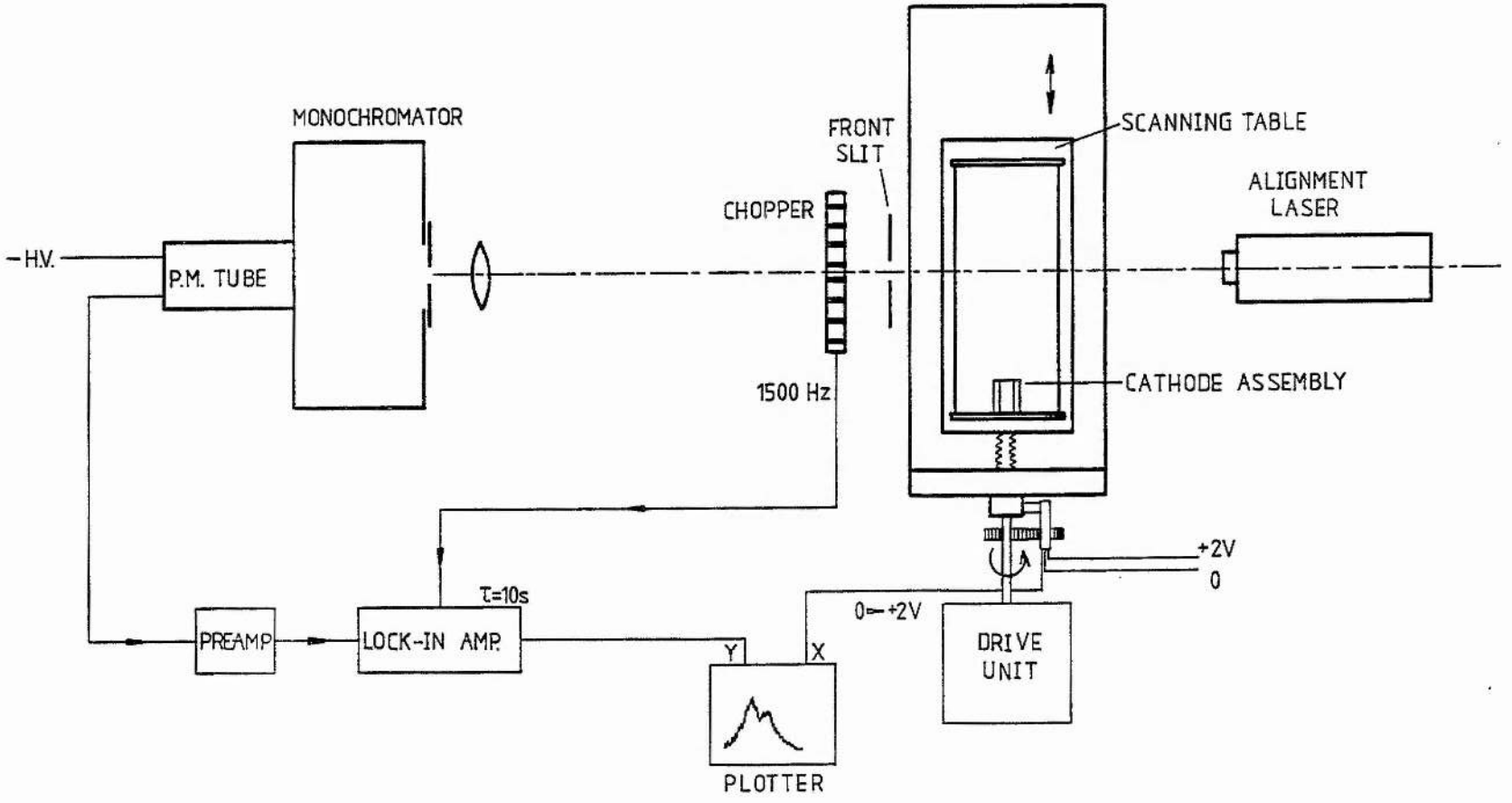

Fig 3.17. Experimental arrangement for the spectral analysis of the discharge glow regions near the cathode.

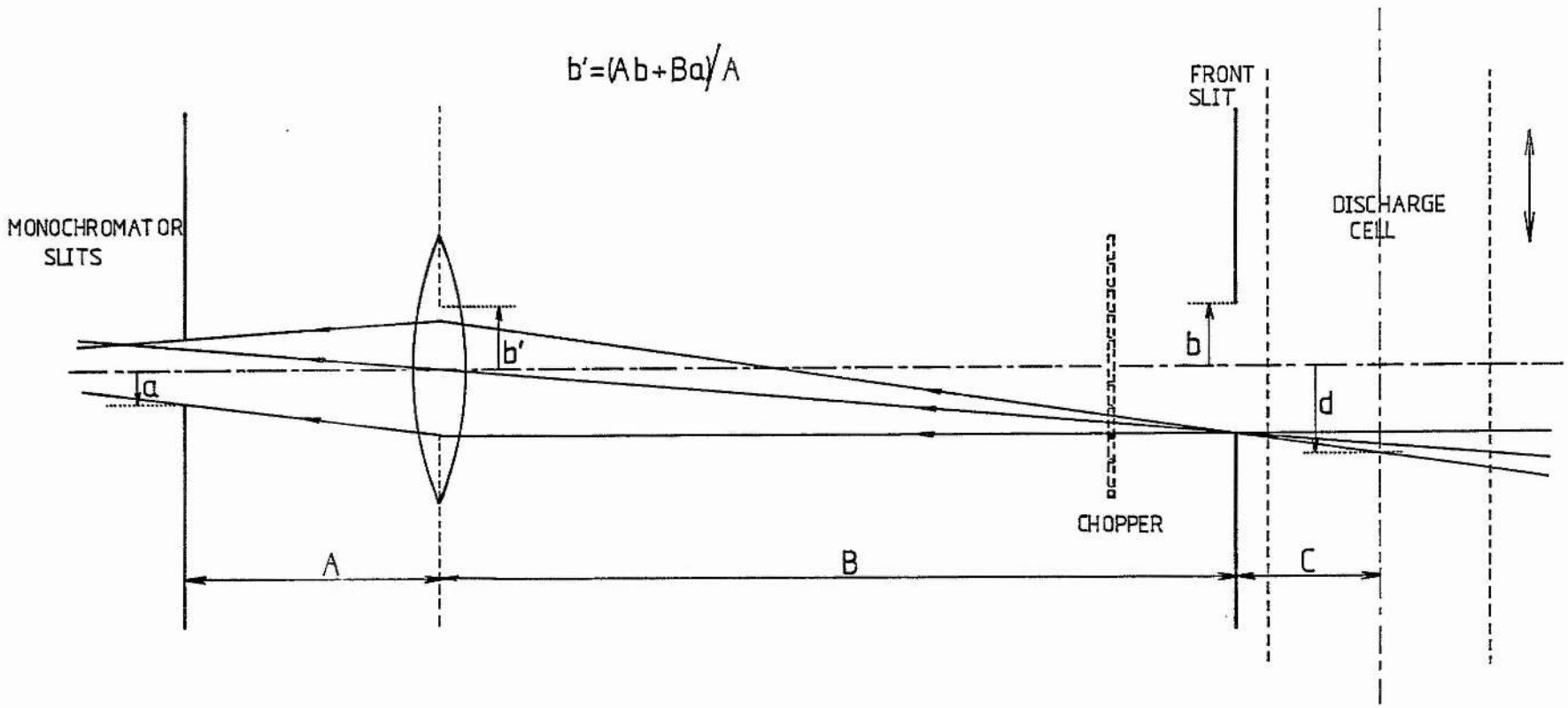

Fig 3.18. A ray diagram to determine the width of the slice of plasma sampled by the monochromator slits. Rays must pass through the front slit of width (b) and through the virtual slit of width (b') to be detected. The width (d) of the plasma slab sampled is 0.013cm for A=5.5cm, B=75.5cm, C=7.2cm, a=0.025cm, b=0.01cm.

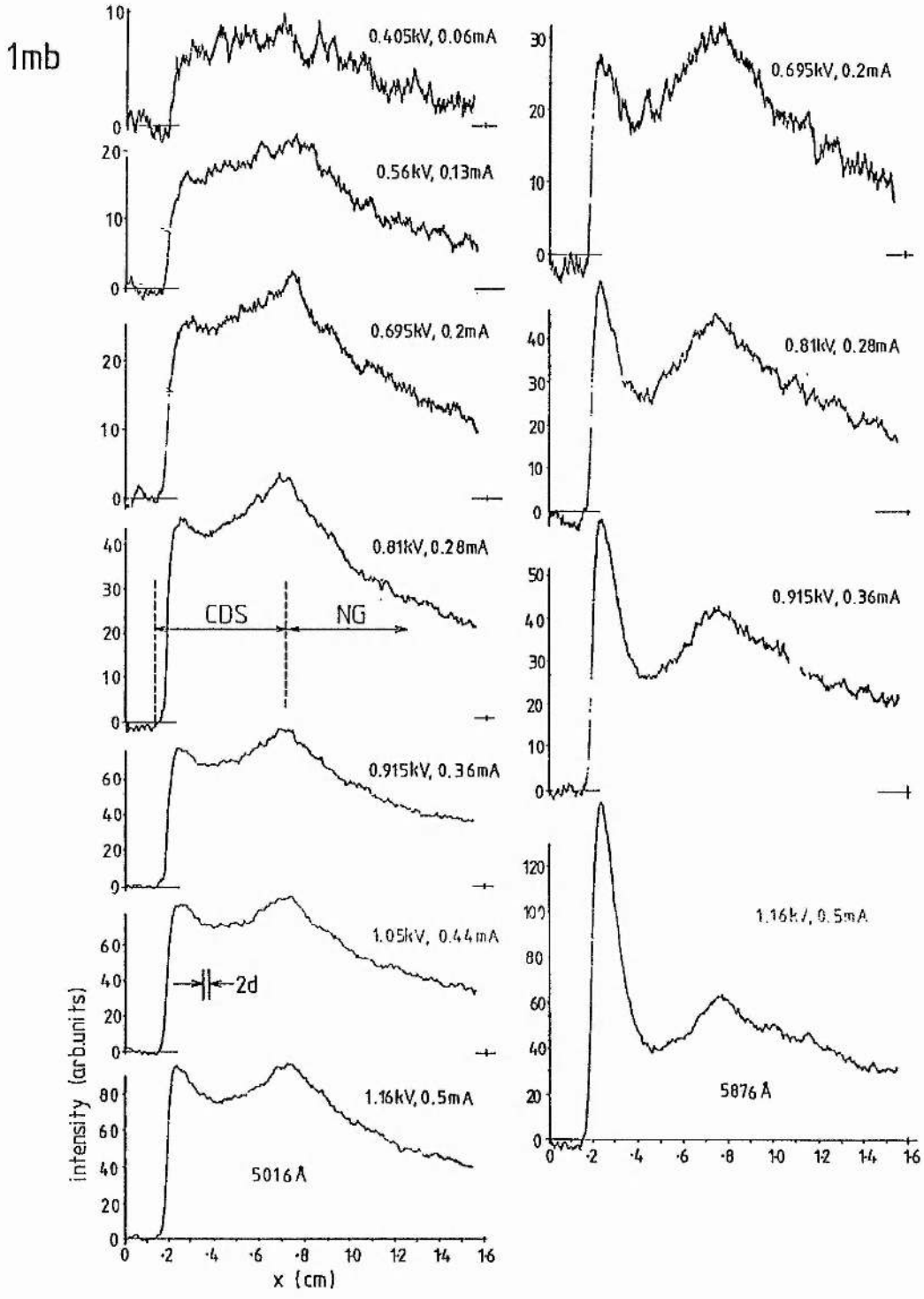

Fig 3.19a. Emission profiles in the CDS and NG regions for a plane cathode at a pressure of 1mb. The width of the 'window' (2d) which is set by the slit dimensions, is shown also.

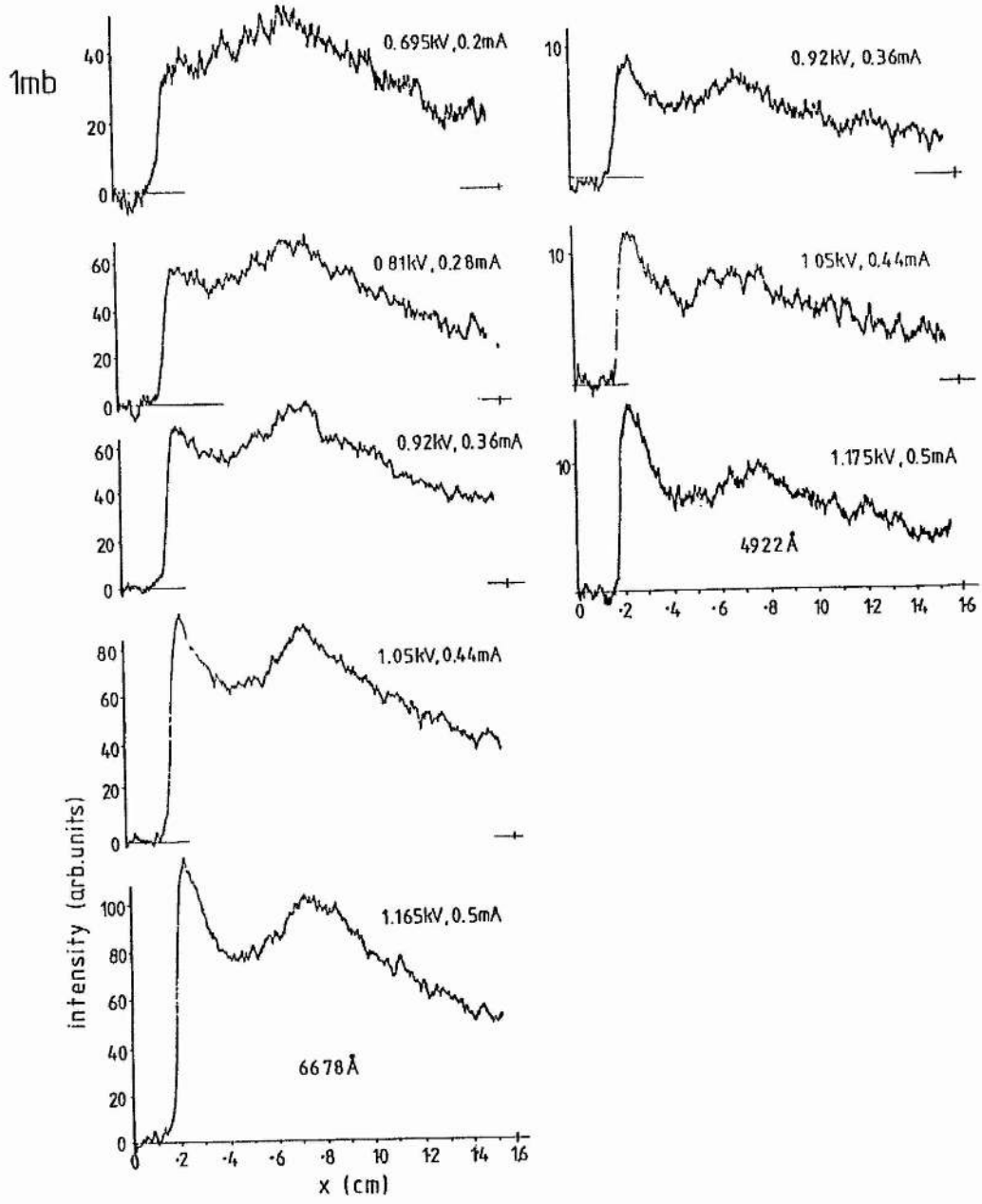

Fig 3.19b. Emission profiles in the CDS and NG regions for a plane cathode at a pressure of 1mb.

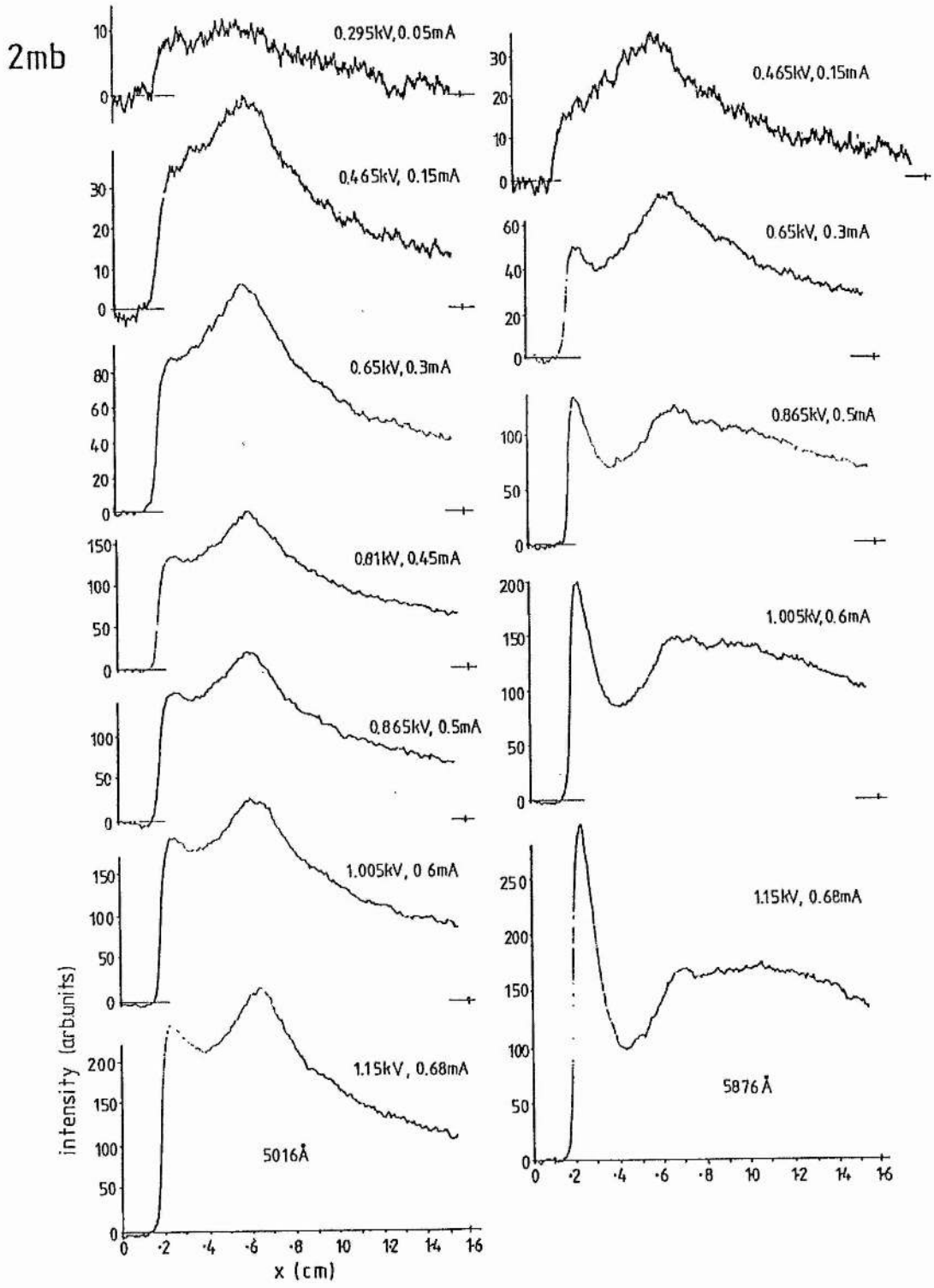

Fig 3.20a. Emission profiles in the CDS and NG regions for a plane cathode at a pressure of 2mb.

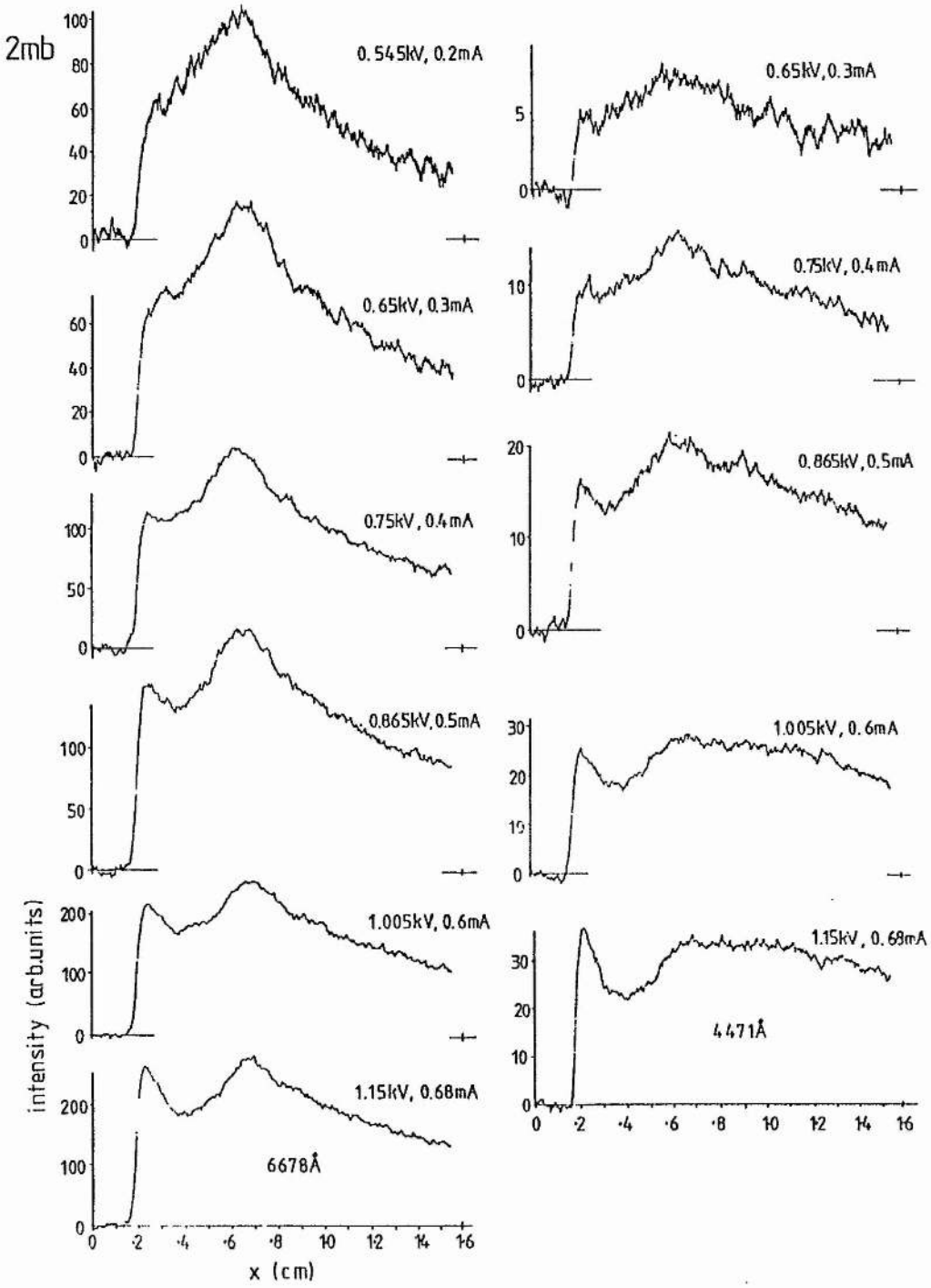

Fig 3.20b. Emission profiles in the CDS and NG regions for a plane cathode at a pressure of 2mb.

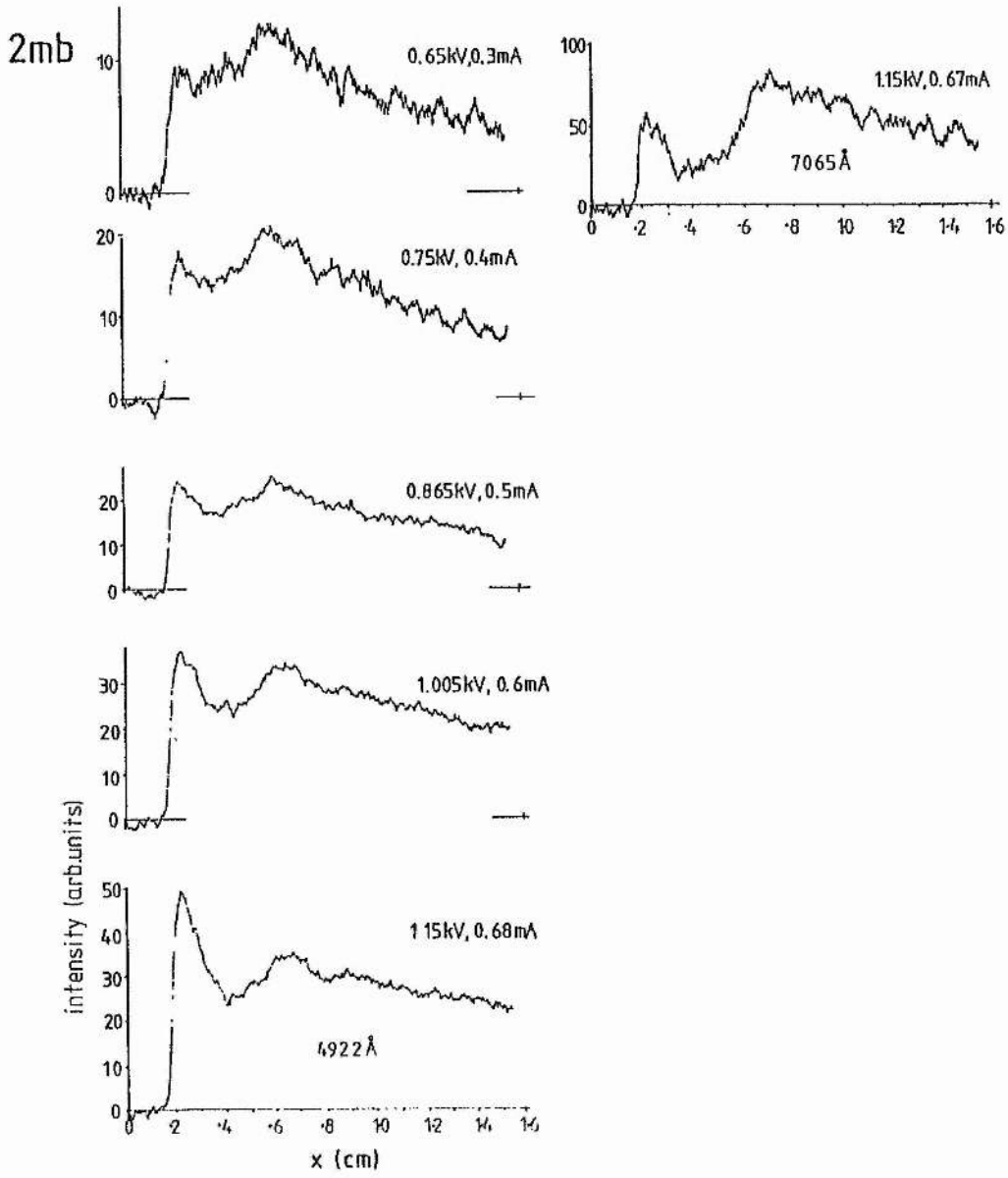

Fig 3.20c. Emission profiles in the CDS and NG regions for a plane cathode at a pressure of 2mb.

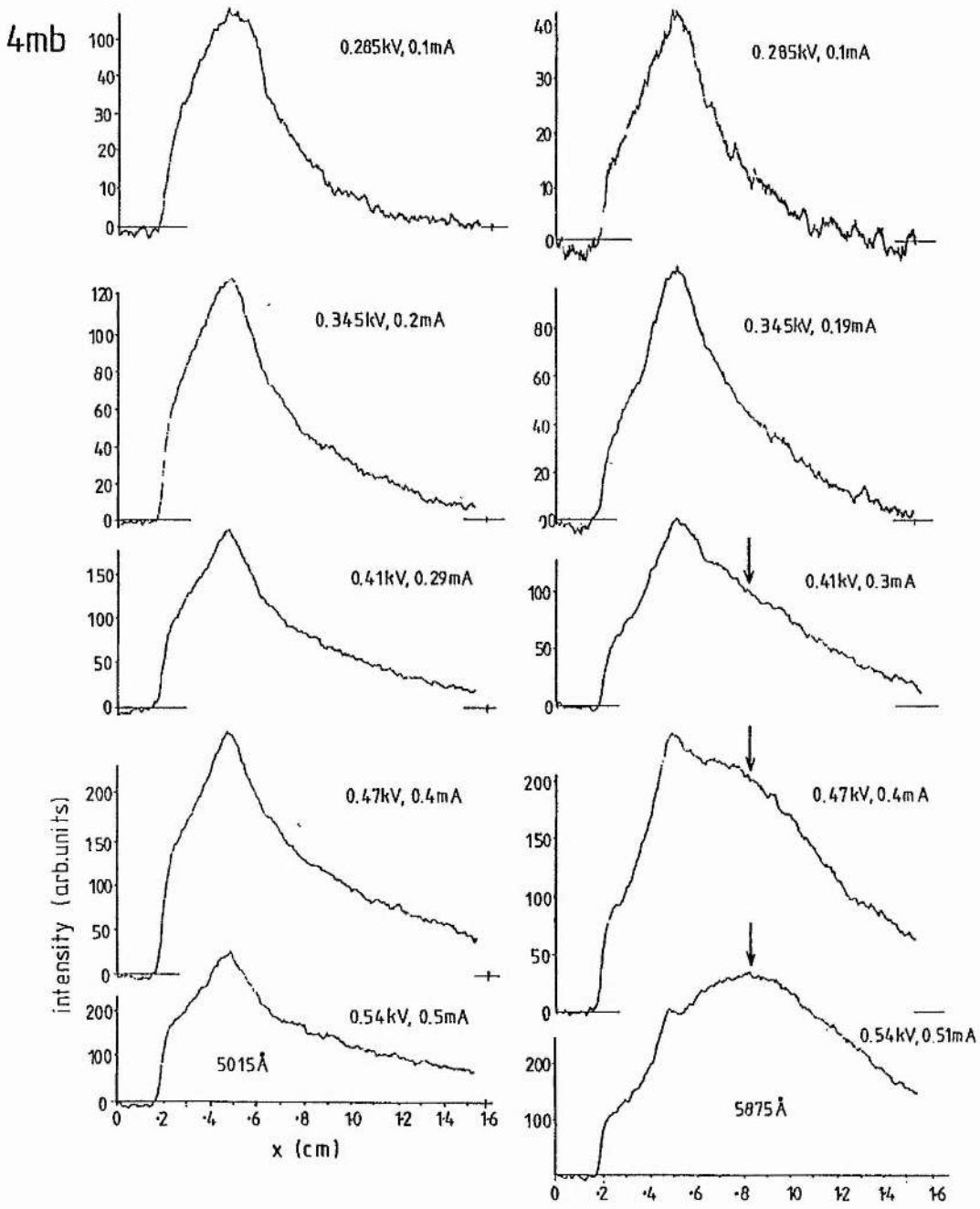

Fig 3.21. Emission profiles in the CDS and NG regions for a plane cathode at a pressure of 4mb. The arrows denote the position of a third peak in the NG region.

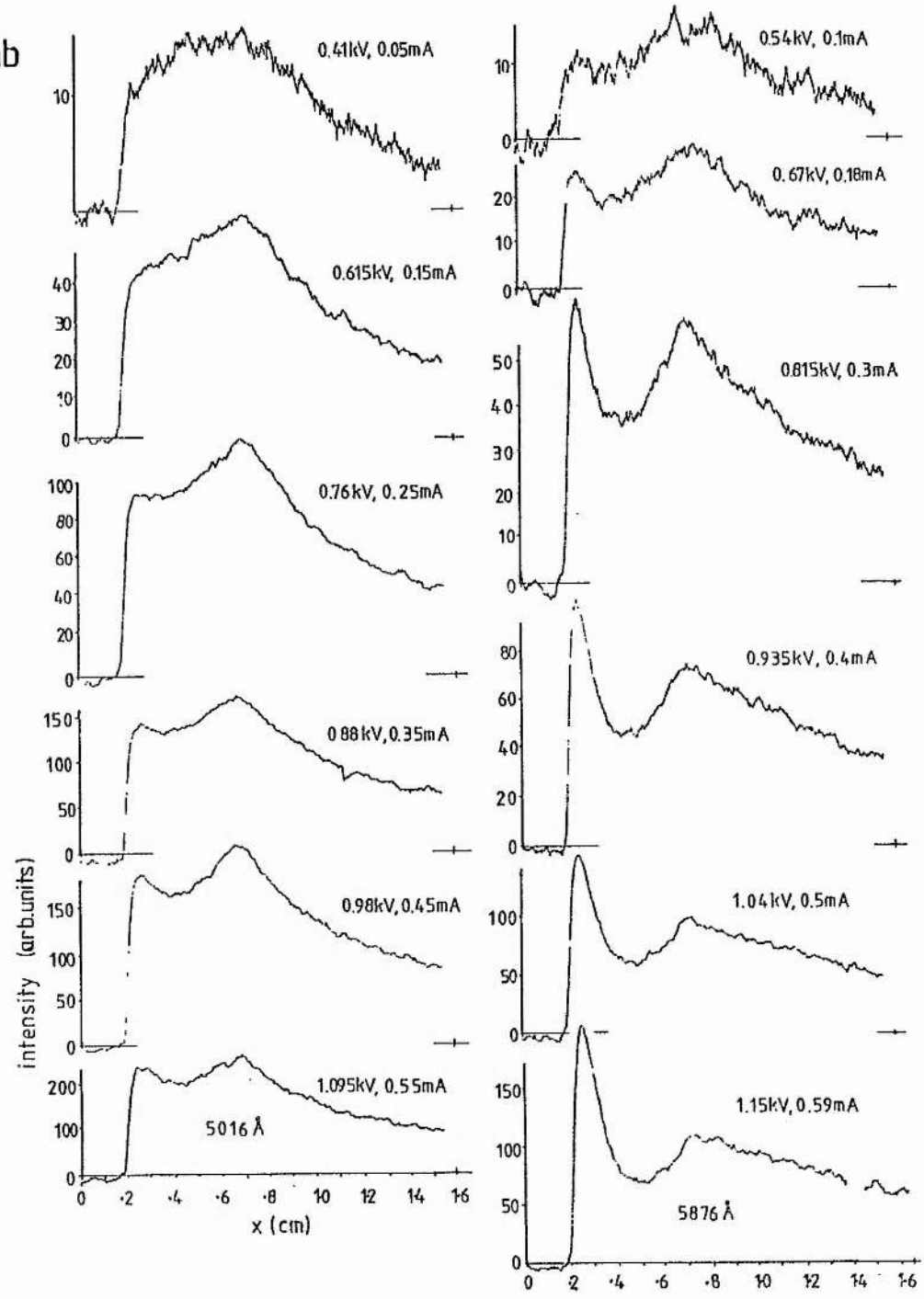

Fig 3.22. Emission profiles in the CDS and NG regions for an electron gun cathode of dimensions 3mm×21mm, at 1mb pressure.

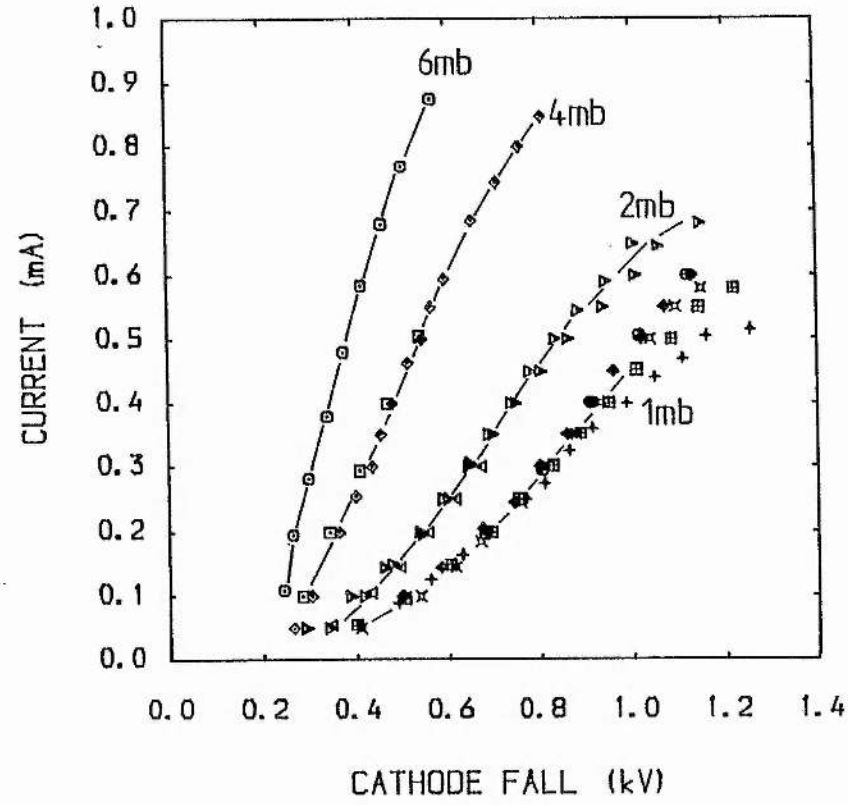

Fig 3.23. Values of the discharge current and Cathode fall taken during the measurements of the emission profiles. The curves show poor reproducibility for larger values of current and Cathode fall, as shown for points around 1.0kV-1.2kV at 1mb. ⊕: electron gun cathode at 1mb.

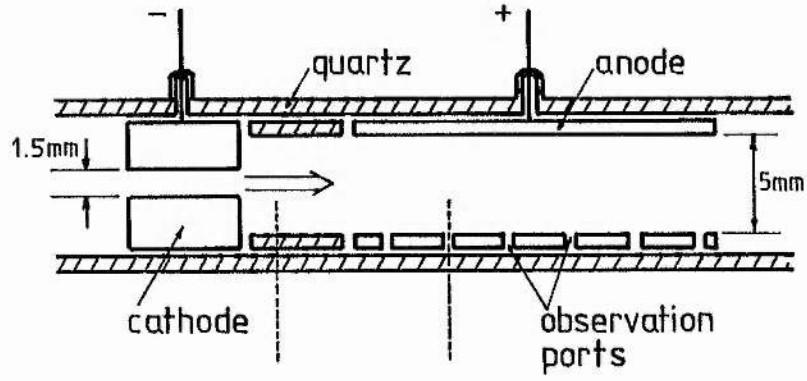

Fig 3.24. The discharge tube used to investigate electron beam production in low pressure argon.

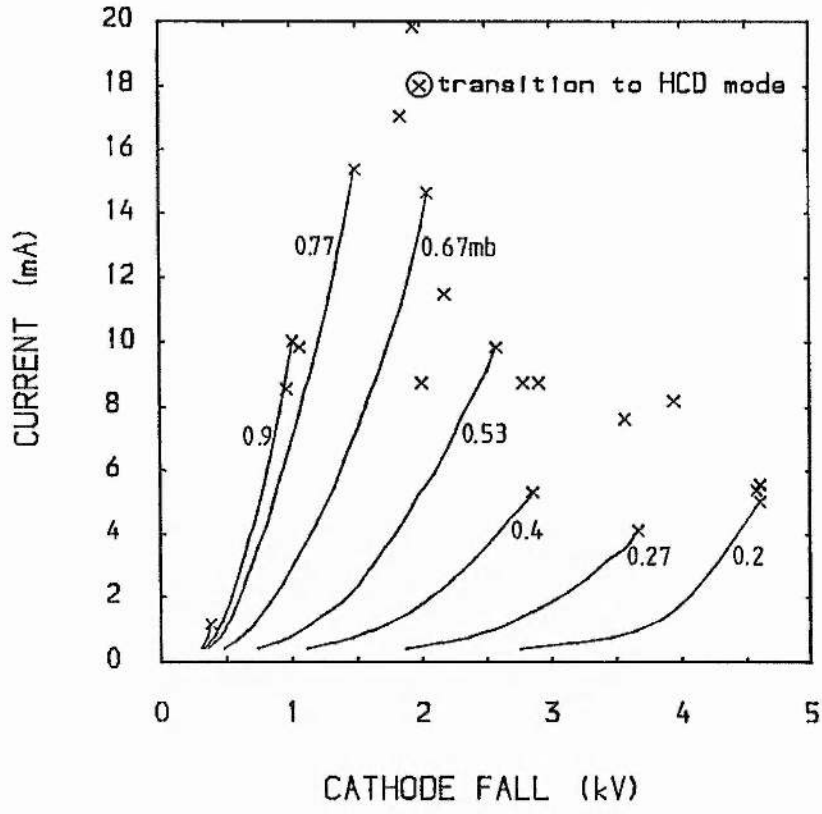

Fig 3.25. The V-I characteristics of an electron beam discharge in argon, with pressure as a parameter. Additional transition points from subsequent runs are included also.

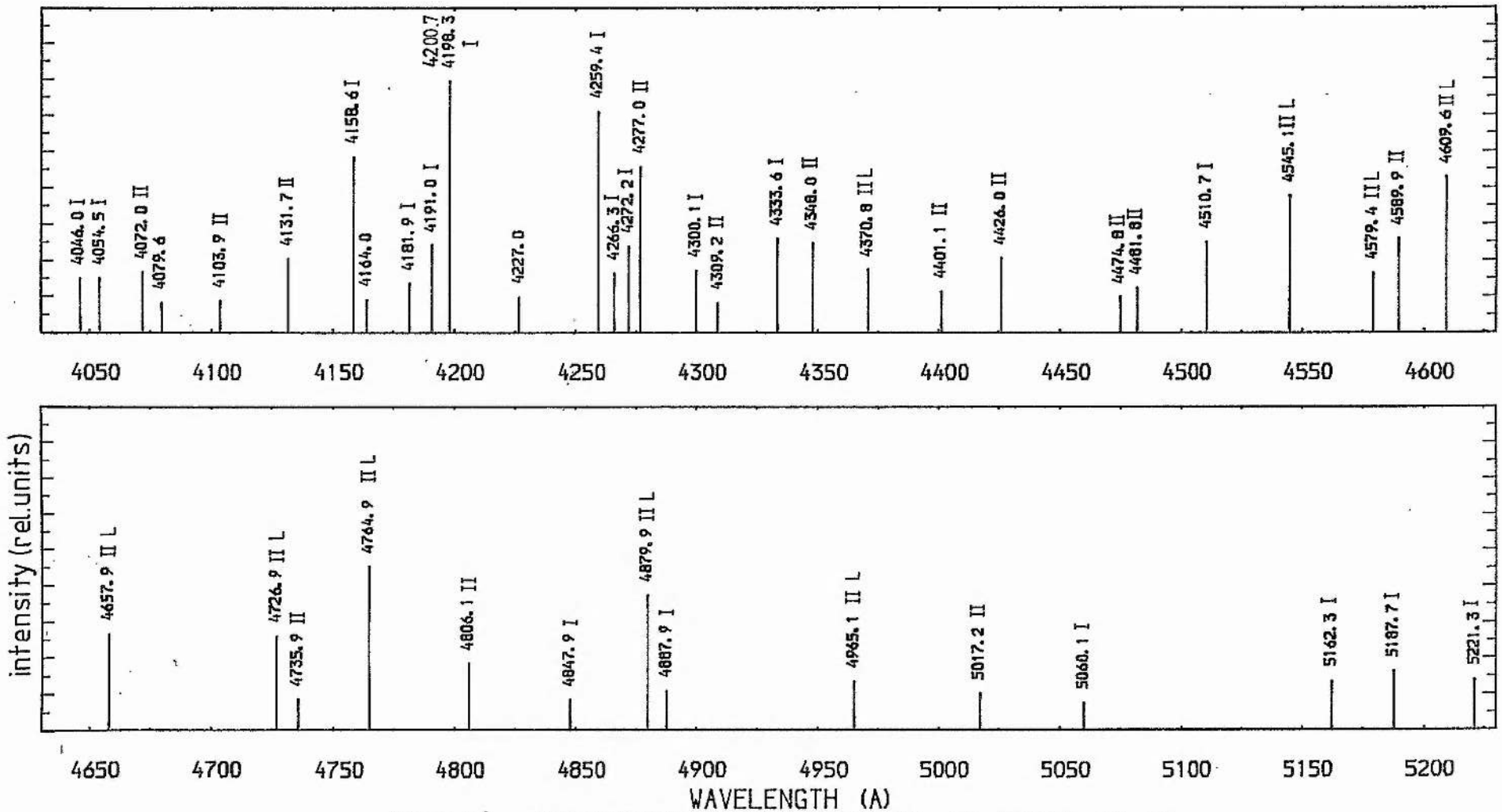

Fig 3.26. The emission spectrum from the NG region of an electron beam plasma in argon at 0.4mb and 0.01mA. I: atomic transitions, II: ionic transitions, L: known laser transitions.

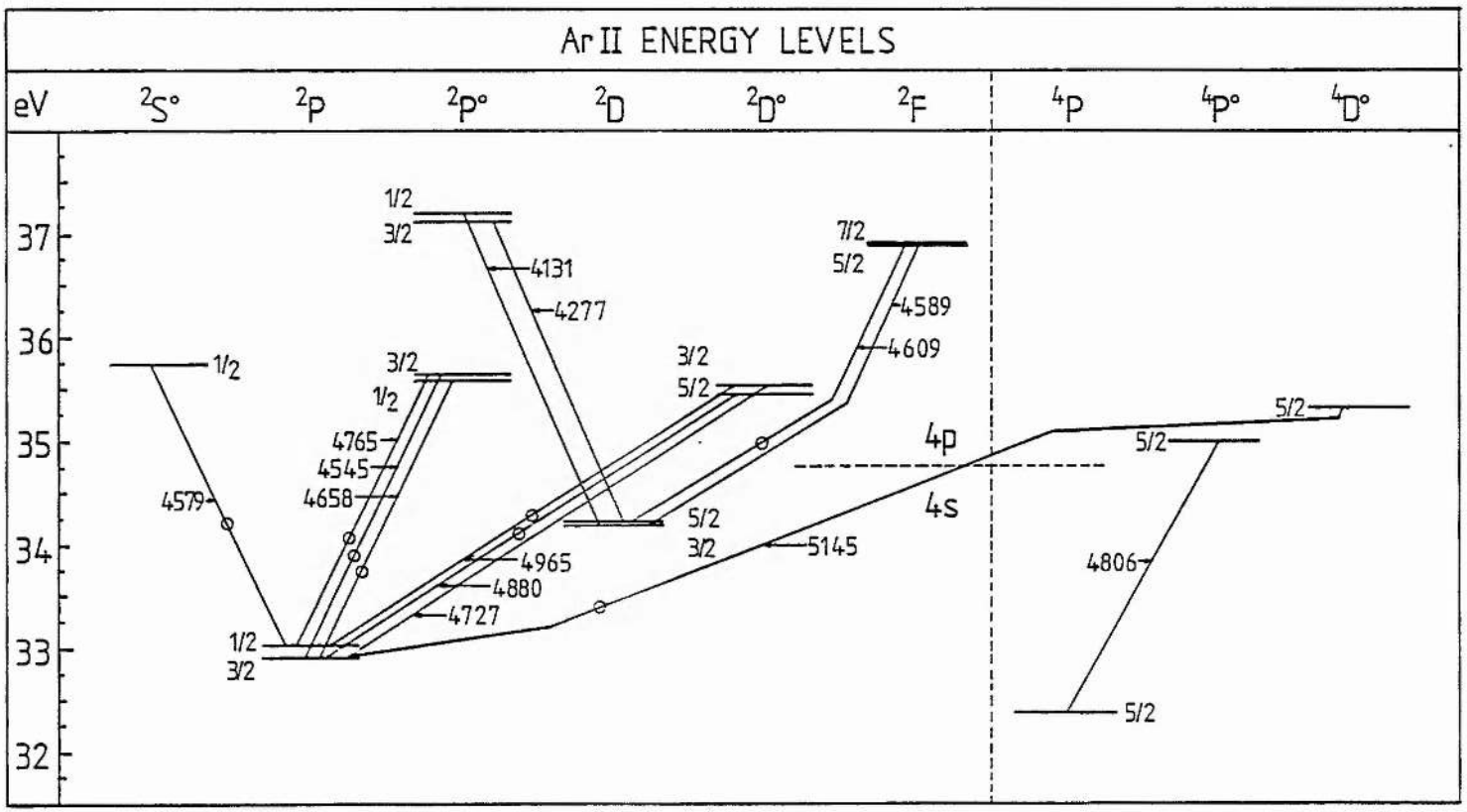

Fig 3.27. Energy levels of the $3p^4 4p$ and $3p^4 4s$ configurations in ArII [25]. The energy scale is referenced from the ground state of ArI. 'O' denotes a known laser transition.

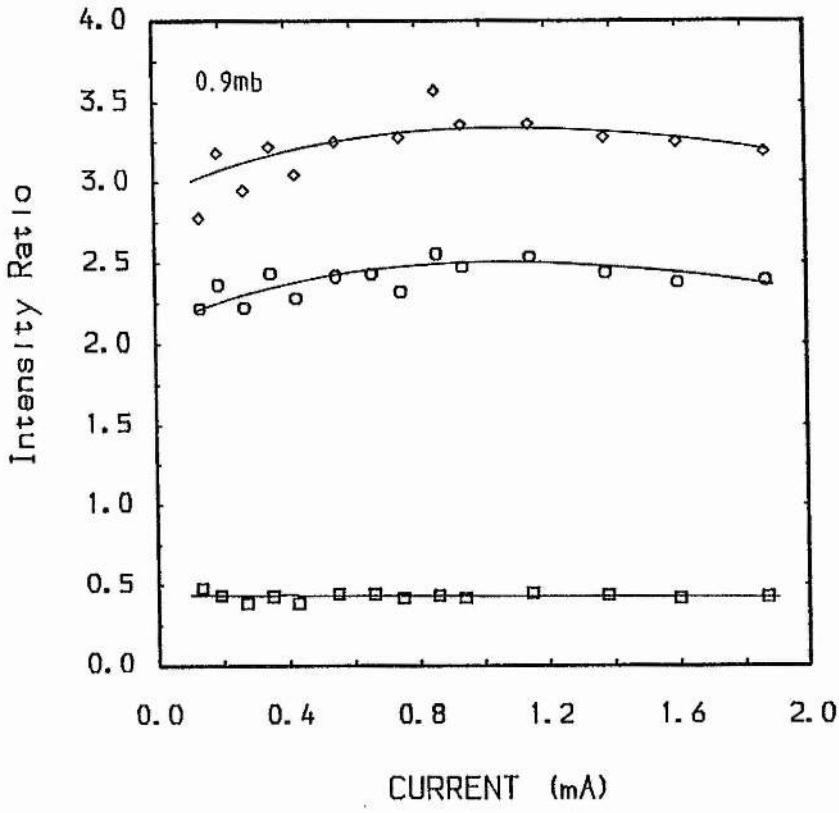

Fig 3.28a. Intensity ratios for ArII levels in an electron beam discharge at 0.9mb. ◇ : 4765A/4806A, ○ : 4880A/4806A, □ : 5145A/4806A.

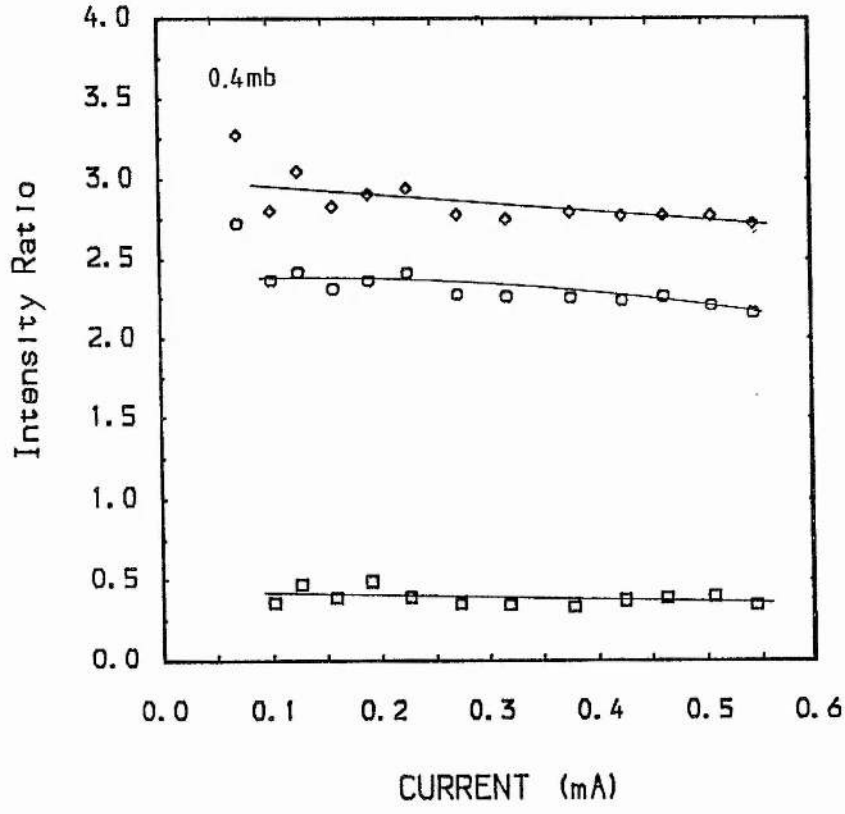

Fig 3.28b. Intensity ratios for ArII levels in an electron beam discharge at 0.4mb. ◇ : 4765A/4806A, ○ : 4880A/4806A, □ : 5145A/4806A.

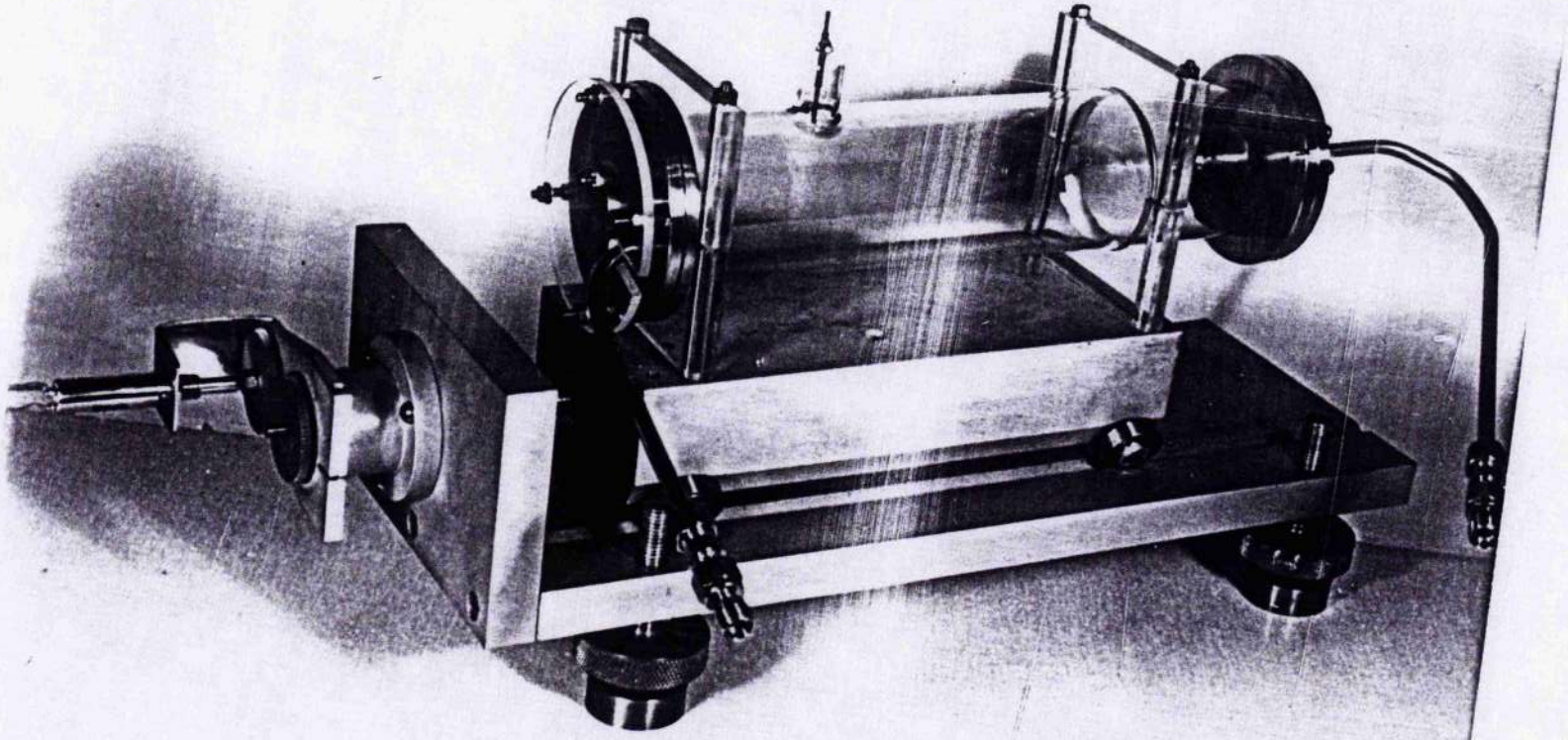

Plate 1. The discharge cell used to investigate electron beam production in helium.

Chapter 4

4 Electron Motion in the Cathode Region of a Helium Discharge

4.1 Introduction

When an electron beam from a high voltage glow discharge is used to generate an electron-beam plasma in a low pressure gas, it is important to understand the processes which sustain the beam plasma region, and the mechanisms by which the fast electrons from the cathode impart their energy to the gas. The physical appearance of the beam plasma region has been depicted in fig 2.13 and consists principally of the CDS sheath and the NG plasma. In this chapter, a theoretical model is developed for helium to gain a better understanding of the basic properties of a high voltage glow discharge, and its possible application to the ion lasers to yield improved operating efficiencies. There are three main aims in the formulation of the model:

1. To provide an understanding of the unusual discharge processes which lead to e-beam production from perforated cathodes;
2. To investigate the general superior performance of high voltage HCD's and e-beam discharges compared to low voltage HCD's;
3. To characterise the ranges of fast electrons in a gas, which are directly related to the physical length of the NG.

A theoretical model of the discharge can be developed by simulating ion and electron motion in the CDS and NG regions. There have been a number of reviews discussing the various techniques for modelling the cathode regions of a glow discharge [1-3]. The general approach involves approximating the electric fields in the cathode regions, and then calculating the charged particle energy distribution functions at each point in the discharge. Self-consistent models go one step further and use the energy distribution functions to calculate charged particle concentrations and space charge densities and then, via Poisson's equation, the electric field is re-defined at all positions. The calculation is repeated until the electric field becomes invariant. Some models treat the CDS and NG together and deal with the boundary region between the two with a modified Langmuir and Tonks/Bohm theory for the NG plasma and CDS positive ion sheath [4]. The presence of a flux of fast, beam-like electrons at the boundary region is a complicating factor, however.

In helium, a few Monte-Carlo calculations using random number generators have been carried out to predict the electron energy distribution function (EEDF) in the CDS sheath using an assumed electric field distribution as a starting point [5],[6]. Helium is a convenient gas to model because the collision cross-sections for electron impact to excite the 10-20 principal atomic states are well known. The EEDF is probably the most important parameter in the discharge to characterise, due mainly to the fact that excitation and ionisation in the helium discharge can be almost entirely attributed to electron collisions. The ion energy distribution function is therefore not considered until the final section of this chapter. In attempting to solve the transport equations for electron motion, it is found that a state of equilibrium between the EEDF and the local

electric field may not exist in the CDS and NG. This is due to the large and rapidly varying electric field close to the cathode, and the flux of fast electrons at the CDS/NG boundary. In simulating electron motion in the cathode regions, it is necessary to use the complete EEDF in calculations to describe the motion of electrons. Unlike the electron motion in the PC. the energy gained by an electron in the CDS is not balanced by energy losses incurred through inelastic collisions, and this leads to a runaway effect of the electron velocity. Even when a linear electric field is assumed in the CDS, together with a small but constant field in the NG, simulating electron motion may demand substantial processing time on a standard mainframe computer. Indeed, the majority of these Monte-Carlo models deal only with 'normal' helium discharges with a Cathode fall of ~150V.

In order to best satisfy the three different aims listed above. a general model is constructed, starting with an assumed electric field distribution, and the EEDF is then calculated at different positions in the discharge. Particular aspects of the general theory related to the three aims are developed at a later stage. Thus, a model is formulated to consider a discharge in helium with the following criteria:

(a) A pair of flat, parallel electrodes of infinite extent with the anode placed in the FDS region;
(b) A variable Cathode fall between 150V (normal regime) and 1.0kV (abnormal regime).

These criteria are adopted because modelling a discharge possessing a two dimensional electric field similar to that expected in a

perforated cathode (fig 3.16b) would be difficult, due to the lack of reliable experimental measurements of the field pattern around the hole aperture. These measurements are needed to make an initial guess of the field distribution and strength. It has been shown in the previous chapter, however, that e-beam production from perforated cathodes is a strong function of the Cathode fall, with the current ratio (η_j) rising rapidly around V_c=1.4kV. It is useful therefore, to simulate a helium discharge with a variable Cathode fall, and pay particular attention to the state of the discharge when $V_c \gtrsim 1.0$kV.

The investigation of electron collisions in nelium by Miller [7] shows that fast electrons (keV) can generate electron/ion pairs with a smaller average energy expenditure than can low energy electrons of a few hundred eV. Electron beams generated by glow discharges are not entirely mono-energetic, however, and the spread of electron energies in the beam undoubtedly affects the overall average efficiency at which new e/i pairs are generated. As the e-beam flux degrades in passing through the gas, ionisation may become less efficient, and certain parts of the NG may be more important in maintaining the production of new e/i pairs. Ionisation in the NG brought about by fast electrons in HCD's (V_c=200V-300V) may be compared to that in e-beam discharges ($V_c \gtrsim 1.0$kV). Degradation with distance of the electron flux from the CDS/NG boundary is also important in characterising the beam energy coupled to the gas in the NG, and in determining the physical length of the NG from the electron ranges. The overall length of the NG is an important factor since it must be matched to the dimensions of the gain volume of the laser. In the longitudinal scheme of fig 1.11, a NG shorter in length than the confining magnet and gas cell leaves regions of the gas along the optic axis unexcited, resulting in a reduction of gain. Conversely,

if the NG is too long, e-beam energy is wasted as the electrons crash into the end mirror or collide with the tube walls. In a hollow cathode discharge using helium at somewhat higher pressure. the length of the NG must be greater than the radius of the circular discharge tube in order to achieve the desired coalescence of NG at the tube centre. If such an overlap is not achieved, the FDS appears at the tube centre, the 'hollow cathode effect' is reduced, and the gain region may take on an annular profile [8].

4.2 The Propagation of Fast Electrons in Helium

4.2.1 Preliminary Assumptions

The following assumptions and simplifications are made in order to minimise the number of calculations required in the simulation of electron motion:

1. The discharge is assumed to form between two flat plate electrodes of infinite extent. so that edge effects around the cathode perimeter and those caused by a build up of wall space charges can be neglected (fig 4.1a).
2. Discharge variables are assumed to vary only with spatial position and not with time.
3. The electric field in the CDS falls linearly with distance, from a maximum at the cathode face decreasing to zero at the CDS/NG boundary. At all positions within the NG, the electric field is

zero.

4. Energy losses due to 'elastic' collisions are negligible.
5. Energy losses incurred during inelastic collisions are considered only for single step ionisation to He^+, and for excitation to the principal atomic levels $ns^1S, np^1P, nd^1D, ns^3S, np^3P, nd^3D$. All the following collision processes are neglected:
   (a) Double ionisation to produce He^{++} from He or He^+
   (b) Simultaneous ionisation and excitation to produce He^{+*} states
   (c) Ionisation via intermediate states such as He^+ and He^*
6. Angular scattering of electrons during elastic and inelastic collisions is not considered for individual impact events. Instead, an empirically determined 'straggling factor' (ke) is introduced, which is a constant (ke=1 or 2).
7. The gas density is taken to be constant in all regions of the discharge, and possible density variations caused by ohmic heating of the gas are neglected.

The complexity of the theoretical model to be developed here can be significantly reduced by adopting a discharge geometry which is effectively one dimensional as shown in fig 4.1a. For this to be the case in practice, it is necessary to ensure that the physical dimensions of the electrodes are greater than the electrode separation. Discharge parameters are therefore only calculated in terms of the X-coordinate. 'Straggling' of the electron path as shown in fig 4.1b is a known experimental effect, and results from the numerous elastic and inelastic collisions that occur when the electron traverses a thick target. The actual path length of an electron in a gas is greater than the observed range (Xo) by a factor of about two

due to the zig-zag path followed by the electron before coming to rest [9]. In the CDS, the electrons suffer relatively few collisions, and straggling is less important than in the longer NG region. Therefore, in the calculations to follow, ke is set at 1.0 in the CDS, and 2.0 in the NG. Spatial variations of the gas temperature in the cathode regions of a helium glow discharge have been investigated extensively by Gunthershulze in connection with a study of the similarity laws for helium [10]. Generally, it is found that the temperature of the gas is at a maximum around the CDS/NG boundary, diminishing with distance further into the NG, or towards the cathode. Gunthershulze estimates the gas temperatures at the CDS/NG boundary to be between 300K-600K at 1mb pressure and $V_c \sim 1.0$kV with a current density of a few $mA.cm^{-2}$. Temperatures of several hundred ^{o}C are also quoted by Francis [11] but there are few direct spectroscopic measurements using the Doppler widths of emission lines. Temperature distributions in the discharge regions are difficult to gauge in practice because the rates of heat dissipation to the surrounding vessel walls and electrodes are difficult to calculate. These factors vary considerably between different experiments. A uniform gas temperature and density throughout the discharge is therefore assumed as a first approximation, and all spatial co-ordinates are scaled according to the similarity law of distance and pressure p.x (mb.cm).

4.2.2 The Collision Cross-sections

A complete set of semi-empirical cross-sections for helium have been calculated by Alkhazov for electron energies up to 20keV, using experimental data to fit curves at low energy and the Born approximation to cover high energies [12]. These cross-sections include single-step ionisation and excitation to the various singlet and triplet atomic levels. The differential cross-section for ionisation reported gives the predicted energy spectrum of the secondary electrons created in ionising collisions. This set of cross-sections are used in this the model and are described in Appendix II.1 of this thesis.

4.2.2.1 Ionisation and Excitation Cross-Sections

The cross-sections for ionisation and for excitation to the various atomic states included in the model are depicted in fig 4.2. For electrons with energies greater than about 30eV, single-step ionisation has the largest cross-section and is the dominant energy loss process. The contrast between the cross-sections for excitation to the singlet states and to the triplet states is quite clear with those of the singlets falling off more gradually at high energy. The general shape of the cross-sections of the singlet $np\,^1P$ states are similar to that of the ionisation cross-section. The impact cross-sections for producing He^{++} and He^{+*} states by single step electron impact are both several orders of magnitude less than those given in rig 4.2, and are thus neglected [13].

4.2.2.2 Differential Cross-Sections

The secondary electrons generated in ionising collisions have a range of energies which are determined by the differential cross-section for ionisation $\sigma_E(\epsilon)$. This represents the probability of generating a secondary with energy $(\epsilon - I_o)$ (eV) from a primary of energy E (eV) with a total energy loss of ϵ (eV), where I_o (eV) is the first ionisation potential. Two examples of the energy spectrum of secondaries are depicted in fig 4.3 using the expression given by Alkhazov for primaries of energy 100eV and 1keV. The probability of generating secondaries has a maximum at zero energy ($\epsilon - I_o = 0$eV) whilst it is least probable that the two electrons share equal energies after the event. The indistinguishability of the two electrons after the collision gives rise to a probability distribution which is, in practice, the sum of two curves. In other words, it is assumed that the faster electron of the pair is the primary electron whilst the slower one is the secondary.

4.2.2.3 Secondary Ionisation

For a primary electron of energy E, the average energy $\overline{\epsilon_s(E)}$ (eV) of the secondary created in an ionising collision can be calculated by taking the average energy over all secondary energies:

$$\overline{\epsilon_s(E)} = \overline{\epsilon'} = \frac{\int_0^{\frac{E-I_o}{2}} \epsilon' \ \sigma_E(\epsilon') \, d\epsilon'}{\int_0^{\frac{E-I_o}{2}} \sigma_E(\epsilon') \, d\epsilon'} \qquad (4.1)$$

with $\epsilon' = \epsilon - I_o$

and therefore

$$\overline{\epsilon_s(E)} = \overline{\epsilon - I_o} = \frac{\int_{I_o}^{\frac{E+I_o}{2}} (\epsilon - I_o)\ \sigma_E(\epsilon)\ d\epsilon}{\int_{I_o}^{\frac{E+I_o}{2}} \sigma_E(\epsilon)\ d\epsilon} \qquad (4.2)$$

The limits of integration are set in accordance with the principle of indistinguishability; to integrate past the point $(E+I_o)/2$ in eq.(4.2) results in counting the the electrons twice. The average total energy $\overline{\epsilon_s(E)} + I_o$ lost in an ionising collision has been calculated using eq.(4.2), and is shown in fig 4.4 as a function of primary energy E. The average energy imparted to the secondary is seen to increase with primary energy and for primaries over 0.3keV, $\overline{\epsilon_s(E)}$ becomes larger than I_o ($\overline{\epsilon_s(E)} + I_o > 2I_o$). A secondary with this average energy may take part in further ionising collisions to generate tertiary electrons.

Although the probability function $\sigma_E(\epsilon)$ for generating secondaries is always largest for producing electrons at 0 eV, a significant number of secondaries may have energies higher than the ionisation potential I_o, and may themselves produce further ionisation. A number of previous theoretical models simulating electron motion in the CDS and NG neglect secondary ionisation partly on the grounds that $\sigma_E(\epsilon)$ peaks at 0 eV [14],[15]. Although this may be a reasonable approximation for low energy primaries, and small Cathode falls ($V_c \sim 150V$), it becomes less accurate for higher energies when a significant number of secondaries are generated in the tail of $\sigma_E(\epsilon)$ (fig 4.3b). Using an expression similar to eq. 4.2, it is possible to calculate the fraction $K(E)$ of electrons in the secondary

distribution $\sigma_E(\epsilon)$ which have energies greater than I_o:

$$K(E) = \frac{\int_{2I_o}^{\frac{E+I_o}{2}} \sigma_E(\epsilon)\, d\epsilon}{\int_{I_o}^{\frac{E+I_o}{2}} \sigma_E(\epsilon)\, d\epsilon} \qquad (4.3)$$

The form of $K(E)$ is shown in fig 4.5 and it is seen that the proportion of secondaries generated with $\epsilon > I_o$ increases with primary energy E and plateaus at around 0.3keV. There is a threshold energy for tertiary production at $E=3I_o$. Many of the secondaries generated with energies only slightly above I_o however, do not ultimately generate tertiary electrons since the cross-sections for ionisation and excitation are comparable in size for electrons with energies between I_o and ~40eV. From a primary of energy E, the overall probability $\mu(E)$ of producing a secondary electron with energy above I_o which subsequently produces an electron/ion pair in a further ionising collision is therefore:

$$\mu(E) = \frac{\int_{2I_o}^{\frac{E+I_o}{2}} \left(\frac{\sigma_i(\epsilon)}{\sigma_i(\epsilon) + \Sigma \sigma_{n,l}(\epsilon)} \right) . \sigma_E(\epsilon)\, d\epsilon}{\int_{I_o}^{\frac{E+I_o}{2}} \sigma_E(\epsilon)\, d\epsilon} \qquad (4.4)$$

where the variables $\sigma_i(E)$ (cm^2) and $\sigma_{n,l}(E)$ are the respective cross-sections for ionisation and for excitation to the atomic level of principal quantum number n (n=2,3,4,...) and angular momentum number l (l=S,P,D,...). This is also shown in fig 4.5 and can be used to assess the importance of secondary ionisation (in an ability to produce tertiaries) for different values of the primary energy E. It

is noted that $\mu(E)$ rises less rapidly than $K(E)$ and levels off at around 0.3keV at a value of about 20%. It seems necessary therefore to take into account ionisation by secondaries if fast electrons (E>0.3keV) are to be expected in the discharge. For a primary energy of 0.15keV, the fraction of electrons which are expected to generate tertiaries is 0.16, so it is questionable as to whether it is reasonable to neglect secondary ionisation even for discharges with Cathode falls as low as 150V.

Values of the average secondary energy $\overline{\epsilon_s(E)}$ can be used to calculate the Loss function L(E) ($eV.cm^2$) for electrons in helium. This is a fundamental parameter for energy loss in a gas, and can be used to compare the energy losses due to excitation and ionisation. L(E) is defined as:

$$L(E) = (\overline{\epsilon_s(E)} + I_o)\,\sigma_i(E) + \sum_{n,l} I_{n,l}\sigma_{n,l} \quad (eV.cm^2) \qquad (4.5)$$

The constant $I_{n,l}$ (eV) is the threshold excitation potential. The form of L(E) is shown in fig 4.6 and it is noticeable that energy loss at low energy (E<50eV) is predominantly by excitation whilst at higher energies (E>0.2keV), it is mainly by ionisation. The loss function can be used directly to calculate the rate of energy loss (dE/dx) ($eV.cm^{-1}$) of an electron travelling through a thin slab of gaseous material (δx):

$$\delta E = N_o \,.\, L(E)\ \delta x \qquad \text{where } N_o = \text{gas density } (cm^{-3})$$

and

$$\left[\frac{\delta E}{\delta x}\right]_{\lim\ \delta x \to 0} = \left[\frac{dE}{dx}\right] = N_o.L(E) \qquad (4.6)$$

The stopping power of a gas of density ρ (gms.cm^{-3}) is derined as $\left[\frac{1}{\rho}\frac{dE}{dx}\right]$ (eV.cm^2.g^{-1}) and therefore:

$$\left[\frac{1}{\rho}\frac{dE}{dx}\right] = K.\ L(E) \qquad (4.7) \qquad \text{where} \quad K=1.506\times10^{23}\ \ g^{-1}$$

Values of the stopping power of helium have been measured experimentally using thin gaseous targets by Berger and Seltzer [16]. A comparison between their data and values calculated here from eq(4.6) and eq(4.5) is made in table 4.1.

	Stopping Power $\left[\frac{1}{\rho}\frac{dE}{dx}\right]$ MeV.cm^2.g^{-1}	
E(keV)	Loss F.	Berger&Seltzer
10.0	20.86	22.66
15.0	14.94	16.41
20.0	12.14	13.07

Table 4.1 Comparison of theoretical and experimental stopping powers in helium

The two sets of data agree to better than 10% for the overlapping energy range 10-20 keV. thereby giving some sense of confidence in the values of L(E) and $\overline{\epsilon_s}(E)$ calculated here from the cross-sections of Alkhazov.

In addition to the energy losses incurred by an electron during ionising collisions, the primary is deflected by a small angle away from its original path during each collision. As the energy E increases beyond a few hundred eV however, this angle of scattering is predominantly in the forward direction [17]. Tran-ngoc et-al [26] have modelled electron motion in the CDS assuming forward scattering only, whilst in a similar model by Boeuf and Marode, electron scattering is treated more rigorously but with an accompanying increase in the complexity of the calculations. In the CDS, it seems reasonable to assume rorward scattering of the primaries, particularly in calculations for a discharge with a large Cathode fall. This approximation is equivalent to using a unity straggling factor in the CDS. For calculations in the NG, a Straggling factor of 2.0 is used throughout, although this is expected to lead to some systematic errors in estimates of the physical size of the region. These estimates can therefore only be used as a rough guide in predicting the total length of the region. The slower secondary electrons from ionisation collisions are also generated with their velocity components mainly in the forward direction [18]. It is assumed here that they travel in the same direction as the primary after the collision. Then, the contribution of the secondaries to the total electron current in the discharge may be added directly to the current flux present due to the primaries. Subsequent excitation and ionisation of the gas by secondaries is confined to a relatively small region of the gas, since the loss function L(E) is larger and the mean free path for collisions shorter for secondaries.

4.2.3 The Computer Simulation

Having made the assumption that electron motion in the cathode regions is essentially a one-dimensional problem, the EEDF can be defined at all positions in the discharge in terms of the current density $j_e(x)$ ($mA.cm^{-2}$). This represents the flux of electron current at position x (cm) from the cathode, and is the sum over all electron energies found at point x:

$$j_e(x) = \int_0^\infty j_e(x,E)\, dE \qquad (4.8)$$

where $j_e(x,E)$ is the current flux due to the fraction of electrons with energy E. The number density $f(x,E)$ of electrons at point x with energy E is found from $f(x,E) = E^{-1/2} j_e(x,E)$. The function $f(x,E)$ is referred to as the EEDF. whilst the energy distribution of electron flux (EDEF) refers to the function $j_e(x,E)$. If the 'swarm' of electrons represented by the flux $j_e(x,E)$ moves through a small distance δx in a field-free region of the gas (fig 4.7), some electrons in the flux distribution collide with helium atoms and may lose kinetic energy. If the gas has density N_o (cm^{-3}), the fraction of electron flux at electron energy E lost through collisions over the distance δx is given by:

$$\delta j_e(x,E) = j_e(x,E)\,(1 - e^{-(\delta x/\lambda(E))}) \qquad (4.9a)$$

where $\lambda(E) = 1/(Q(E).N_o)$ and $Q(E) = \sigma_i(E) + \sum_{n,l} \sigma_{n,l}(E)$

$\lambda(E)$ (cm) is the average mean free path between inelastic collisions and $Q(E)$ (cm^2) is the total inelastic collision cross-section. The

remaining electron flux, comprised of electrons still retaining energy E, emerges from the slab at $x+\delta x$.

The EDEF referring to the current flux $j_e(x,E)$ is not treated as a continuous function in the calculations to follow, but instead is split up into a large number (k) of separate energy 'cells' with each cell containing electrons with the same kinetic energy (fig 4.8). A similar approach is made by Kagan to model a low voltage helium discharge [15]. The EDEF therefore consists of a finite number of cells and the current flux $j_e(x,E_k)$ represents the electron flux at point x due to electrons with energy E_k. Thus eq.4.9a becomes:

$$\delta j_e(x,E_k) = j_e(x,E_k)\,(1- e^{-(\delta x/\lambda(E_k))}) \qquad (4.9b)$$

The fraction $\delta j_e(x,E_k)$ of current flux represents those electrons which have lost energy in inelastic collisions within $x \rightarrow x+\delta x$. Accordingly, the flux of these electrons must be transferred to cells of lower energy. The electron flux remaining in the k^{th} cell at point $x+\delta x$ is therefore:

$$j_e(x+\delta x,E_k) = j_e(x,E_k)\, e^{-(\delta x/\lambda(E_k))} \qquad (4.10)$$

However, this cell may also receive contributions of flux at point $x+\delta x$ from cells of nigher energy in which electrons have lost energy in collisions. All electrons in the EDEF are taken to have energies which are exact multiples of the cell separation δE, which is set at 0.984eV. This is an exact rraction of the first ionisation potential in helium (I_o) which is taken to be 24.6eV. The quantity $\delta j_e(x,E_k)$ of electron flux which represents those electrons judged to have collided with helium atoms, can be subdivided into two smaller

fractions to represent those electrons taking part in ionising collisions and those in excitation collisions. The corresponding flux losses due to ionisation $\delta j_{ion}(x,E_k)$ and to excitation $\delta j_{ex}(x,E_k)$ are therefore:

$$\delta j_{ion}(x.E_k) = \delta j_e(x,E_k) \left(\frac{\sigma_i(E_k)}{\sigma_i(E_k) + \sum_{n,l} \sigma_{n,l}(E_k)} \right) \quad (4.11a)$$

$$\delta j_{ex}(x,E_k) = \delta j_e(x,E_k) \left(\frac{\sum_{n,l} \sigma_{n,l}(E_k)}{\sigma_i(E_k) + \sum_{n,l} \sigma_{n,l}(E_k)} \right) \quad (4.11b)$$

The energy losses incurred in both types of collision are constrained here to be exact multiples of the cell separation δE. For example, in all excitation collisions it is assumed that the energy loss can be set at a value of I_{ex} with $I_{ex} = 22 \times \delta E$. This is an average value calculated from the excitation potentials $I_{n,l}$ weighted according to the relative cross-sections of the different excited states. Consequently, the flux loss $\delta j_{ex}(x,E_k)$ must be added as a cascade contribution to the current flux in the cell at energy $E_k - I_{ex}$ at point $x+\delta x$. In ionising collisions, the energy loss is not simply the ionisation potential I_o ($I_o = 25 \times \delta E$) in all cases, since the secondary electrons can carry away kinetic energy ($\epsilon - I_o$) at the expense of the primary. The secondary energy ($\epsilon - I_o$) is therefore quantised in steps of δE as shown in fig 4.9, to take into account all possible secondary energies between $\epsilon = 0eV$ and $\epsilon = (E - I_o)/2$. If $\delta j_{ion}(x,E_k)$ represents the total flux of ions judged to have taken part in ionising collisions, the fraction used in generating secondaries with the specific energy ϵ_m' is therefore:

$$\delta j_s(x,E_k,\epsilon'_m) = \delta j_{ion}(x,E_k) \cdot \sigma_E(\epsilon'_m) \Big/ \sum_{m=1}^{m=N} \sigma_E(\epsilon'_m) \quad (4.12)$$

where $\epsilon'_m = (m-1)\,\delta E$

and $N\,\delta E \sim (E - I_o)/2$ or $N \sim (E - I_o)/2\,\delta E$

The sum in the denominator of eq.(4.12) is used to normalise $\sigma_E(\epsilon'_m)$. The total energy loss for primaries to generate secondaries with energy ϵ'_m is thus $(\epsilon'_m + I_o)$ and the fraction of flux is therefore added as a cascade contribution to the cell with energy $(E_k - (\epsilon'_m + I_o))$. At the same time, the flux of secondaries with energy ϵ'_m (equal in size to $\delta j_s(x,E_k,\epsilon'_m)$ is itself added to the EDEF for values of k=m. In practice, this corresponds to additions to energy cells with small k numbers. The inelastic collisions experienced by a flux of electrons moving through a thin region of gas $x \rightarrow x+\delta x$ which result in energy loss and cascading of the electron flux between cells in the EDEF are represented graphically in fig 4.10.

The model developed so far examines the changes in electron flux $j_e(x,E_k)$ in each of the cells in the EDEF as the 'swarm' moves away from the cathode and through the discharge regions. The CDS and NG are thus divided into a large number of thin slabs and as the electron flux traverses each slab, the fraction of flux $\delta j_e(x,E_k)$ lost from each energy cell is calculated, and the collision products assigned to the appropriate energy cells. The physical widths of the slabs are selected with the requirement that the probability of a collision in a given cell for a given electron is small (<0.1). As the initial electron 'swarm' moves away from the cathode face under the action of the electric field in the CDS, the electrons in the EDEF gain energy

from the field as well as lose energy through collisions. Accordingly, as the electrons accelerate in the CDS, they must be raised into higher energy cells in the EDEF. The field in the CDS $E(x)/p$ ($V.cm^{-1}.mb^{-1}$) is assumed linear and is given by:

$$\frac{E(x)}{p} = -\frac{1}{p}\frac{dV}{dx} = \frac{2V_c}{pd_c}\left(1 - \frac{x}{d_c}\right) \qquad (4.13)$$

This is shown in fig 4.11, and the equation can be used to arrive at the following formula giving the width of the region of gas δx in the CDS over which the field potential changes by an amount δV:

$$p.\delta x \approx p.d_c\left[\left(1-\frac{x}{d_c}\right) - \left(\left(1-\frac{x}{d_c}\right)^2 - \frac{\delta V}{V_c}\right)\right] \qquad (4.14)$$

If the potential δV changes by 0.984eV as the electron 'swarm' advances through δx ($x \rightarrow x+\delta x$) in the CDS, each electron flux component $j_e(x+\delta x, E_k)$ can be raised into the next highest energy cell as the swarm reaches $x+\delta x$. Thus, eq.(4.14) is used to define the widths of the slabs in the CDS, so that the voltage drop across every slab is 0.984eV. Values of the total width of the CDS from the similarity parameter $p.d_c$ (mb.cm) for different values of Cathode fall V_c are taken from von Engel [19]. These values are listed in table 4.2.

Cathode Fall V_c(kV)	$p.d_c$ (mb.cm)
0.15	1.733
0.20	1.663
0.30	1.435
0.40	1.263
0.50	1.140
0.60	1.038
0.70	0.965
0.80	0.912
0.90	0.870
1.00	0.835

Table 4.2 Values of the CDS width parameter $p.d_c$.

Strictly speaking, all dimensions in the discharge should be scaled in units of (mb.cm) according to the similarity parameter p.x. For convenience, a helium pressure of 1mb is used in subsequent calculations, but the discharge parameters are presented in the correct format, and are scaled in terms of p.x (mb.cm).

In the field free NG region, δx is selected using a different set of criteria. Since the field is assumed to be negligible, only the cascading electron flux need be calculated for each slab of discharge. If the initial EDEF is allowed to contain 10 units of electron flux at x=0, an energy cell is judged to have emptied of flux when its population drops below 10^{-6}. After identifying the cell with highest energy E_{kmax} still containing flux at the point of interest in

the NG, the value of δx is selected as equal to 0.1 $\lambda(E_{kmax})$. The whole electron 'swarm' is then advanced by the same distance δx, and the cascading flux computed. The very low energy electrons generated in the NG from cascading, with energies less than I_o appear to have long collision mean free paths when referring to fig 4.2, but they are less directional than the fast electrons. For low energies, the assumptions of forward scattering during inelastic collisions and negligible effects due to elastic scattering are probably invalid. The motion of such electrons must be dealt with using two dimensional transport equations taking into account diffusion and recombination [20]. The eventual fate of these slow electrons is therefore not addressed in this model. Instead, only the directional flux of fast electrons in the NG is of interest and therefore the flux in all energy cells below I_o is ignored. As the cascading between energy cells in the EDEF continues as the 'swarm' advances through the NG, a point is reached when the flux density in all cells in the EDEF drops below 10^{-6}, and the calculation is then assumed to be complete. The calculations have been carried out on the VAX 11/780-5 computer at St Andrews, and the relevant programmes are included in Appendix II.2 of this thesis. The range of the Cathode fall (0.15kV-1.0kV) for which calculations have been carried out is limited by the constraints of the computer used.

4.3 Electron Motion in the CDS

4.3.1 Electron Energy Distribution Functions

To begin the calculation of electron motion in the CDS, an initial EDEF at the cathode face is defined. The form of the EDEF is determined by the energies of the electrons released from the cathode by secondary emission resulting from ion, metastable and photon impacts. It has been shown by Helm, however, that secondary emission by ion impact is the dominant process in helium discharges [21]. Secondary electron emission from various metals caused by helium ion impacts has been discussed by Carter & Colligon, and it is shown that electrons are emitted with energies governed by initial ion energy [22]. Typical ion energies expected at the cathode face are calculated here from the results of Davis and Vanderslice [23] and range from ~3eV for V_c~0.15kV up to ~50eV for V_c~1.0kV. The spectrum of emitted electrons for such ion energies is approximately a trapezoid in profile as shown in fig 4.12. This shape is therefore adopted as the initial EDEF, and an arbitrary initial flux of 10 units is assigned to the profile. Models based on Monte-Carlo techniques tend to adopt a simplified uniform flux distribution between 0-10eV, or a δ-function of flux at 0eV, initially [5],[6].

The 'swarm' of electrons at the cathode face represented by fig 4.12 rapidly accelerates away from the cathode face under the action of the electric field in the CDS. The form of the EDEF at different stages in the CDS has been calculated for a Cathode fall of 0.2kV, and the results are depicted in fig 4.13. The electrons

quickly gain energy in the region close to the cathode at small p.x, where the electric field is largest. As some electrons in the primary group lose energy through collisions, a secondary group forms with energies about ~25eV below that of the primary group. These in turn suffer collisions and, aided by a degree of 'smearing out' of the high energy region of the EDEF caused by the different energy losses during collisions, a 'tail' of intermediate energy electrons builds up as the 'swarm' approaches the CDS/NG boundary. Simultaneously, the flux of low energy electrons consisting mainly of slow secondary electrons produced in ionising collisions builds up. The presence of a distinct group of primary electrons and a 'tail' of high energy electrons at the CDS/NG boundary has been established experimentally by Gill and Webb [24] and, independently, by Pringle and Farvis [25]. In comparison, the EDEF at the CDS/NG boundary shown in fig 4.13 agrees well with the EDEF observed by Gill and Webb in the same region, as shown in fig 2.2a.

The evolution of the EDEF in the CDS has been calculated for a Cathode fall of 1.0kV with the results shown in fig 4.14. In this case, electrons in the primary group appear to be attenuated to a lesser degree by collisions throughout the CDS, and this is due to a more rapid initial gain in velocity close to the cathode. when the electrons quickly climb to energies beyond the impact cross-section maxima around 0.1keV. A secondary group forms as the primaries traverse the CDS, but the 'tail' of intermediate energy electrons and peak of low energy electrons are both noticeably absent.

The motion of electrons in the CDS has been modelled for other intermediate values of the Cathode fall V_c, and the EDEF at the CDS/NG boundary is shown in fig 4.15 for several values of V_c. It is clear that the proportion of high energy electrons to reach the CDS/NG

boundary region increases as the Cathode fall is raised. At a Cathode fall of ~1.0kV, the EDEF contains electron flux concentrated mainly in the primary group with a few slightly slower electrons in the 'tail' group. At the boundary region, the proportion of electron flux in the primary group as a fraction of the total electron flux has been calculated, as shown in fig 4.16. Thus, the proportion of primaries arriving at the CDS/NG boundary increases as V_c is raised, and the EDEF appears to contain electrons which are more mono-energetic, with energies corresponding to the Cathode fall.

4.3.2 Ionisation and Excitation Rates in the CDS

Once the EDEF has been calculated at all points in the CDS for a particular value of the Cathode fall, it is possible to calculate ionisation and excitation rates in the CDS, as well as a number of other discharge parameters which can be used to characterise the discharge. These rates are normalised for a current flux at the cathode face of one electron per second. The multiplication coefficient M(x) of the current flux is given by:

$$M(x) = \frac{j_e(x)}{j_e(0)} = \frac{\sum_{k=1}^{k_{max}} j_e(x,E_k)}{\sum_{k=1}^{k_{max}} j_e(0,E_k)} \qquad (4.15)$$

This is shown in fig 4.17 for six different values of the Cathode fall. Excellent agreement is obtained between the values calculated from eq.(4.15) for V_c=0.15kV and those given by Tran-Ngoc et-al for the same voltage [26]. Between V_c=0.15kV and 0.4kV, M(x) tends to rise more steeply for larger values of V_c but for V_c>0.4keV, a

different trend is predicted. For these higher values of Cathode fall, the current flux increases at the same rate initially but towards the CDS/NG boundary, the curves for higher V_c begin to level off. This effect can probably be attributed to the fewer collisions experienced by electrons which have gained sufficient energy to be well past the impact cross-section maxima around 0.1keV. The average energy $\overline{E(x)}$ (eV) at points in the CDS is calculated from the following equation:

$$\overline{E(x)} = \frac{\sum_{k=1}^{k_{max}} E_k \cdot j_e(x,E_k)}{\sum_{k=1}^{k_{max}} j_e(x,E_k)} \qquad (4.16)$$

The form of $\overline{E(x)}$ for different values of V_c is shown in fig 4.18. Once again, the values of $\overline{E(x)}$ given by Tran-Ngoc et-al for V_c=0.15kV agree well with those calculated from eq.(4.16). Values of $\overline{E(x)}$ always increase with distance p.x, peak at some distance well into the CDS, and then decrease slightly as the 'swarm' approaches the boundary region. In the region where $\overline{E(x)}$ increases with distance, the energy gained by the 'swarm' from the electric field is greater than that lost through collisions. After reaching the maximum value of $\overline{E(x)}$, each curve shows a downward trend and the situation is reversed. It is noted that the position of the peak, as a fraction of the CDS thickness $p.d_c$, shifts closer to the boundary region as V_c is increased. The values of $\overline{E(x)}$ at the boundary region ($p.x=p.d_c$) support the notion that the electron flux at the boundary becomes more mono-energetic as the Cathode fall is raised.

The Townsend ionisation coefficient $\alpha_T(x)/p$ ($cm^{-1}.mb^{-1}$) is calculated using the following expression:

$$\frac{\alpha_T(x)}{p} = \frac{1}{j_e(x,E_k)} \cdot \frac{\sum_{k=1}^{k_{max}} \delta j_{ion}(x,E_k)}{p.\delta x} \qquad (4.17)$$

The form of the ionisation coefficient for increasing Cathode fall is shown in fig 4.19 where again, the agreement is good at V_c=0.15kV with values quoted by Tran-Ngoc et-al. For each curve, there is a maximum value of $\alpha_T(x)/p$ at a certain distance into the CDS and this peak is seen at a position progressively closer to the cathode for higher values of V_c. In addition, the peak is more pronounced for higher values of Cathode fall. Similar behaviour is observed for the total ion production rate $\alpha_i(x)/p$ ($cm^{-1}.mb^{-1}$) and the excitation rate $\alpha_{ex}(x)/p$ ($cm^{-1}.mb^{-1}$) which are given by:

$$\frac{\alpha_i(x)}{p} = \frac{1}{j_e(0)} \frac{\sum_{k=1}^{k_{max}} \delta j_{ion}(x,E_k)}{p.\delta x} \qquad (4.18a)$$

$$\frac{\alpha_{ex}(x)}{p} = \frac{1}{j_e(0)} \frac{\sum_{k=1}^{k_{max}} \delta j_{ex}(x,E_k)}{p.\delta x} \qquad (4.18b)$$

These two parameters are depicted in fig 4.20 and fig 4.21. The position of maximum ion production in the CDS appears to shift from the CDS/NG boundary when V_c=0.15kV to a narrow region very close to the cathode face when V_c=1.0kV. Ions generated close to the cathode face are immediately accelerated toward the cathode face by the intense electric field in this region. Thus on collision, they release more electrons by secondary emission. Compared with ions generated in the NG, they are less likely to be lost before colliding with the cathode through the usual loss mechanisms of diffusion or recombination with slow electrons. In a discharge with a large

Cathode fall, such a region of ion production may be important in the maintenance of the discharge current. The curve profiles of excitation rates shown in fig 4.21 are similar to those of ionisation, particularly at high Cathode fall. More information can be gained, however, if the excitation profiles are subdivided into the excitation rates for the individual atomic levels in helium.

4.3.3 Excitation Profiles in the CDS

Spatial profiles in the CDS for the production rates of nine excited states of HeI are shown in fig 4.22, for a Cathode fall of 0.2kV. Immediately next to the cathode, there is a region of width ~0.05 mb.cm where no excitation occurs. Here, the electrons moving away from the cathode have not gained energy from the E-field in the CDS above the excitation threshold potentials. At about 0.1 mb.cm, several sharp peaks appear principally for the production rates of triplet states. This region probably corresponds to the Cathode glow. The triplet production rates then fall away with distance from the cathode, and then rise slowly towards the CDS/NG boundary. The curves for the production of singlet states generally do not have sharp peaks near the cathode and do not dip in the central part of the CDS. The production rates for these same nine levels for a Cathode fall of 1.0kV are shown in fig 4.23. Since the E-field next to the cathode is then larger, the electrons are accelerated more rapidly and excitation begins closer to the cathode. The production rates for all levels are seen to peak close to the cathode, although the peaks are again sharper for the production of triplet states. In all cases, the production rates are higher in the region immediately next to the

cathode than at the CDS/NG boundary.

In a glow discharge, the intensity of the emission lines originating from those levels shown in fig 4.22 and fig 4.23 are directly proportional to the population of these levels, and therefore to the production rates. Cascade pumping of certain levels from higher states is important if there is significant recombination in the plasma, as shown in fig 3.21. A calculation of the cascade contributions to the levels shown in fig 4.22 from higher levels (which themselves are pumped by direct electron impact) has not been carried out here. However, if cascade pumping of these levels is small compared with the production rates shown, then good qualitative agreement is obtained with the observed emission profiles shown in fig 3.19. As the Cathode fall is raised to around 1.0kV, it is observed experimentally that the Cathode glow region becomes more prominent in comparison with the glow intensity at the CDS/NG boundary. Emission lines corresponding to transitions between triplet states are observed to be significantly more intense in the Cathode glow that at the CDS/NG boundary. Therefore, it seems likely that the Cathode glow region is generated mainly by the electron flux from the cathode. If the production of excited species in the CDS by the flux of ions from the NG is important, the production rates are likely to be highest in a region very close to the cathode, where the ions gain most energy from the E-field.

4.4 Electron Motion in the NG

4.4.1 Electron Energy Distribution Functions

The EDEF expected at the CDS/NG boundary or at the start of the NG region has been calculated in the previous section for values of the Cathode fall between 0.15kV and 1.0kV. These are used as the starting EDEF's at the beginning of the NG in the same way as the trapezoid distribution is used at the start of the CDS region. The boundary region is therefore re-defined as the point where x=0. Calculations of the development of the EDEF in the NG are simplified since the E-field is assumed to be zero, and flux redistribution between energy cells in the EDEF is calculated purely from the collision losses. The evolution of the EDEF in the NG has been calculated for ten different values of V_c between 0.15kV and 1.0kV. It has been found that by setting the slab width δx equal to one tenth of the mean free path corresponding to cell E_{kmax} ($\lambda(E_{kmax})/10$), computation times became excessive to achieve a final state whereby all cells have a flux density less than 10^{-6}. To overcome this problem, at a distance into the NG when the total ionisation rate is found to have decayed to a value less than 2% of the maximum value, δx is increased by a factor of ten to equal $\lambda(E_{kmax})$.

The development of the EDEF in the NG for V_c=0.2kV is depicted in fig 4.24. It is evident that electron flux from the primary group and 'tail' group of cells decay at about the same rate. Only the low energy cells around 30eV gain flux. This is because the impact

cross-sections for electrons with energies between ~0.1keV and ~0.2keV are roughly the same. More interesting behaviour is predicted for the development of the EDEF when the Cathode fall is 1.0kV as shown in fig 4.25. At the boundary region when p.x=0, the EDEF contains flux principally in the primary component with a small 'tail' component. Further into the NG, this primary component loses flux to lower energy cells in the 'tail' group to generate a broader secondary peak about 25eV below that of the primary. Further peaks are observed at yet lower energies (separated by ~25eV), but these tend to merge together to produce a broad hump in the EDEF which shifts toward lower energy, whilst at the same time broadening, as the 'swarm' penetrates further into the NG.

For a depth factor (p.x) of 5.0 mb.cm, the EDEF is remarkably similar to the EDEF measured in the NG experimentally by Yu et-al [27], and the two distributions are shown in fig 4.26 for comparison. The similarities are discussed further in section 4.4.3.

4.4.2 Ionisation and Excitation Rates in the NG

The production rates of ions and excited atoms in the NG region can be calculated using the expressions applicable to the CDS (eq.4.18) with the lower limit of the sum reset to count from k=25. The respective production rates are shown in fig 4.27 and for a given value of the Cathode fall, both rates show similar behaviour with increasing distance p.x. However, the ionisation rates (fig 4.27a) decay slightly more rapidly with distance than do the excitation rates (fig 4.27b). For low values of V_c, ionisation and excitation appear to be confined to a region close to the cathode. These curves peak at

the CDS/NG boundary at p.x=0 and decay within a distance of a few mb.cm. As the Cathode fall is raised, the curve profiles extend to larger values of p.x with a plateau region forming over the initial stages of the development of the 'swarm'. For V_c=1.0kV, both rates actually increase slightly with distance over the initial plateau region and exhibit a small maximum at about 10 mb.cm. After this point, both rates decay to approach the x-axis asymptotically. Thus, the character of the NG changes as V_c is increased. For a low Cathode fall, ionisation and excitation are centred mainly at the CDS/NG boundary. As V_c is raised, the production rates become more uniformly spread with only a small maximum located well into the NG.

A plateau region in ion production for V_c=1.0kV leading to a region in the NG with a uniform ionisation rate is a useful property of the high voltage glow discharge in helium. It is likely to be at least partly responsible for the improved efficiencies achieved with longitudinally pumped e-beam lasers (fig 1.11) [28]. A region with more uniform ionisation can be envisaged using two cathodes set to ionise the same region of gas as shown in fig 4.27a (inset). This type of geometry is investigated further in Chapter 5.

4.4.3 Electron Ranges and the Length of the NG

It is difficult to assign precise values to the overall length of the NG owing to the asymptotic behaviour of the ionisation and excitation rates as they approach the x-axis. This is borne out by experimental observations where the NG/FDS boundary normally appears very diffuse. Cut-off points may be assigned to the curves in fig 4.27 using various criteria, but are calculated here from the

gradient of the curve at its inflection point on the final downward trend. The point at which the gradient intercepts the x-axis is the 'extrapolated range' X_o (cm) [29]. These ranges are therefore calculated assuming an origin (x=0) at the CDS/NG boundary. The intercept points have been determined for values of V_c between 0.15kV and 1.0kV and are shown in fig 4.28. The ranges are proportional to the gas temperature T (K) as a multiple of the absolute temperature T_o=273K , and to the reciprocal of the gas pressure. Therefore, the ordinate is scaled as $X_o.p.\frac{1}{T}$ (mb.cm.K^{-1}). The ranges calculated from the ionisation curves can be fitted to a simple power law:

$$X_o(i) = \frac{T}{p}. q V_c^r \qquad (4.19a)$$

where r=1.548 , $q=8.409.10^{-2}$ and V_c is in kV.

The ranges $X_o(ex)$ calculated from the excitation curves are slightly larger, particularly at low V_c, and can be fitted to the following expression:

$$X_o(ex) = \frac{T}{p}. q(V_c^r + sV_c + t) \qquad (4.19b)$$

where $s=8.89.10^{-3}$ and $t=3.42.10^{-2}$

There have been a number of other studies of electron ranges in the NG of a helium discharge at a few mb with Cathode falls up to 1-2kV. These are invariably measurements of the total length of the NG and usually have wide error margins owing to the diffuse nature of the NG/FDS boundary. Brewer and Westhaver report measurements of the length of the NG in helium with Cathode falls in the range 0.2-1.0kV based on spectroscopic estimates [30]. Their data is shown in fig 4.29 together with curves calculated from eq.4.19 for T=300K. No

mention is made in this study of gas heating by the discharge current and it is unclear whether the gas pressures have been corrected for heating effects. Gas heating effectively reduces the gas density and leads to larger electron ranges. They conclude that the length of the NG is determined essentially by the ranges of the fastest electrons at the CDS/NG boundary, namely, those electrons with energies corresponding to the Cathode fall. Lehmann calculated electron ranges based on measurements of current flow in an ionisation chamber containing helium at 0.1-4.0mb [31]. Brewer and Westhaver observe close agreement between their data and those of Lehmann although no mention is made of the errors in measurement of individual range estimates, which are presumably significant owing to the diffuse NG/FDS boundary. Woolsey et-al investigated electron ranges in a helium NG at 0.7-4.0mb using a magnetic lens arrangement placed around the NG [32]. They conclude that the ranges may be slightly shorter than the visual length of the NG by a factor of up to 1/3 under some conditions. Using eq.4.19, this is predicted to be the case for low values of Cathode fall when the ratio $X_o(i)/X_o(ex)$ is equal to 0.6 for V_c=0.15kV and 0.7 for 0.2kV. In section 4.4.1, good agreement has been found between the calculated EDEF profile in the NG for V_c=1.0kV at a distance p.x = 5.0mb.cm and the experimental profile reported by Yu et-al [27]. The latter EDEF has been recorded at a sample point 17 cm from the cathode face with p=1.07mb corresponding to an apparent distance of p.x=18.2mb.cm. To make a valid comparison between the two EDEF's, the experimental ranges must be corrected for gas temperature variations in the discharge which have not been reported by Yu et-al. In this case, they are likely to be significant since the cathode used is concave to focus the electron flux into a narrow beam, and the discharge is run at 300mA. An average temperature of 900K necessary

to bring the two ranges into agreement does not seem unreasonable for such discharge conditions.

4.5 Efficiency of Ion Production in a Helium Discharge

Electron/ion pairs are generated in the NG by the e-beam flux from the cathode which can therefore be taken as a source term S(ions.s^{-1}) for ionisation. Ions are lost from the NG by a number of mechanisms and the rate of change of ion density n_i with time can be expressed as:

$$\frac{dn_i}{dt} = + S - \underbrace{(-D_i \nabla^2 n_i + \alpha_r n_i n_e + \beta_{ct} n_m n_i + \text{to cathode})}_{\text{loss terms}} \qquad (4.20)$$

The rate of change is normally zero representing a state of stable equilibrium. and the source term is then exactly balanced by the loss terms. The first loss term represents the rate of diffusion of ions which is always in a direction of decreasing ion density, proportional to the density gradient and to the ion diffusion coefficient D_i. Volume recombination is represented by the second term, where the coefficient α_r encompasses radiative, dielectronic, and collisionally assisted recombination. The recombination rate is proportional to both the ion density n_i and the density of slow electrons n_e, and recombination at the vessel walls is of course the final stage of the diffusion process. Strictly speaking, the third term, representing loss through asymmetric charge transfer, is not a loss term for ions, but only for helium ions. It is dependent on the density of metal atoms n_m, and on the charge transfer coefficient β_{ct}. This third

term is the most important with regard to generating laser action from a metal vapour, and its possible enhancement in relation to the other loss terms must therefore be examined carefully. The fourth term represents the ion flux toward the cathode which is necessary to maintain the discharge current.

For a discharge to act as ion source in a charge transfer laser, the third term in eq.4.20 must be optimised and the other loss terms reduced as far as possible, so that helium ions are used to generate M^{+*} ions. The metal density n_m may be raised initially, but cannot be increased indefinitely without affecting the stability of the discharge. This is due to the low ionisation potential of the metal atoms compared with helium. Alternatively, a high ion density n_i is required. but this also enhances the other loss rates unless steps are taken to reduce them individually. Diffusion can be inhibited to some extent by applying a longitudinal magnetic field around the discharge vessel to keep the plasma away from the vessel walls, resulting in a larger ion density gradient. Such a scheme has already been discussed in Chapter 1. For a fixed source term, losses to the cathode may be reduced by using a cathode with a large coefficient for secondary emission. In this case, fewer ions are needed to maintain the overall discharge current. Diffusion and recombination losses in a helium discharge have been discussed by Persson [20] and Franck [33]. Yu et-al have examined the balance between charge transfer losses and recombination losses in a Helium/Mercury laser for both transverse and longitudinal e-beam generated plasmas [14].

Little attention has been paid to the source term S, to ascertain whether ions may be generated more efficiently under certain discharge conditions. This overall efficiency is important because low ionisation efficiencies result in larger input power levels to

maintain the necessary ionisation rate S, and unwanted heat production in the vessel. The source rate is clearly directly proportional to the electron flux, but not necessarily to the electron energy. If a single electron with energy E_k' is identified at the CDS/NG boundary, and followed through the NG, the total number of ions generated N_i during its lifetime and by secondaries in the cascade can be calculated. The quantity E_k'/N_i therefore represents the average energy $W(E_k')$ required to generate an ion/electron pair and is given by:

$$W(E_k') = E_k'/N_i = E_k' \left[\sum_{x=0}^{all\,x} \left(\sum_{k=1}^{k_{max}} \delta j_{ion}(x, E_k) \right) \right]^{-1} \qquad (4.21)$$

where x=0 is defined as the CDS/NG boundary. The form of $W(E_k')$ for increasing E_k is shown in fig 4.30 together with the results of Miller [7]. It is seen that the energy spent in generating an ion/electron pair falls with increasing energy E_k'. The efficiency of ionisation is defined as $I_o/W(E_k')$ and is shown in fig 4.31. This quantity is not to be confused with the ionisation efficiency which is defined simply in terms of the ionisation cross-section of the gas [19]. Thus, ions are more efficiently generated by electrons with energies above 1keV.

In a real discharge, electrons at the CDS/NG boundary have a range of energies. For an initial flux of N electrons per second leaving the cathode in a discharge with a Cathode fall of V_c, the discharge current may be determined from the size of the multiplication coefficient at the boundary $M(d_c)$, where it is a reasonable approximation to assume that the discharge current is carried principally by the electron flux. Thus, the power into the discharge is given by $P = V_c.N.e.M(d_c)$ (Watts). The number of electron/ion pairs generated by this electron flux can be calculated

from the ionisation rates given in fig 4.20 and fig 4.27a. The number of ions W_i generated per Watt of input power, and therefore the ion production rate, is given by:

$$W_i(V_c) = \frac{N\left(p \sum_{x=0}^{\text{all}x} (\alpha_i(x)/p)\delta x\right)}{V_c . N . e . M(d_c)} \qquad (4.22)$$

where x=0 is defined from the cathode face.

This is shown in fig 4.32 which gives the separate contributions from ion production in the CDS and from the NG. It is shown that ion production rate in the CDS and NG are roughly equal for a 'normal' discharge with a Cathode fall of 150V. For a discharge operating well into the 'abnormal' regime with a higher Cathode fall, the majority of the ions in the discharge are generated in the NG region. It is concluded that ions are generated more efficiently for higher values of the Cathode fall and indeed, the curve of $W_i(V_c)$ is still rising for the largest value of V_c investigated. This is an important result, and increased efficiency for the production of ground state helium ions is probably one of the reasons why high voltage HCD's show improved lasing characteristics over ordinary hollow cathode devices. Therefore, e-beam plasmas are particularly well suited for metal vapour/helium lasers in which charge transfer is the principal pumping mechanism.

4.6 Plasma Processes in a Perforated Cathode

The increase of the current density generated by an e-gun cathode compared with that produced by a plane cathode implies that the secondary emission processes at the cathode are more efficient in the e-beam discharge. The expected perturbation of the equipotentials in the CDS around the hole aperture of an e-gun cathode is shown fig 3.16b. The separation of the equipotentials in the cavity are larger than at the cathode face, so the electric fields in the cavity are lower than at the cathode face. Those equipotentials which mark the extent of the Cathode glow region are shown schematically in fig 4.33. The internal glow in the cavity may therefore represent an extended region of Cathode glow, in agreement with visual observations of this internal glow. The properties of the internal Cathode glow are therefore likely to be similar to those of the external Cathode glow. Species generated in the Cathode glow at the cathode face are therefore expected to be produced to some extent by the same mechanisms in the internal glow. Such species are then trapped by the cavity. Compared with those generated in the external Cathode glow, they are less likely to be lost via diffusion, and have a higher probability of striking the cathode to release more secondary electrons. This is partly the basis for the 'hollow cathode effect' as discussed by Francis [11].

The production of excited species in the Cathode glow of a plane cathode is calculated to become more important as V_c is raised, as shown in fig 4.23. Such species when generated in the internal Cathode glow of an e-beam discharge emit UV photons as they decay which can release secondary electrons from the cathode walls. Ion and metastable production in the Cathode glow of a plane cathode also

become more important as V_c is raised, as shown in fig 4.34. If generated in the internal Cathode glow, they are also trapped by the cavity.

An increase of the effective secondary electron emission coefficient for processes in the hole cavity can also be attributed the motion of particles normally incident on the cathode face. If these particles pass into the cavity, they are likely to make glancing angle impacts at the cathode walls, and it is known that the coefficient for such impacts is larger than for collisions at normal incidence [34]. The flux of particles incident on the cathode face have been examined by Davis and Vanderslice using an electrostatic energy analyser and a magnetic mass analyser, sampling species through a pinhole in the cathode [23]. They demonstrate that the energy distribution of rare gas ions present at the cathode face is in close agreement with a simple theoretical model of ion motion in the CDS. This model assumes that ions originate in the NG, and progress through the CDS with their motion determined by a large number of symmetric charge transfer collisions of the type:

$$He^{+}_{fast} + He_{slow} \geqslant He_{fast} + He^{+}_{slow} \qquad (4.23)$$

Few ions are found to reach the cathode with energies comparable with eV_c. As V_c is increased, however, and $p.d_c$ decreases slightly, higher ion energies are detected at the cathode, and a larger proportion have energies close to eV_c. It is also suggested that ionic species such as He^{++} and He_2^+ pass through the CDS without suffering multiple charge transfer collisions, and are observed at the cathode with energies close to eV_c. The presence of relatively large numbers of He_2^+ ions, with energies much less than eV_c, have been observed also by Davis and

Vanderslice. They suggest that they are generated in a region very close to the cathode by the process:

$$He^{*} + He \geqslant He_2^{+} + e \qquad (4.24)$$

where He^{*} is a metastable state.

This observation ties in well with the calculated peak of the metastable production rate shown in rig 4.34. Therefore, such ions may be produced in the internal Cathode glow also.

In summary, secondary emission processes are more efficient for e-gun cathodes than for plane cathodes. This may be due to the following processes:

1. The production of species such as He^{+}, He^{*} (metastable), He_2^{+}, and He^{*} (giving UV photons) occurs in an extended Cathode glow region inside the cathode cavity. Such species are trapped within the cavity and eventually collide with the cathode walls to release secondary electrons.
2. Fast ions (He^{+}. He_2^{+}. and He^{++}) from the NG pass into the cathode cavity and release secondary electrons by glancing angle impacts with the cathode walls. Such impacts have higher γ coefficients than do impacts at normal incidence.

References

1. Segur P., Yousfi M., Boeuf J.P., Marode E., Davies A.J. and Evans J.G., 'Electrical Breakdown and Discharges in Gases', Part A, pp 331-395 (1981)
2. Emeleus K.G., J.Phys.D., 14, 2179 (1981)
3. Emeleus K.G and Coulter J.R.M., J.Phys.D., 16, 2181 (1983)
4. Emeleus K.G., Int.J.Electron., 36, 1 (1974)
5. Ohuchi M. and Kubota T. J.Phys.D., 16, 1705 (1983)
6. Boeuf J.P. and Marode E., J.Phys.D., 15, 2169 (1982)
7. Miller W.F., Dissertation Thesis, Purdue University, USA, (1956)
8. Gill P. and Webb C.E., J.Phys.D., 11, 245 (1978)
9. O'Neill F.. 'Physics and Technology of High Power E-beam pumped KrF* Lasers', (unpublished) Rutherford Appleton Lab, (1982)
10. Gunthershultze A.. Z.fur.Physik 49, 358 (1928)
11. Francis G., 'Handbuch Der Physik', Vol XXII, Springer-Verlag, pp 53-203 (1956)
12. Alkhazov G.D.. Sov.Phys-Tech.Phys., 15, 66 (1970)
13. Massey H.S.W., Burhop E.H.S. and Gilbody H.B., 'Electronic and Ionic Impact Phenomena', Vol I, Oxford University Press, (1971)
14. Yu Z., Rocca J.J., Collins G.J. and She C.Y., Phys.Lett., 96A, 125 (1983)
15. Kagan Y.M., J.Phys.D.. 18, 1113 (1985)
16. Berger M.J. and Seltzer S.M., 'Tables of Energy Losses and Ranges of Electrons and Positrons', NASA report SP-3012 (1965)
17. Labahn R.W. and Callaway J., Phys.Rev., 135, 1539 (1964)
18. Massey H.S.W. and Burhop E.H.S., 'Electronic and Ionic Impact Phenomena'. Oxford University Press, (1952)
19. von-Engel A., 'Ionised Gases'. Oxford University Press, (1965)

20. Persson K.B., J.Appl.Phys., 36. 3086 (1965)

21. Helm H., Beitr. Plasmaphysik, 18, 233 (1979)

22. Carter G. and Colligon J.S., 'Ion Bombardment of Solids', Heinemann (1968)

23. Davis W.D and Vanderslice T.A., Phys.Rev., 131, 219 (1963)

24. Gill P. and Webb C.E., J.Phys.D., 10, 299 (1977)

25. Pringle D.H. and Farvis W.E.J., Phys.Rev., 96, 536 (1954)

26. Tran Ngoc An., Marode E. and Johnson P.C., J.Phys.D., 10, 2317 (1977)

27. Yu Z., Rocca J.J. and Collins G.J., J.Appl.Phys., 54, 131 (1983)

28. Rocca J.J., Meyer J.D. and Collins G.C., Phys.Lett., 90A, 358 (1982)

29. American Institute of Physics Handbook, ed. D.E.Gray, (1972)

30. Brewer A.K. and Westhaver J.W., J.Appl.Phys., 8, 779 (1937)

31. Lehmann J.F., Proc.Roy.Soc., 115, 624 (1927)

32. Woolsey G.A., Reynolds R.M. and Clark L.P., Phys.Lett., 25A, 9, 656 (1967)

33. Franck G., Held R. and Pfeil H.D., Z.Physik 256, 73 (1972)

34. Oliphant M.L.E., Proc.Roy.Soc., A127, 373 (1930)

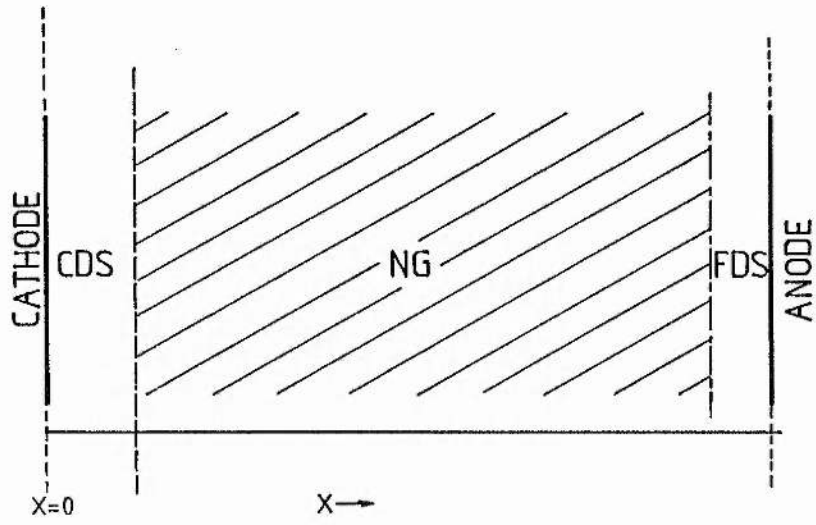

Fig 4.1a. An idealised glow discharge between infinite electrodes with distance X (cm) measured from the cathode.

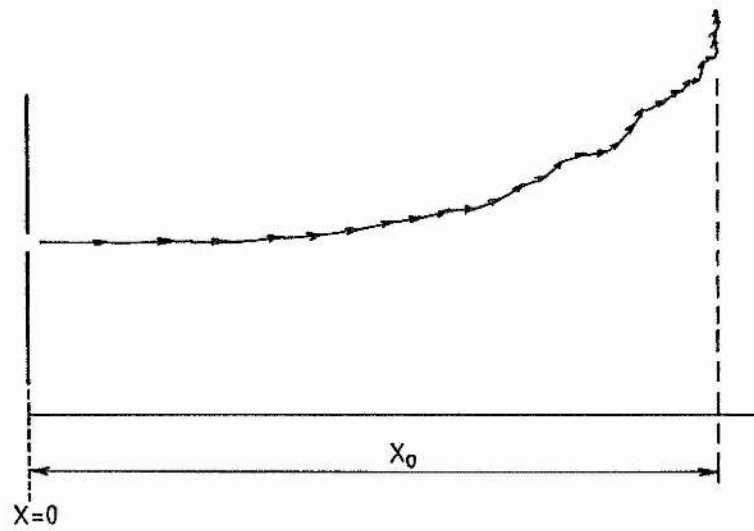

Fig 4.1b. The Straggling effect of the electron trajectory in a gas medium, where X_o denotes the range of the electron.

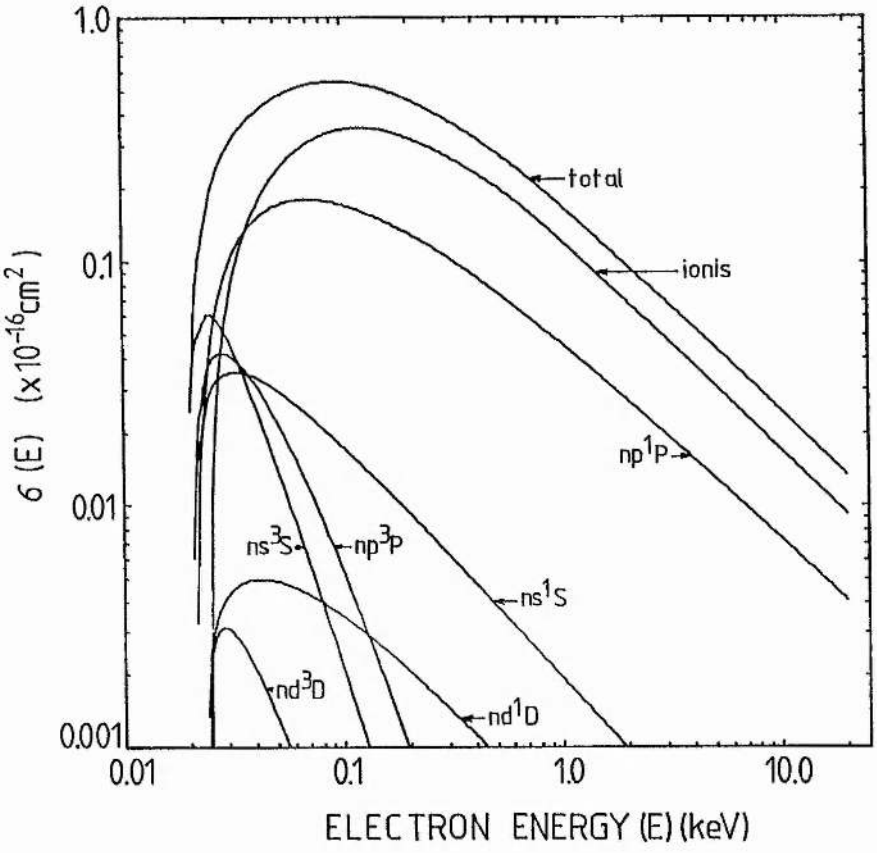

Fig 4.2. The set of inelastic collision cross-sections for helium as used in this study, after Alkhazov [12].

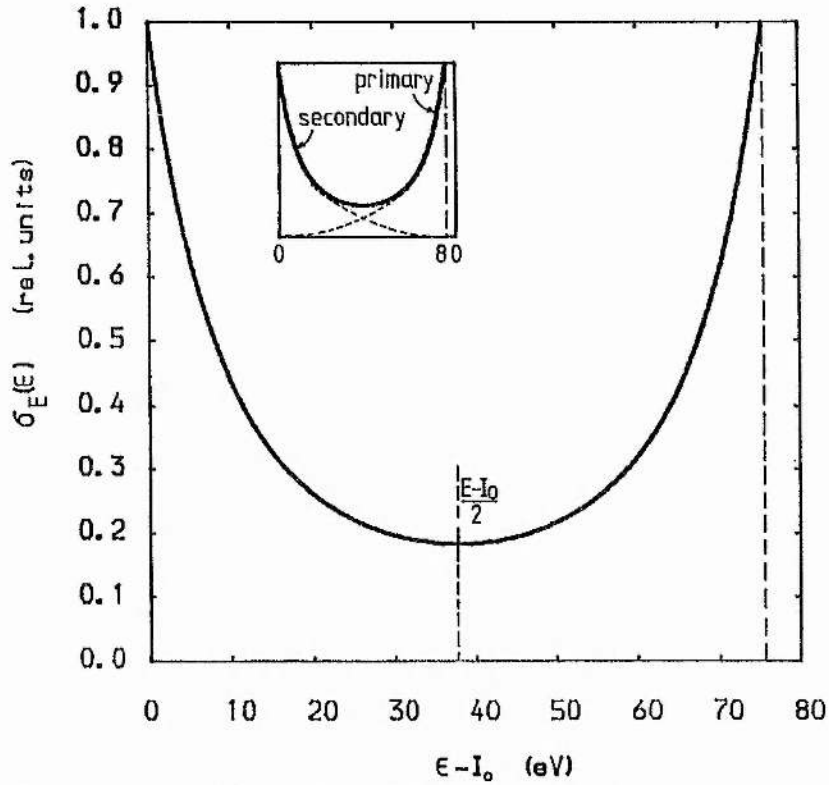

Fig 4.3a. The distribution in energy of the scattered electrons produced in ionising collisions from a primary electron with energy 100eV. The individual probability distributions for the primary and secondary electrons, which are added to give the full symmetrical form of $\sigma_E(\epsilon)$, are shown inset.

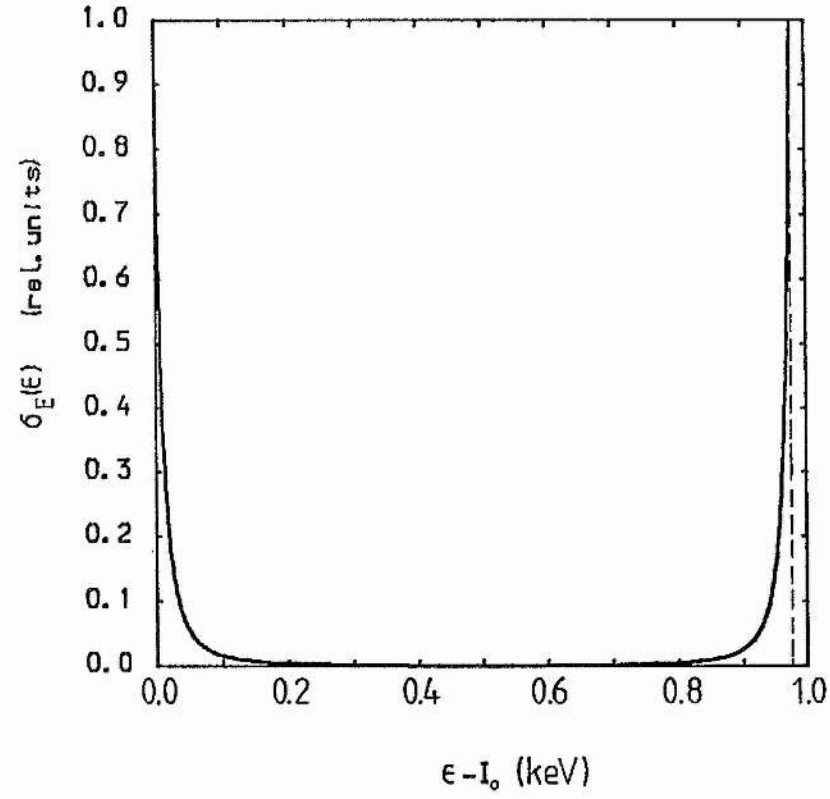

Fig 4.3b. The distribution in energy of scattered electrons generated from a primary electron of 1.0keV.

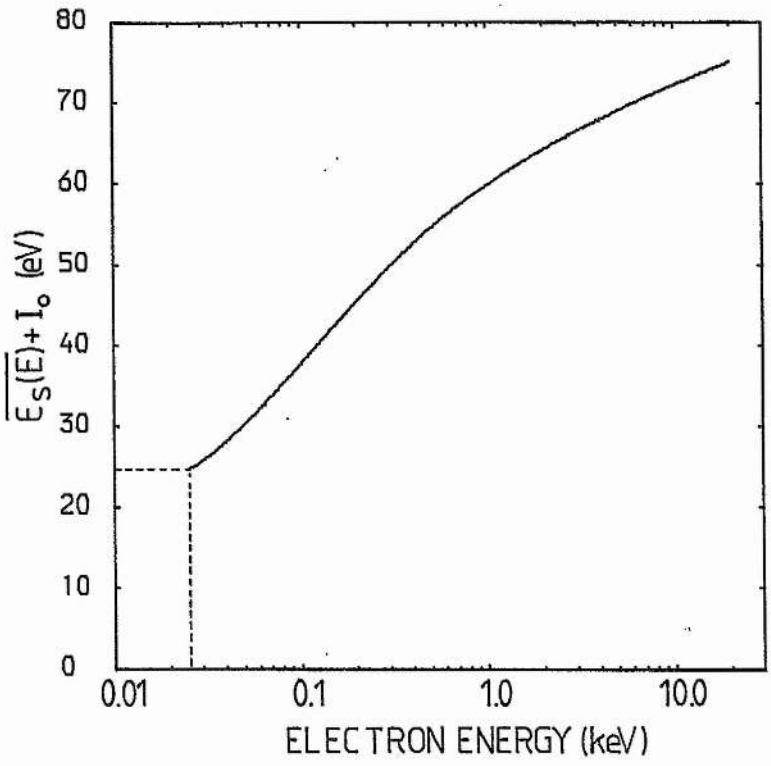

Fig 4.4. The average total energy lost in an ionising collision, as a function of primary energy E.

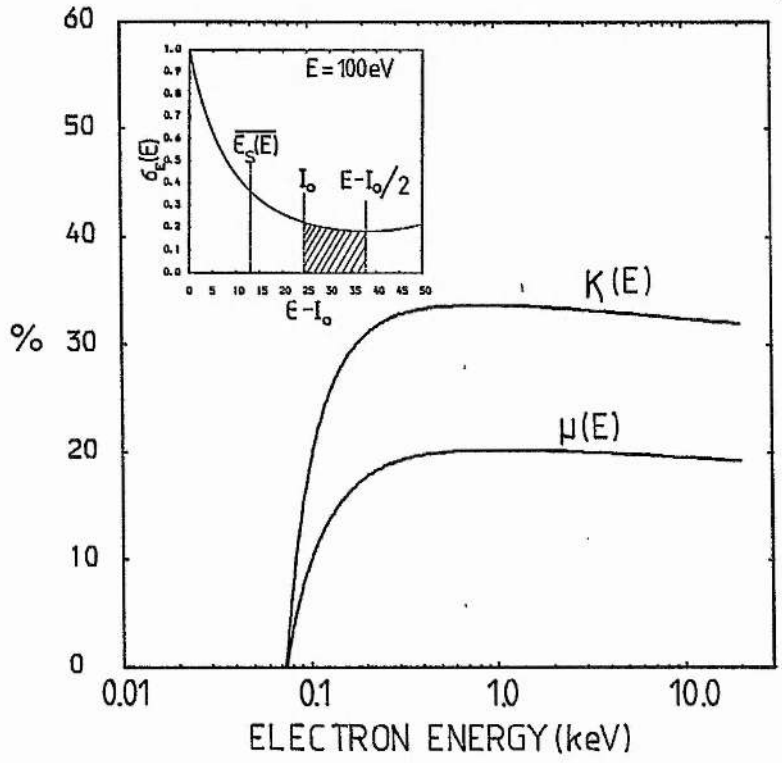

Fig 4.5. The fraction K(E) of electrons in the secondary energy distribution (shown inset) generated with energies greater than I_o. and the fraction μ(E) of secondary electrons derived from an initial electron with energy E which subsequently generate tertiary electrons.

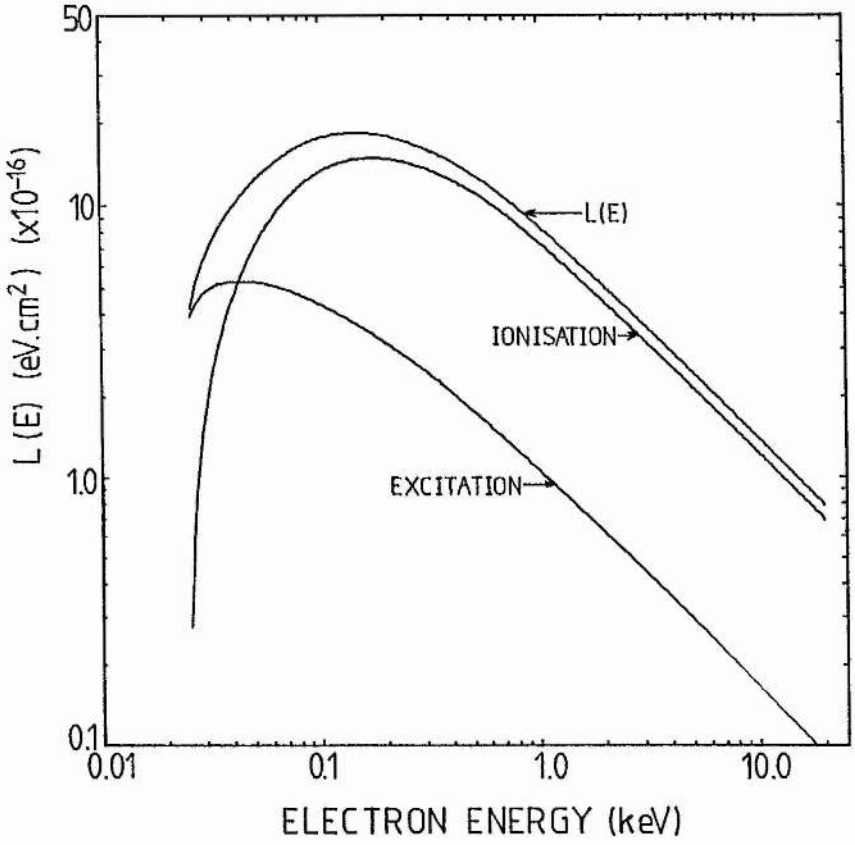

Fig 4.6. The loss function L(E) as a function of electron energy E.

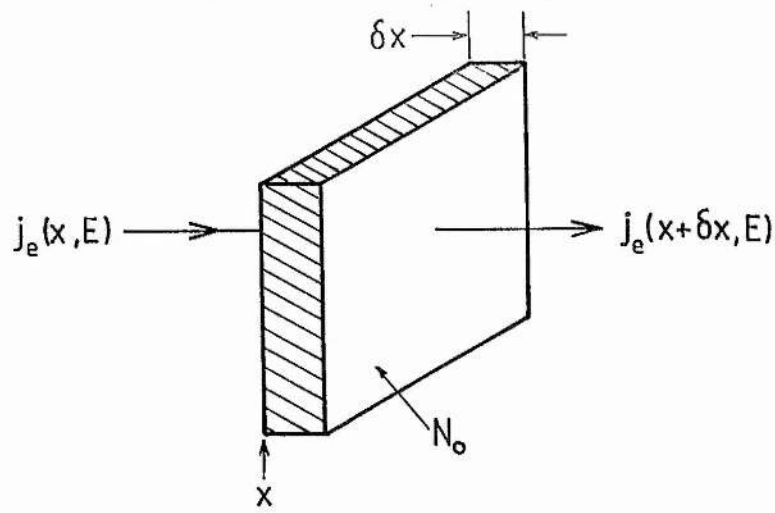

Fig 4.7. The passage of a flux of electrons $j_e(x,E)$ through a slab of gaseous material of width δx and density N_o (cm^{-3}).

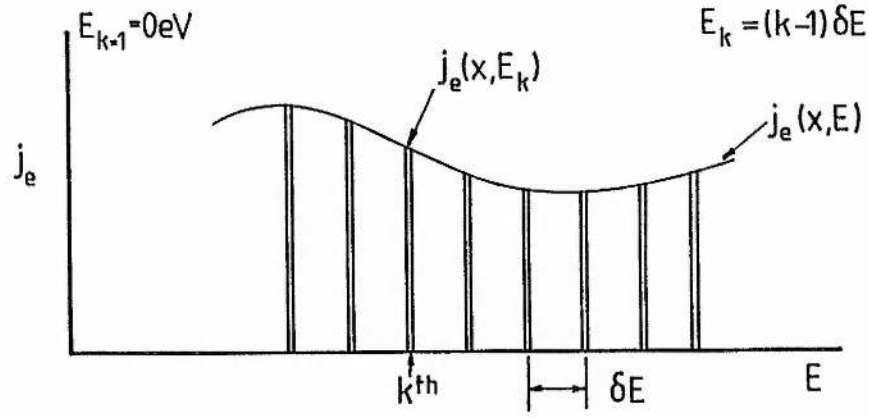

Fig 4.8. The continuous electron energy distribution function $j_e(x,E)$ is divided into a series of separate energy cells with separation δE. Cell populations are described by energy distribution function $j_e(x,E_k)$.

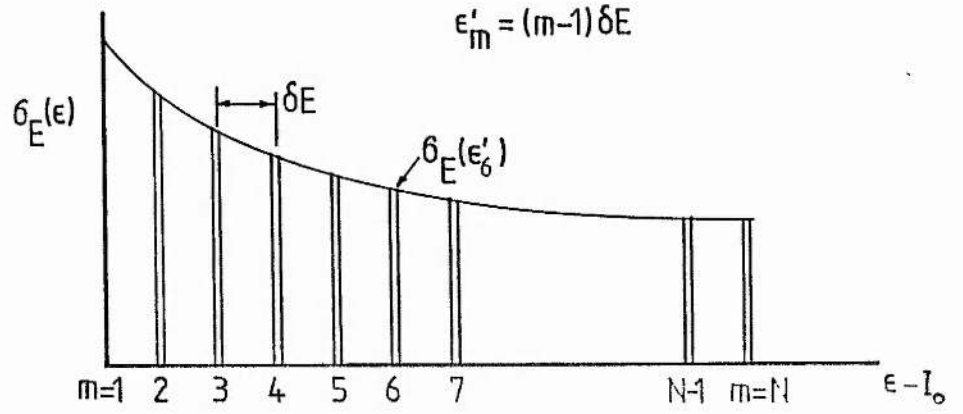

Fig 4.9. The secondary energy distribution function $\sigma_E(\epsilon)$ is divided into a number of separate energy cells, with cell populations described by the distribution function $\sigma_E(\epsilon'_m)$.

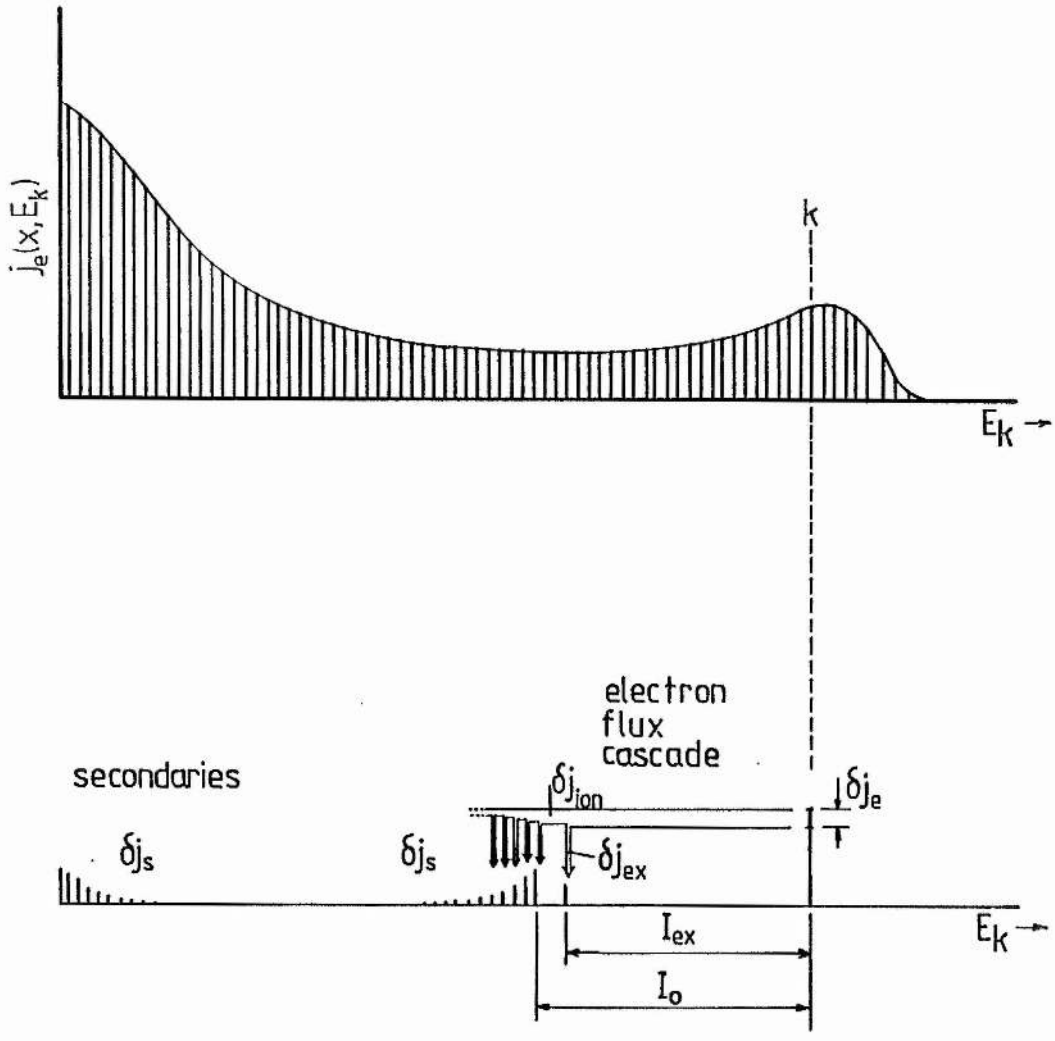

Fig 4.10. The cascade of electron flux from a cell (k) in the distribution function $j_e(x, E_k)$ to cells of lower energy and lower (k) number.

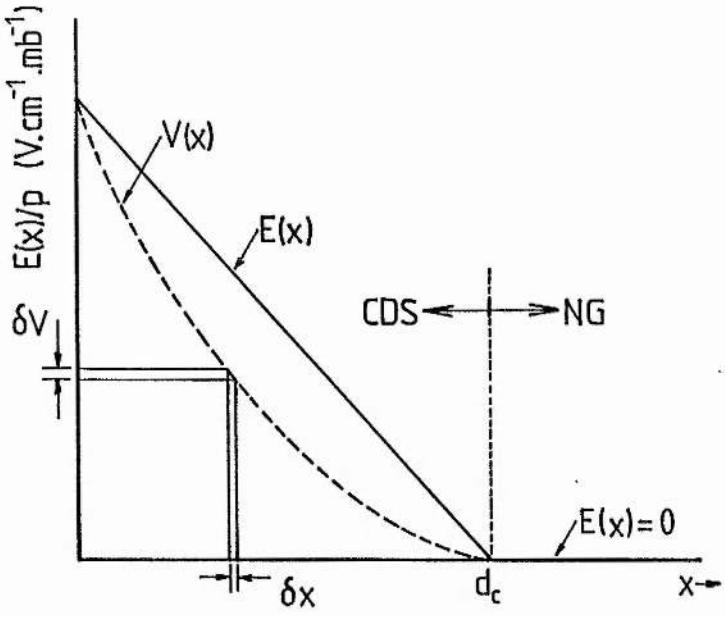

Fig 4.11. The assumed electric field distributions in the Cathode dark space and Negative glow regions.

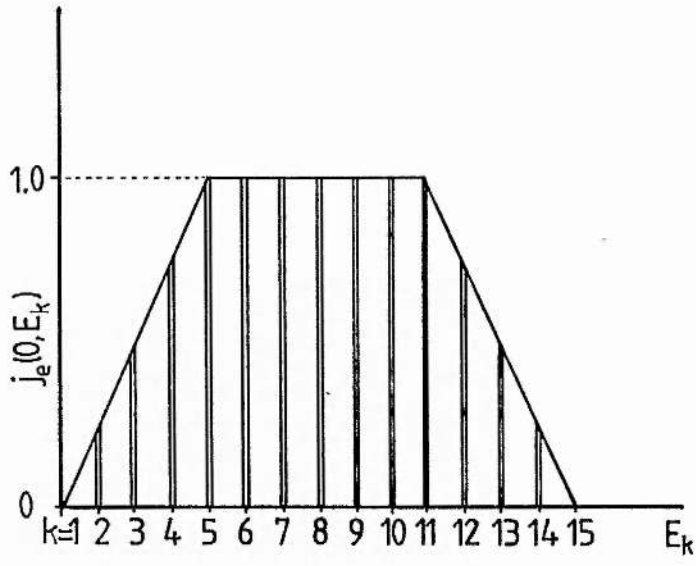

Fig 4.12. The initial trapezoid shaped energy distribution function defined at the cathode. It contains ten units of electron flux.

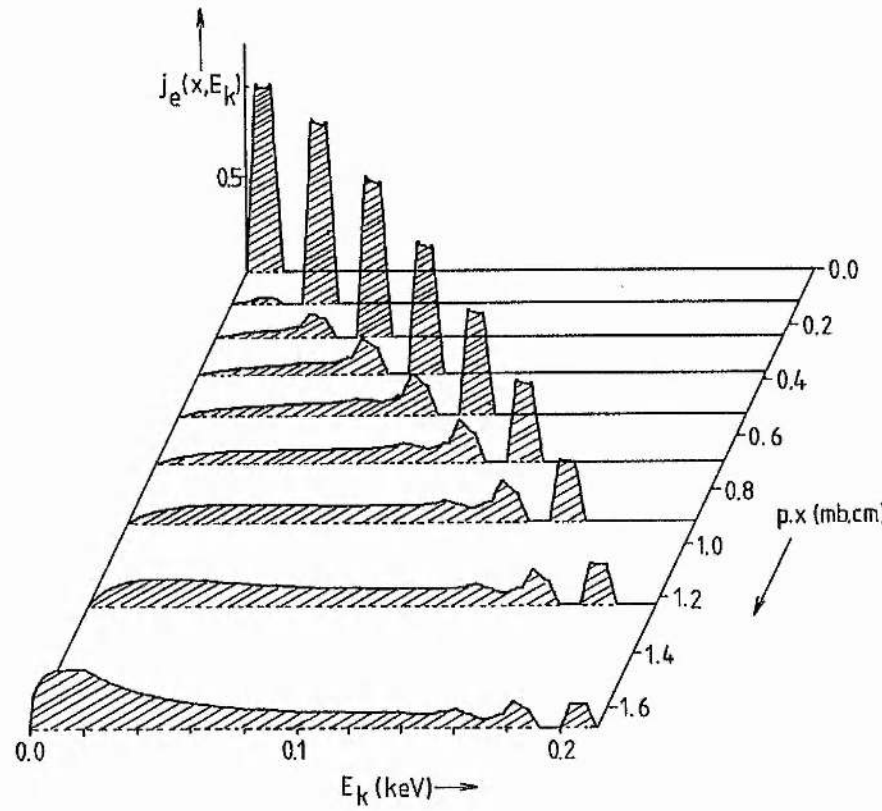

Fig 4.13. The development of the electron energy distribution function in the Cathode dark space for a Cathode fall of 0.2kV.

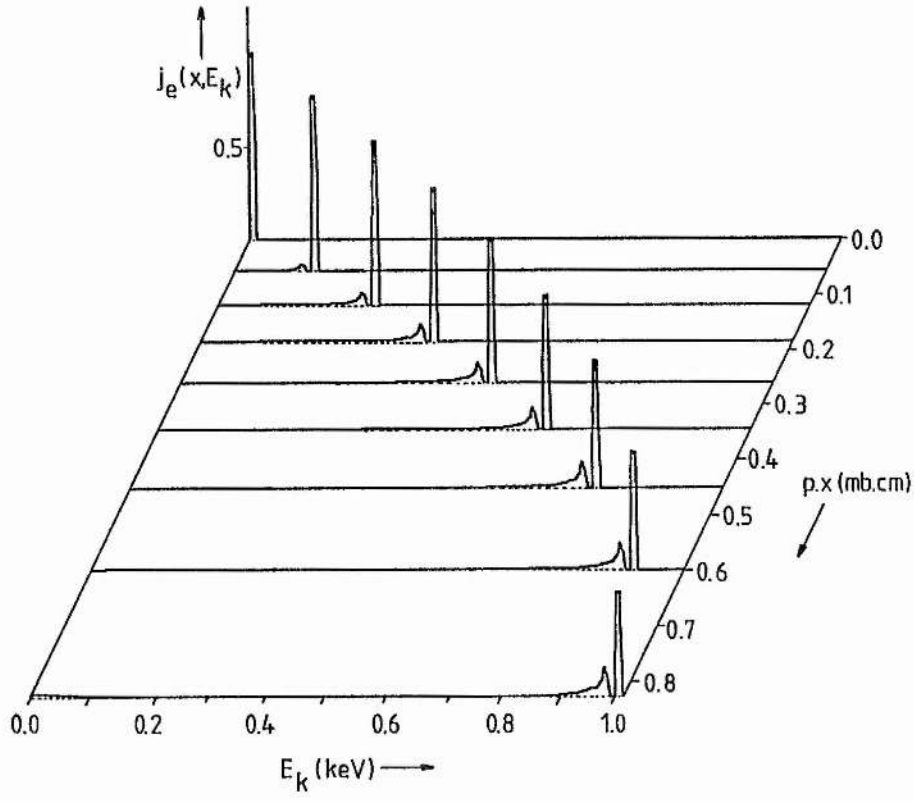

Fig 4.14. The development of the electron energy distribution function in the Cathode dark space for a Cathode fall of 1.0kV.

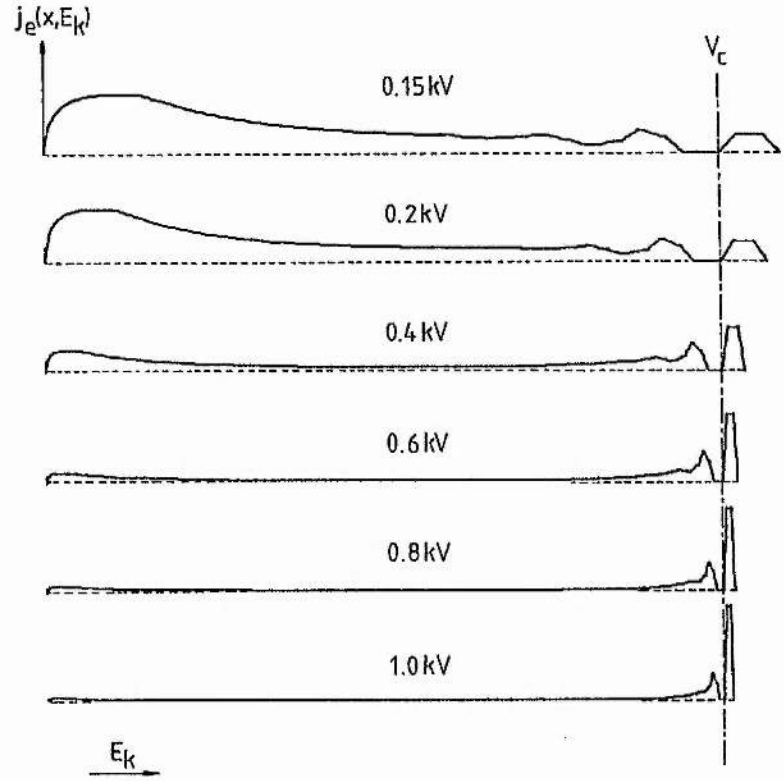

Fig 4.15. The electron energy distribution function at the Cathode dark space/Negative glow boundary, for different values of the Cathode fall.

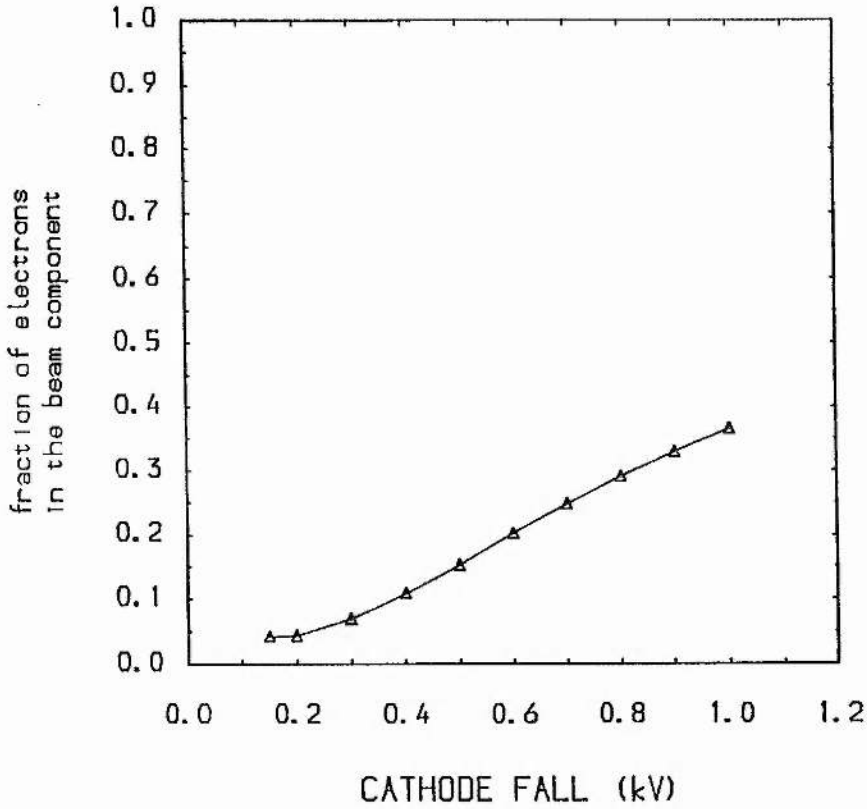

Fig 4.16. The fraction of electron flux in the primary component of the electron energy distribution function, at the Cathode dark space/Negative glow boundary. Electrons in this group traverse the dark space without suffering collisions.

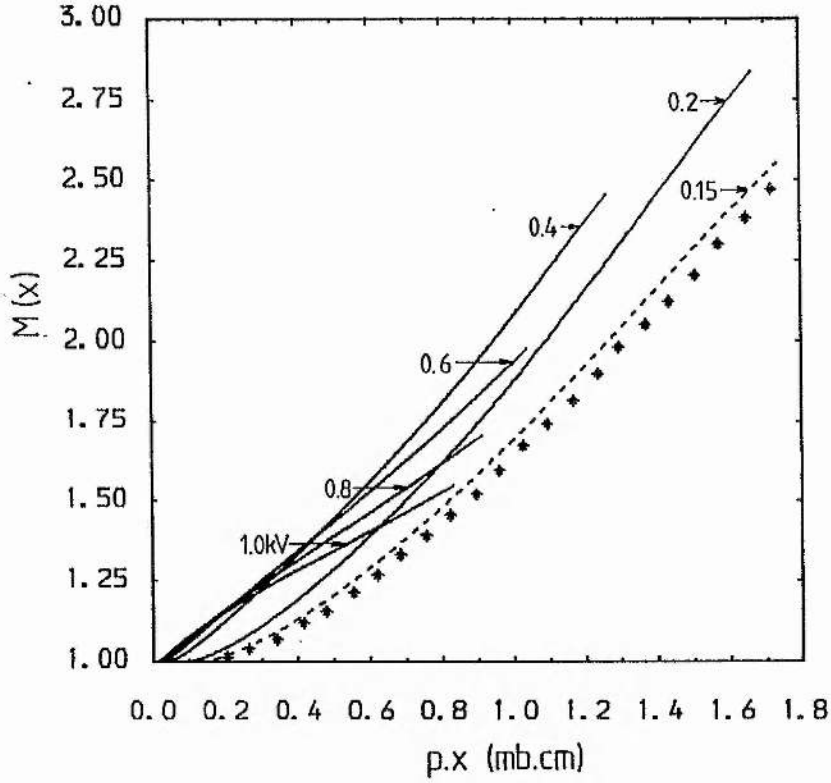

Fig 4.17. The multiplication factor for electron flux in the Cathode dark space, with Cathode fall as a parameter. * : Tran-Ngoc et-al for V_c =0.15kV.

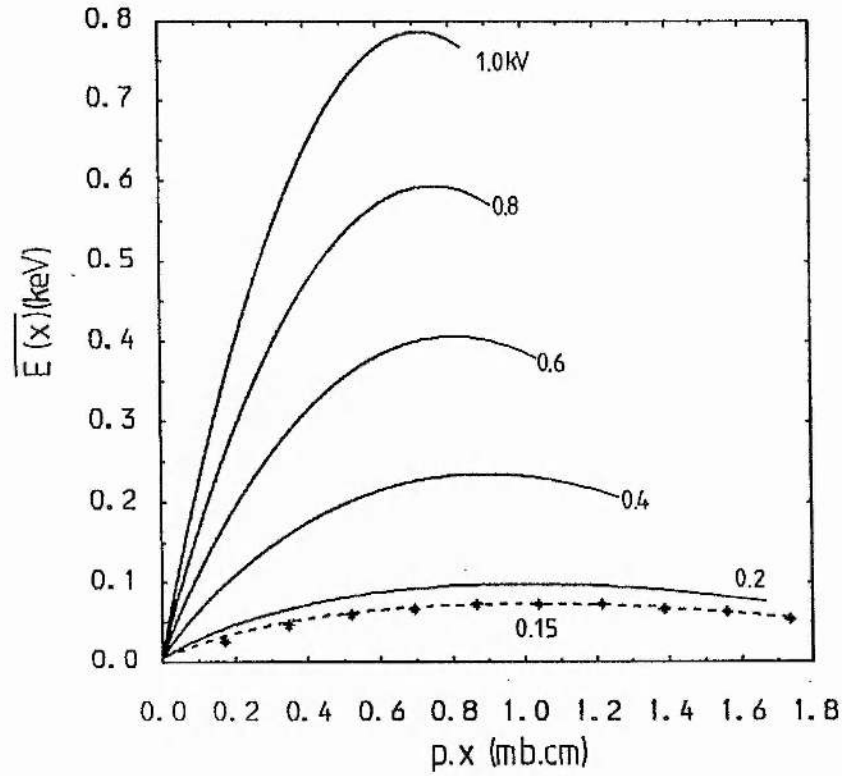

Fig 4.18. The average electron energy in the Cathode dark space for different values of the Cathode fall. * : Tran-Ngoc et-al for V_c =0.15kV.

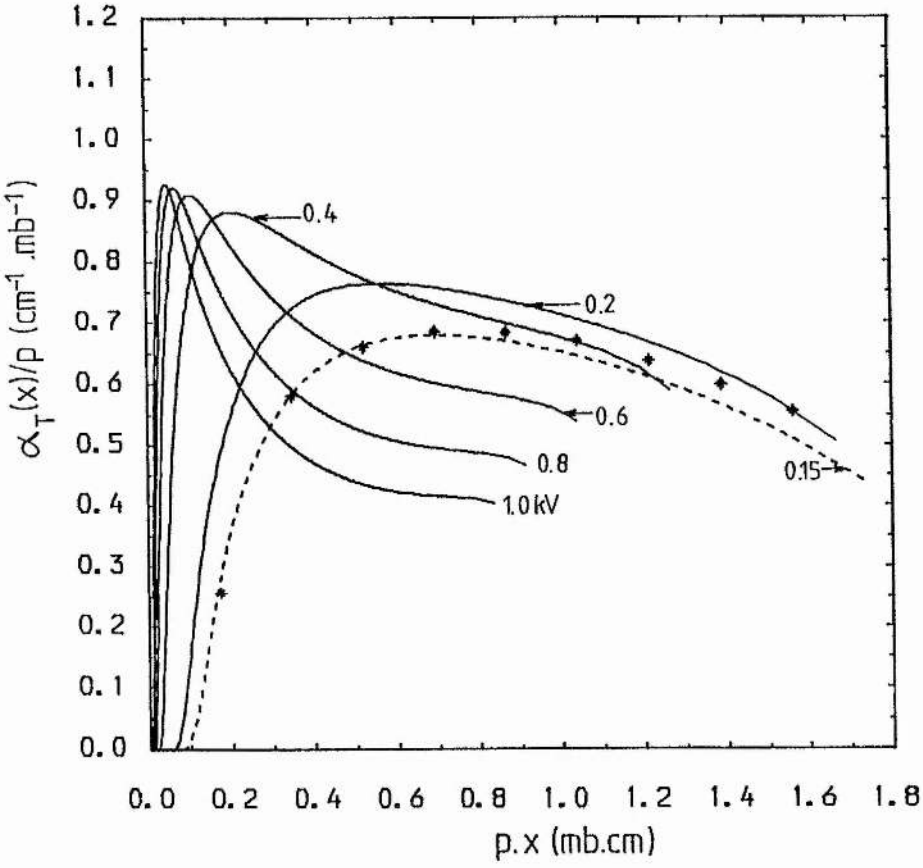

Fig 4.19. The Townsend ionisation coefficient in the Cathode dark space, with Cathode fall as a parameter. * : Tran-Ngoc et-al for V_c =0.15kV.

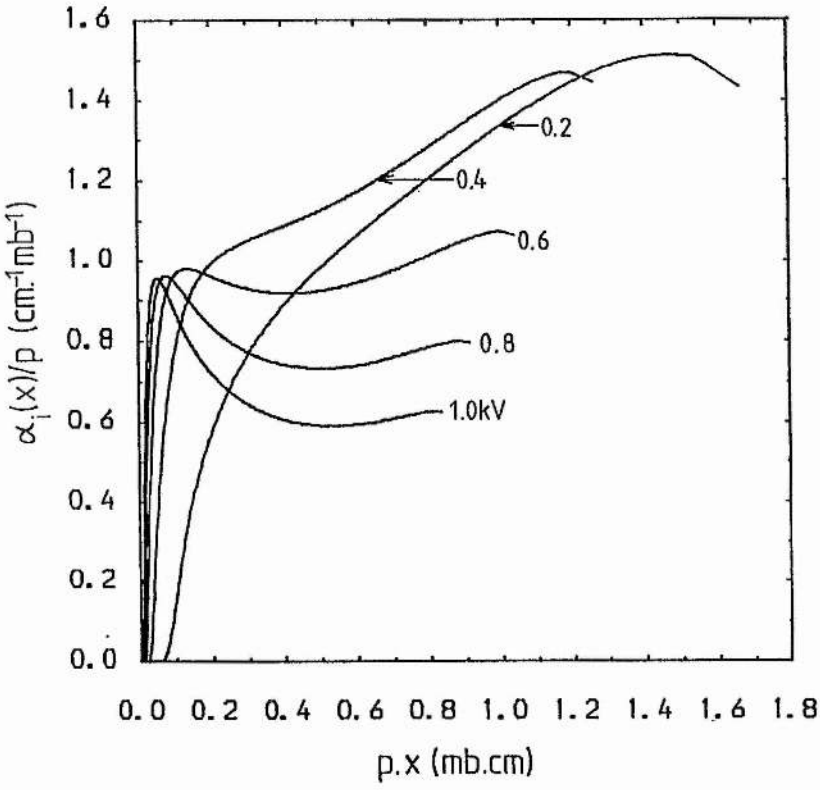

Fig 4.20. The ion production rate in the Cathode dark space for different values of the Cathode fall.

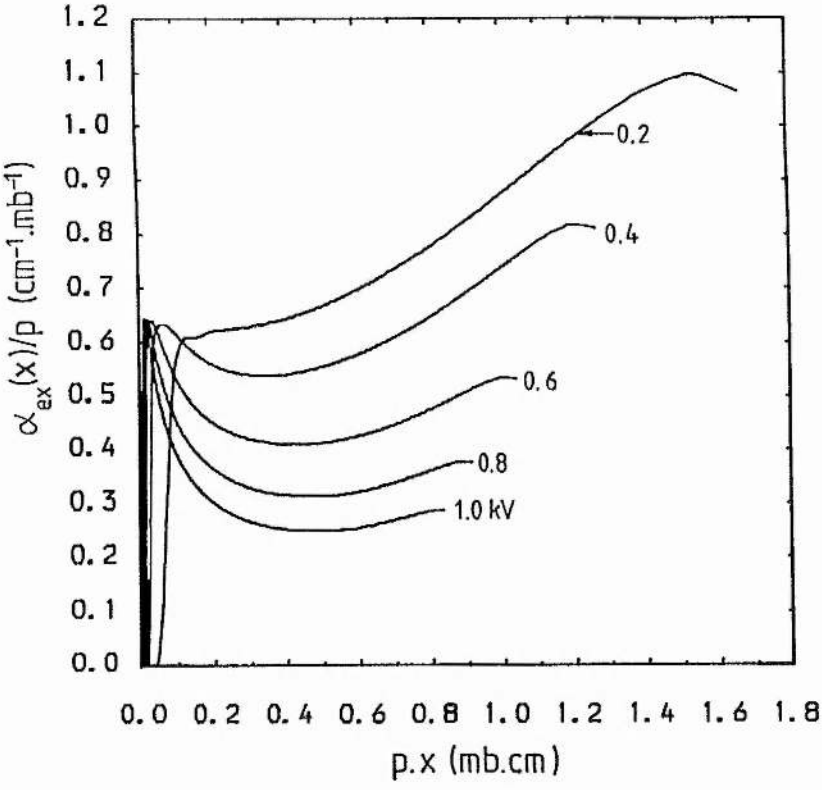

Fig 4.21. The total production rate of excited HeI states in the Cathode dark space, with Cathode fall as a parameter.

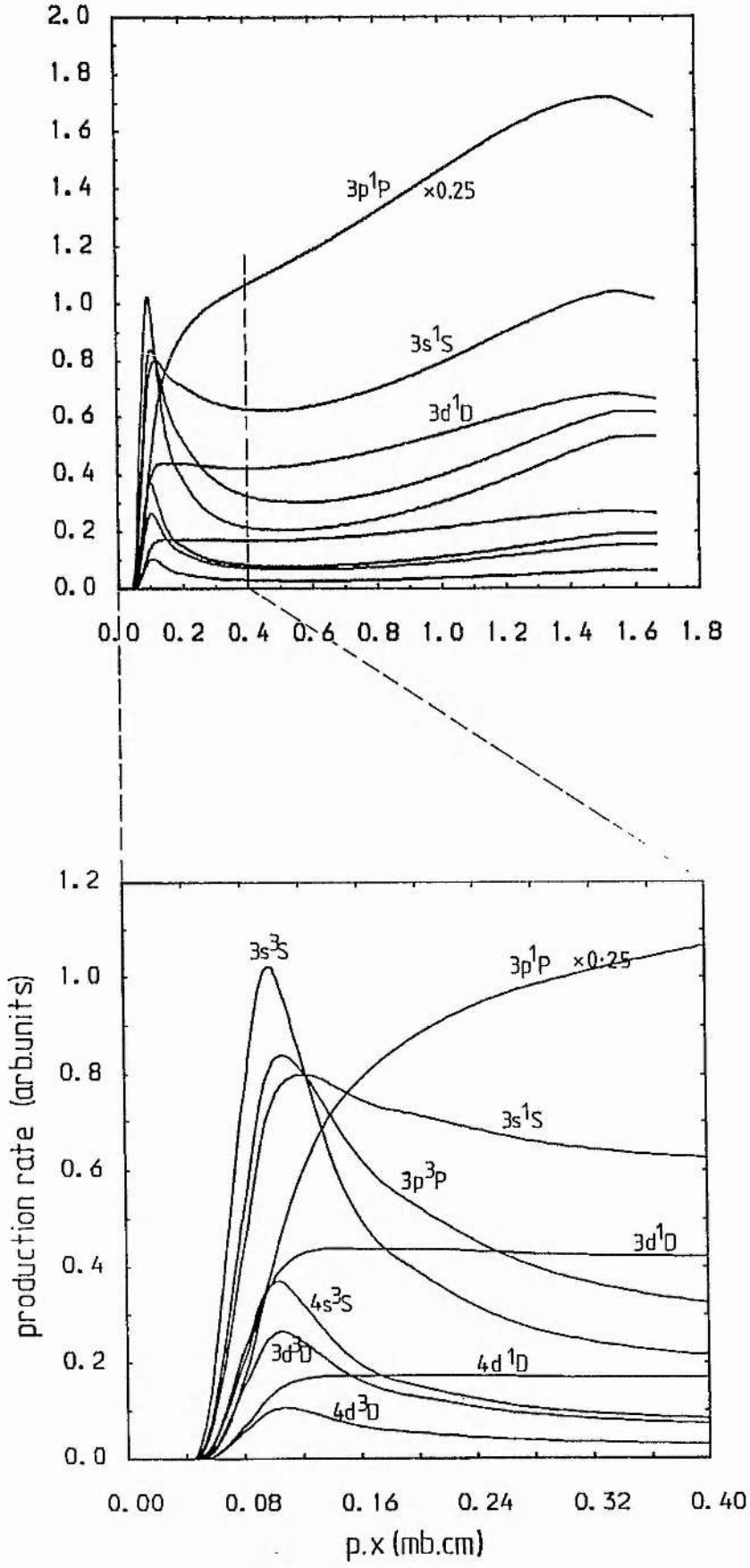

Fig 4.22. Production rates of individual HeI states in the Cathode dark space for a Cathode fall of 0.2kV.

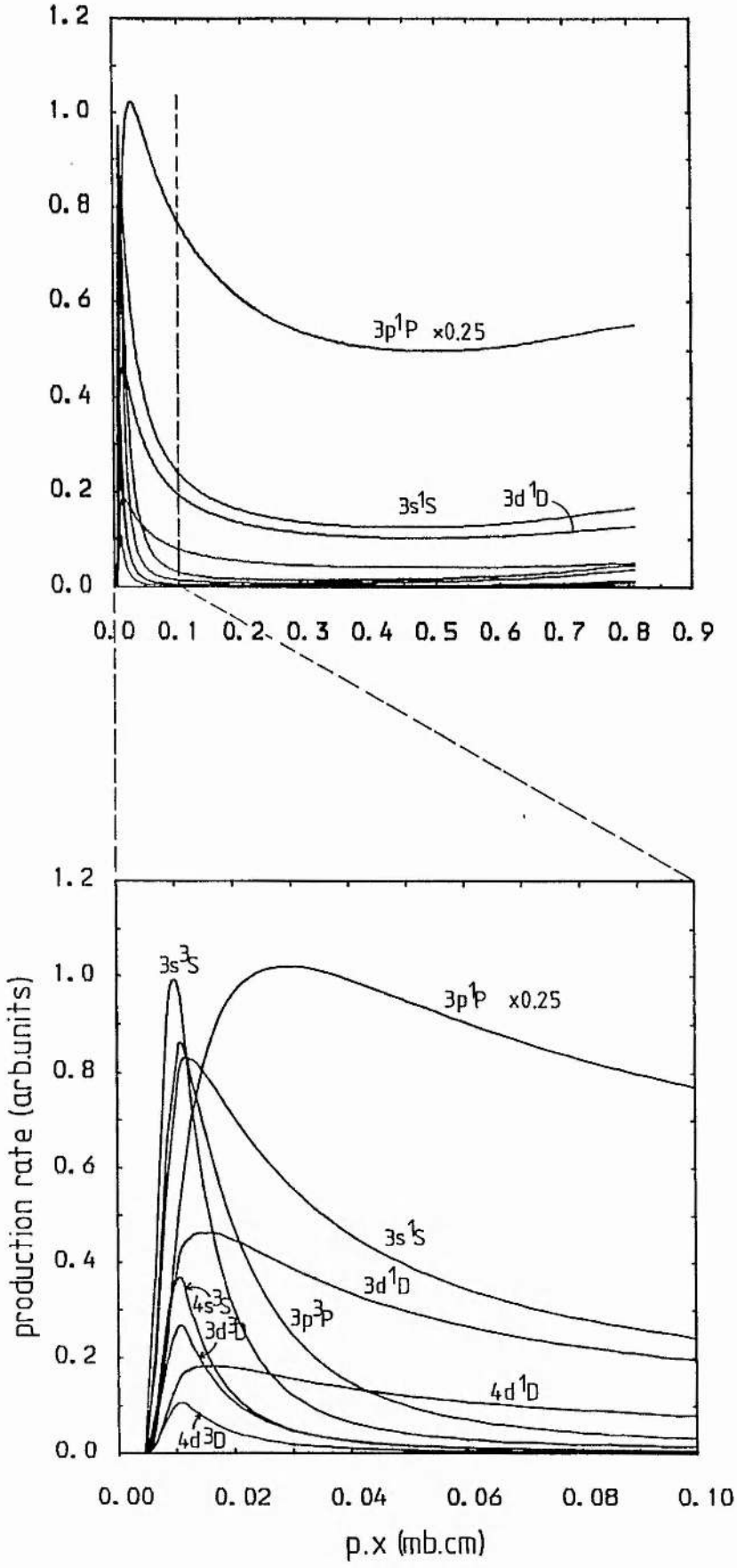

Fig 4.23. Production rates of individual HeI states in the Cathode dark space for a Cathode fall of 1.0kV.

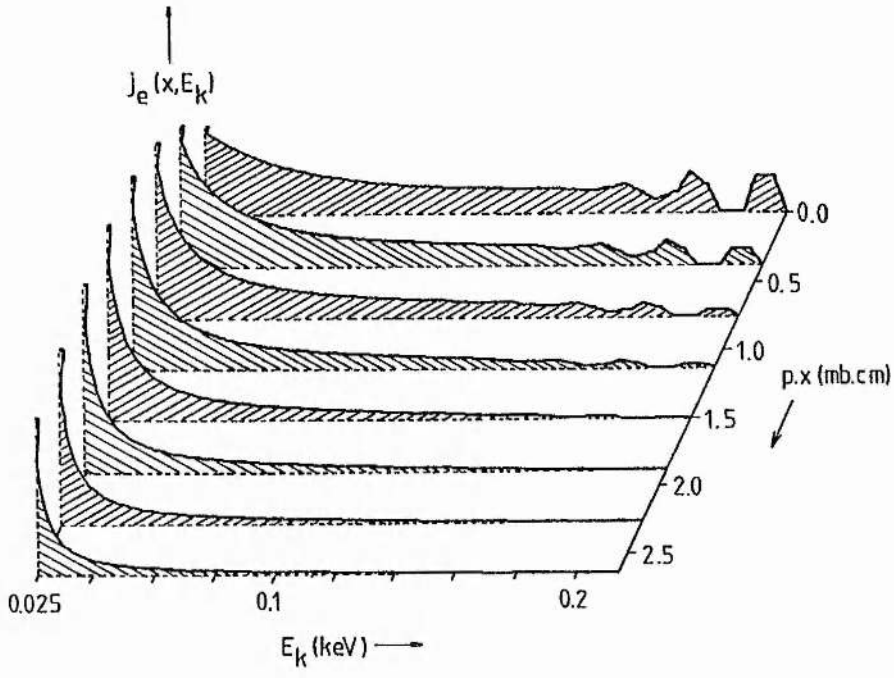

Fig 4.24. The development of the electron energy distribution function in the Negative glow for a Cathode fall of 0.2kV.

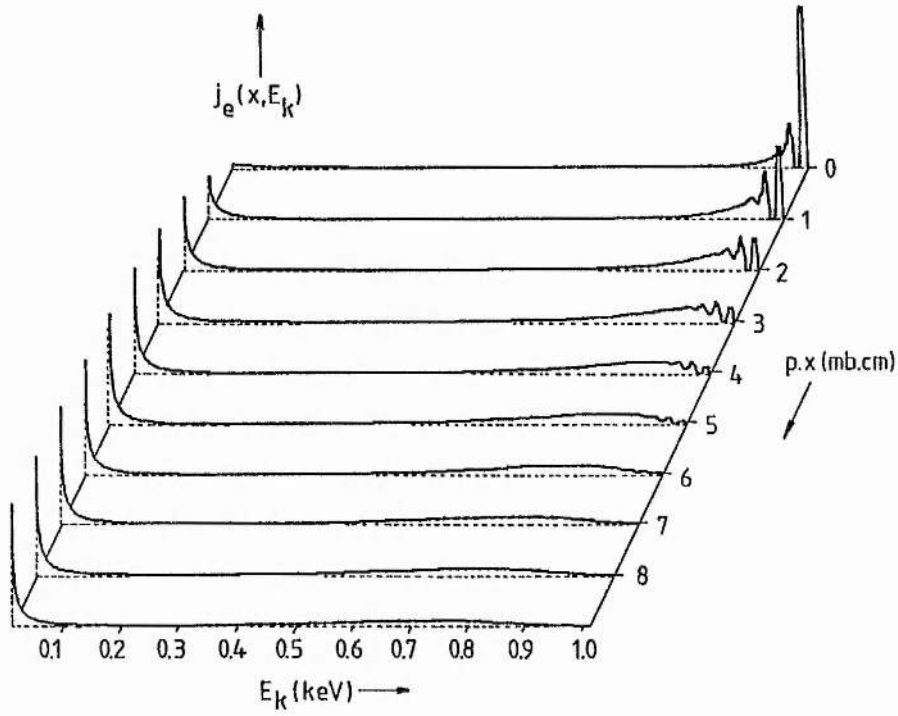

Fig 4.25. The early stages of the development of the electron energy distribution function in the Negative glow for a Cathode fall of 1.0kV.

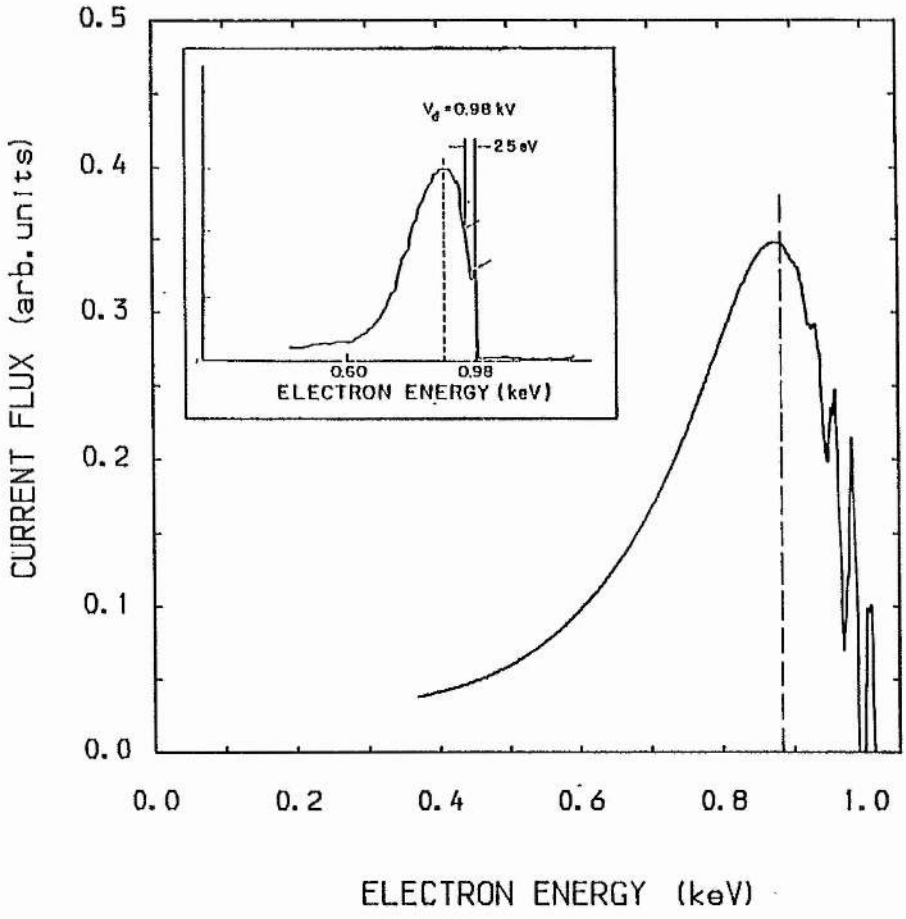

Fig 4.26. The electron energy distribution function in the NG for a depth factor of 5.0mb.cm, with a Cathode fall of 1.0kV. The energy distribution measured experimentally by Yu et-al is shown inset.

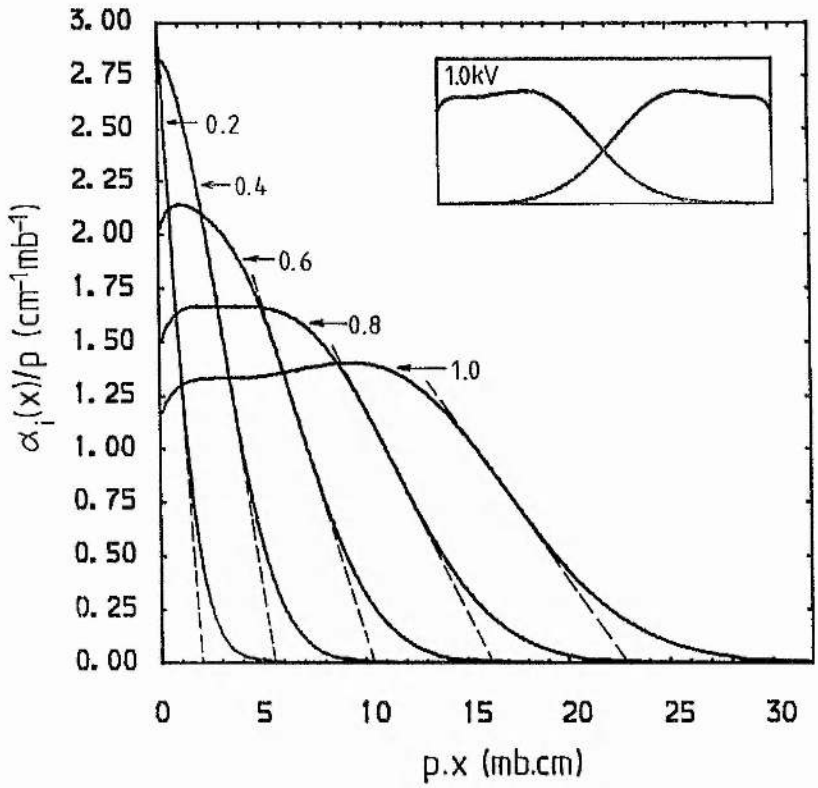

Fig 4.27a. The ion production rate in the Negative glow, with Cathode fall as a parameter. The superposition of two profiles from two opposing cathodes (shown inset) may produce a Negative glow region with more uniform ionisation.

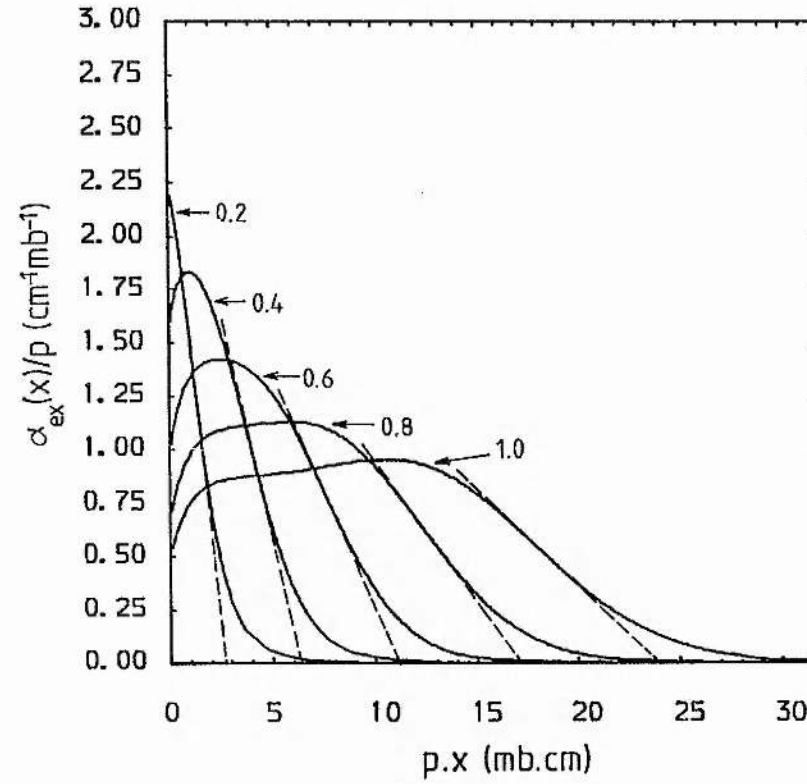

Fig 4.27b. The total production rate of excited HeI states in the Negative glow for different values of the Cathode fall.

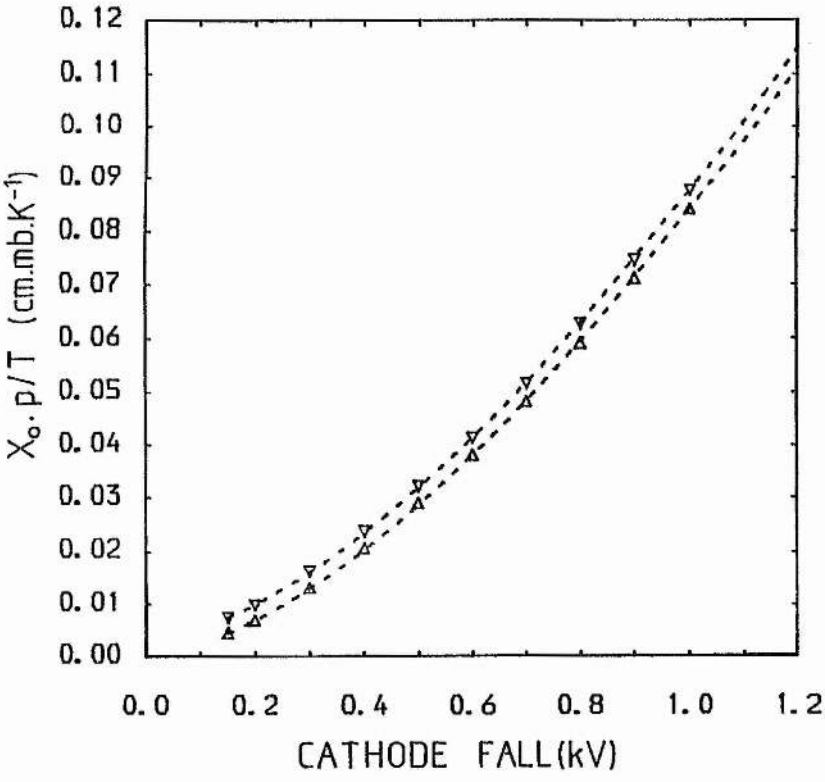

Fig 4.28. Extrapolated range criteria for the length of the Negative glow region. Δ : from ionisation rates, ∇ : from excitation rates, broken lines are from eq.4.19a and eq.4.19b.

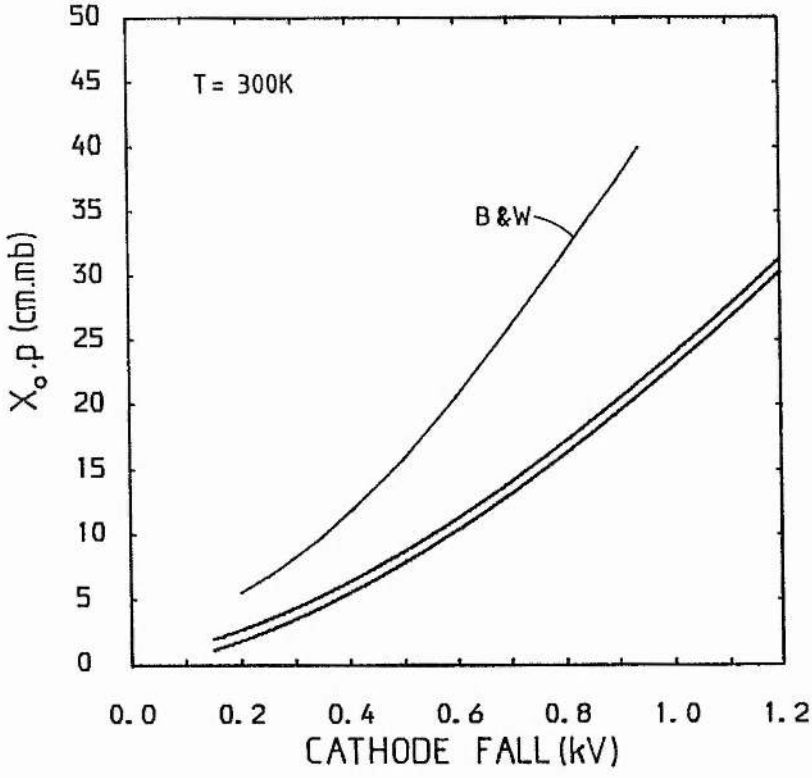

Fig 4.29. Range criteria for a gas temperature of 300K. The results of Brewer & Westhaver are included for comparison [30].

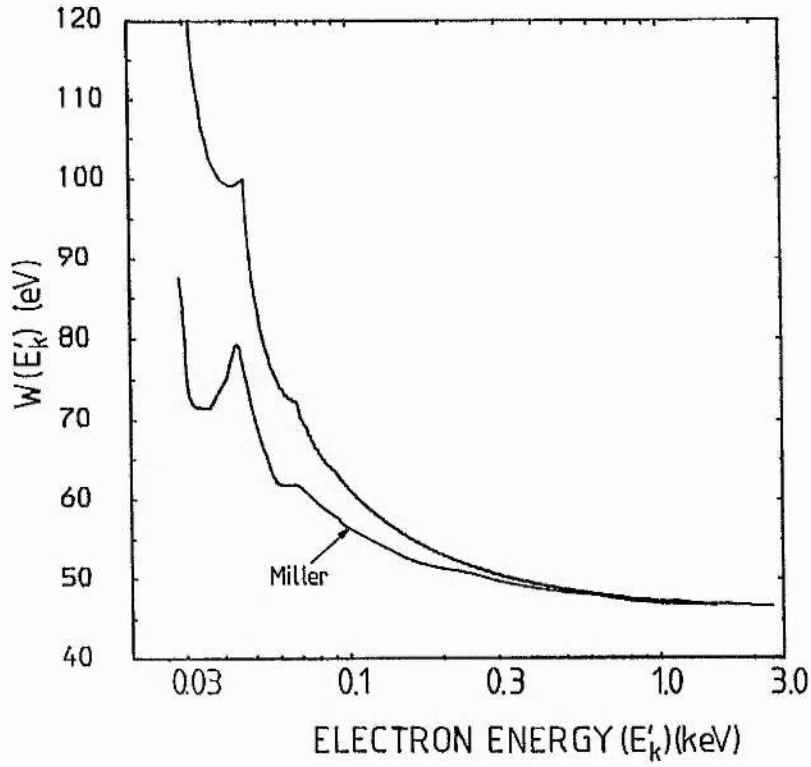

Fig 4.30. The average energy $W(E_k')$ required to generate an electron/ion pair, over the lifetime of an electron with an initial energy E'. The results of Miller are included for comparison [7].

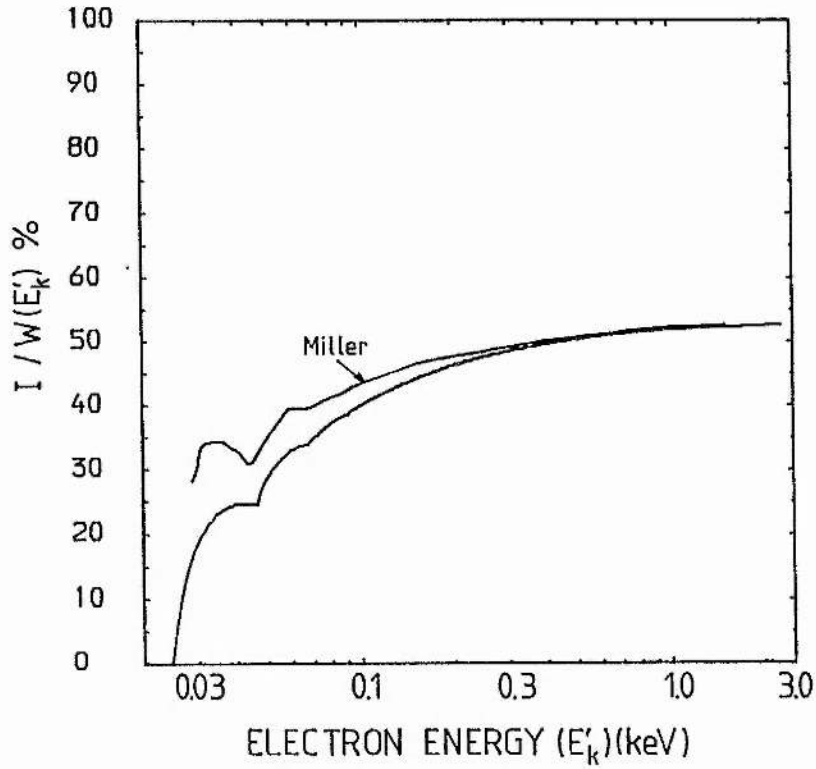

Fig 4.31. The efficiency of ionisation for an electron with an initial energy E_k'.

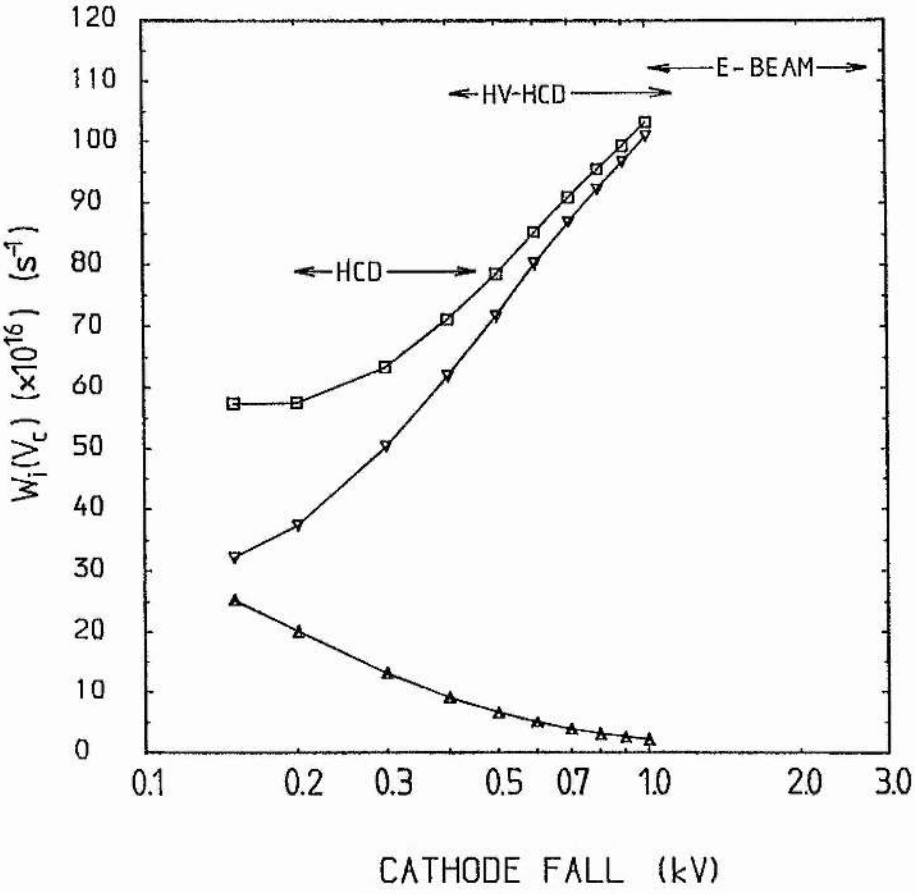

Fig 4.32. The rate of ion production in the Cathode dark space and Negative glow regions of a helium discharge, for an input power level of 1 Watt. ▲ : production rate in the CDS, ▽ : production rate in the NG, □ : total production rate.

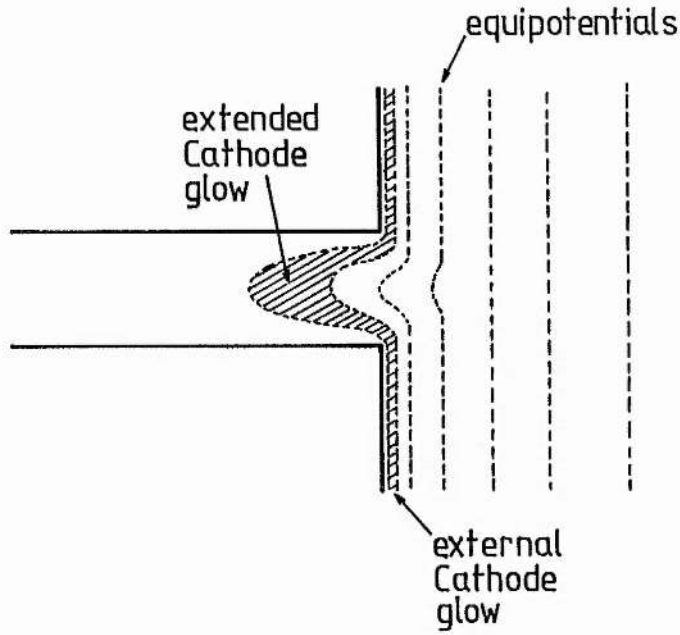

Fig 4.33. The expected equipotential distribution in the Cathode dark space region of an electron gun cathode. An extended Cathode glow region is defined by the perturbed equipotentials.

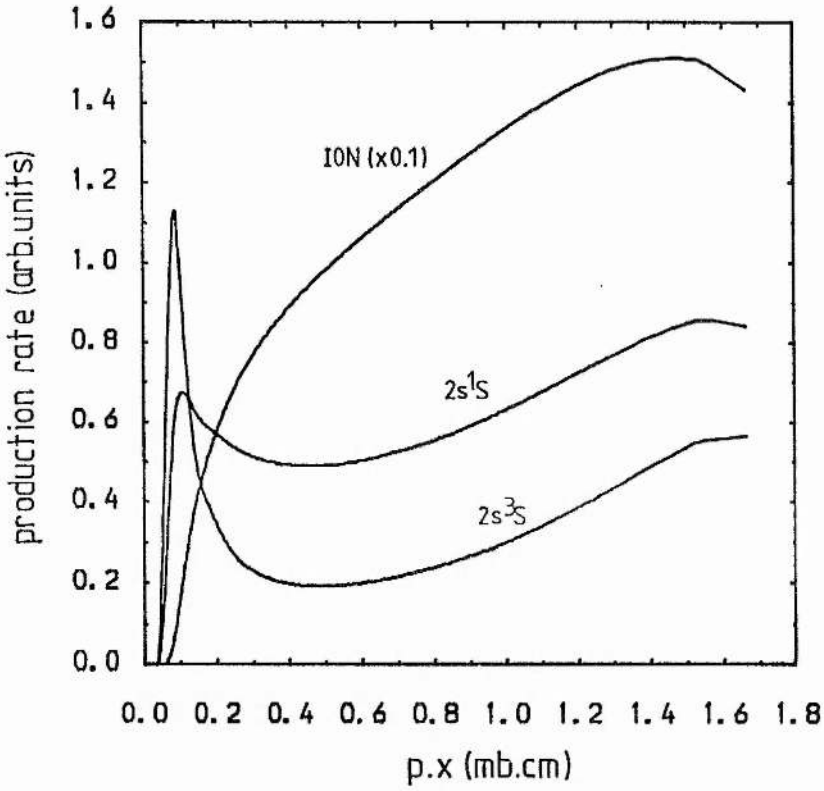

Fig 4.34. The production rates of helium ions and metastables at a Cathode fall of 0.2kV.

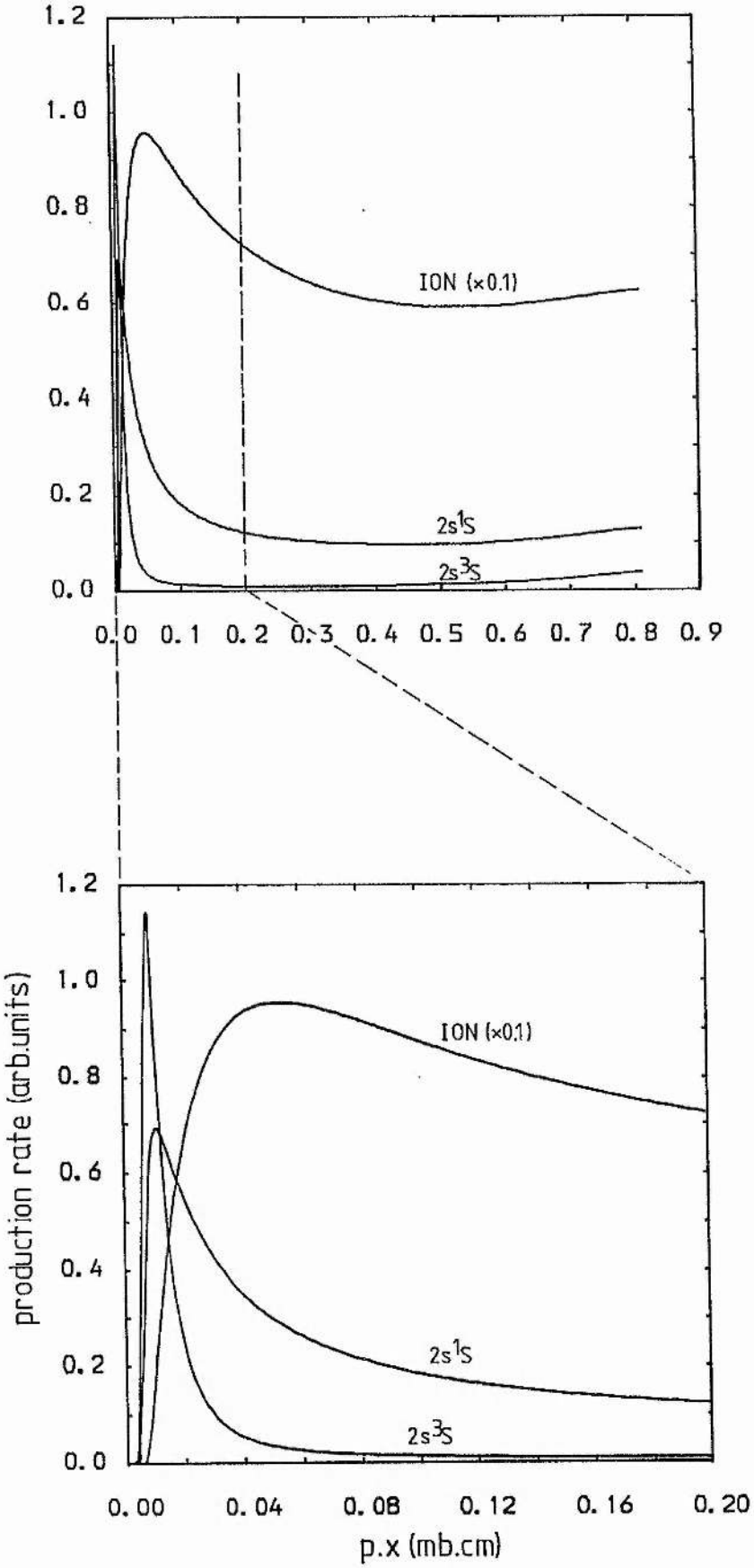

Fig 4.35. The production rates of helium ions and metastables at a Cathode fall of 1.0kV.

Chapter 5

5 Electron Gun Configurations for Laser Plasmas

A single electron gun operating with a Cathode fall of up to 5 kV, and giving a beam current of up to 1 amp, has been used by Rocca et-al for longitudinal pumping of several types of ion metal vapour lasers [1] (fig 1.11). Despite the improved operating characteristics reported for this system compared with the performance of previous hollow cathode discharges, there are several drawbacks in using such a geometry. Firstly, an electro-magnet generating a field of up to 0.3-0.4T must be employed to maintain the e-beam collimation over the length of the active medium, which is about 1 metre. Such a magnet is physically large, uses considerable power (typically10 kVA) and must be adequately cooled. Secondly, the ranges of the electrons in the e-beam are chosen to be compatible with the length of the active medium to ensure optimum coupling of the beam power to the laser gas. Therefore, the electron energies at each end of the gas cell are expected to be markedly different, and the production of excited species may diminish in the region furthest from the electron gun. Two electron guns, firing electron beams into the active medium from both ends of the electro-magnet, have been employed to provide more uniform excitation [2]. Nevertheless, the electro-magnet must still be employed to maintain the collimation of the two beams.

With the aim of developing an e-beam pumped discharge which requires a somewnat lower magnetic field than 0.4T, a number of discharge geometries have been investigated here. Essentially, a number of electron guns are employed, spaced at regular intervals

along the discharge tube. The aim is to provide excitation of the gas by each e-gun over a distance of approximately 10cm. Although an electro-magnet has not been employed, the field strength necessary to provide some degree of collimation over this distance should be considerably less that 0.4T. In addition, the current generated by the single e-gun for the system used by Rocca et-al [1] can be divided between the e-guns of the multiple array, thus reducing the current required from each e-gun to achieve the same overall input power level. A discharge tube incorporating three cathode/anode pairs has been constructed to carry out preliminary investigations of a multiple e-gun array in helium. A second discharge tube has been constructed with water cooling to investigate a multiple e-beam discharge in argon.

5.1 Electron Gun Cathode Geometries

5.1.1 Experimental Arrangement

A quartz discharge tube with three independent cathode/anode pairs is shown in fig 5.1. The stainless steel electron guns are 2.5cm in length, with hole apertures of diameter 3.5mm. The separation between the guns is 6.0cm, and three Tungsten pin anodes are set midway between adjacent e-guns. Helium is flowed through the discharge tube throughout the investigation to purge impurities, and the gas handling system is identical to that described in section 3.3.1. The tube has been heated for 60 hours using heating tapes

before running the discharge, and a 'running in' procedure has been followed for each cathode face, as described in section 3.3.1. During the 'running in' procedure, the sidelight emission from the NG of a single e-gun has been examined using the same optical arrangement as described in section 3.4.1. Slight traces of hydrogen (H_α and H_β lines) have been observed in the spectrum recorded, which otherwise contains known helium emission lines only. The V-I characteristics of the discharge, with electrode pairs connected in a number of different configurations, have been recorded. Good reproducibility of the V-I curves is achieved by following the acquisition method described in section 3.3.1.

5.1.2 Results

Simultaneous e-beam production from the two faces of a single electron gun has been investigated, as shown in fig 5.2a. Two electron beams, of roughly equal intensity, are produced by the cathode when the two anodes are earthed. Beam production from one face may be disrupted by isolating one of the anodes. The V-I characteristics of the e-gun operating in the single beam mode have been recorded for each face of the cathode, and then for simultaneous operation in the twin beam mode. To determine whether there are interaction effects between the internal plasmas in the hole cavity, the current passed by the cathode operating in the twin beam mode, as a ratio of the sum of the currents passed by each face operating separately, has been calculated for particular values of pressure and Cathode fall. A set of such current ratios are shown in fig 5.3. Although there is some scatter in the points calculated, there is a

general trend whereby the current ratios increase slightly for higher values of Cathode fall. It is possible that long-lived species such as He^* (metastable) are carried from the first plasma region to the second by the gas flow. Therefore, two separate power supplies have been used to investigate interaction effects in a single e-gun also, as shown in fig 5.2b. The current I_1 is set, and then monitored as I_2 is increased. The results are shown in fig 5.4 for gas pressures of 1mb and 2mb. They demonstrate that there is an interaction effect, although small, with I_1 increasing slightly as I_2 is raised. This may be due to a degree of cross-ionisation by slow electrons in the internal plasmas of the two separate e-beam discharges. However, it may also be due to eventual fate of ions generated in the two NG regions, which pass into the hole cavity from opposite directions. Since two CDS regions are present, the ions are trapped within the cavity, and must eventually collide with the cavity walls.

Two e-beam discharges can be used to excite the same region of gas using counter-propagating beams, as shown in fig 5.5. A similar cathode geometry has been employed by Persson to generate overlapping NG's for a study of diffusion and recombination in the NG [3]. It is found here that individual ballasting of the two electron guns is not necessary to achieve stable operation of the two guns simultaneously. However, ballasting may become important when operating at high current levels, as found for the separate anodes of a 'flute' type hollow cathode discharge [4]. Current ratios for the twin gun system have been calculated, to investigate interaction effects between the two electron beams, and are depicted in fig 5.6. For low values of Cathode fall, the e-beams do not overlap, the degree of cross-ionisation in the two NG's is small, and the current ratios are near unity as expected. As V_c is raised, the NG's begin to overlap

and the current ratios rise. The ratios start to increase at lower values of V_c for lower gas pressures, as predicted by the range criteria (eq.4.19). As the current ratios rise further, a kink is observed in the curves for 1mb and 2mb. This suggests that the ionisation cycle in the compound discharge is somehow interrupted, over a small range of Cathode fall values. One explanation for this effect is that the electrons from one e-gun then have a range equal to the gun separation, and reach the CDS/NG boundary region of the other e-gun. They are prevented from drifting further by the other CDS sheath region. The presence of such slow electrons in the boundary region will reduce the effect of the positive space charge of the ions, and thus reduce the fields in the CDS. As V_c is raised further and the electron energies increase, their ranges in the gas also increase. In this case, they pass through the opposite CDS/NG boundary region, are reflected by the electric fields in the CDS, and pass back into the main body of the two overlapping NG's. This would explain why the current ratios increase again as V_c is raised further.

A potentially useful effect is observed when a voltage is applied between the outermost two e-gun cathodes 'A' and 'B', leaving the centre cathode at floating potential. When the discharge is run at low current, two electron beam plasmas are observed, with one produced by the cathode at floating potential (fig 5.7a). This floating electrode acts simultaneously as an anode for the cathode 'A' and as a cathode for 'B'. As the discharge current is raised to about 3mA, however, the discharge transposes to another mode in which a single e-beam is produced, and a filament of PC is formed along the axis of the tube, and passes through the centre cathode (fig 5.7b). The V-I characteristics for the twin beam mode are shown in fig 5.8a, which

shows the total voltage (V_t) applied to the end electrodes, and the floating potential (V_f) of the centre electrode. The floating potential is approximately one half of the overall voltage when the discharge operates in the twin beam mode, as shown in fig 5.9. When a voltage is applied between points 'A' and 'C' shown in fig 5.7a, to leave two electrodes at floating potential, three e-beam plasmas are generated, although the multiple beam mode is again only stable below 3.0mA, as shown in fig 5.8b.

It is unfortunate that this multiple beaming effect using floating electrodes is not stable at higher current levels. As to a reason why the discharge is stable in the multiple beam mode at low current, it is known that the size of the electric field parameter E/p ($V.cm^{-1}.mb^{-1}$) required to maintain the flow of charged particles in the PC must be increased for smaller tube diameters [5]. Therefore, at low current, the value of E/p across the bore of the central electrode is probably too small to overcome the diffusion losses for charged particles in the bore, in order to maintain a PC region. However, the applied potential is clearly adequate to sustain two almost independent CDS and NG plasma regions. Therefore, by reducing the bore diameter to increase the diffusion losses for a PC glow, it might be possible to increase the operating range of discharge in the multiple beam mode.

Since the e-beam plasma is generated along the central axis of an e-gun cathode, a discharge tube has been constructed in order to confine the entire e-beam plasma to a central region of the same diameter as the cathode hole. This geometry is shown in rig 5.10, and adjacent electrodes are used as anodes in this case. The separation between the electrodes is set at 0.5mm to establish an obstructed discharge and prevent gas breakdown across the electrode gap. It is

found that an e-beam plasma cannot be maintained at low current (~1mA) using such a geometry, is somewhat unstable, and does not yield reproducible V-I characteristics. The discharge is observed to switch on and off intermittently, with a period of several seconds. Oscillations of this nature have been observed with other types of obstructed glow discharges also [6]. It is suggested that these oscillations are due to a build-up of space charge in the inter-electrode gap, which then acts to extinguish the discharge.

An e-beam plasma is generated at a voltage of 2-3kV as indicated by the V-I characteristics in fig 5.11. It is shown that the V-I curves are unusually steep and small variations in the Cathode fall produce large changes in the discharge current. The position of the anode very close to the cathode face undoubtedly gives rise to a degree of perturbation of the equipotentials in the CDS region, as shown in rig 2.13. Electrons in the e-beam plasma may be formed as a divergent beam and collide with the walls of the anode instead of generating a NG region along the bore. By increasing the inter-electrode spacing whilst maintaining an obstructed mode criterion (ie. gap<d_c), the perturbation of the equipotentials may be reduced, enabling more stable operation of this type of geometry. The inclusion of a small electro-magnet around the discharge tube to generate a longitudinal magnetic field, thereby reducing the beam divergence, may improve the stability of the discharge also.

5.2 A Multiple e-beam Discharge using Argon

5.2.1 Experimental Arrangement

The discharge cell shown in fig 5.12 (and plate 2) has been constructed to investigate the behaviour of a multiple e-beam discharge in argon. The cell has been designed to allow the addition of further segments at a later stage, although the operation of only one segment is reported here. The cell consists of an aluminium body which houses the two e-gun cathodes, and two stainless steel end flanges through which the vacuum and water connections are made. The cathodes are slid along the central bore and are held in place by vacuum lead throughs in the aluminium body, which are used also to connect the cathodes to the power supply. The cathodes are anodised to provide electrical isolation from the main body, which also acts as an anode, and is held at earth potential. The cathodes are 2.0cm in length with 2.0mm holes to generate the e-beams, and only the walls of the holes are left un-anodised. A CDS sheath region is expected to form next to the anodised cathode faces which are exposed to the discharge. The ion concentration in such a sheath is likely to be less than in the sheath region at the hole entrance, however, since the electron flux derived from the anodised surfaces will be less than that carried in the e-beam filament. The weaker sheath region may be used to reflect stray electrons back into the central discharge region, however, and for this reason the cathode faces are machined slightly concave. To overcome the serious sputtering problems encountered with the previous argon e-beam discharge, the cathodes

have been made from aluminium which is more resistant to sputtering than stainless steel [7]. In addition, an admixture of oxygen at 0.01mb-0.025mb in the gas supply can be used to maintain the thin layer of oxide on the cathode surface, in this case the bore of the cathode, to reduce sputter damage considerably [8]. Therefore, a small amount of oxygen has been introduced into the argon flow entering the discharge cell. Spontaneous emission from the e-beam glow has been collected from the cell viewed 'end-on' using the optical arrangement described in section 3.4.1. The axis of the cell has been aligned with the optical arrangement using a He-Ne laser.

5.2.2 Results

A spectrum of the e-beam discharge glow has been recorded at low discharge current (0.3mA, 0.39kV), and is shown in fig 5.13. The argon pressure is set at 0.7mb with an admixture of oxygen at 0.06mb to maintain the thin oxide layer along the cathode bores. The spectrum contains numerous ArII lines, and their relative intensities are found to be similar to those observed for the previous argon e-beam discharge (section 3.5.2). The most intense emission line is at 4765Å, and the ten principal lines in the spectrum are listed in table 5.1. It is noted that the emission line at 5145Å is, once again, not observed at low current. During subsequent experiments to monitor the intensities of these principal emission lines as the discharge parameters are changed, it is found that the discharge current is not steady, and current 'glitches' are observed with a frequency of $\sim$1Hz. These bursts of current appear more frequently as the discharge is run for periods of several hours. They also increase

	Wavelength (A)	Transition	Intensity (arb.units)
1.	4764.9 (II) L	$4p^2P_{3/2}$-$4s^2P_{1/2}$	8.98
2.	4277.5 (II)		8.12
3.	4609.6 (II) L	$4p^2F_{7/2}$-$4s^2D_{5/2}$	6.93
4.	4198.3 (II)		6.49
5.	4879.9 (II) L	$4p^2D_{5/2}$-$4s^2P_{3/2}$	6.39
6.	4259.4 (I)		6.33
7.	4158.6 (I)		6.18
8.	4545.1 (II) L	$4p^2P_{3/2}$-$4s^2P_{3/2}$	6.16
9.	4200.7 (I)		5.62
10.	4657.9 (II) L	$4p^2P_{1/2}$-$4s^2P_{3/2}$	5.29

Table 5.1. The ten most prominent lines in the e-beam discharge at 0.3mA, 0.39kV and 0.7mb. 'L' denotes a known laser transition.

in frequency as the discharge current is raised. By increasing the ballast resistor on the power supply from 20kΩ to 200kΩ, however, the discharge is found to be generally more stable. The intensities of the principal ArII lines in the spectrum nave been recorded as the discharge current is increased, and the intensities of two ArI lines at 4259Å and 4158Å have been monitored also. Values of the Cathode fall over the current range investigated are shown in fig 5.14. The current range is limited to about 20mA by the ballast resistor used to stabilise the discharge current. All spectral line intensities are observed to increase almost linearly with rising discharge current, suggesting single-step electron excitation of both ArI and ArII states. However, the intensities of all ArII lines appear to increase

slightly faster than the intensities of both ArI lines as shown in fig 5.15. Here, ratios of line intensities have been calculated using the intensity of the emission line at 4259Å as a common denominator throughout. Interestingly, the ratios increase most noticeably for the ArII lines which correspond to known laser transitions. The intensity of the line at 5145Å remains weak in comparison to the other ArII lines over the current range investigated.

After running the discharge for approximately 12 hours continuously, the frequency of the current 'glitches' is observed to increase, and this prevents further spectral analysis. These current bursts are accompanied by bursts of RF emission between 0-800MHz as shown in fig 5.16. There appears to be an envelope function within which the RF radiation is emitted. On examining the e-gun cathodes, it is found that a layer of oxide builds up along the bores during operation reducing the diameters to about 1.9mm. After re-drilling the cathodes to 2.0mm and replacing the guns in the discharge cell, it is possible to run the discharge with a relatively stable discharge current once again. The build-up of a thick oxide layer is probably caused by operating with the partial pressure of oxygen set too high. In subsequent runs, the oxygen pressure is reduced to 0.02mb. However, after several hours of operation, the discharge current becomes unstable once again. At a discharge current of 10mA, an audible 'ring' can be heard from the discharge cell, and this persists as the current is raised further. It is found that the instabilities encountered are not prevented by connecting 5kΩ ballast resistors to the individual cathodes.

Instabilities in DC glow discharges have been discussed extensively by Francis [6]. The instabilities encountered here may be caused by the presence of O^- ions in the discharge, and the minimum

partial pressure of Oxygen required to maintain the thin oxide layer along the cathode bore will probably be determined by trial and error. It will depend on the sputtering rate in the cavity, and therefore on the discharge current and on the Cathode fall. The instabilities may be caused by intermittent arcing from the cathode edges to the aluminium body also, which may be prevented by improved design of the cathode segments. It has been suggested that the glow-arc transition of a cold cathode discharge may be prevented by limiting the current available for the arc to form, by reducing the capacitance of external circuitry of the power supply [8]. Instabilities may also be reduced by running the cathode 'hot' to drive off volatile gases. Extensive studies into the formation of temporary arcs in hollow cathode discharges using aluminium cathodes coated with an oxide layer have been carried out by Rozsa et-al [9]. It is suggested that arcing occurs as a result of non-uniformities in the thickness of the thin oxide layer on the cathode. Relatively stable operation is reported after this oxide layer is removed by sputtering, to expose a clean metal surface.

RF emission has not been detected from the e-beam plasmas in helium discussed in section 3.3.2 of this thesis. However, UHF emission between 1-10GHz has been generated by an e-beam discharge in helium for current densities of around $0.1A.cm^{-2}$ [10]. Such RF emission is caused by an interaction between the plasma generated by the e-beam (the NG) and the e-beam itself. These 'plasma oscillations' have been investigated by Wada and Knechtli, and are shown to increase in intensity as e-beam current increases, or as the surrounding gas pressure is reduced [11]. Serious degradation of the quality of the e-beam has been observed at the onset of these oscillations [10]. This is accompanied by a sharp change in the

spectral characteristics of the e-beam plasma. However, if a similar 'plasma oscillations' in the argon e-beam discharge are occurring, the excitation of ArII levels compared with ArI levels would be expected to diminish, at the onset of such oscillations. This is not observed to be the case, as shown in fig 5.13.

Further investigations are necessary to determine the nature of the current instabilities observed here, to enable the e-beam discharge to operate stabily at higher current levels, and with a smaller ballast resistance. The presence of numerous ArII emission lines in the spectrum of the e-beam plasma is an encouraging feature, however. The behaviour of electrons in the CDS and NG regions of an abnormal glow discharge in argon is undoubtedly similar to that in an abnormal helium discharge. The proportion of 'fast' electrons at the CDS/NG boundary and in the NG is therefore likely to increase as the Cathode fall is raised. Such electrons are able to excite ArII levels directly, and this is confirmed by the presence of strong ArII emission lines even at low discharge currents. It follows that the average electron energy in the e-beam discharge is expected to be markedly higher than in an equivalent Positive column discharge. Further investigations are needed to establish whether ArII levels are pumped favourably in a high current electron beam discharge.

Compact, air-cooled argon ion lasers using a low current (5A-10A) Positive column discharge are used to generate laser action at 4880Å, and have been developed commercially in recent years. Such lasers have very low operating efficiencies because the pumping rate to the $3p^4\ 4p^2D_{5/2}$ level is dependent on the square of the discharge current, which is limited by the cooling efficiency of the unit. However, since the production of ArII states in the e-beam discharge is maintained at low current levels, laser action generated in an e-beam

discharge, running at comparable input power levels to these Positive column devices, may be more efficient. Laser action on one or more of the ArII lines listed in table 5.1 may well be possible using an e-beam discharge of this type.

References

1. Rocca J.J., Meyer J.D. and Collins G.J., Appl.Phys.Lett., 40, 300 (1982)
2. Rocca J.J., Meyer J.D.. Farrell M.R. and Collins G.J., J.Appl.Phys, 56, 790 (1984)
3. Persson K.G., J.Appl.Phys., 36, 3086 (1965)
4. Piper J.A. and Webb C.E., J.Phys.D., 6, 400 (1973)
5. von Engel A., 'Ionised Gases', O.U.P (1965)
6. Francis G., 'Handbuch der Physik, XXII, p53-203 (1956)
7. Maitland A., private communication
8. Dugdale R.A., 'Glow Discharge Materials Processing', Mills and Boon (1971)
9. Rozsa K.. Apai P., Janossy M., Bergou J., Fujii K., Rubin G., Denton M.B., Phillips H. and Hopf F.A., Hungarian Academy of Sciences, Central Research Institute for Physics, Report KFKI-1985-43 and KFKI-1982-97
10. Yu Z., Rocca J.J. and Collins G.J., J.Appl.Phys., 54, 131 (1983)
11. Wada J.Y. and Knechtli R.C., Phys.Fluids., 12, 1497 (1969)

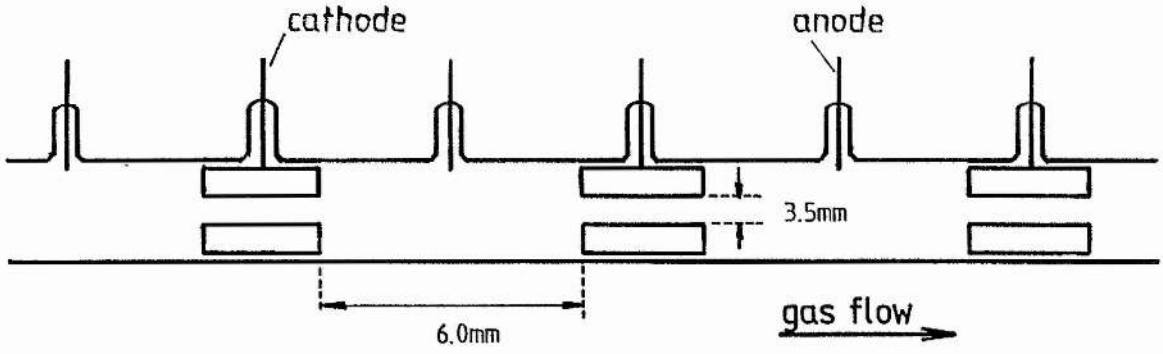

Fig 5.1. A multiple electron gun geometry incorporating three anode/cathode pairs.

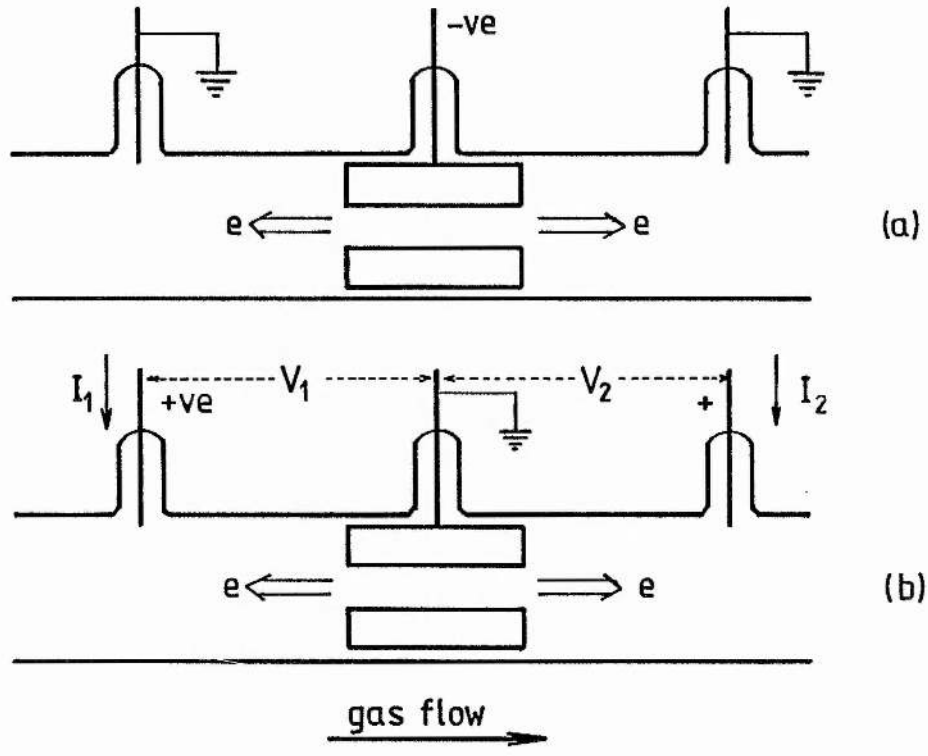

Fig 5.2. Simultaneous electron beam production from two faces of the same e-gun cathode.

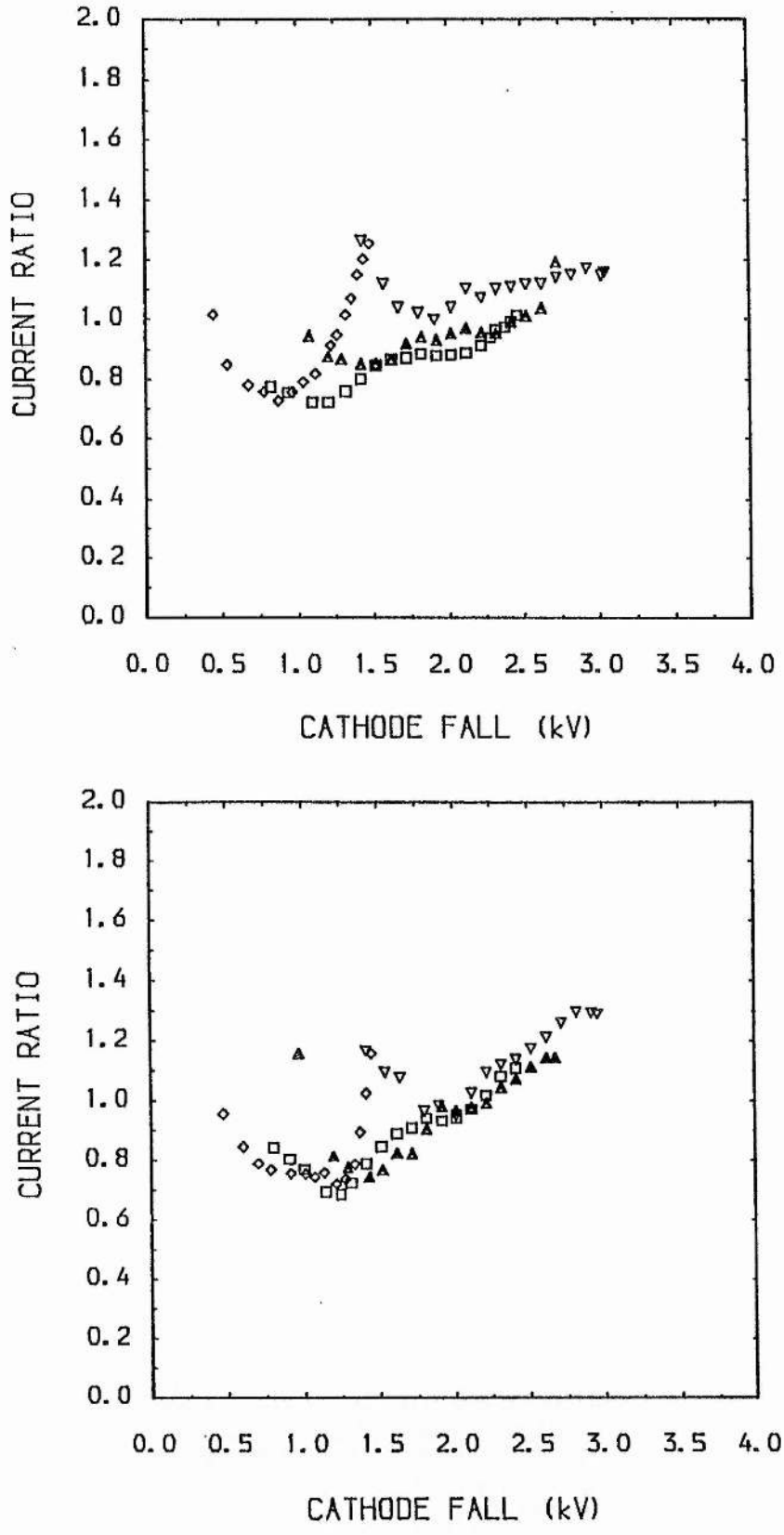

Fig 5.3. Current ratios for twin beam production by a single electron gun cathode. Two sets data are generated by using different cathode/anode pairs. ▽ : 1mb, △ : 2mb, □ : 3mb, ◇: 4mb.

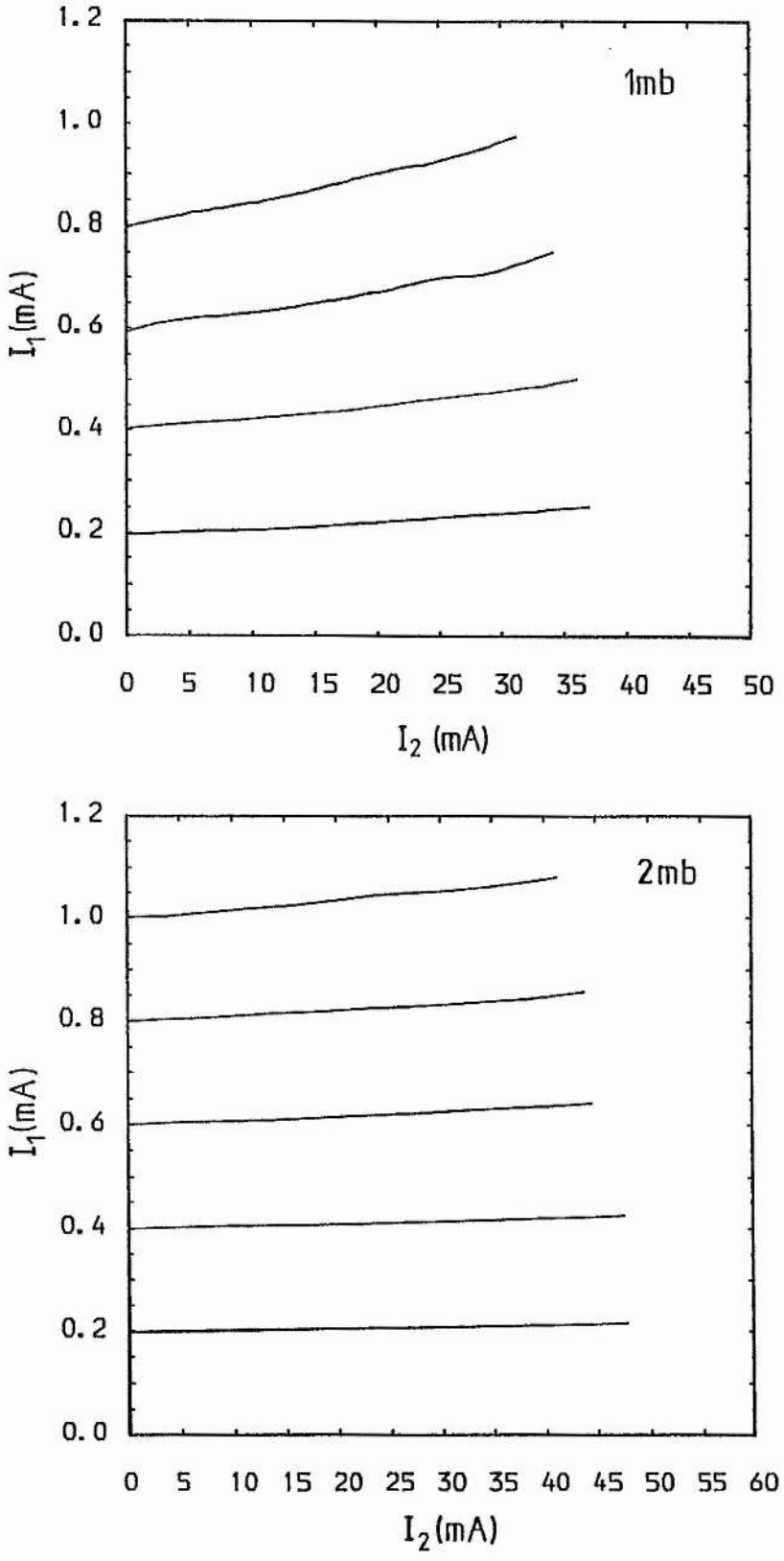

Fig 5.4. The discharge currents derived from each face of a single e-gun cathode operating in a twin beam mode.

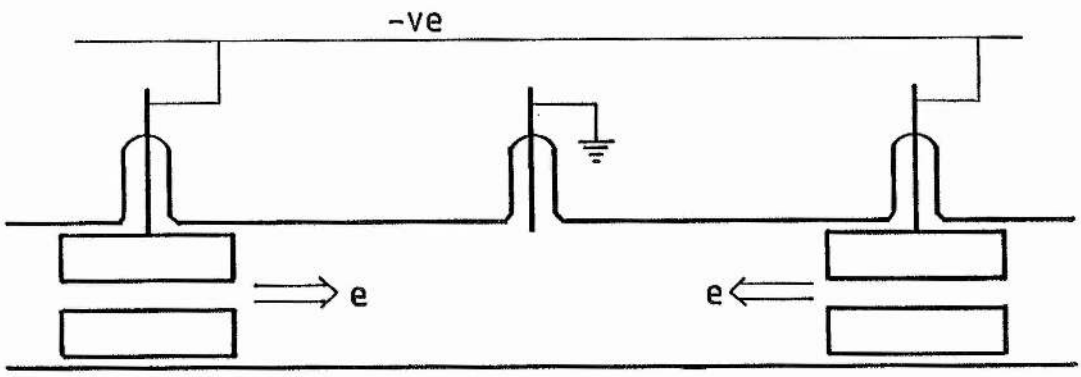

Fig 5.5. Excitation of a region of gas by two counter propagating electron beams.

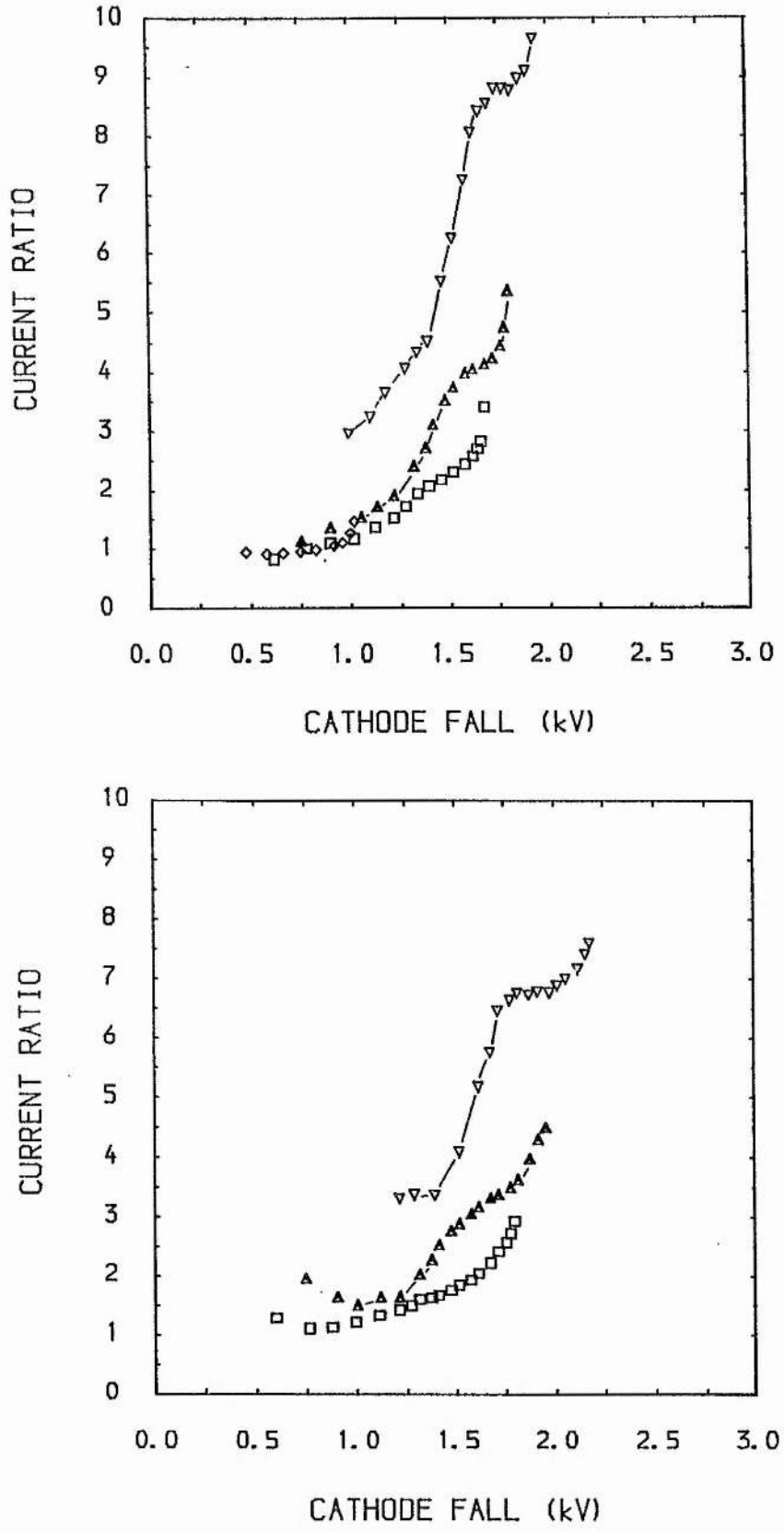

Fig 5.6. Current ratios for a twin electron gun system with overlapping NG plasma regions. Two sets of data are generated by using two different anode/cathode pairs. ▽ : 1mb, △ : 2mb, □ : 3mb.

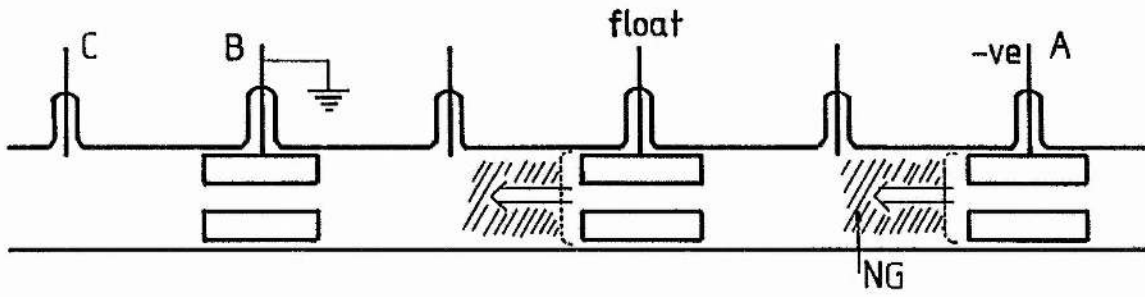

Fig 5.7a. Production of two electron beam plasmas at low discharge current, using a central electrode at floating potential.

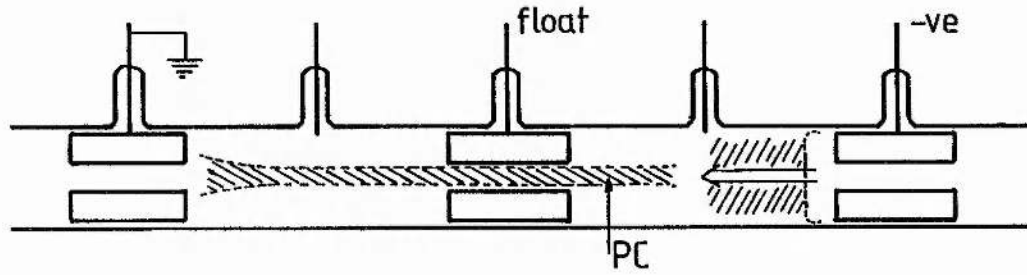

Fig 5.7b. The formation of a Positive column along the central axis of the discharge tube for discharge currents larger than ~3mA.

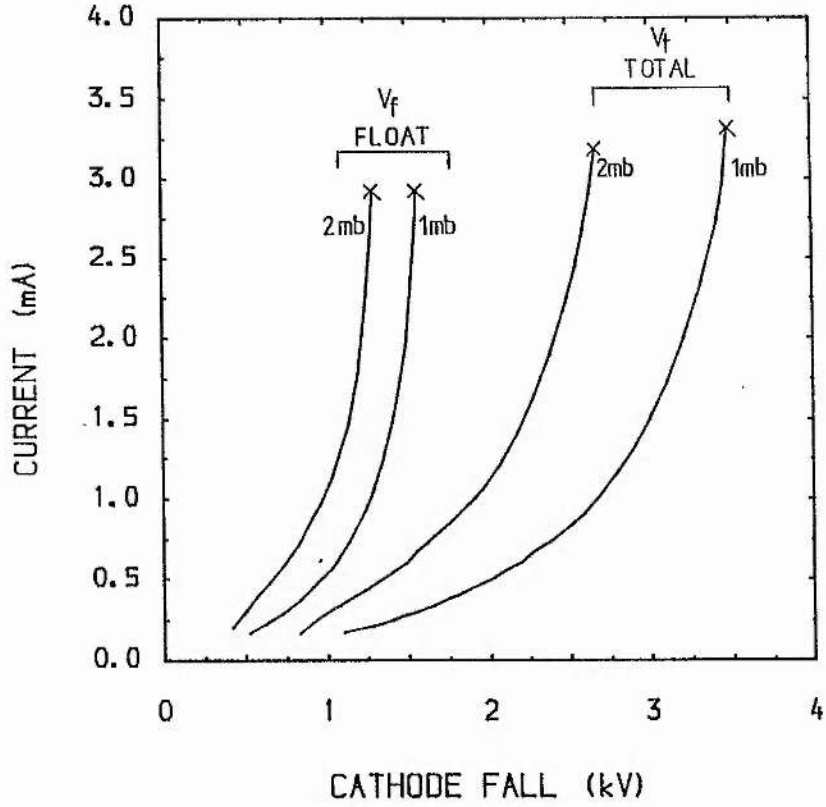

Fig 5.8a. The V-I characteristics of the discharge for the production of two electron beam plasmas, with the centre electrode at floating potential. × : transition point to the single beam mode with a Positive column region.

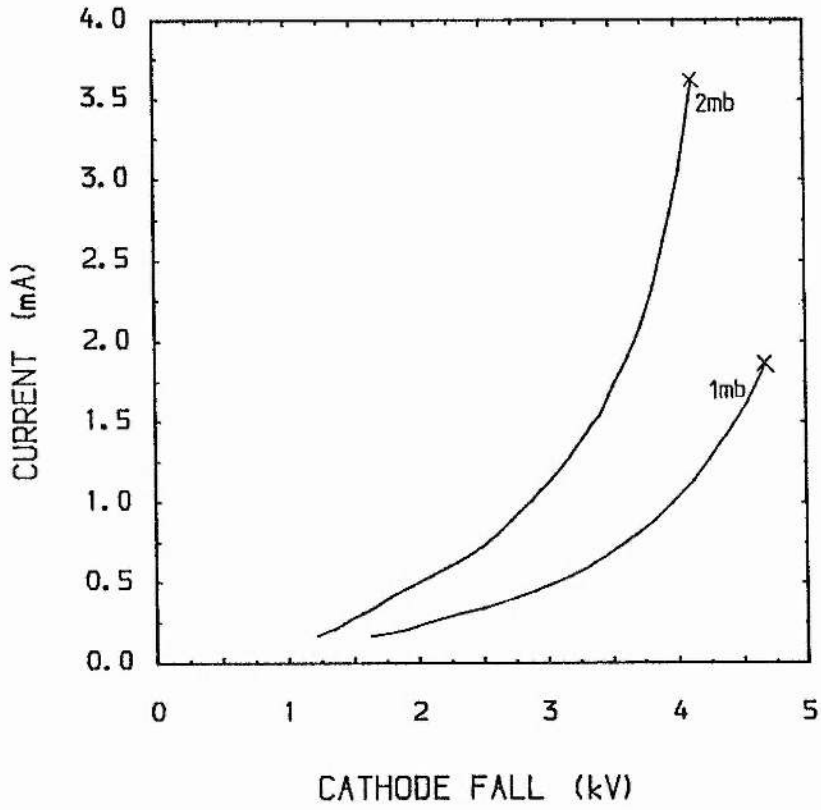

Fig 5.8b. The V-I characteristics for a discharge generating three electron beam plasmas, with two intermediate electrodes at floating potential. The voltage shown is applied to the end electrodes.

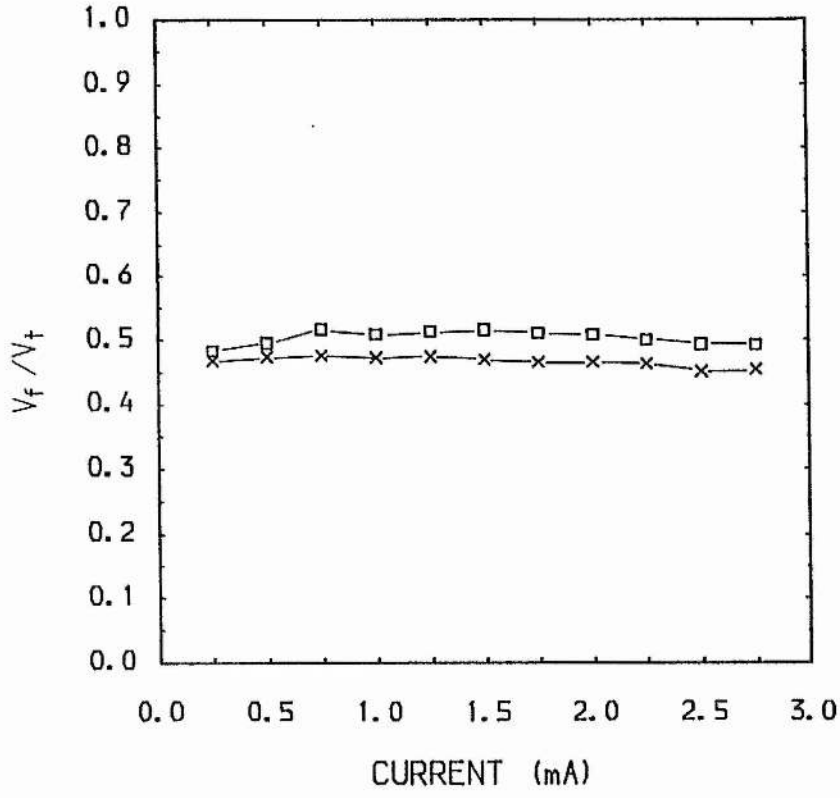

Fig 5.9. The floating potential V_f of the centre electrode, as a fraction of the overall tube voltage V_t, for operation in the twin beam mode. × : 1mb, □ : 2mb.

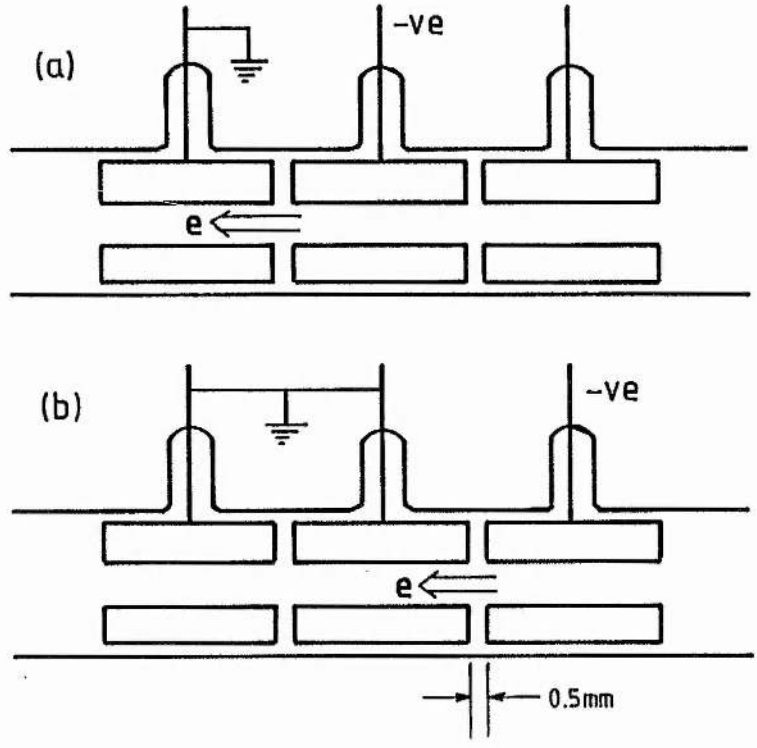

Fig 5.10. Electron beam production along the central axis of a geometry consisting of closely spaced anode/cathode pairs.

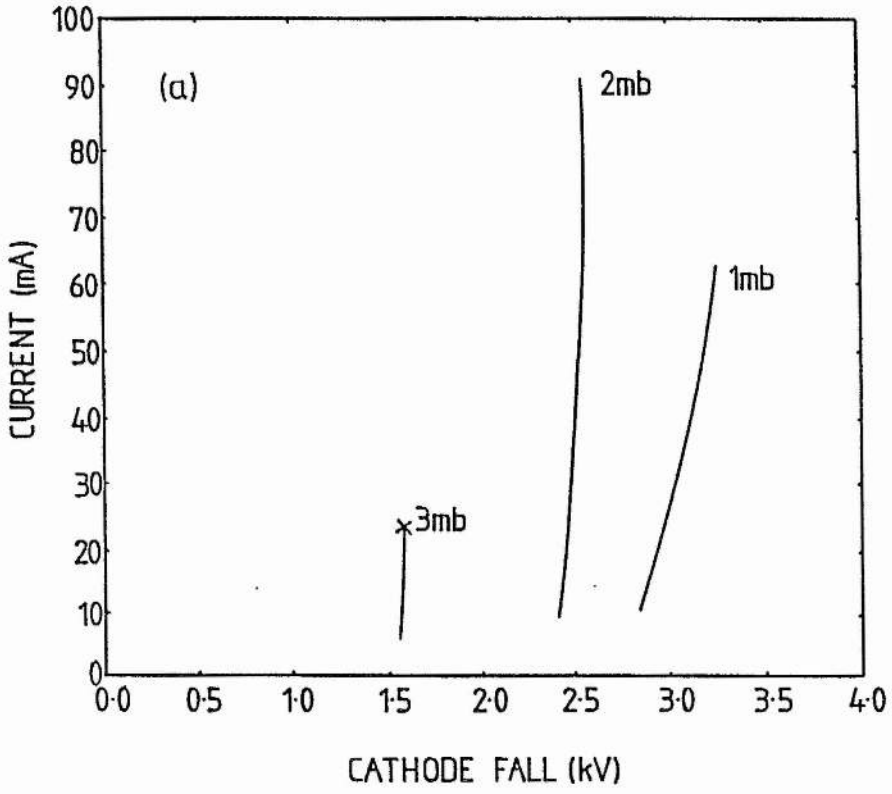

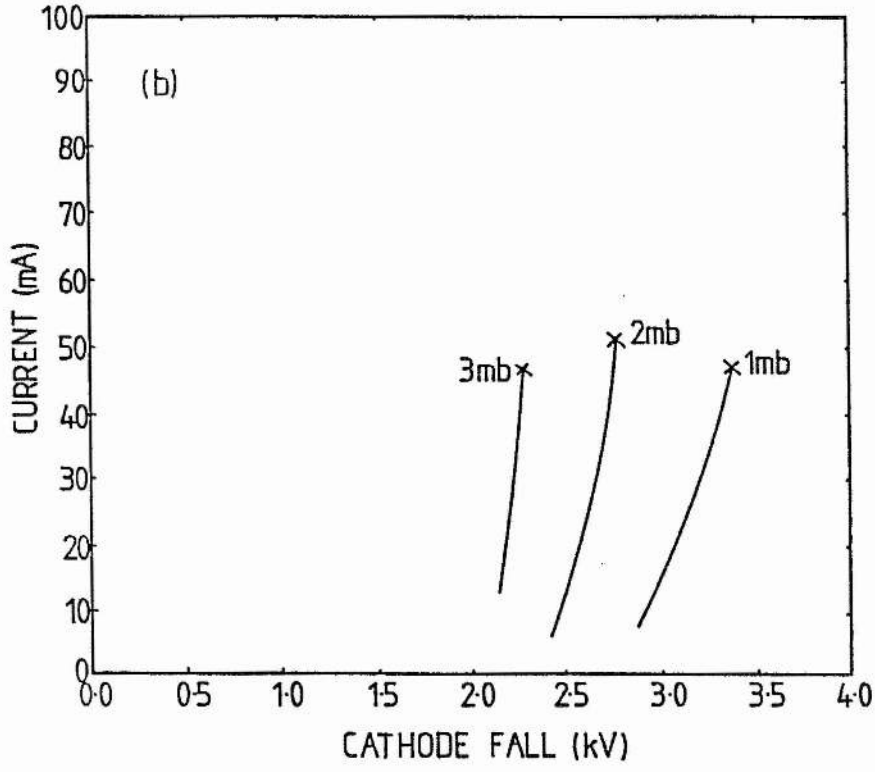

Fig 5.11. The V-I characteristics for electron beam production along the central axis of a geometry consisting of closely spaced anode/cathode pairs. × : transition point to the HCD mode.

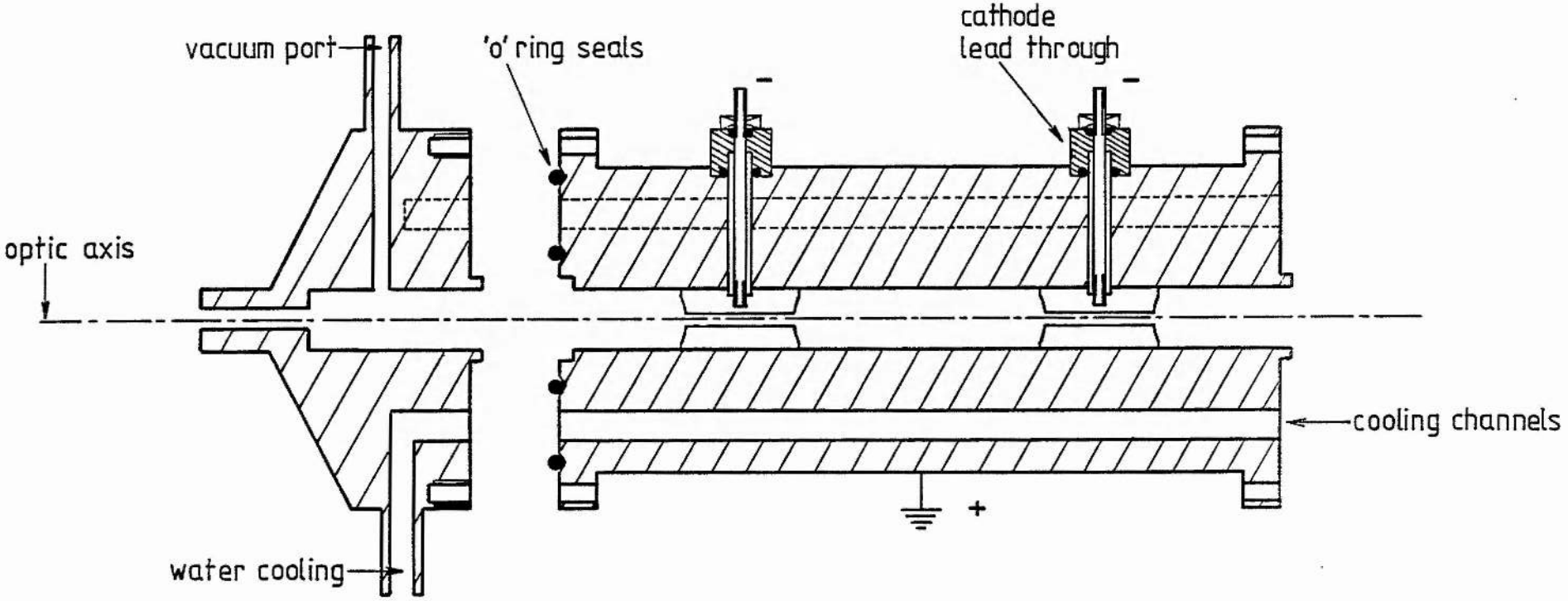

Fig 5.12. The discharge cell used to investigate electron beam production from multiple e-gun cathodes in argon.

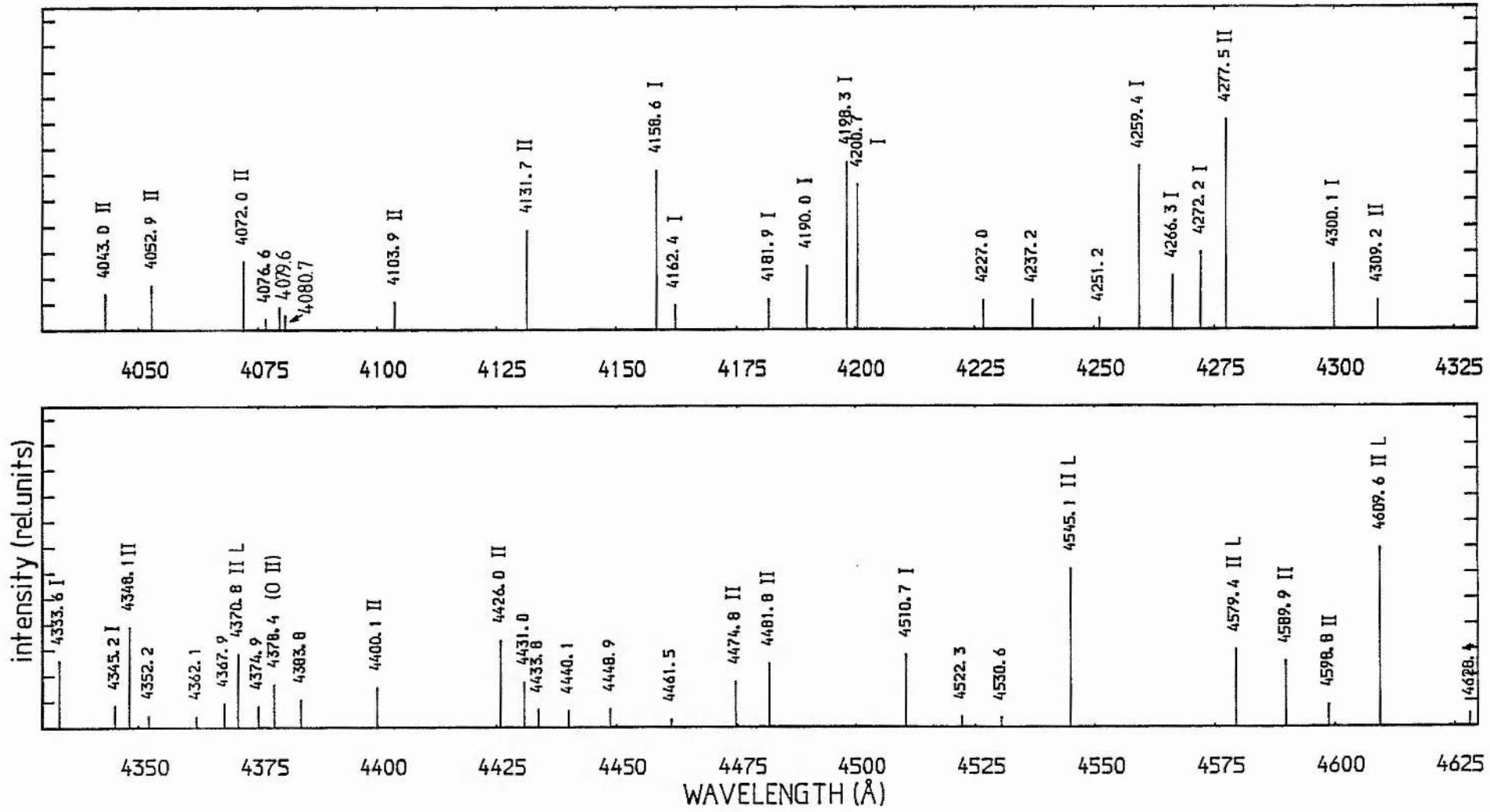

Fig 5.13a. A spectrum of the e-beam plasma glow in argon at 0.3mA, 0.39kV and 0.7mb, with an oxygen admixture at 0.06mb. I: atomic transitions, II: ionic transitions, L: known laser transitions.

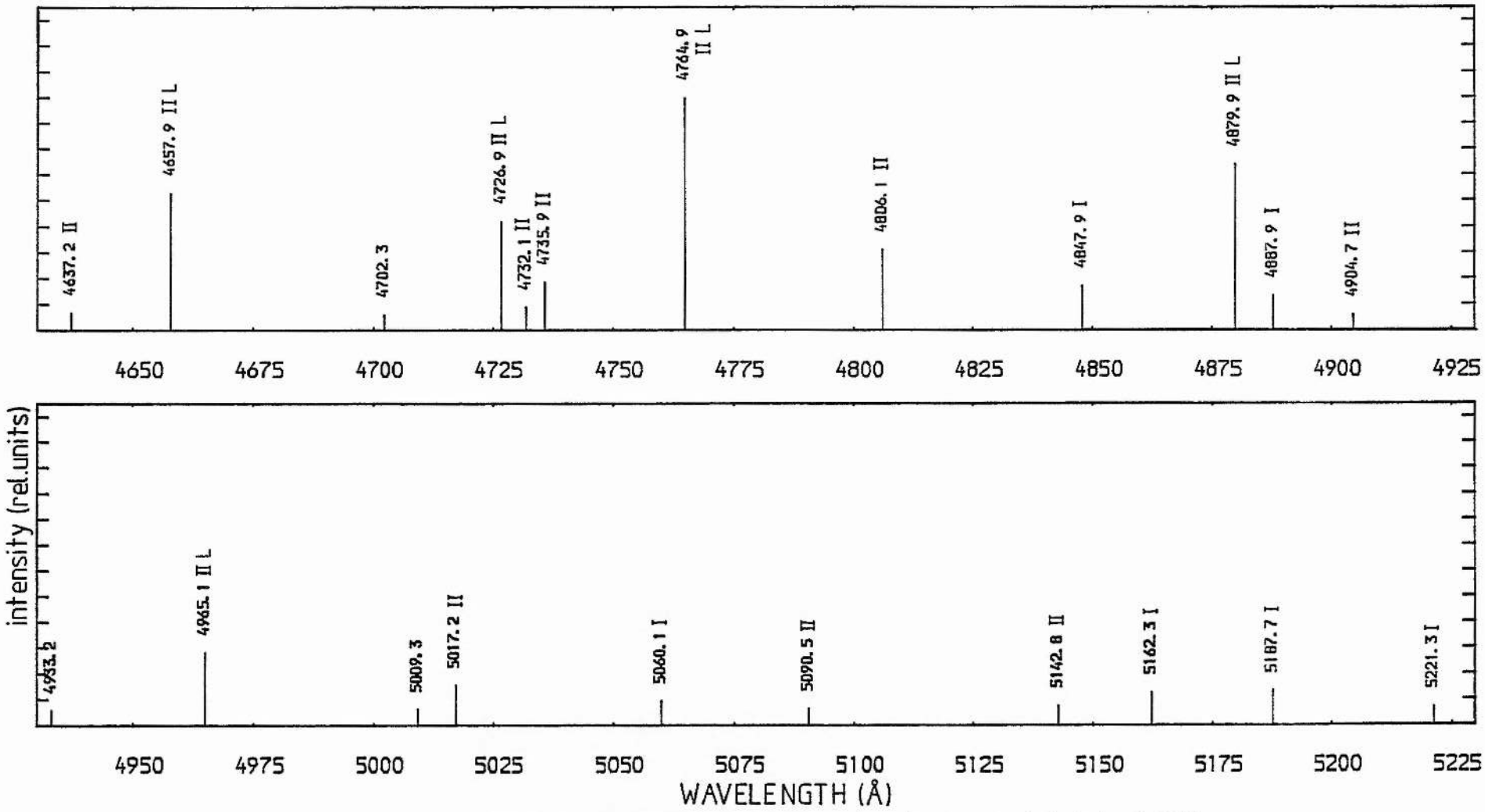

Fig 5.13b. A spectrum of the e-beam plasma glow in argon at 0.3mA, 0.39kV and 0.7mb, with an oxygen admixture at 0.06mb. I: atomic transitions, II: ionic transitions, L: known laser transitions.

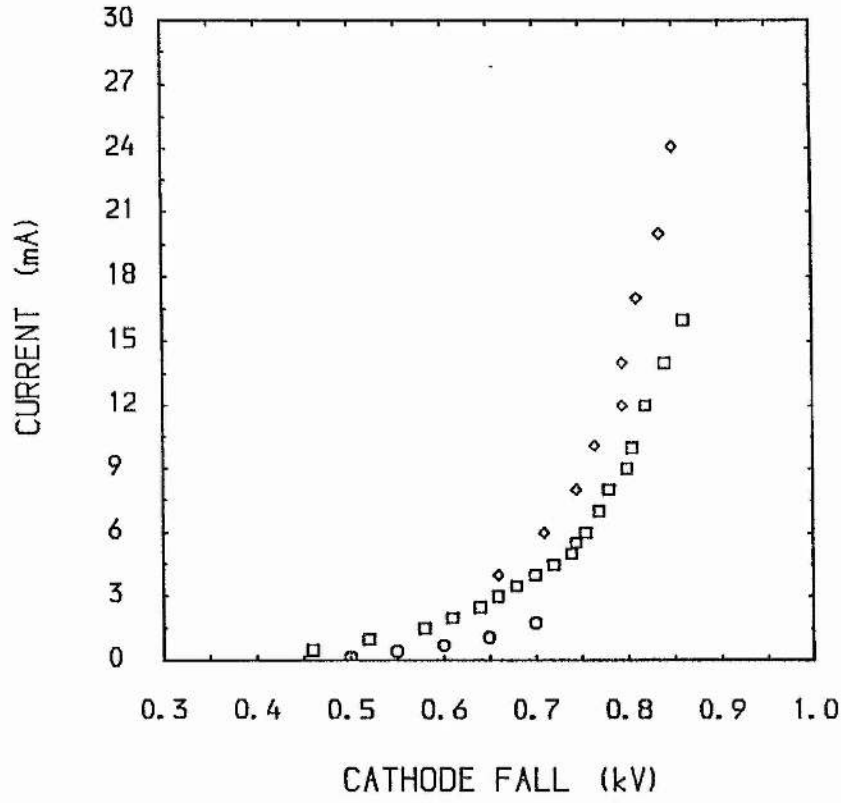

Fig 5.14. Values of the discharge current and Cathode fall taken during the measurements of spectral line intensities. ◇ : 0.4mb, □ : 0.4mb (subsequent run), ○ : 0.27mb.

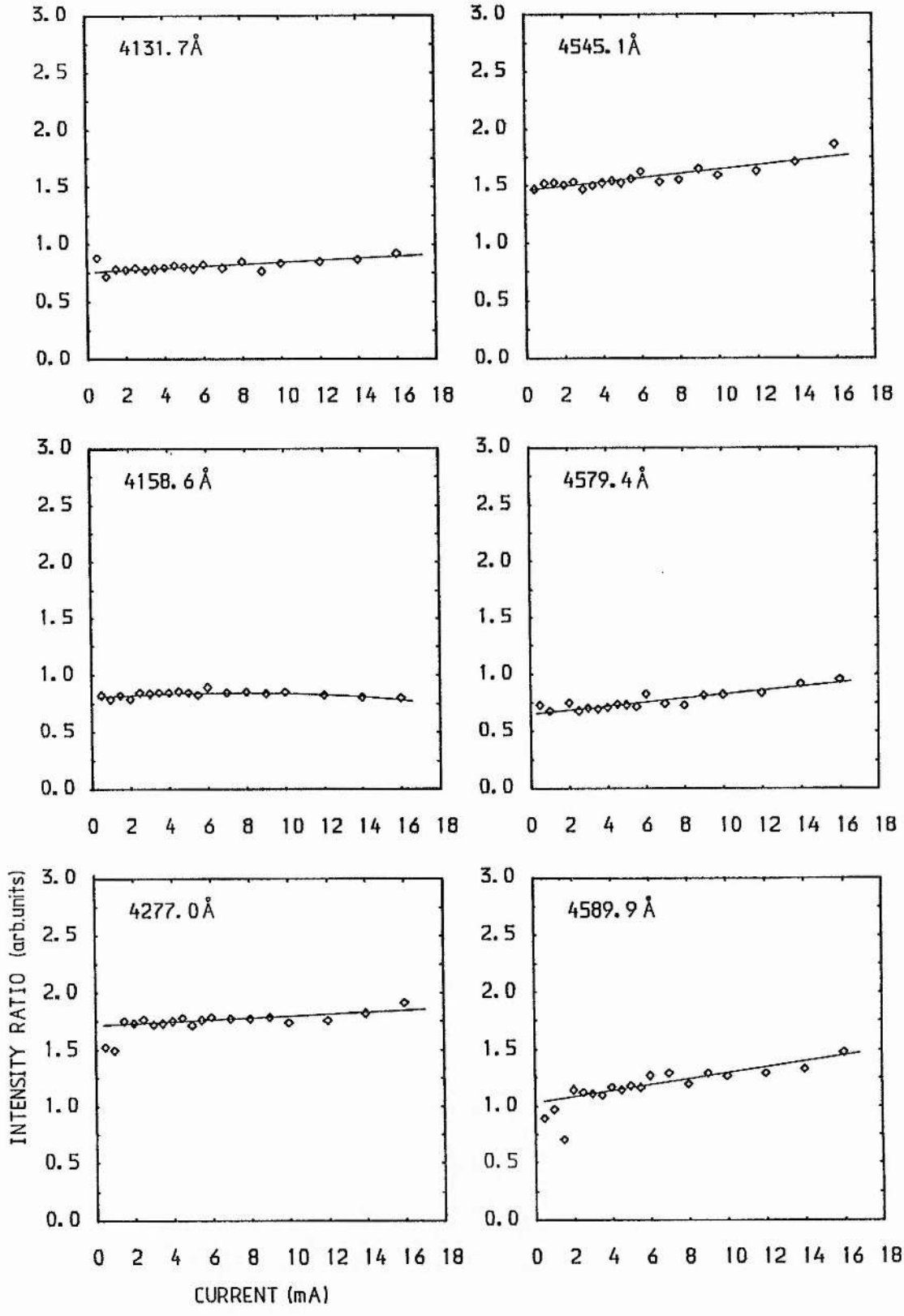

Fig 5.15a. Intensity ratios of the principle ArII emission lines in the e-beam plasma, using the intensity of the emission line at 4259Å as a common denominator. The ratios for the line at 4158Å (ArI) are almost constant over the current range investigated, as would be expected.

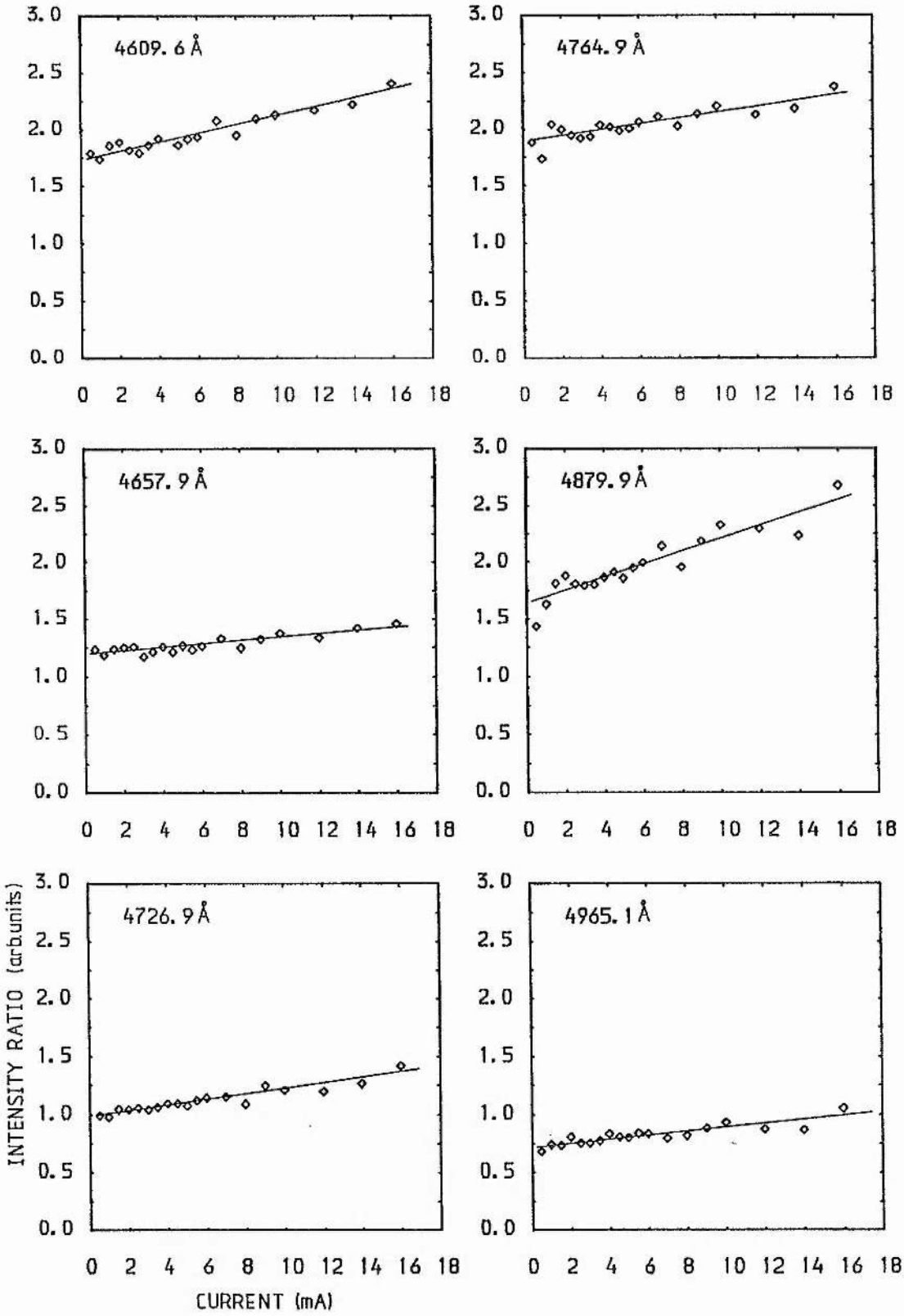

Fig 5.15b. Intensity ratios of the principle ArII emission lines in the e-beam plasma, using the intensity of the emission line at 4259Å as a common denominator.

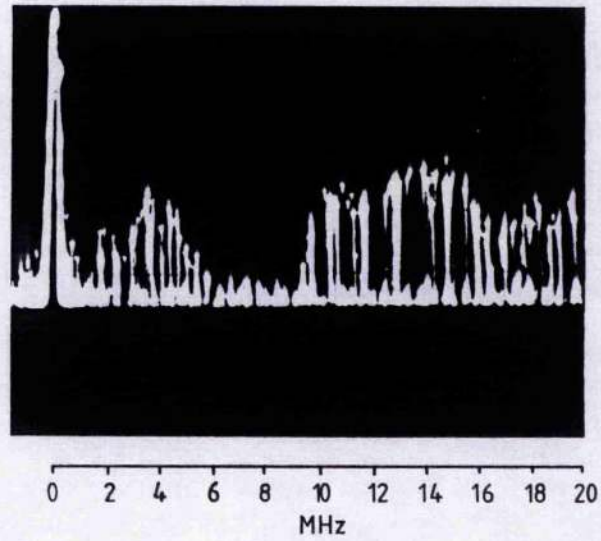

Fig 5.16a. RF emission from the e-beam plasma in argon at 0.4mb, 1.0mA and 0.48kV.

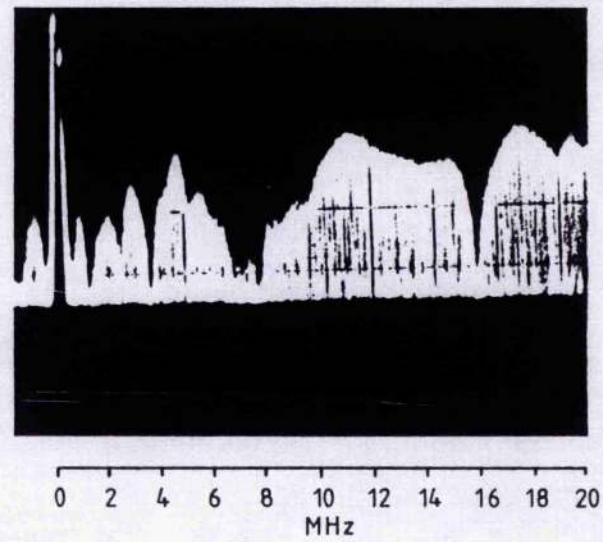

Fig 5.16b. RF emission from the e-beam plasma in argon at 0.4mb, 15.0mA and 0.875kV.

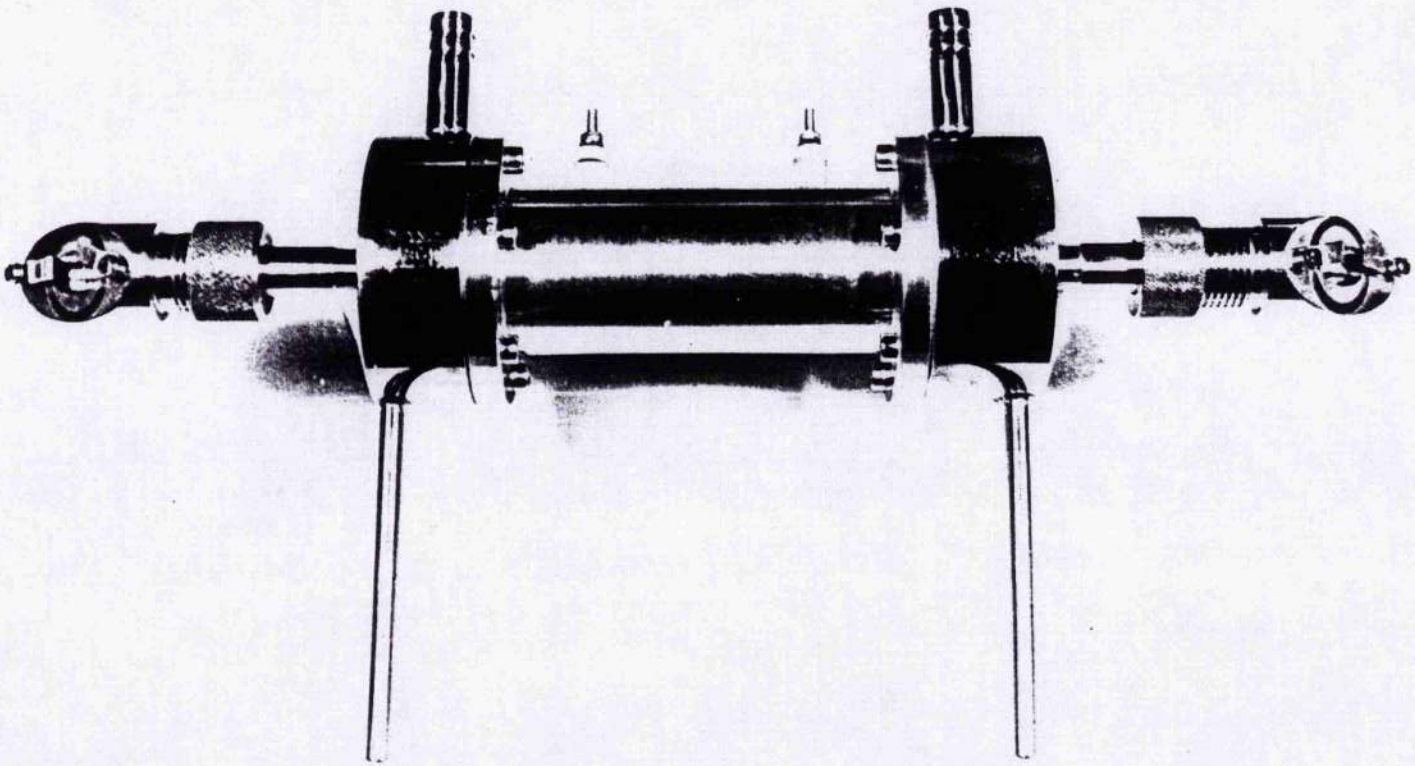

Plate 2. The discharge cell used to investigate electron beam production from multiple electron gun cathodes in argon.

Appendix I

It has been proposed by Bayless et-al [1] that a continuous glow discharge can be used as a source of electrons to achieve continuous pumping of a gaseous laser medium. The transverse pumping geometry suggested is used in conjunction with a thin metal foil separating the gun and laser volumes as shown in fig a.1. This scheme allows the electron gun and the laser medium to be operated independently. To examine the practicality of such a scheme, both the coupling efficiency of beam energy to the gas and the loss of electron energy to the foil element must be determined. A similar set of calculations have been carried out by Dutov et-al [2] for electron energies in the range 100-250keV using a Monte Carlo simulation. Those calculations, however, are confined to CO_2-N_2-He mixtures at pressures of around one atmosphere, and based on discharge tube diameters of about 10cm. The following calculations are based on gas cells containing pure helium, neon or argon.

The energy (ΔE) lost by an electron passing through a slab of material of density (ρ) and thickness (Δx) is given by

$$\Delta E = \left[\frac{1}{\rho}\frac{dE}{dx}\right]\rho.\Delta x \qquad (a.1)$$

with

$$S_p = \left[\frac{1}{\rho}\frac{dE}{dx}\right] \quad [eV.cm^2.g^{-1}]$$

where S_p is the stopping power of the material, which is a function of the electron energy (E). The total penetration depth into the medium

(X_o) of electrons with initial energy (E_o) can be found by taking the integral of (a.1):

$$X_o = \int_0^{E_o} (ke.\rho.S_p)^{-1}\, dE \qquad (a.2)$$

with ke = 2

where (ke) is a 'Straggling factor', a constant value, which is included to take into account the zig-zag path followed by electrons traversing thick targets [3]. The Straggling factor accounts for multiple scattering of the electrons in both the gas and metal foil, and the calculation is then simplified to motion in one dimension. Therefore, individual elastic and inelastic collisions are not considered, and the attenuation is calculated on the basis of a continuous loss of electron energy. This type of model is known as a 'continuous slowing down approximation' (CSDA).

Tabulated values of the stopping power for electrons of energies between 10keV and 1MeV are available [4] and penetration depths into helium, neon and argon have been calculated from eq a.2, as a function of initial electron energy E_o and gas density ρ (in mb). The results are shown in figs a.2, a.4 and a.6. In practice, the individual electrons have different collision case histories, so the ranges calculated here represent average values. The electron energy and gas pressure must be chosen so that the penetration depth matches the diameter of the gain tube (typically 1-2cm for a metal vapour/rare gas laser). A similar range calculation has been carried out to estimate the transmission efficiency (ϵ) of electrons through thin titanium foils of various thicknesses. This efficiency is plotted in

figs a.3, a.5 and a.7, together with the coupling efficiency (η) of electron energy into the gas contained within a 2cm diameter tube. Titanium is often used as a window element in preference to steel or aluminium foils since it has a higher tensile strength for a given beam attenuation. Bayless et-al report an experimental figure of $(50\pm6)\%$ for the transmission efficiency of 100keV electrons through a 13.8 micron titanium foil. This agrees well with the figure of 57% calculated here.

The thinnest foil element which can be used for practical reasons is about 10 microns. This thickness of foil is sufficient to withstand a pressure differential of about 500mb. Electrons with energies greater than about 60keV are required, therefore, to penetrate through a 10 micron foil. For efficient energy coupling to the gas, an electron must have an energy lower than about 20keV, preferably, in the case of helium. In neon, the coupling is efficient below about 30keV and in argon, below about 40keV. An overall efficiency, which is the ratio of coupled energy to the initial energy, also has been calculated as a function of electron energy. This is shown in figs a.3, a.5 and a.7 for a foil thickness of 10 microns, a 2cm gas cell diameter, and a gas pressure of 500mb. The resulting sharp peak in efficiency around 65-70keV is found for all three rare gases. Electrons of this energy lose about 40keV during their passage through the foil and subsequently emerge with energy of about 20keV, thereby enabling them to couple efficiently with the gas. However, a device operating around this small energy range is susceptible to foil damage through substantial heating by the beam if run continuously. Metal foils of this thickness cannot rapidly dissipate heat thus leading to large internal temperature gradients and structural stresses.

The conclusion reached from this analysis is that the overall efficiency of this scheme is low in the case of helium, reaching a peak of about 18% around a small range of electron energies. For neon and argon, the overall efficiencies are generally higher, and peak at 35% and 44% respectively, with the peaks extending over a somewhat broader range of energies. Both factors reflect the greater attenuation of electron energy by these heavier gases. Therefore, argon gas is better suited to work as a laser medium than a helium/metal vapour mixture. However, such a device is probably limited to operating in a pulsed mode.

Finally, electrons with energy somewhat higher than that corresponding to the peak efficiency are required for two reasons. Firstly, the transmission losses through the foil decrease quite rapidly with increasing electron energy in the range 70-100keV (thus reducing foil damage). Secondly, electrons which overshoot the gas medium provide more uniform excitation of the gas volume. Electrons with energies in the range 60-70keV, corresponding to the leading edge of the overall efficiency curve, do not produce excitation across the full 2cm gap.

Electron beam excitation of a helium/metal vapour mixture using electrons of energies in the range (10-100keV) in conjunction with a thin 10 micron titanium foil window and a gain medium of 2cm width, is shown to be inefficient. Probably less than about 10% of the beam energy is coupled into the laser gas. However, using the same general scheme with argon gas as a gain medium, it is shown that a pulsed or quasi-CW system might be feasible using electrons of energies [70-100keV].

References

1. Bayless J.R. and Knechtli R.C., IEEE., J.Q.E., QE-10, 213 (1974)

2. Dutov A.I., Minaev S.V. and Nikolaev V.B., Sov. J.Q.E., 9, 995 (1979)

3. O'Neill F., 'Physics and Technology of High Power E-Beam Pumped KrF^{*} Lasers', (unpublished), Rutherford Appleton Lab, (1982)

4. Berger M.J. and Seltzer S.M., 'Tables of Energy Losses and Ranges of Electrons and Positrons', NASA report SP-3012, (1964)

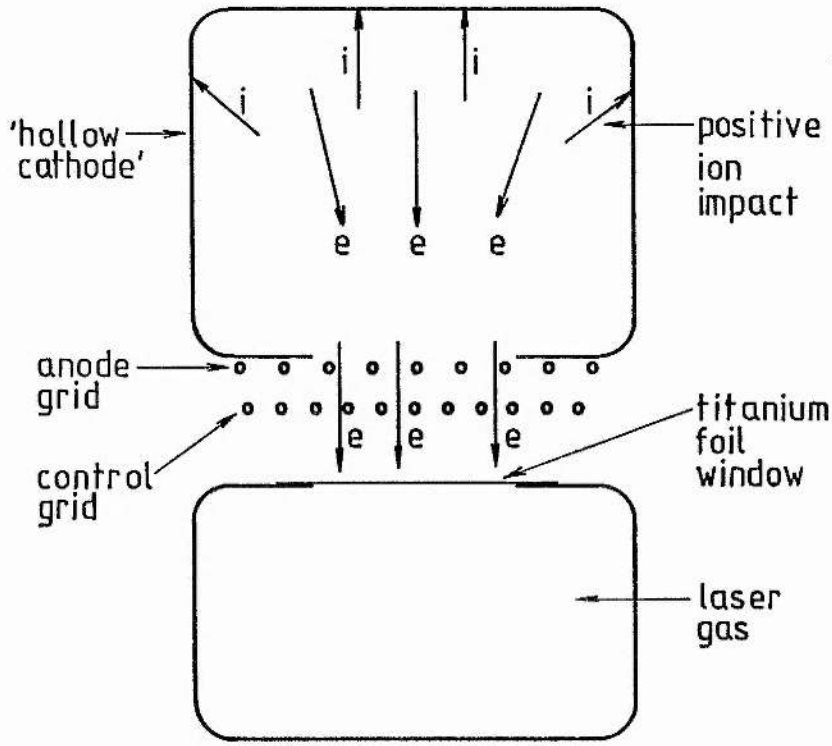

Fig a.1. Transverse e-beam pumping of a gas laser. Electrons are generated by secondary emission in the e-gun, and the control grid is used to adjust the beam current.

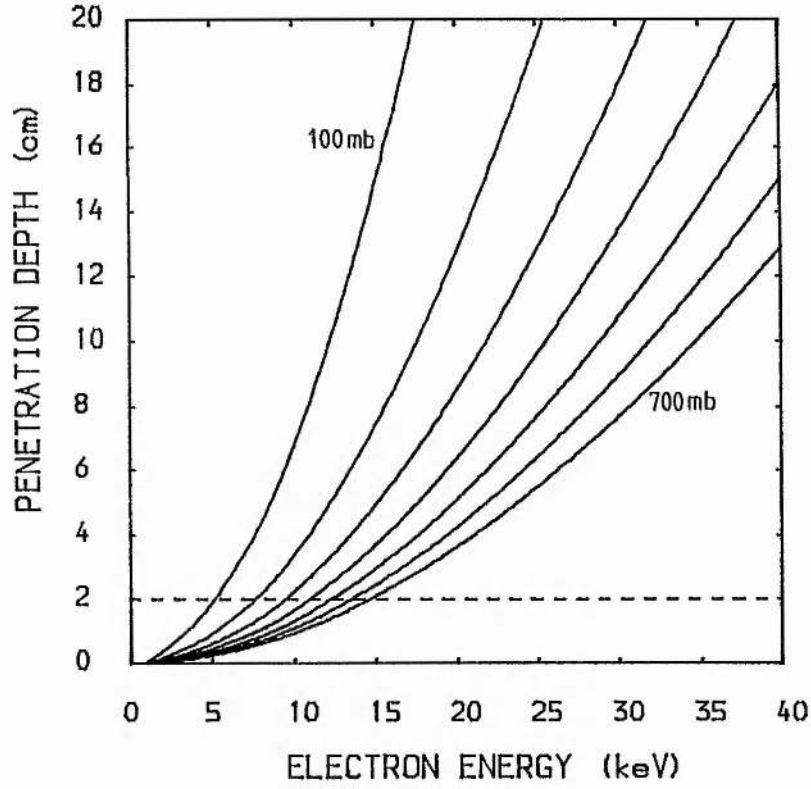

Fig a.2. Penetration depths of fast electrons in helium as a function of initial energy, with pressure as a parameter.

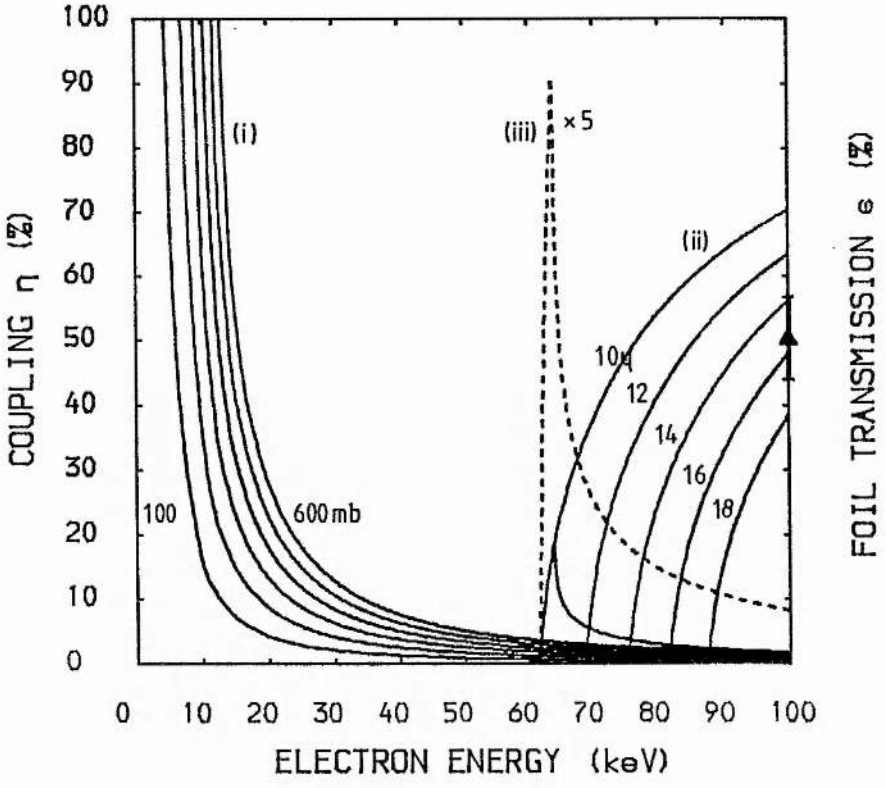

Fig a.3. (i) Coupling efficiency (η) of electrons to a helium cell 2cm wide, with pressure as a parameter. (ii) Transmission efficiency (ε) of electrons through thin titanium foils, with foil thickness as a parameter. (iii) Overall coupling efficiency of beam energy to the gas cell. (▲-Bayless et-al)

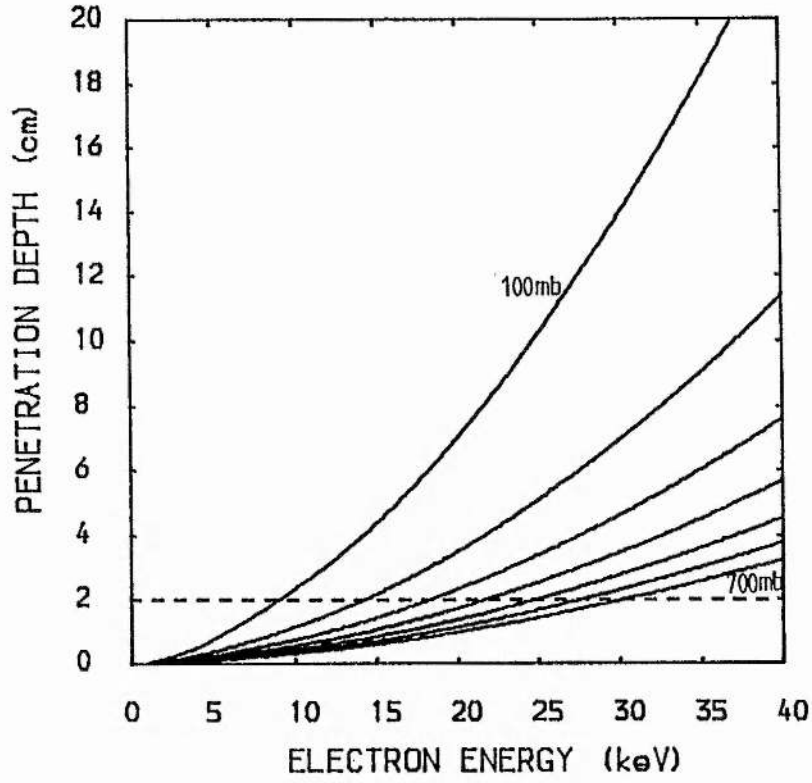

Fig a.4. Penetration depths of fast electrons in neon as a function of initial energy, with pressure as a parameter.

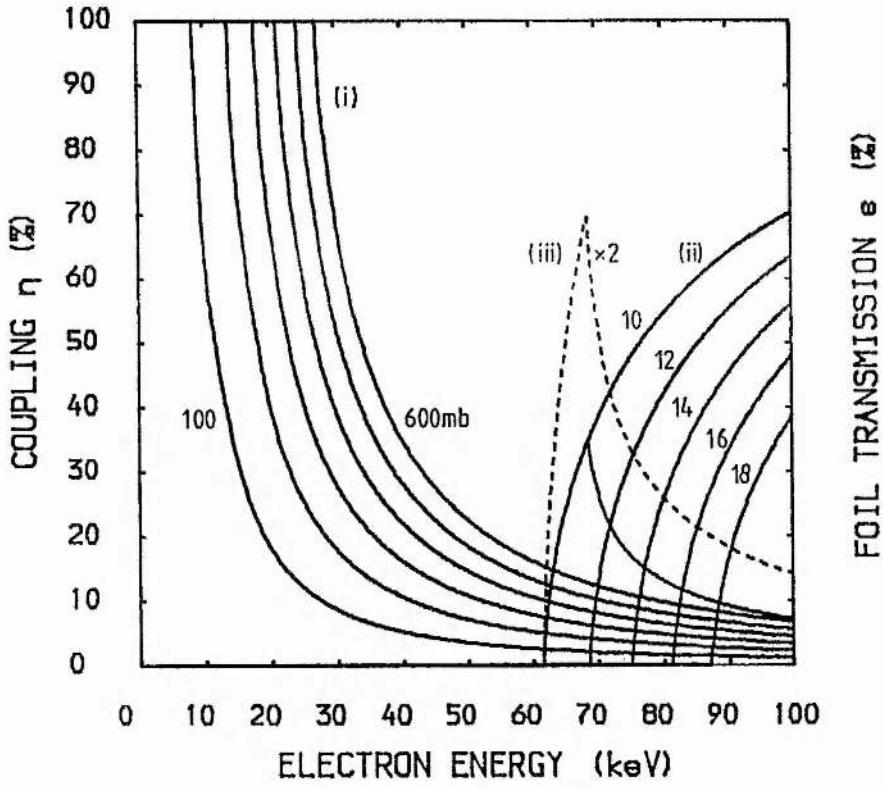

Fig a.5. (i) Coupling efficiency (η) of fast electrons to a gas cell of neon, with pressure as a parameter. (ii) Transmission efficiency (ε) in the titanium foils. (iii) Overall coupling efficiency.

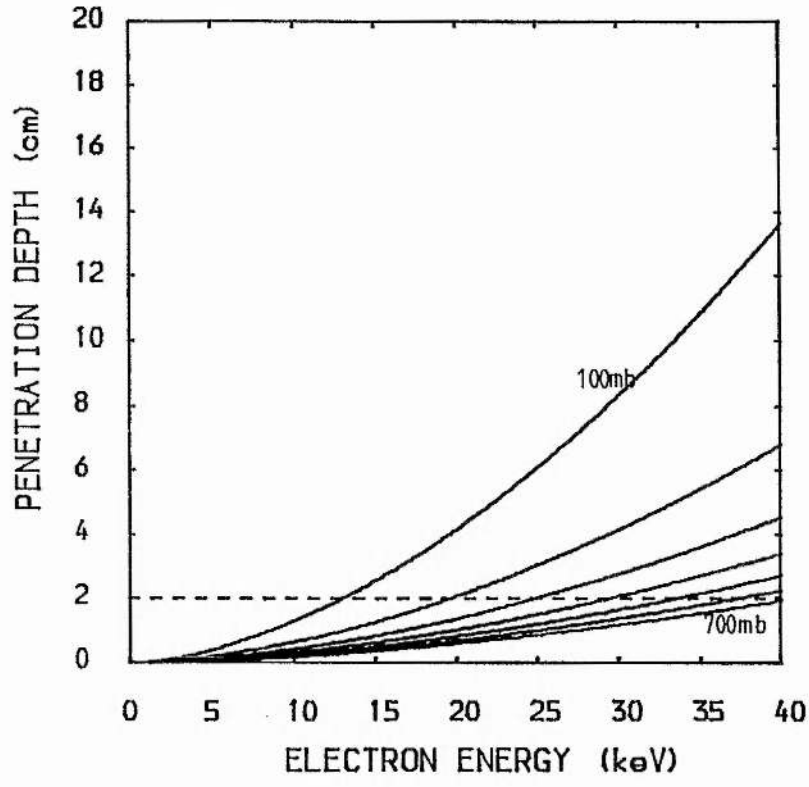

Fig a.6. Penetration depths of fast electrons in argon as a function of initial energy, with pressure as a parameter.

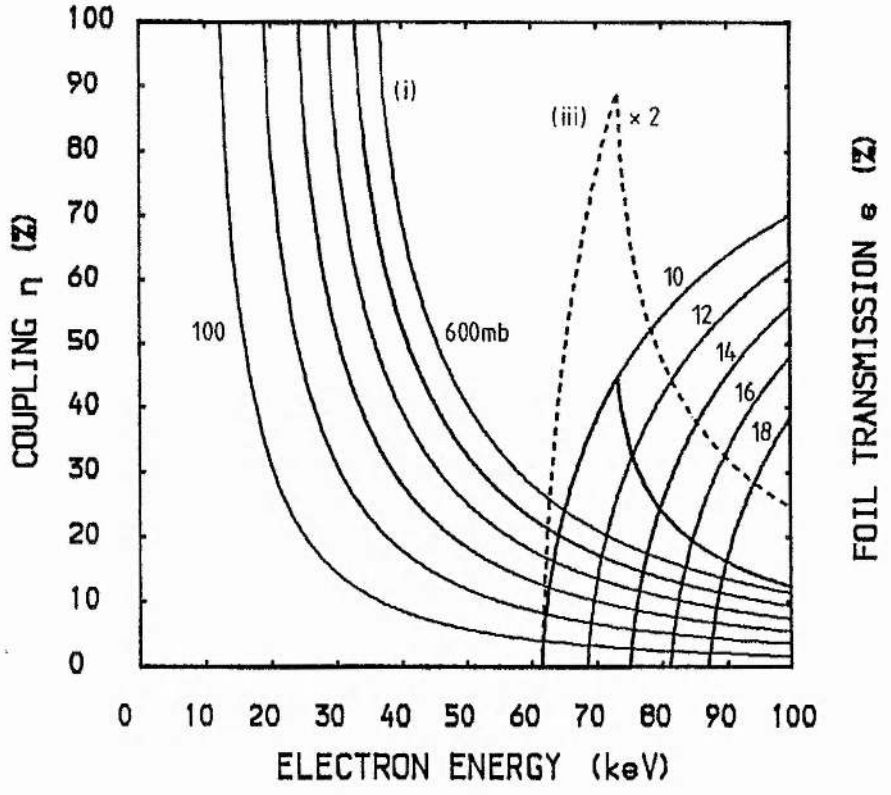

Fig a.7. (i) Coupling efficiency (Π) of electrons to a gas cell of argon, with pressure as a parameter. (ii) Transmission efficiency (ε) in the titanium foils. (iii) Overall coupling efficiency.

Appendix II.1

The Inelastic Collision Cross-Sections in Helium

The cross-sections developed by Alkhazov [1] which have been used in this study are given below. The energy units used throughout are Rydbergs (13.6eV) and the cross-sections are given in units of 10^{-16} cm^2 unless otherwise stated.

1. The ionisation cross-section $Q_i(E)$

The cross-section for ionisation at electron energy E is given by the following expression:

$$Q_i(E) = \frac{8.br}{E.F(E)} \left\{ \left[\frac{1}{I_o}\left(1-\frac{I_o}{E}\right) - \frac{1}{E+W} \ln \frac{E}{I_o} \right] + \left(1-\frac{I_o^2}{E^2}\right) M_i^2 \ln\left(d+\left[C_1(E-I_o)\right]^{\frac{1}{2}}\right) \right\} \quad (a.3)$$

$$F(E) = 1+\frac{A}{E}\,\frac{1+(A/E)}{1+(BE)}$$

where I_o=1.8079, M_i^2=0.49, d=1.6, C_1=0.15, W=67.7, A=5.34, B=0.027, and br=0.8791 are all constants.

2. The differential cross-section $\sigma_E(\epsilon)$

This is represented by the following expression:

$$\sigma_E(\epsilon) = \frac{8}{E.F(E)} \left\{ \left[\frac{1}{\epsilon^2} + \frac{1}{\epsilon_1^2} - \frac{E+I_o}{E+W}\,\frac{1}{\epsilon\epsilon_1} \right] + 2\left[\frac{1}{\epsilon^2} + \frac{1}{\epsilon_1^3} \right] M_i^2 I_o^2 \ln\left(d+\left[C(E-I_o)\right]^{\frac{1}{2}}\right) \right\} \quad (a.4)$$

$\epsilon_1 = E+I_o-\epsilon$, $F(E) = 1+(W/E)$

The units of $\sigma_E(\epsilon)$ are set arbitrarily and in all calculations, a normalised version of eq.(a.4) is used.

3. The excitation cross-sections

Electron-impact excitation from the helium ground state to the states np^1P, ns^1S, nd^1D, ns^3S, np^3P and nd^3D are considered here and only levels whose cross-sections are more than 1% of the peak of $Q_i(E)$ around ~100eV are taken into account. The cross-sections for excitation to np^1P states are given by the following expression:

$$Q_{np^1P}(E) = \frac{4.br\,[1-((U_{np^1P})^2/E^2)]}{E.U_{np^1P}.G(E)}\; f_{np^1P} \ln[d'+C'(E-U_{np^1P})] \qquad (a.5)$$

$$G(E) = 1+\frac{A'}{E}\,\frac{1+(B'/E)}{1+(D'E)^4}$$

where A'=0.96, B'=1.3, C'=0.65 and D'=0.05 are constants, U_{np^1P} are the excitation threshold potentials [2] and f_{np^1P} are the oscillator strengths for the transitions. The values of U_{np^1P} and f_{np^1P} used are tabulated below:

Transition	U_{np^1P}	f_{np^1P}
$1s^1S-2p^1P$	1.5623	0.2762
$-3p^1P$	1.7000	0.0734
$-4p^1P$	1.7481	0.0307
$-5p^1P$	1.7705	0.0157

Table a.1

The cross-sections for excitation to the other atomic states are represented by the following series of expressions:

$$Q_{ns\,^1S} = \frac{4\,B_0}{U_{ns\,^1S}} \frac{(1-U_{ns\,^1S}/E)}{E} \qquad (a.6a)$$

$$Q_{nd\,^1D} = \frac{4\,B_n}{U_{nd\,^1D}} \frac{(1-U_{nd\,^1D}/E)}{(E+U_{nd\,^1D})} \qquad (a.6b)$$

$$Q_{ns\,^3S} = \frac{4\,B_n}{U_{ns\,^3S}} \frac{(1-U_{ns\,^3S}/E)}{E^3} \qquad (a.6c)$$

$$Q_{nd\,^3D} = \frac{4\,B_n}{U_{nd\,^3D}} \frac{(1-U_{nd\,^3D}/E)}{E^2(E+U_{nd\,^3D})} \qquad (a.6d)$$

$$Q_{np\,^3P} = \frac{4\,B_n}{U_{np\,^3P}} \frac{(1-U_{np\,^3P}/E)}{(E+U_{np\,^3P})^3} \qquad (a.6e)$$

The parameter B_n for each group of levels is given by:

$$B_n = br\,(B_o/n^3) \qquad (a.7)$$

Values of $U_{nl\ L}$ and B_o are given in table a.2 below:

Level		$U_{nl\ L}$	B_o
ns^1S	$2s^1S$	1.5179	0.36
	$3s^1S$	1.6876	
	$4s^1S$	1.7431	
nd^1D	$3d^1D$	1.6989	0.33
	$4d^1D$	1.7477	
ns^1S	$2s^3S$	1.4593	2.24
	$3s^3S$	1.6727	
	$4s^3S$	1.7372	
np^3P	$2p^3P$	1.5436	10.8
	$3p^3P$	1.6940	
	$4p^3P$	1.7456	
nd^3D	$3d^3D$	1.7477	1.24
	$4d^3D$	1.7702	

Table a.2

References

1. Alkhazov G.D., Sov.Phys.-Tech.Phys., 15, 66 (1970)

2. Bashkin S. and Stoner J.O., 'Atomic Energy Levels and Grotrian Diagrams', vol I, (1975)

Appendix II.2

The simulation of electron motion in the cathode regions of a helium glow discharge has been carried out using two Fortran programmes. The first, 'darksp1.for', performs calculations of the electron flux in the Cathode dark space. The second, 'herange1.for', is used for calculations in the Negative glow. Modified versions of these two programmes have been used to calculate a number of discharge parameters. The number of calculations performed by the programmes increases when higher values of the Cathode fall are selected initially. The maximum processing time on the St Andrews VAX 11/780-5 computer is one hour. This limits the selection of the Cathode fall to values less than about 1.0kV, as shown in fig a.8.

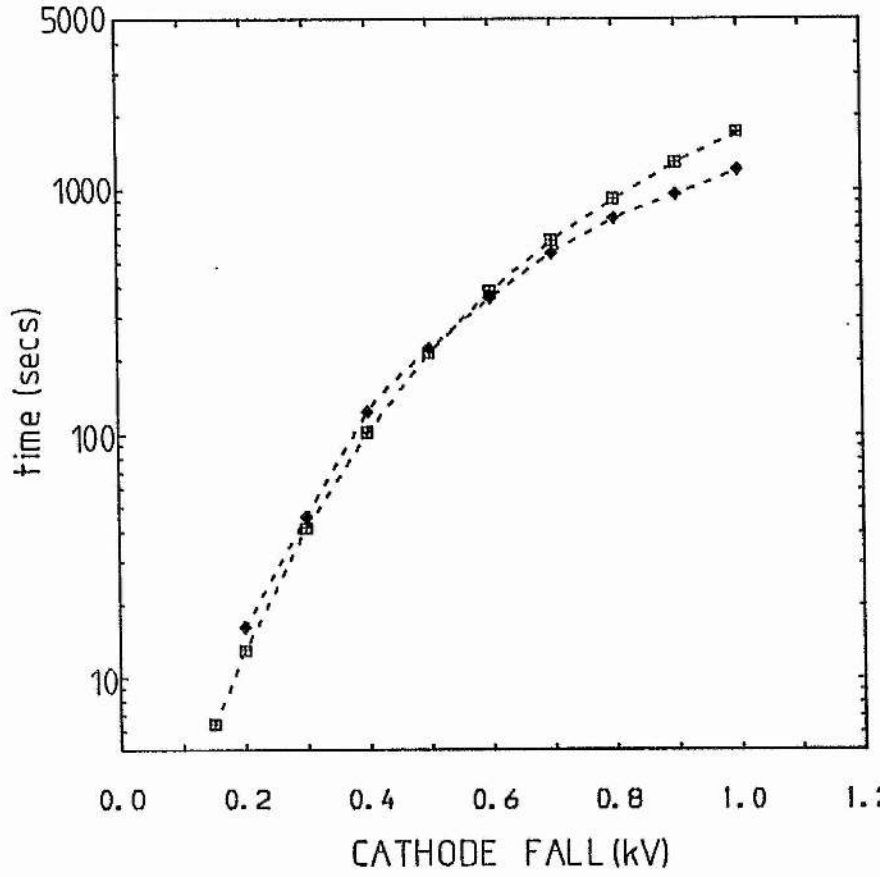

Fig a.8. The processing time for the programmes 'darksp1.for'(⊞) and 'herange1.for' (⊕) for selected values of the Cathode fall.

DARKSP1.FOR

```
      real f(5000),df,f1,dex,dion,dsumx
      real ftot,nmin,crs,dsum,fetot,mtot
      real po,f3(5000),pen(5000),ion(5000),exc(5000)
      real ex,r1,e(5000),np,sum1,sum2,sum3,ge,qn1p
      real bn,d1,qn1s,dx(5000),qi(5000)
      real qextot,fei,qr2(5000),qion,qsig,i2,qr1(5000)
      real bohr,cons,temp,na,un1p(5),fn1p(5),a,b,c,d,ds,un1s(5)
      real un3p(5),ai,bi,ci,di,w,mi2,io,ke,exx,qn3s,qn3p
      real sum5,sum6,sum7,sum8,sum9,sum10,sum12,ei,epj,de1,de2
      real fo(3000,300),eps(7500),sig(7500)
      real cpu,un3s(5),un1d(5),un3d(5),qn1d,qn3d,cfall
      real fxm,p,foxj,dxr,fx,f5(5000)
      integer j,m,n,x,de,nochar,u,jo,xv,xr,r,xm,ro,xu,m1,x1,m3,en
      integer u2,jj,m2
      integer*4 ist,ifn
      call actim(ist)
      nochar=233
      u=1
      ro=0
      ke=1.0
      bohr=8.7975e-17
      na=6.023e+23
      cons=8.3138e+4
      temp=273.0
      dsum=0.0
      dsumx=0.0
      p=1.0
      np=(na*p*ke)/(cons*temp)
      io=1.8079
      i2=13.6*io
      de=1
      u2=2
      en=1032
      cfall=((float(en))-15.0)*0.984
      m=en
      exx=0.0-1.0
      write(81,50) m
C       SELECT ELECTRON ENERGY E
      do 20 x=1,m
      exx=exx+(float(de))
      ex=exx*0.984
      e(x)=ex
C       EXCITATION COLLISION CROSS-SECTIONS AT ENERGY E
      un1p(1)=1.5623
      un1p(2)=1.7
      un1p(3)=1.7481
      un1p(4)=1.7705
      fn1p(1)=0.2762
      fn1p(2)=0.0734
      fn1p(3)=0.0307
      fn1p(4)=0.0157
      qtn1p=0.0
      a=0.96
      b=1.3
      c=0.65
      d=0.05
      ds=2.0
      ex=ex/13.6
      qn1p=0.0
      do 21 j=1,4
```

```
      crs=un1p(j)
      if(ex.lt.crs) goto 21
      sum1=1+((d*ex)**4)
      sum1=(1+(b/ex))/sum1
      ge=1+((a/ex)*sum1)
      sum2=ds+(c*(ex-un1p(j)))
      sum2=log(sum2)
      sum2=(fn1p(j)*sum2)/(ex*un1p(j))
      sum2=(4*sum2)/ge
      sum2=(1-((un1p(j)/ex)**2))*sum2
      sum2=sum2*bohr
      qn1p=qn1p+sum2
21      end do
      un1s(2)=1.5179
      un1s(3)=1.6876
      un1s(4)=1.7477
      qn1s=0.0
      do 22 j=2,4
      crs=un1s(j)
      if(ex.lt.crs) goto 22
      sum1=(1-(un1s(j)/ex))**0.5
      sum1=(4*sum1)/(ex*un1s(j))
      bn=0.36/(j**3)
      qn1s=qn1s+((bn*sum1)*bohr)
22      end do
      un3s(2)=1.4593
      un3s(3)=1.6727
      un3s(4)=1.7372
      qn3s=0.0
      do 23 j=2,4
      crs=un3s(j)
      if(ex.lt.crs) goto 23
      sum1=(1-(un3s(j)/ex))**0.5
      sum1=(4*sum1)/((ex**3)*un3s(j))
      bn=2.24/(j**3)
      qn3s=qn3s+((bn*sum1)*bohr)
23      end do
      un3p(2)=1.5436
      un3p(3)=1.694
      un3p(4)=1.7456
      qn3p=0.0
      do 24 j=2,4
      crs=un3p(j)
      if(ex.lt.crs) goto 24
      sum1=(1-(un3p(j)/ex))**0.5
      sum1=(4*sum1)/((ex+un3p(j))**3)
      sum1=sum1/un3p(j)
      bn=10.8/(j**3)
      qn3p=qn3p+((bn*sum1)*bohr)
24      end do
      un1d(3)=1.6989
      un1d(4)=1.7477
      qn1d=0.0
      do 25 j=3,4
      crs=un1d(j)
      if(ex.lt.crs) goto 25
      sum1=(1-(un1d(j)/ex))**0.5
      sum1=(4*sum1)/((ex+un1d(j))*un1d(j))
      bn=0.33/(j**3)
      qn1d=qn1d+((bn*sum1)*bohr)
```

```
25      end do
      un3d(3)=1.7477
      un3d(4)=1.7702
      qn3d=0.0
      do 26 j=3,4
      ors=un3d(j)
      if(ex.lt.ors) goto 26
      sum1=(1-(un3d(j)/ex))**0.5
      sum1=(4*sum1)/((ex+un3d(j))*(ex**2))
      sum1=sum1/un3d(j)
      bn=1.24/(j**3)
      qn3d=qn3d+((bn*sum1)*bohr)
26      end do
      qextot=qn1s+qn1p+qn3s+qn3p+qn3d+qn1d
      qion=0.0
      if(ex.lt.io) goto 27
        ai=5.34
      bi=0.027
      ci=0.15
      di=1.6
      w=67.7
      mi2=0.49
      sum1=1+((bi*ex)**3)
      sum1=(1+(ai/ex))/sum1
      fei=((ai/ex)*sum1)+1
      sum1=(ci*(ex-io))**0.5
      sum1=log((sum1+di))
      sum1=sum1*mi2
      sum1=(1-((io/ex)**2))*sum1
      sum2=ex/io
      sum2=log(sum2)
      sum2=sum2/(ex+w)
      sum3=1-(io/ex)
      sum3=sum3/io
      sum3=sum3-sum2+sum1
      qi(x)=(sum3*8.0)/(ex*fei)
      qion=qi(x)*bohr
27    qsig=qion+qextot
      if(qsig.eq.0.0) goto 28
      qr1(x)=qion/qsig
      qr2(x)=qextot/qsig
28    dx(x)=qsig*np
      if(ex.lt.io) goto 20
      sum12=0.0
      de1=0.984/13.6
      de2=(ex+(24.55/13.6))**0.5
      sum5=(ci*(ex-io))**0.5
      sum5=log((di+sum5))
      sum5=mi2*sum5
      sum5=sum5*(io**2)
      sum6=1+(w/ex)
      sum6=8.0/(ex*sum6)
      sum7=(ex+io)/(ex+w)
      epj=io-de1
      do 10 j=1,300
      eps(j)=epj+de1
      epj=eps(j)
      if(epj.lt.de2) goto 13
      jo=j
      goto 11
```

```
13      ei=ex+io-epj
        sum8=1/(ei**3)
        sum8=sum8+(1/(epj**3))
        sum8=2*(sum8*sum5)
        sum9=1/(ei*epj)
        sum9=sum7*sum9
        sum10=1/(ei**2)
        sum9=sum10-sum9
        sum10=1/(epj**2)
        sum9=sum8+sum9+sum10
        sig(j)=sum6*sum9
        eps(j)=eps(j)-io
        sum12=sig(j)+sum12
10      end do
        jo=301
11      do 12 j=1,300
        if(j.eq.jo) goto 14
        fo(x,j)=sig(j)/sum12
12      end do
        goto 20
14      fo(x,j)=0.0
20      continue
        f(1)=0.0
        f(2)=0.25
        f(3)=0.5
        f(4)=0.75
        f(12)=0.75
        f(13)=0.5
        f(14)=0.25
        do 29 x=15,m
        f(x)=0.0
29      end do
        do 39 x=5,11
        f(x)=1.0
39      continue
        po=0.0
c       write(81,53) po
        do 47 x=1,m
        f5(x)=f(x)
c       write(81,52) e(x),f5(x)
47      end do
        d1=0.835
        m2=m-15
c       write(81,50) m
c       write(83,50) m2
c       write(84,50) m2
c       write(86,50) m2
c       write(87,50) m2
c       write(88,50) m2
        do 30 r=1,m2
        xm=r+13
        sum1=d1-po
        if(r.ne.m2) goto 49
        dxr=sum1
        goto 46
49      sum2=(sum1**2)-((0.984*(d1**2))/cfall)
        dxr=sum1-(sum2**0.5)
46      pen(r)=dxr+po
        po=pen(r)
        ion(r)=0.0
```

```
      exc(r)=0.0
      ftot=0.0
      fetot=0.0
      if(xm.lt.23) goto 31
      do 35 x=1,xm
      if(x.lt.23) goto 35
      xv=x
      xu=1
      fx=f(x)
      if(fx.eq.0.0) goto 35
      df=0.0-(dxr*dx(x))
      df=(1-(exp(df)))*f(x)
      f(x)=f(x)-df
      dion=df*qr1(x)
      dex=df*qr2(x)
      ion(r)=dion+ion(r)
      dsum=dsum+dion
      exc(r)=exc(r)+dex
      dsumx=dsumx+dex
      xv=xv-22
      if(xv.lt.1) goto 35
      f(xv)=f(xv)+dex
      xv=xv-3
      if(xv.lt.1) goto 35
      do 36 j=1,300
      foxj=fo(x,j)
      if(foxj.eq.0.0) goto 35
      f1=fo(x,j)*dion
      f(xv)=f(xv)+f1
      f(xu)=f(xu)+f1
      xu=xu+1
      xv=xv-1
36      end do
35      end do
31    do 38 x=1,xm
      x1=x+1
      f3(x1)=f(x)
38      end do
      m1=xm+1
      do 32 x=2,m1
      f(x)=f3(x)
      fx=f(x)
      ftot=ftot+fx
      fetot=fetot+(fx*e(x))
32      end do
      f(1)=0.0
      fetot=fetot/ftot
c     write(87,52) pen(r),fetot
      mtot=ftot/10.0
c     write(88,52) pen(r),mtot
      ion(r)=ion(r)/(dxr*(1.0e+1))
      exc(r)=exc(r)/(dxr*(1.0e+1))
c     write(84,52) pen(r),ion(r)
c     write(86,52) pen(r),exc(r)
      ion(r)=ion(r)/(ftot*0.1)
c     write(83,52) pen(r),ion(r)
      ro=ro+1
      if(ro.ne.134) goto 30
c     write(81,53) po
      do 37 x=1,m
```

```
      f5(x)=f(x)
c     write(81,52) e(x),f5(x)
37      end do
      ro=0
30      continue
c     write(81,53) po
      do 45 x=1,m
      f5(x)=f(x)
      write(81,52) e(x),f5(x)
45      continue
      write(81,53) dsum
      write(81,53) dsumx
50      format(I6)
52      format(2e10.5)
53      format(1e10.5)
54      format(3e10.5)
55      format(7e10.5)
      call actim(ifn)
      cpu=0.01*(ifn-ist)
      write(81,53) cpu
      stop
      end
```

HERANGE1.FOR

```
      real fun,roo,nmin,k1,ion1,ion2,ion3
      real po,crs,dfx,dsum,pen(5000),ion(5000),exc(5000)
      real ex,ftot,r1,e(5000),np,sum1,sum2,sum3,ge,qn1p
      real bn,energy(5000),qn1s,dx(5000),qi(5000)
      real qextot,fei,qr2(5000),qion,qsig,i2,qr1(5000)
      real bohr,cons,temp,na,un1p(5),fn1p(5),a,b,c,d,ds,un1s(5)
      real un3p(5),ai,bi,ci,di,w,mi2,io,ke,exx,qn3s,qn3p
      real sum5,sum6,sum7,sum8,sum9,sum10,sum12,ei,epj,de1,de2
      real fo(3000,300),eps(7500),sig(7500)
      real cpu,p,un3s(5),un1d(5),un3d(5),qn1d,qn3d
      real dion,dex,fxm,foxj,f1,f2,dxr,df,fx,f(5000),f5(5000)
      integer j,m,n,x,de,nochar,u,jo,xv,xr,r,xm,ro,xu,m1,m2,m3,en
      integer u2,jj
      integer*4 ist,ifn
      call actim(ist)
      nochar=233
      u=1
      ro=0
      roo=0.0
      ke=2.0
      bohr=8.7975e-17
      na=6.023e+23
      cons=8.3138e+4
      temp=273.0
      p=1.0
      np=(na*p*ke)/(cons*temp)
      io=1.8079
      i2=13.6*io
      de=1
      u2=2
      dsum=0.0
      open(unit=60,name='darked3.dat',status='old')
      read(60,50) en
      energy(en)=(float(en)-15.0)*0.984
      m=en
      exx=0.0-1.0
C       SELECT ELECTRON ENERGY E
      do 20 x=1,m
      exx=exx+(float(de))
      ex=exx*0.984
      e(x)=ex
C       EXCITATION COLLISION CROSS-SECTIONS AT ENERGY E
      un1p(1)=1.5623
      un1p(2)=1.7
      un1p(3)=1.7481
      un1p(4)=1.7705
      fn1p(1)=0.2762
      fn1p(2)=0.0734
      fn1p(3)=0.0307
      fn1p(4)=0.0157
      qtn1p=0.0
      a=0.96
      b=1.3
      c=0.65
      d=0.05
      ds=2.0
      ex=ex/13.6
      qn1p=0.0
      do 21 j=1,4
      crs=un1p(j)
```

```
      if(ex.lt.crs) goto 21
      sum1=1+((d*ex)**4)
      sum1=(1+(b/ex))/sum1
      ge=1+((a/ex)*sum1)
      sum2=ds+(c*(ex-un1p(j)))
      sum2=log(sum2)
      sum2=(fn1p(j)*sum2)/(ex*un1p(j))
      sum2=(4*sum2)/ge
      sum2=(1-((un1p(j)/ex)**2))*sum2
      sum2=sum2*bohr
      qn1p=qn1p+sum2
21      end do
      un1s(2)=1.5179
      un1s(3)=1.6876
      un1s(4)=1.7477
      qn1s=0.0
      do 22 j=2,4
      crs=un1s(j)
      if(ex.lt.crs) goto 22
      sum1=(1-(un1s(j)/ex))**0.5
      sum1=(4*sum1)/(ex*un1s(j))
      bn=0.36/(j**3)
      qn1s=qn1s+((bn*sum1)*bohr)
22      end do
      un3s(2)=1.4593
      un3s(3)=1.6727
      un3s(4)=1.7372
      qn3s=0.0
      do 23 j=2,4
      crs=un3s(j)
      if(ex.lt.crs) goto 23
      sum1=(1-(un3s(j)/ex))**0.5
      sum1=(4*sum1)/((ex**3)*un3s(j))
      bn=2.24/(j**3)
      qn3s=qn3s+((bn*sum1)*bohr)
23      end do
      un3p(2)=1.5436
      un3p(3)=1.694
      un3p(4)=1.7456
      qn3p=0.0
      do 24 j=2,4
      crs=un3p(j)
      if(ex.lt.crs) goto 24
      sum1=(1-(un3p(j)/ex))**0.5
      sum1=(4*sum1)/((ex+un3p(j))**3)
      sum1=sum1/un3p(j)
      bn=10.8/(j**3)
      qn3p=qn3p+((bn*sum1)*bohr)
24      end do
      un1d(3)=1.6989
      un1d(4)=1.7477
      qn1d=0.0
      do 25 j=3,4
      crs=un1d(j)
      if(ex.lt.crs) goto 25
      sum1=(1-(un1d(j)/ex))**0.5
      sum1=(4*sum1)/((ex+un1d(j))*un1d(j))
      bn=0.33/(j**3)
      qn1d=qn1d+((bn*sum1)*bohr)
25      end do
```

```
      un3d(3)=1.7477
      un3d(4)=1.7702
      qn3d=0.0
      do 26 j=3,4
      ors=un3d(j)
      if(ex.lt.ors) goto 26
      sum1=(1-(un3d(j)/ex))**0.5
      sum1=(4*sum1)/((ex+un3d(j))*(ex**2))
      sum1=sum1/un3d(j)
      bn=1.24/(j**3)
      qn3d=qn3d+((bn*sum1)*bohr)
26      end do
      qextot=qn1s+qn1p+qn3s+qn3p+qn3d+qn1d
      if(ex.lt.io) goto 27
        ai=5.34
      bi=0.027
      oi=0.15
      di=1.6
      w=67.7
      mi2=0.49
      sum1=1+((bi*ex)**3)
      sum1=(1+(ai/ex))/sum1
      fei=((ai/ex)*sum1)+1
      sum1=(oi*(ex-io))**0.5
      sum1=log((sum1+di))
      sum1=sum1*mi2
      sum1=(1-((io/ex)**2))*sum1
      sum2=ex/io
      sum2=log(sum2)
      sum2=sum2/(ex+w)
      sum3=1-(io/ex)
      sum3=sum3/io
      sum3=sum3-sum2+sum1
      qi(x)=(sum3*8.0)/(ex*fei)
      qion=qi(x)*bohr
27    qsig=qion+qextot
      if(qsig.eq.0.0) goto 28
      qr1(x)=qion/qsig
      qr2(x)=qextot/qsig
28    dx(x)=qsig*np
      if(ex.lt.io) goto 20
      sum12=0.0
      de1=0.984/13.6
      de2=(ex+(24.55/13.6))*0.5
      sum5=(oi*(ex-io))**0.5
      sum5=log((di+sum5))
      sum5=mi2*sum5
      sum5=sum5*(io**2)
      sum6=1+(w/ex)
      sum6=8.0/(ex*sum6)
      sum7=(ex+io)/(ex+w)
      epj=io-de1
      do 10 j=1,300
      eps(j)=epj+de1
      epj=eps(j)
      if(epj.lt.de2) goto 13
      jo=j
      goto 11
13      ei=ex+io-epj
      sum8=1/(ei**3)
```

```
      sum8=sum8+(1/(epj**3))
      sum8=2*(sum8*sum5)
      sum9=1/(ei*epj)
      sum9=sum7*sum9
      sum10=1/(ei**2)
      sum9=sum10-sum9
      sum10=1/(epj**2)
      sum9=sum8+sum9+sum10
      sig(j)=sum6*sum9
      eps(j)=eps(j)-io
      sum12=sig(j)+sum12
10      end do
      jo=301
11      do 12 j=1,300
      if(j.eq.jo) goto 14
      fo(x,j)=sig(j)/sum12
12      end do
      goto 20
14      fo(x,j)=0.0
20      end do
      do 29 x=1,m
      read(60,55) f(x)
29      end do
      xm=m
      dfx=1.0e-6
      m2=m*300
      po=0.0
      k1=10.0
      ion2=0.0
      do 30 r=1,m2
32    fxm=f(xm)
      if(xm.eq.22) goto 43
      if(fxm.gt.dfx) goto 31
      xm=xm-1
      goto 32
31    xr=xm
      dxr=1/(dx(xr)*k1)
      pen(r)=dxr+po
      po=pen(r)
      ion(r)=0.0
      exc(r)=0.0
      ftot=0.0
      do 35 x=23,xm
      xv=x
      xu=23
      fx=f(x)
      ftot=ftot+fx
      if(fx.eq.0.0) goto 35
      df=0.0-(dxr*dx(x))
      df=(1-(exp(df)))*f(x)
      f(x)=f(x)-df
      dion=df*qr1(x)
      dex=df*qr2(x)
      ion(r)=dion+ion(r)
      dsum=dsum+dion
      exc(r)=exc(r)+dex
      xv=xv-22
      if(xv.lt.23) goto 35
      f(xv)=f(xv)+dex
      xv=xv-3
```

```
      if(xv.lt.23) goto 35
      do 36 j=1,300
      foxj=fo(x,j)
      if(foxj.eq.0.0) goto 35
      f1=fo(x,j)*dion
      f(xv)=f(xv)+f1
      if(j.lt.23) goto 33
      f(xu)=f(xu)+f1
      xu=xu+1
33    xv=xv-1
      if(xv.lt.23) goto 35
36      end do
35      end do
      if(ftot.eq.0.0) goto 34
      ion(r)=ion(r)/(dxr*(1.0e+1))
      exc(r)=exc(r)/(dxr*(1.0e+1))
      write(82,52) pen(r),ion(r)
      write(83,52) pen(r),exc(r)
34    if(k1.eq.1.0) goto 30
      ion1=ion(r)
      if(ion1.lt.ion2) goto 38
      ion2=ion1
      ion3=ion2/50.0
38    if(ion1.gt.ion3) goto 30
      k1=1.0
30      continue
43      m=r
      write(82,50) m
      write(83,50) m
50      format(I6)
52      format(2e10.5)
53      format(1e10.5)
54      format(3e10.5)
55    format(10x,1e10.5)
      call actim(ifn)
      cpu=0.01*(ifn-ist)
      write(81,53) cpu
      stop
      end
```

Appendix III

The following papers have been published during the course of this work.

ELECTRON BEAMS FROM GLOW DISCHARGE ELECTRON GUNS IN HELIUM

R.J.Carman and A.Maitland
Dept of Physics, University of St Andrews, North Haugh,
St Andrews, Fife, Scotland. KY16 9SS

Introduction

We have investigated the characteristics of glow discharge electron guns generating beams of electrons at several keV in helium at 1-6mb pressure. Electron guns of similar design have been used by Rocca et-al to pump metal vapour/rare gas mixtures and generate laser action at a number of wavelengths in the visible region [1],[2]. These guns can be used to excite the active medium of the laser directly without using differential pumping of the laser and gun regions, or thin foil window elements. Rocca et-al have reported an output power of 1.2W CW from an e-beam pumped helium/zinc laser, which represents a ten-fold increase in power over that obtained from a hollow cathode He/Zn laser [3].

Cold cathode electron guns employing an internal cavity as a source of low energy electrons can generate collimated electron beams in low pressure argon (0.01mb) as discussed by Boring and Stauffer [4]. Measurements in low pressure hydrogen (0.1mb) have been reported by Popa et al [5]. We have investigated a similar effect in helium at a few mb pressure when a distinct e-beam can be derived from a small hole drilled in the cathode face. The beaming phenomenon is examined for a range of hole sizes and gas pressures, and for a few multiple hole e-guns in helium.

Experimental arrangement

The discharge cell used is shown in Fig.1 and consists of a quartz tube 300mm long, 65mm I.D., held between two stainless steel end-flanges. The cathode assembly is fitted into one end-flange and is isolated from it by a quartz spacer. The stainless steel electron gun is interchangable and held in a stainless steel support-mount which can be withdrawn from the rear of the flange. The discharge is confined to the front surface of the electron gun, which is 6mm in diameter, by an aluminium shield which is placed close to the cathode body with a gap of about 0.5mm to prevent breakdown. The anode is a tungsten pin set in a side limb in the quartz tube and, together with the end-flanges, is held at earth potential. The cathode assembly carries a negative potential of a few kV. The cell is evacuated by a diffusion pump before U.H.P. helium is admitted, via a needle valve, to maintain a flow of gas through the cell for the duration of the experiment in order to purge impurities.

The discharge is operated in the 'abnormal' glow regime with only the cathode dark space (CDS) and negative glow (NG) regions present. The anode is located in the faraday dark space (FDS) and under these conditions, the tube voltage is equal to the cathode fall voltage, with a small correction for the anode sheath voltage.

Results

The generation of electron beams from drilled cathodes was investigated using a wide range of hole sizes from 1-5mm in diameter and 1.5mm-21mm in depth. The characteristics of an ordinary plane cathode were also recorded for comparison. A typical set of V-I characteristics are shown in Fig.2 and two modes of operation are revealed, in agreement with the observations of Rocca et-al [1]. In the high impedance or beam mode, an electron beam is generated and a narrow beam filament is seen to stretch from the hole aperture, through the CDS and into the NG. There is also a dim internal plasma in the hole cavity which is considerably less intense than the NG. A critical point is reached however, when the discharge impedance suddenly drops, the beam production ceases, and the NG extends into the hole producing an intense glow which is the well known 'hollow cathode' discharge. Beam production from the larger holes, of diameter 4mm and 5mm, was only observed at relatively low pressure, in the range 1-2mb. Beam collimation is also seen to degrade for all guns as the pressure is increased beyond 3-4mb.

Comparison between different e-guns is complicated by the presence of edge effects around the cathode perimeter which must be taken into account when comparing the V-I characteristics. The characteristics of the plane cathode are therefore used as a baseline and the ratio (η) of the discharge current derived from the drilled and plane cathodes is calculated for identical values of the pressure and cathode fall. The

ratios shown in Fig.3 for a 3mm diameter cavity of depth 15mm, demonstrate that more current may be derived from the drilled cathode than from the simple plane type. Between 1mb and 3mb, the current ratios are similar and at around 1.5kV, there is a sharp increase in (η), which rises to a factor of 5 at around 3kV. At higher pressures, the rise in (η) occurs at a progressively lower cathode fall. The same behaviour is observed for hole diameters of 2mm and 4mm. For 1mm, no discernable variation of (η) could be identified whilst at 5mm, the current ratios are much larger, but are observed only over a small range of low cathode fall voltages.

A further series of current ratios have been calculated for cavities of diameter 3mm, with different overall depths. The results are depicted in Fig.4 for 1mb pressure. The current ratios are again similar in size at low voltages and increase sharply at around 1.5kV. However, a saturation effect can be clearly identified with the shallower holes saturating first. The e-gun of depth 10mm is beginning to saturate at about 3kV. The same saturation effect is observed, using the same set of guns, at all pressures up to 4mb.

Several types of multi-hole guns were also investigated and in all cases, e-beams were produced from the separate cavities simultaneously. The characteristics of these guns are broadly similar to those with single cavities.

Discussion

When an electron gun operates in the beam mode, the region of high electric field in the CDS is located in front of the hole aperture and the expected equipotential distribution is shown in Fig.5. The distortion of the electric field at the hole entrance depends on the ratio of the CDS thickness to the hole diameter, and the electric field acts as an electron lens. Electrons are released from the cathode face and the hole wall by secondary emission processes caused by particles and photons from the NG. Electrons released from the hole wall are accelerated by the field at the wall and are drawn into a region around the hole axis. On passing into the CDS, they are further accelerated to form the e-beam. The beam direction is determined by the fields in the CDS and is essentially normal to the cathode surface (Fig.6). The internal plasma is partially sustained by inelastic electron collisions which generate metastables, electron/ion pairs and UV photons which may produce further secondary emmission. As the beam discharge approaches the transition point at which it changes into a hollow cathode discharge, the gradient of the V-I characteristic (Fig.2) increases rapidly and is accompanied by a rapid rise in the ratio (η) just before the transition point is reached (Fig.3).

The fact that currents drawn from cathodes with holes are greater than those drawn from a plane cathode (Fig.3 and Fig.4) implies that the secondary emission processes are more efficient in holes. As to a possible reason for this we note the following:

1. Charged particles are likely to collide with the walls of the hole at glancing angles. Such impacts are known to have larger (γ) values than do impacts at normal incidence [6].
2. Production of species such as He^{*}, He_2^{+}, and UV photons may be greater in a hole than at a plane cathode surface. Such species are known to produce secondary electrons and an increased production rate would naturally lead to increased electron emission.

References

1. Rocca J.J., Meyer J. and Collins G.J., Phys.Lett., 87A., 237, (1982)
2. Rocca J.J., Meyer J. and Collins G.J., Appl.Phys.Lett., 43, 37, (1983)
3. Piper J.A. and Gill P., J.Phys.D., 8, 127, (1975)
4. Boring K.L. and Stauffer L.A., Proc.Nat.Elect.Conf., 19, 535, (1963)
5. Popa G., Sandulovicіu M., Croitoru P. and Moldovan C., J.de.Phys., coll. C7-187, (1979)
6. Oliphant M.L.E., Proc.Roy.Soc., A127, 373, (1930)

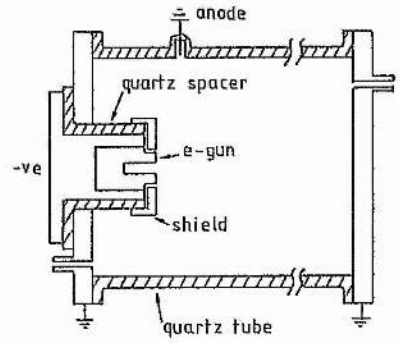

Fig. 1. The discharge cell.

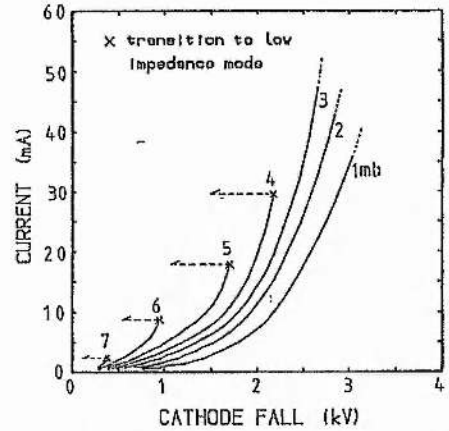

Fig. 2. V-I characteristics for a 3mm diameter hole, 21mm in depth.

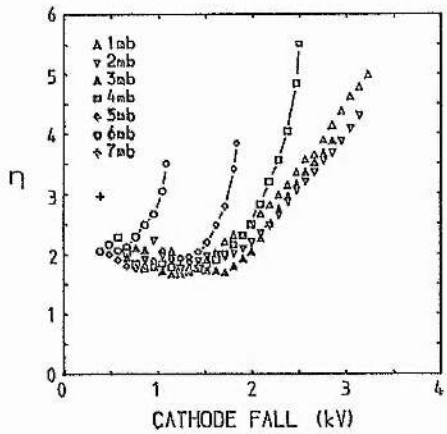

Fig. 3. Current ratios for a 3mm diameter hole, 15mm in depth with pressure as a parameter.

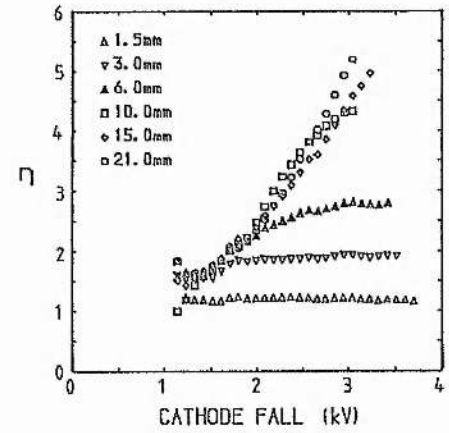

Fig. 4. Current ratio for 3mm diameter holes with depth as a parameter.

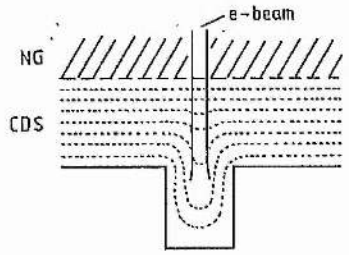

Fig. 5. Expected equipotential distribution in the gun cavity

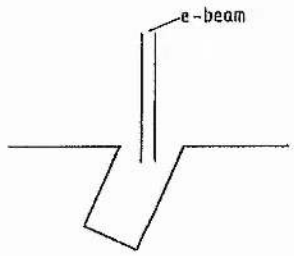

Fig. 6. Electron beam derived from a skewed hole

(12) UK Patent Application (19) GB (11) 2 153 140 A

(43) Application published 14 Aug 1985

(21) Application No 8431116

(22) Date of filing 10 Dec 1984

(30) Priority data
(31) 8333880 (32) 20 Dec 1983 (33) GB
8333879 20 Dec 1983
8413791 30 May 1984

(51) INT CL⁴
H01J 3/02 1/30 // 1/20

(52) Domestic classification
H1D 12847Y 1284 1286 12C 17A3 17AY 17D 1D12 1D1 1D4 1E1 1EY 1J2 1JY 1L 31 34 4A12 4A4 4A7 4A8B 4A8Y 4E3A 4E3Y 4K3B 4K8
U1S 1719 1724 2284 H1D

(56) Documents cited
GB A 2117173 GB 1490463 GB 0763670
GB A 2023922 GB 1370656 GB 0603088
GB 1557094 GB 1136144

(58) Field of search
H1D

(71) Applicant
English Electric Valve Company Limited (United Kingdom),
106 Waterhouse Lane, Chelmsford, Essex

(72) Inventors
Dr Arthur Maitland
Hugh Menown
Ian Arthur Strudwick
Clifford Robert Weatherup
Robert John Carman

(74) Agent and/or Address for Service
D G Rouse,
The General Electric Company plc, Central Patent Dept, Marconi Research Centre, Great Baddow, Chelmsford, Essex

(54) Apparatus for forming electron beams

(57) An envelope containing a gas filling includes a cathode 3 having, except for one or more portions or (as shown) notes 5 formed in a front surface thereof, all surfaces which would otherwise be exposed to the gas filling covered with an electrically insulating material, such as glass, and an anode 9 such that upon application of a suitably high voltage between the cathode and anode an electron beam is formed directed away from the front surface of the cathode. A grid 11, alternatively located in hole 5, modulates the beam; the anode may be located behind the front surface of the cathode, and still form a beam in front of the front surface. Fig. 18 shows such an arrangement in which the anodes and cathodes form an addressable crossed matrix. The front cathode surface may be oblique with respect to the hole or holes therein (Fig. 20) or may be curved (Fig. 21) to form a plurality of beams focussed to a point. The apparatus may comprise a CRT display when provided with a phosphor layer 2 or may be used for electron beam welding. The described beam arrangement can form the cathode of the thyratron (Figs. 22–24) or can be used to heat a separate thermionic cathode or can be used to ionise the gas filling locally in front of a conventionally heated thyratron cathode. Materials of electrodes and gas filling are given.

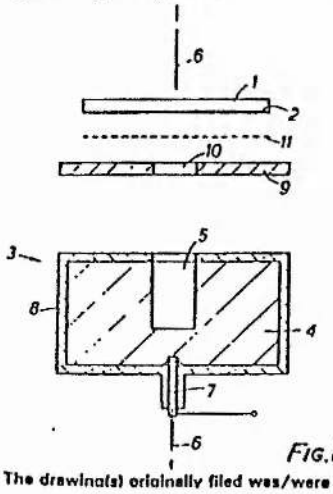

Fig.1.

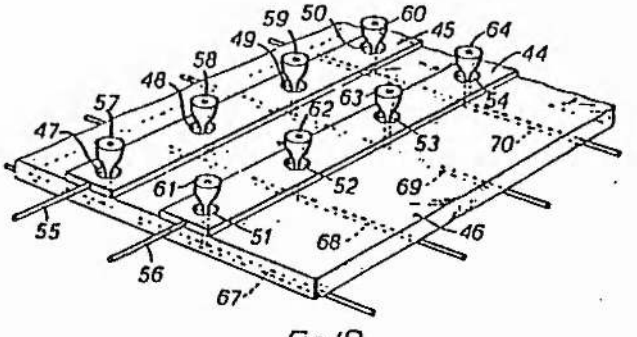

Fig.18.

GB 2 153 140 A

SPECIFICATION

Apparatus for forming electron beams

This invention relates to apparatus for forming electron beams, and to apparatus requiring the formation of electron beams, such as, for example, display devices and thyratrons.

The present invention seeks to provide improved apparatus for forming electron beams.

According to a first aspect of the invention there is provided apparatus for forming an electron beam comprising, within an envelope, an anode member; a cathode member of electrically conductive material; and a gas filling, and wherein, except for part of a front surface of said cathode member, at least substantially the whole of the surface of said cathode member which would otherwise be exposed to the gas filling within said envelope is covered with an electrically insulating material; the whole arrangement being such that upon the application of a suitably high voltage between said anode member and said cathode member an electron beam is formed extensive in a direction away from said part of said front surface.

According to a second aspect of the invention there is provided apparatus for forming an electron beam comprising, within an envelope, an anode member; a cathode member of electrically conductive material and having a hole in a front surface thereof; and a gas filling, and wherein, except within said hole, at least substantially the whole of the surface of said cathode member which would otherwise be exposed to the gas filling within said envelope is covered with an electrically insulating material, the whole arrangement being such that upon the application of a suitably high voltage between said anode member and said cathode member an electron beam is formed extensive in a direction away from said hole.

According to a third aspect of the invention, the anode member is located in front of the front surface of the cathode member.

Preferably a control grid electrode is included through which operation the electron beam passes, enabling the intensity or energy of the electron beam, to be modulated.

Preferably the apparatus includes a plurality of elongate cathode members arranged in a grid formation, and a plurality of elongate anode members arranged in a grid formation with said grid of anode members superimposed over said grid of cathode members, but spaced therefrom, with said anode members in crossing relationship with said cathode members to form a matrix, each of said cathode members having a series of holes entering into its surface facing said grid of anode members and each of said anode members having a series of holes passing therethrough, with each hole in an anode member aligned with a hole in a different one of the cathode members, and all surfaces of said cathode members, except for surfaces within said holes in said cathode members, which would otherwise be exposed to said gas filling are isolated therefrom by electrically insulting material, and the whole arrangement being such that by applying a high potential between one of said anode members and one of said cathode members an electron beam is formed at the crossing point of said last-mentioned two members, said electron beam being extensive in the space between the mouth of the hole in the cathode member at said crossing point and said anode member, said beam being arranged to penetrate through the corresponding hole in said addressed anode member.

It will be appreciated that by suitably addressing selected ones of said anode and cathode members an electron beam may be created which, by varying the selection of anode and cathode members addressed may be caused to be animated.

Preferably, insulating material is interposed between said grid of cathode members and said grid of anode members, which insulating material has passages therethrough aligned with said holes in said cathode and anode members whereby to permit communication between one cathode hole and the appropriate anode hole but impede communication between that cathode hole and any other anode hole.

Preferably, said last-mentioned interposed insulating material is provided in the form of a slab having holes extending between its major surfaces and forming the said passages.

A control grid electrode may be located on the side of the grid of anode members other than that on which the grid of cathode members is located, or alternatively it may be located between the grid of cathode members and the grid of anode members, and where insulating material is interposed between the cathode and anode grids the control grid electrode may be embedded in the interposed insulating material.

The anode member may be to one side of the axis of the electron beam formed in operation, such that said beam passes by said anode. It has been found by the inventors that the electron beam may be formed along the axis of the hole even though the anode member is displaced to the side of its path.

According to a forth aspect of the invention the anode member is located behind said front surface of the cathode member, and again in this configuration the electron beam may be formed along the axis of the hole, rather than along the shortest path between the anode and cathode members.

Preferably the anode member is co-axial with the cathode member. Preferably a grid is included through which in operation the electron beam passes, enabling it to be modulated

in intensity or energy, although of course, this may be achieved by varying the high voltage between the anode and cathode members.

Preferably there are included a plurality of elongate anode members, each having apertures therein; and a plurality of stemmed cathode members, each having a hole in the front surface thereof and arranged such that its stem extends through one of said apertures, such that each anode member is located behind the front surfaces of cathode members whose stems pass through apertures in said anode member, whereby by applying a high potential between an anode member and one of the cathode members extending through an aperture therein an electron beam is formed extensive in a direction away from the hole in said one of the cathode members.

As previously described where the grid of anode members are located in front of the grid of cathode members, by addressing selected cathode and anode members an electron beam may be formed in a desired location, or number of such beams formed simultaneously if cathode members may be individually addressed.

Preferably a cathode member extending through an aperture in one anode member is electrically connected to another cathode member extending through an aperture in another anode member and also preferably a connector connecting two cathode members is spaced from the anode members by electrically insulating material.

Preferably where the apparatus in accordance with this invention is included in a display device a phosphor layer is included and is arranged so that when an electron beam is formed it impinges upon a spot upon said layer whereby to excite the same and preferably said envelope has a portion formed as a faceplate on the interior of which said phosphor layer is provided.

According to a feature of this invention a video signal reproducing apparatus includes apparatus as described above.

According to a feature of the invention in its third aspect a cathode ray tube apparatus comprises a plurality of elongate cathode members arranged in a grid formation, a plurality of elongate anode members arranged in a grid formation with said grid of anode members superimposed over said grid of cathode members, but space therefrom, with said anode members in crossing relationship with said cathode members to form a matrix, each of said cathode members having a plurality of holes entering into its surface facing said grid of anode members and each of said anode members having a plurality of holes passing therethrough, with each hole in an anode member aligned with a hole in a different one of the cathode members and, superimposed over said grid of anode members on the side thereof remote from said grid of cathode members, a phosphor screen, the two grids being enclosed within an envelope having a gas filling from which all surfaces of said cathode members, except for surfaces within said holes in said cathode members, which would otherwise be exposed to said gas filling are isolated therefrom by electrically insulating material, and the whole arrangement being such that by applying a high potential between one of said anode members and one of said cathode members an electron beam is formed at the crossing point of said last-mentioned two members, said electron beam being extensive in the space between the mouth of the hole in the cathode member at said crossing point and said anode member, said beam penetrating through the corresponding hole in said addressed anode member to impinge upon a spot upon said phosphor whereby to excite the same.

According to a fifth aspect of the invention the longitudinal axis of said hole is oblique to the normal of said front surface, and the electron beam is formed normal to said front surface of said hole. The inventors discovered that, when the hole is arranged with its longitudinal axis inclined to the normal of the front surface, an electron beam is not formed parallel to the aforesaid axis as might be expected but is in fact, surprisingly, formed in a direction normal to the front surface. Where in this specification the term "normal" is used, it should be taken to include "substantially normal". Apparatus utilising this principle may be useful where, for example, space is restricted and it would not be possible to employ a device in which the hole is arranged normal to the surface of the cathode. Also manufacture of the device is facilitated since only the direction of the front surface need be accurately machined.

Such apparatus may include a plurality of holes in said front surface, at least one of said holes having its longitudinal axis oblique to the normal of said front surface at that hole, such that upon the application of said suitably high voltage electron beams are formed extensive normal to said front surface at and in a direction away from respective holes. Since the configuration of the front surface was found by the inventors to determine the direction of electron beams produced, a desired pattern of electron beams or concentration of electron beams may be achieved without costly machining. For example, if a plurality of beams which are mutually parallel are required the holes need not be drilled in precise relationship to each other, as might have been thought, as only the front surface need be made flat. Of course the front surface can be curved if more complex patterns are required, and because of leniency in the disposition of the holes the cathode member may be more conveniently shaped for a desired application.

According to a sixth aspect of the invention

there is provided apparatus for forming electron beams comprising, within an envelope, an anode member; a cathode member of electrically conductive material having a front surface which is curved; and a gas filling, and wherein, except for a plurality of discrete parts of the said front surface, at least substantially the whole of the surface of said cathode member which would otherwise be exposed to the gas filling within said envelope is covered with an electrically insulating material, the whole arrangement being such that upon the application of a suitably high voltage between said anode member and said cathode member electron beams are formed extensive normal to said front surface at and in a direction away from respective parts.

It is preferred that, where there are a plurality of electron beams formed, the front surface is curved such that they are focussed or concentrated at a point or small region. This is a particularly useful configuration providing apparatus suitable for inclusion in an electron beam welder, or as a point source of soft X-rays or incandescent black body radiation.

According to a seventh aspect of this invention there is included a layer of phosphor material on a viewable screen arranged such that upon the application of said suitably high voltage the electron beam impinges upon said phosphor layer and so excites the same.

According to a feature of the seventh aspect of this invention a display apparatus comprises, within an envelope, a layer of phosphor material on a viewable screen; remote from said phosphor layer, a metallic cathode member having a hole formed in a front surface thereof; between said cathode member and said phosphor layer, an apertured anode electrode; and a gas filling, and wherein, except within said hole, at least substantially the whole of the surface of said cathode member which would otherwise be exposed to the gas filling within said envelope is covered with an electrically insulating material, the whole arrangement being such that upon the application of a suitably high voltage between said anode member and said cathode member an electron beam is formed extensive in the space between the mouth of the hole in said cathode member and said anode member, and is arranged to penetrate through an aperture in said anode member to impinge upon said phosphor layer and so excite the same.

Preferably said envelope has a portion formed as a faceplate upon the inner surface of which said phosphor layer is provided.

The apparatus may include a modulating grid provided to affect the strength or intensity of the electron beam impinging upon said phosphor layer.

Said modulating grid may be a perforated grid or gauze provided either between said anode member and said phosphor layer or between said anode member and said cathode member. In other embodiments of the invention said modulating grid comprises a ring grid provided within the mouth of said hole in said cathode member. In this last mentioned case preferably an electrical connection for said grid is taken out, in insulated fashion through said cathode member in a direction away from said anode member, i.e. through the base of said cathode member.

Where, as is preferable, electrical connection to said cathode member is provided for by means of an electrical connector connected to the base of said cathode member, said last mentioned connector is preferably in the form of a hollow cylinder with an electrical connector for said grid passing, in insulated fashion, therethrough.

There may be provided a single hole in said cathode member with a corresponding single aperture in said anode member but alternatively a plurality of holes may be provided in said cathode member with a corresponding plurality of holes in said anode member. Where a plurality of holes and apertures are provided these may be in ring formation, with or without a central disposed hole and aperture.

According to a feature of the second aspect of the invention thyratron apparatus comprises, within an envelope, an anode member; a cathode member of electrically conductive material and having a hole in a front surface thereof; and a gas filling, and wherein, except within said hole, at least substantially the whole of the surface of said cathode member which would otherwise be exposed to the gas filling within said envelope is covered with an electrically insulating material, the whole arrangement being such that upon the application of a suitably high voltage between said anode member and said cathode member an electron beam is formed extensive in a direction away from said hole.

Preferably said cathode member has a plurality of holes in the front surface thereof, such that upon application of a suitably high voltage electron beams are formd extensive in a direction away from respective holes, and it is preferred that said front surface is curved, such that some focussing of the electron beams to a point may be obtained. Also it is preferred, where the front surface is curved, that at least one of said holes has its longitudinal axis oblique to the normal of said front surface at that hole. The cathode member may form the cathode of a thyratron, or advantageously thermionic material may be included and arranged such that when an electron beam or beams are formed they heat the same. This heating may be direct or indirect. For example, a substrate carrying the thermionic material may be exposed to the electron beam or beams and heat transmitted to the thermionic material by conduction.

Alternatively, when the electron beam is formed, it may be arranged to ionize the gas filling in a localised region, and so improve operating characteristics of a thyratron, and advantageously the longitudinal axis of the hole is oblique to the normal of said front surface at the hole, enabling the cathode member to be accommodated in a restricted space. Of course, more than one such cathode member may be employed.

According to an eighth aspect of the invention said front surface is shaped to focus said electron beam. Thus even where only one hole is employed the electron beam may be focussed. Each point of the surface around the mouth of the hole and at its edge may be thought of as directing components of the electron beam normal to the surface at respective points. Thus by providing the surface with a certain configuration, for example a convex shape or advantageously a frusto-conical configuration, with the hole being centrally located, a desired degree of focussing may be obtained. For example, the electron beam may be focussed to a point or it could be focussed merely enough to aid in further collimation of the electron beam.

Generally the, or each hole in a cathode member is blind, and preferably of circular cross-section.

Preferably said insulating material insulating surfaces of said cathode member, or plurality of cathode members, from said gas filling is glass, but where said cathode member, or members, is of an anodisable metal, such as aluminium or titanium, the insulating material may be anodisation.

Preferably said cathode and anode members are of Kovar (R.T.M.) but other metals or alloys may be used, such as aluminiumm copper or tungsten, or of molybdenum, tantalum or other refractory metals for high current use.

Generally said envelope is of glass or quartz.

Preferably the side wall and base surfaces of each hole is entirely free of a covering of electrically insulating material.

A number of gases, or mixture of gases, may be used for said gas filling including helium and/or argon and/or deuterium and/or neon. The hole size and voltages applied are related to the type of gas employed. Typically, hole sizes for argon are 0.2 to 0.1 of the size of those for helium, giving the possibility of more compact devices.

Preferably said gas filling is at a pressure of between 0.5 and 2.5 mB.

Normally the higher voltage utilised to address the anode and cathode members is from 1 to 5 kV and preferably between 1 and 2.5 kV.

The invention is further described by way of example with reference to the accompanying drawings in which:

Figure 1 is a schematic cross-section of one simple electronic display device in accordance with the present invention;

Figure 2 and 3 illustrate modifications of the device illustrated in Fig. 1, like references being used for like parts in Figs. 1 to 3;

Figure 4 and 5 are explanatory graphs;

Figure 6 shows, in longitudinal cross-section, another example of an electron beam device in accordance with the present invention;

Figure 7 is a schematic cross-section through a flat screen cathode ray display device in accordance with the present invention;

Figure 8 illustrates in perspective part of the insulating slab 20 of Fig. 7;

Figure 9 illustrates, part broken away, one elongate anode member A used in the device of Fig. 7;

Figure 10 illustrates, part broken away, one elongate cathode member C utilised in Fig. 7;

Figure 11 is a perspective view, part broken away, of an assembly of cathode and anode members with the slab of insulating material shown in Fig. 8 sandwiched therebetween;

Figure 12 is a schematic diagram illustrating the operation of the device illustrated in Figs. 7 to 11;

Figure 13 is a schematic cross-section through another flat screen cathode ray device in accordance with the present invention;

Figure 14 illustrates in perspective part of the device of Fig. 13;

Figure 15 illustrates in perspective part of the device of Fig. 13; with like references being used for like parts;

Figure 16 is a schematic cross-section of a display device in accordance with the invention;

Figure 17 is a schematic cross-section of another display device in accordance with the invention;

Figure 18 is a perspective view, part broken away, and

Figure 19 a cross-sectional view, of yet another device in accordance with the invention;

Figure 20 shows a longitudinal section of a further apparatus in accordance with the invention;

Figure 21 is a longitudinal section of another apparatus in accordance with the invention;

Figure 22 illustrates a thyratron in accordance with the invention;

Figure 23 illustrates another thyratron in accordance with the invention;

Figure 24 shows yet another thyratron in accordance with the invention;

Figure 25 illustrates a cathode member in accordance with the invention;

Figure 26 shows another cathode member; and

Figure 27 illustrates another device in ac-

cordance with the invention.

Referring to Fig. 1, a device comprises a quartz envelope of which only one portion 1 is shown. The envelope portion 1 is provided as a faceplate having on its interior a layer 2 of phosphor material similar to that used in conventional cathode ray display tubes. Associated with the phosphor layer 2 is a transparent metal layer (not shown but somewhat akin to the transparent metal layer forming part of the screen of a conventional cathode ray tube) between the layer 2 and the faceplate. The faceplate formed by the portion 1 of the envelope of the device is transparent.

Within the envelope and at the end thereof opposite to the faceplate portion 1, is a cathode member 3 which comprises a block 4 of Kovar having a blind hole 5 formed therein, in this case by drilling coaxially with the axis of cylindrical symmetry 6 of the device. The open mouth of the hole 5 faces the phosphor layer 2. In the base of the block 4, adjacent the blind end of the hole 5, a connecting pin 7 is inserted so as to enable electrical connection to be made to the Kovar block 4.

All of the external surfaces of the Kovar cathode block 4, with the exception of the wall and base surfaces of the blind hole 5, which would otherwise be exposed to a gas filling within the envelope of the device are covered by electrically isolating material represented at 8. In this example, the insulating material 8 is glass.

Between the cathode 3 and the phosphor layer 2 is an anode electrode 9 which has a circular hole 10 passing therethrough. Circular hole 10 is coaxially aligned with the blind hole 5 within the Kovar block 4.

It will be noted that the cathode 3 is devoid of a heater as such, or any electron emissive cathode material, such as barium.

The envelope of the tube is filled with helium at a pressure of between 0.2 and 10 mB.

As so far described the device is in its simplest form. For the moment it will be assumed that grid 11, shown between the anode electrode 9 and the phosphor layer 2, is absent.

Provided that the dimensions of the cathode and anode holes 5 and 10 and the spacing of the anode 9 to the cathode 3 is suitably chosen, a type of electrical discharge will be established between the anode 9 and the cathode 3 which results in the formation of an electron beam along the axis 6 of the coaxially aligned anode and cathode holes when a potential difference in the range of from several hundred volts to several thousand volts is established between the anode 9 and the block 4 of cathode 3. Within limits, the electron beam acquires energy approximately equal to the anode to cathode potential difference and so extends into the region beyond the anode hole 10 to impinge, finally, upon the phosphor layer 2 thus exciting it.

Thus, in operation, whenever a potential as aforesaid is established between anode 9 and block 4 of cathode 3, the resulting electron beam causes a spot to appear on the screen 1 due to excitation of the phosphor layer 2. Whilst the aforementioned dimensions and spacing may be arrived at empirically, in the particular example illustrated in Fig. 1, the cathode and anode holes were of 5 mm diameter. With a gas filling of helium at a pressure of 2 mB and a potential difference between anode 9 and cathode 3 of approximately 1.5 kV, the device was found to operate with a spacing between the plane of the anode 9 and the surface of the phosphor layer 2 of up to a few centimetres, and a spacing between the anode 9 and the cathode 3 of at least 3 mm. With the above-mentioned potential difference of 1.5 kV the current drawn from the cathode, was of the order of 15 mA.

Reverting to the aforementioned grid 11—by introducing a control grid, modulation of the intensity or energy of the electron beam arriving at the surface of the phosphor layer 2 may be achieved by varying a potential applied to the grid 11. Alternatively or additionally varying the potential between the anode 9 and the cathode 3 will produce or enhance a modulation effect but, of course, it is much less convenient to apply modulation at high potential.

Referring to Fig. 2, the essential difference between the device shown in Fig. 2 and the device shown in Fig. 1 resides in the fact that a mesh grid such as 11 in Fig. 1 is not provided between the anode 9 and the phosphor layer 2. Instead, a ring grid 11′ is provided within the mouth of the blind hole 5 in the Kovar block 4. Electrical connection is made to the ring grid 11′ by means of a connector passing out through the base of the Kovar block 4. In fact, instead of a pin 7 making contact with the block 4 the contact, here referenced 7′, is cylindrical with the connecting lead for the grid 11′ passing coaxially therethrough in insulated fashion. Although not shown in Fig. 2, insulting material would be provided to support the connecting lead for the grid 11 within the cylindrical connector 7′.

Referring to Fig. 3, in this case, compared to Fig. 1, the position of the grid 11 is changed. Instead of providing this between anode 9 and the phosphor layer 2 it is provided between the anode 9 and the cathode 3. In some cases this may be preferred since a relatively lower voltage is required compared to that required with the grid in the position shown in Fig. 1.

The graph of Fig. 4 shows the relationship between beam current I and cathode fall voltage V (i.e. the voltage applied between anode and cathode) for different gas filling pressures,

for a device as described above having cathode and anode holes of 5 mm in diameter.

In any of the embodiments described above with reference to Figs. 1, 2 and 3, instead of a single cathode hole and a single anode hole a plurality of blind holes may be provided in the Kovar block 4 with each cathode hole being coaxially aligned with a corresponding hole passing through the anode member 9. Typically in such a case, the holes will be arranged in a ring formation, with or without cathode and anode holes on-centre. The effect achieved using a plurality of cathode and anode holes in a simple device as illustrated in Figs. 1 to 3, is that the areas of excitation thus created in the phosphor layer 2 tend to merge to produce a larger illuminated spot (or other prescribed pattern as determined by the pattern of holes on the faceplate 1) than would otherwise be the case.

The graph of Fig. 5 shows parameters for this last-mentioned case corresponding to those shown in the graph of Fig. 4 for this embodiment shown in Fig.. 1.

One application for a device as described above is in large area displays such as those sometimes found in public places in order to impart information, e.g. in airport terminals or sports areas. By arranging devices such as those described above in rows and columns and addressing individual devices appropriately, letters and words—and even graphics—may be produced.

Referring to Fig. 6, another device in accordance with the invention includes a glass envelope 12 which is of generally circular cross-section and has a transversely extending side-arm 13 about mid-way along its length. An anode member 14 extends through the end wall of the side-arm 13 and into the main part of the volume enclosed by the envelope 12.

A cathode member 15 passes through an end wall of the envelope 12. It has a stem portion 15A and an enlarged end 15B with a blind hole 16 of circular cross-section in its front surface. All of the surfaces of the cathode member 15 contained within the envelope 12, except for the side wall and base surfaces of the hole 16, are coated with a layer of glass 17. The envelope 12 contains helium at a pressure of 2 mB.

In operation, a potential difference of about 1 kV is applied across the anode and cathode members 14 and 15 and an electron beam is formed along the axis A–A of the hole 16.

The envelope 12 has a length of about 7 cm and a diameter of about 3.5 cm.

The anode and cathode members 14 and 15 are separated by approximately 1 cm in the axial direction and 0.5 cm in the transverse direction. The diameter of the hole 16 is 5 mm, with a depth (i.e. axial length) of 3 mm.

Referring to Figs. 7 to 11 a display device comprises a plurality of elongate cathode members C1 to C4 arranged parallel to one another to form a grid. Each cathode member, as shown in Fig. 10, comprises a bar of Kovar having at regular intervals along its length blind holes 18. The holes 18 extend into the same planar surface of the cathode member. Each cathode member is provided with an electrical connector (not shown) by means of which it may be individually addressed.

Superimposed above the grid of cathode members is a grid of parallel elongate anode members A1 to A5 each of which consists of a bar of Kovar having a series of holes 19 passing therethrough from one planar face to its opposite planar face as illustrated in Fig. 9. The pitch of the holes 19 in an anode member corresponds to the spacing between the cathode members in the cathode grid and the spacing of the anode members in the anode grid corresponds to the pitch of the cathode holes 18 in a cathode member so that each cathode hole 18 is aligned with an anode hole 19 at the crossing point of the anode and cathode conductors in which those particular holes appear.

Sandwiched between the grid of cathode members and the grid of anode members is a slab 20 of glass which has rows and columns of holes 21 therein extending from one major planar face to its opposite major planar face, as illustrated in Fig. 8. The rows and columns of holes are spaced such that when the slab is sandwiched between the grid of cathode members and the grid of anode members, as shown in Fig. 11, each aligned cathode and anode hole at the crossing point of an anode and cathode member is also aligned with a hole in the slab of insulating material 20. Thus, the holes 21 in the insulating slab 20 permit communication between appropriate ones of the cathode and anode holes 18 and 19 but impede communication between each cathode hole and other than the anode holes with which it is directly aligned. Thus the tendency for so-called "long path" discharges to take place is reduced.

Superimposed over the grid of anode members is a phosphor screen comprising of a layer of phosphor material 22 on the inside of part of an enclosing envelope which is formed as a faceplate 23. Associated with the layer 22 of phosphor material is a transparent layer of conductive material (somewhat akin to the transparent metal layer of the phosphor screen of a conventional cathode ray tube device) between the phosphor layer 22 and the faceplate 23. The envelope in this case is of glass and encloses the anode and cathode members together, of course, with the interposed slab of insulating material 20.

The envelope has a gas filling of helium and, as illustrated only in Fig. 7, each cathode member C is entirely covered with an electrically isolating layer 24 of glass, except within

the holes 18. Thus, save for the wall and base surfaces of the holes 18 all surfaces of the cathode members which would otherwise be exposed to the helium gas filling are isolated therefrom. In fact, save for the interior surfaces of the holes 18 as aforesaid, all surfaces at cathode potential are so isolated from the gas filling. In this particular case the wall and base surfaces of the holes 18 are entirely free from glass. In this particular example the cathode and anode holes 18 and 21 are of circular cross-section with a diameter of 5 mm. The helium gas filling is at a pressure of 2 mB. The distance separating the grid of cathode members from the grid of anode members (i.e. the thickness of the slab 20) is a few millimetres whilst the distance separating the grid of anode members from the phosphor layer 22 is in the region of 0.5 to 2 cm.

If now, and referring particularly to Fig. 12, a 1.5 kV potential difference is established between cathode member C2 and anode member A4 then an electron beam will be formed in the region of the crossing point of members C2 and A4 which beam extends from out of the mouth of the cathode hole 18 at the crossing point through the corresponding hole in the insulating slab 20 to penetrate through the corresponding anode hole 19 in anode members A4 and impinge upon the phosphor screen to form a spot as represented at S in Fig. 12. By addressing different combinations of anode members and cathode members corresponding spots may be caused to appear on the screen at any of the crossing points and by suitably changing the combination of crossing points selected an animated display may be achieved.

No mention has so far been made of grid 25 shown in Fig. 7 as located between the grid of anode members A and the phosphor layer 22. The purpose of this grid, if provided, is to modulate the intensity or energy of the electron beams arriving at the phosphor.

Alternatively, with or without the grid 25, the overall intensity or energy of the electrons beams may be modulated or adjusted by appropriate alterations to the anode to cathode discharge current as determined by the voltage applied between the cathode and anode members.

In another embodiment a grid 26 is embedded in the slab 20, as shown in Figs. 13 and 14, and may comprise a gauze or as metal plate having holes which correspond to the anode and cathode holes, as illustrated in Figs. 15.

It will be noted particularly the absence of any form of conventional electron gun. No cathode heaters are employed in the device illustrated, the cathodes being cold cathodes, and no cathode material such as barium is employed.

With reference to Fig. 16, another embodiment of the invention includes a cathode member 27 of Kovar having a hole 28 of about 5 mm diameter in its front surface and being enclosed in a glass envelope 29 which also contains helium gas at a pressure of about 2 mB and has a layer of phosphor on its inner surface to form a screen 30. The surfaces of the cathode member 27, except the side wall and base of the hole 28, are covered in a glass layer 31, which electrically insulates the cathode member 27 from the helium gas filling. Electrical connection to the cathode member 27 is made via a pin 32 which is sheathed with a layer 33 of glass.

An anode member 34 is located between the front surface of the cathode member 27 and the phosphor screen 30, being about 2 cm from the cathode member 27, and 2 cm from the screen 30. The anode member 34 is also offset from the axis X–X of the hole 28, being about 2 cm to the right as shown.

When a 1.5 kV potential difference is established between the cathode member 27 and the anode member 34, an electron beam is formed along the axis X–X of the hole, even though the anode member 34 is offset from that axis. The electron beam impinges on the phosphor screen 30 to form a spot.

The intensity of the spot may be varied by modulating the voltage applied to a grid electrode 35, shown in this embodiment to be positioned between the screen 30 and the anode member 34, although it could be located between the anode and cathode members 34 and 27.

A further embodiment of the invention is illustrated schematically in Fig. 17. A cathode member 36 of Kovar has a hole 37 in its front surface and is coated with an electrically insulating layer of glass 38. The cathode member 36 is contained within a glass envelope 39 having on its inner surface a layer of phosphor which acts as a screen 40, and enclosing helium gas at 2 mB pressure. The cathode member 36 is electrically connected via a pin 41, which is also coated in glass 42, forming a stem. In this embodiment a Kovar anode member 43 is located behind the front surface of the cathode member 36 and is positioned co-axially with it about the pin 41.

When in operation a potential difference of 1.5 kV is applied between the cathode and anode members 36 and 43, an electron beam forms along the axis Y–Y of the hole 37 and impinges on the screen 40.

As in the previously described embodiments, a modulating grid may also be included, and/or modulation may be carried out by varying the potential difference applied.

The hole 37 has a diameter of about 5 mm and the front surface of the cathode member 36 may be between a few millimetres and a few centimetres from the screen 40.

Yet another embodiment of the invention is now described with reference to Figs. 18 and

19. A plurality of Kovar strips, only two of which 44 and 45 are shown, are arranged parallel to each other on a glass slab 46. Each of the strips has a plurality of apertures through it, only four of which, 47, 48, 49 and 50; 51, 52, 53 and 54 are shown for each strip. Each strips forms an anode member, electrical signals being applied to them via rods 55 and 56.

Cathode members 57 to 64 are of Kovar and have stems extending through the apertures in the strips 44 and 45, there being one cathode member to each aperture, and passing through the glass slab 46. The surfaces of each cathode member, including the connecting pin comprising its stem, are coated in glass layers 65 and 66 except for the side wall and base of the single hole in each ones front surface.

The ends of the cathode members 57 to 64 on the side of the glass slab 46 other than the anode strips 44 and 45 are connected via rods 67, 68, 69 and 70, such that one cathode member associated with one strip is electrically connected to a cathode member associated with each of the other strips, giving a crossing relationship between the cathode and anode members. Thus, by applying a potential difference between a suitable cathode member and anode strip, an electron beam may be formed in front of that cathode member.

By placing the structure within an envelope filled with helium at 2 mB pressure, and having a phosphor screen on its inner surface, a display may be produced.

The front surfaces of the cathode members 57 to 64 may be as little as 5 mm from the surface of the screen, and a potential difference between the anode and cathode members of 1.5 kV would be required.

With reference to Fig. 20, a thorated tungsten cathode member 71 has a stem 72 via which electrical connection is made, and is covered with a layer 73 of electrically insulating glass which also extends to the stem 72. An anode member 74 surrounds and is coaxial with the stem 72.

The cathode member 71 has a front surface 75 in which is formed a blind hole 76 of circular cross-section, being 5 mm deep and having a diameter of about 1.5 mm, and having surfaces which are free of the layer 73 of glass. The front surface 73 is inclined with respect to the hole 76 such that the longitudinal axis of the hole 76, shown as broken line 77, is oblique to the normal 78 of the front surface 75 at that point, the angle between them being about 30°.

The cathode and anode arrangement is enclosed within a glass envelope which also contains a gas filling of deuterium at about 2 mB pressure.

In operation, when a suitably high voltage, say 2 kV, is established between the anode and the cathode members 74 and 71, an electron beam is formed extensive in a direction away from the hole 76 and normal to the front surface 75. If, as illustrated a wall 79, which might be for example the wall of the envelope or some other obstruction, is present, this could restrict the space available to the arrangement. By giving a suitable incline to the front surface 75 the hole 76 can have a depth which might not be possible if its longitudinal axis 77 were arranged to be parallel to the normal 78 to the front surface 75.

With reference to Fig. 21, a thorated tungsten cathode member 80 is connected to stem 81 and is contained within an envelope (not shown) together with a deuterium gas filling at about 2 mB pressure and an anode member 82, which is coaxial with and surrounds the stem 81.

The cathode member 80 and stem 81 are coated with a layer 83 of glass which electrically insulates them from the deuterium gas filling.

A plurality of holes 84 or formed in a front surface 85 of the cathode member 80, each of them being of circular cross-section with a diameter of about 1.5 mm and a depth of 5 mm and having surfaces which are free of the layer 83 of glass. The front surface 85 is curved, for example, it may be parabolically or spherically shaped, rather than the flat surface 75 shown in Fig. 20.

In operation, when a voltage of about 2 kV is applied between the cathode and anode members 80 and 82 a plurality of electron beams are formed extensive normal to the front surface 85 at and in directions away from respective holes, and come to a focus at a point 86 which is located according to the configuration of the front surface 85.

Although the holes 84 are illustrated as being disposed mutually parallel, they could be arranged in some other way, since their attitude does not affect the directions of the electrons beams which are formed during operation.

Apparatus according to the invention in which the surface is curved to produce such focussing might find application in an electron beam welder, for example, in which case the piece being welded may also be for example contained within the envelope. It might also find application in the production of a point source of soft X-rays, having a wavelength of about 6.10^{-10}m, for use in spectroscopy for example, or to generate a point source of incandescent black body radiation.

With reference to Fig. 22, a thyratron in accordance with the invention includes a glass envelope 87, containing a gas filling, an anode 88, a screen grid 89 and control grids 90 and 91, such as might be found in a conventional thyratron. However, instead of the conventionally provided heated cathode, the cath-

ode comprises a cathode member 92 of tungsten having a plurality of holes 93 in its front surface, facing the anode 88. The surface of the cathode member 92 is entirely covered with a glass layer 94 except for the walls and bases of the holes 93. When the thyratron is required to become conducting a suitably high voltage is applied between the anode 88 and the cathode member 92 such that an electron beam is formed extensive in a direction away from each hole. The gas filling becomes ionized and a conduction path is established between the anode 88 and cathode member 92.

Referring to Fig. 23, another thyratron in accordance with the invention includes a glass envelope 95 containing a gas filling, an anode 96, a screen grid 97 and controls grids 98 and 99. It also includes a conventional heated cathode, comprising a hollow cylinder 100 of thermionic material and a heater filament 101.

Two cathode members 102 and 103 are located within the glass envelope 95. Each has a hole 104 and 105 in its front surface and is coated with a glass layer 106 and 107. The longitudinal axes of the holes 104 and 105 are oblique to the front surfaces of the cathode members 102 and 103. The cathode members 102 and 103 also have stem portions 108 and 109 which are surrounded by coaxial anode members 110 and 111 respectively.

During operation of the thyratron, the thermionic material 100 is heated by the heater filament 101 causing electrons to be emitted from its surface. The emitted electrons ionize that part of the gas filling between the controls grids 98 and 99 and the cathode to establish a primary discharge. Then conventionally, to trigger the thyratron, a positive voltage pulse is applied to the control grids 98 and 99, allowing the discharge to penetrate through them to initiate the main discharge, and thus to render the thyratron conducting. However, in addition to this, a voltage may be applied between the cathode members 102 and 103 and the cathode members 110 and 111 respectively, such that electrons beams are formed extensive of the holes 104 and 105 and normal to the front surfaces of the cathode members 102 and 103, their path being shown by broken lines 112 and 113. These beams may be formed simultaneously with, or shortly before or after, the application of the voltage pulse to the control grids 98 and 99. The beams are arranged to pass through apertures in the control grids 98 and 99 and penetrate into the volume beyond them, to ionize the gas filling.

The cathode members could be located elsewhere within the envelope 95 if it is desired to promote ionization in other regions of the thyratron, and of course only one, or more than two cathode members could be used.

With reference to Fig. 24, another thyratron includes a glass envelope 114, gas filling, an anode 115, a screen grid 116 and control grids 117 and 118. The thyratron includes a thermionic cathode 119 having thermionic material 120 carried by a substrate 121 of high thermal conductivity which may be nickel, for example. A cathode member 122 of tungsten is positioned on the substrate side of the cathode 120. The cathode member 122 has a plurality of holes 123 in its front surface which is concave. The surface of the cathode member 122, except for the walls and bases of holes 123, are covered with a layer 124 of glass. An anode member 125 surrounds the cathode member 122.

In operation, a voltage is applied between the anode member 125 and the cathode member 122 such that a beam of electrons is formed extensive of each hole. The curved surface of the block 122 gives a focussing effect, and the electrons are directed to impinge on the substrate 121, their kinetic energy being converted into heat. Heat is conducted to the thermionic material 120 causing electrons to be emitted to produce ionization of the gas filling.

With reference to Fig. 25, a cathode member is formed by inserting a tungsten cylindrical rod 126 into a hollow tube 127 of an electrically insulating material, such as a ceramic or glass.

Fig. 26 illustrates another cathode member in which a tungsten rod 128 is inserted into a hollow metal tube 129, which may also be of tungsten, and a ceramic tube 130 is fitted over the metal tube 129. Any metal surfaces which would be exposed in use to a gas filling may then be covered with an insulating layer. By employing cathode members of this type no drilling is required, as it is with those previously described.

With reference to Fig. 27, a device in accordance with the invention comprises within an envelope (not shown) which also contains a gas filling, a cylindrical cathode member 131 having a stem portion 132 via which electrical connection is made to the cathode member 131. The cathode member 131 has a front surface 132 of circular transverse cross-section which is of a 'dished' or frusto-conical configuration, the front surface being inclined such that the length of the cathode member 131 along its axis Z–Z increases from its centre to its circumference. Other surface configuration may of course be employed if desired. A hole 133 is located in the centre of the front surface 132 and is coaxial with axis Z–Z of the cathode member 131. The surfaces of the cathode member 131 and the stem portion 132 are covered with a layer 134 of electrically insulating glass, and an anode member 135 surrounds

and is coaxial with the stem portion 132.

When a voltage is applied between the cathode member 131 and the anode member 135 an electron beam is formed extensive of the hole 133. The beam is formed in a direction normal to the front surface 132. Since at the edge of the hole 133 the front surface 132 is inclined, components of the beam at points around the edge of the hole 133 are directed towards the axis Z–Z, such that the beam is brought to a focus F. The position of the focus F depends on the amount of inclination of the front surface. Such a device may thus produce a lens-like action, without the need for electron lens.

If the front surface is flat then a beam is produced which, although it is highly collimated, tends to diverge to some extent because of, for example, scattering processes. By using a front surface having a small degree of dishing, this tendency may be counteracted.

CLAIMS

1. Apparatus for forming an electron beam comprises, within an envelope, an anode member; a cathode member of electrically conductive material; and a gas filling, and wherein, except for part of a front surface of said cathode member, at least substantially the whole of the surface of said cathode member which would otherwise be exposed to the gas filling within said envelope is covered with an electrically insulating material, the whole arrangement being such that upon the application of a suitably high voltage between said anode member and said cathode member an electron beam is formed extensive in a direction away from said part of said front surface.

2. Apparatus for forming an electron beam comprising, within an envelope, an anode member; a cathode member of electrically conductive material and having a hole in a front surface thereof; and a gas filling, and wherein, except within said hole, at least substantially the whole of the surface of said cathode member which would otherwise be exposed to the gas filling within said envelope is covered with an electrically insulating material, the whole arrangement being such that upon the application of a suitably high voltage between said anode member and said cathode member an electron beam is formed extensive in a direction away from said hole.

3. Apparatus as claimed in claim 2 and wherein the anode member is located in front of the front surface of the cathode member.

4. Apparatus as claimed in claim 3 and including a control grid electrode through which in operation the electron beam passes.

5. Apparatus as claimed in claim 3 or 4 and including a plurality of elongate cathode members arranged in a grid formation, and a plurality of elongate anode members arranged in a grid formation with said grid of anode members superimposed over said grid of cathode members, but spaced therefrom, with said anode members in crossing relationship with said cathode members to form a matrix, each of said cathode members having a series of holes entering into its surface facing said grid of anode members and each of said anode members having a series of holes passing therethrough, with each hole in an anode member aligned with a hole in a different one of the cathode members, and all surfaces of said cathode members, except for the surfaces within said holes in said cathode members, which would otherwise be exposed to said gas filling are isolated therefrom by electrically insulating material, and the whole arrangement being such that by applying a high potential between one of said anode members and one of said cathode members an electron beam is formed at the crossing point of said last-mentioned two members, said electron beam being extensive in the space between the mouth of the hole in the cathode member at said crossing point and said anode member, said beam being arranged to penetrate through the corresponding hole in said addressed anode member.

6. Apparatus as claimed in claim 5 and wherein insulating material is interposed between said grid of cathode members and said grid of anode members, which insulating material has passages therethrough aligned with said holes in said cathode and anode members whereby to permit communication between one cathode hole and appropriate anode hole but impede communication between that cathode hole and any other anode hole.

7. Apparatus as claimed in claim 6 and wherein said interposed insulating material is provided in the form of a slab having holes extending between its major surfaces and forming the said passages.

8. Apparatus as claimed in claim 5, 6 or 7 and including a control grid electrode located on the inside of the grid of anode members other than that on which the grid of cathode members is located.

9. Apparatus as claimed in claim 5, 6 or 7 and wherein a control grid electrode is located between the grid of cathode members and the grid of anode members.

10. Apparatus as claimed in claim 9 when dependent on claim 6 or 7 and wherein the grid electrode is embedded in the interposed insulating material.

11. Apparatus as claimed in claim 2 and wherein the anode member is located to one side of the axis of the electron beam formed in operation.

12. Apparatus as claimed in claim 2 and wherein the anode member is located behind said front surface of the cathode member.

13. Apparatus as claimed in claim 12 and wherein the anode member is co-axial with

the cathode member.

14. Apparatus as claimed in claim 12 or 13 and including a grid electrode through which in operation the electron beam passes.

15. Apparatus as claimed in claim 12, 13, or 14 and wherein there are included a plurality of elongated anode members, each having apertures therein; and a plurality of stemmed cathode members, each having a hole in the front surface thereof and arranged such that its stem extends through one of said apertures, such that each anode member is located behind the front surfaces of cathode members whose stems pass through apertures in said anode member, whereby by applying a high potential between an anode member and one of the cathode members extending through an aperture therein an electron beam is formed extensive in a direction away from the hole in said one of the cathode members.

16. Apparatus as claimed in claim 15 and wherein a cathode member extending through an aperture in one anode member is electrically connected to another cathode member extending through an aperture in another anode member..

17. Apparatus as claimed in claim 16 and wherein a connector connecting two cathode members is spaced from the anode members by electrically insulating material.

18. Apparatus as claimed in any preceding claim and including a phosphor layer arranged so that when an electron beam is formed it impinges upon a spot upon said layer whereby to excite the same.

19. Apparatus as claimed in claim 18 and wherein said envelope has a portion formed as a faceplate on the interior of which said phosphor layer is provided.

20. A video signal reproducing apparatus including apparatus as claimed in any preceding claim.

21. Cathode ray tube apparatus comprising a plurality of elongate cathode members arranged in a grid information, a plurality of elongate anode members arranged in a grid formation with said grid of anode members superimposed over said grid of cathode members, but spaced therefrom, with said anode members in crossing relationship with said cathode members to form a matrix, each of said cathode members having a plurality of holes entering into its surface facing said grid of anode members and each of said anode members having a plurality of holes passing therethrough, with each hole in an anode member aligned with a hole in a different one of the cathode members and, superimposed over said grid of anode members on the side thereof remote from said grid of cathode members, a phosphor screen, the two grids being enclosed within an envelope having a gas filling from which all surfaces of said cathode members except for surfaces within said holes in said cathode members, which would otherwise be exposed to said gas filling are isolated therefrom by electrically insulating material and the whole arrangement being such that by applying a high potential between one of said anode members and one of said cathode members, an electron beam is formed at the crossing point of said last-mentioned two members, said electron beam being extensive in the space between the mouth of the hole in the cathode member at said crossing point and said anode member, said beam penetrating through the corresponding hole in said addressed anode member to impinge upon a spot upon said phosphor screen whereby to excite the same.

22. Apparatus as claimed in claim 2 and wherein the longitudinal axis of said hole is oblique to the normal of said front surface, and the electron beam is formed normal to said front surface at said hole.

23. Apparatus as claimed in claim 22 and including a plurality of holes in said front surface, at least one of said holes having its longitudinal axis oblique to the normal of said surface at the hole, such that upon the application of said suitability high voltage electron beams are formed extensive normal to said front surface at and in a direction away from respective holes.

24. Apparatus as claimed in claim 23 and wherein said front surface is curved.

25. Apparatus for forming electron beams comprising, within an envelope, an anode member; a cathode member of electrically conductive material having a front surface which is curved; and a gas filling, and wherein, except for a plurality of discrete parts of the said front surface, at least substantially the whole of the surface of said cathode member which would otherwise be exposed to the gas filling within said envelope is covered with an electrically insulating material, the whole arrangement being such that upon the application of a suitably high voltage between said anode member and said cathode member electron beams are formed extensive normal to said front surface at and in a direction away from respective parts.

26. Apparatus as claimed in claim 24 or 25 and wherein said front surface is curved such that the electron beams formed are focussed at a point.

27. Apparatus as claimed in claim 22, 23, 24, 25 or 26 and wherein said anode member co-axially surrounds and is behind said front surface of said cathode member.

28. Apparatus as claimed in claim 2 and including a layer of phosphor material on a viewable screen arranged such that upon the application of said suitably high voltage the electron beam impinges upon said phosphor layer and so excites the same.

29. Apparatus as claimed in claim 28 and wherein said anode member has an aperture therein and is located between said cathode

member and said phosphor layer, said electron beam being arranged to penetrate through said aperture.

30. Apparatus as claimed in claim 29 and wherein the hole in said cathode member and said aperture in said anode member are coaxially aligned.

31. Apparatus as claimed in claim 28, 29 or 30 and wherein said envelope has a portion formed as a faceplate upon the inner surface of which said phosphor layer is provided.

32. Apparatus as claimed in any of claims 28 to 31 including a modulating grid provided to affect the strength or intensity of the electron beam impinging upon said phosphor layer.

33. Apparatus as claimed in claim 32 and wherein said modulating grid is a perforated grid or gauze provided between said anode member and said phosphor layer.

34. Apparatus as claimed in claim 32 and wherein said modulating grid or gauze is provided between said anode member and said cathode member.

35. Apparatus as claimed in claim 32 and wherein said modulating grid comprises a ring grid provided within the mouth of said hole in said cathode member.

36. Apparatus as claimed in claim 35 and wherein an electrical connection for said grid is taken out, in insulated fashion, through said cathode member in a direction away from said anode member.

37. Apparatus as claimed in any of claims 28 to 36 wherein electrical connection to said cathode member is provided for by means of a first electrical connector connected to the base of said cathode member.

38. Apparatus as claimed in claim 37 and wherein said first electrical connector is preferably in the form of a hollow cylinder.

39. Apparatus as claimed in claim 38 and wherein, where said modulating grid comprises a ring grid provided within the mouth of said hole in said cathode member and an electrical connection for said grid is taken out, in insulated fashion, through said cathode member in a direction away from said anode member, a second electrical connector for said grid passes through said hollow cylinder.

40. Apparatus as claimed in any of claims 28 to 39 wherein a plurality of holes are provided in said cathode member and a corresponding plurality of holes are provided in said anode member.

41. Display apparatus comprising, within an envelope, a layer of phosphor material on a viewable screen; remote from said phosphor layer, a metallic cathode member having a hole formed in a front surface thereof; between said cathode member and said phosphor layer, an apertured anode electrode; and a gas filling, and wherein, except within said hole at least substantially the whole of the surface of said cathode member which would otherwise be exposed to the gas filling within said envelope is covered with an electrically insulating material, the whole arrangement being such that upon the application of a suitably high voltage between said anode member and said cathode member an electron beam is formed extensive in the space between the mouth of the hole in said cathode member and said anode member, and is arranged to penetrate through an aperture in said anode member to impinge upon said phosphor layer and so excite the same.

42. Thyratron apparatus comprising, within an envelope, an anode member; a cathode member of electrically conductive material and having a hole in a front surface thereof; and a gas filling, and wherein, except within said hole, at least substantially the whole of the surface of said cathode member which would otherwise be exposed to the gas filling within said envelope is covered with an electrically insulating material, the whole arrangement being such that upon the application of a suitably high voltage between said anode member and said cathode member an electron beam is formed extensive in a direction away from said hole.

43. Apparatus as claimed in claim 42 and wherein said cathode member has a plurality of holes in the front surface thereof, such that upon application of a suitably high voltage electron beams are formed extensive in a direction away from respective holes.

44. Apparatus as claimed in claim 43 and wherein said front surface is curved.

45. Apparatus as claimed in claim 44 and wherein at least one of said holes has its longitudinal axis oblique to the normal of said front surface at that hole.

46. Apparatus as claimed in any of claims 42 to 45 and including thermionic material arranged such that when an electron beam, or beams are formed they heat the same.

46. Apparatus as claimed in claim 42 and wherein, when said electron beam is formed it is arranged to ionize the gas filling in a localised region.

48. Apparatus as claimed in claim 47 and wherein the longitudinal axis of said hole is oblique to the normal of said front surface at the hole.

49. Apparatus as claimed in claim 2 and wherein said front surface is shaped to focus said electron beam.

50. Apparatus as claimed in claim 2 or 49 and wherein said front surface is substantially frusto-conical, the hole being centrally located.

51. Apparatus as claimed in any of claims 2 to 50 and wherein the or each hole in a cathode member is blind.

52. Apparatus as claimed in any of claims 2 to 51 and wherein the or each hole in a cathode member is of circular cross-section.

53. Apparatus as claimed in any of claims 2 to 52 and wherein the side wall and base surfaces of the or each hole in a cathode member is entirely free of a covering of electrically insulating material.

54. Apparatus as claimed in any preceding claim and wherein said insulating material insulating surfaces of said cathode member or plurality of cathode members from said gas filling is glass.

55. Apparatus as claimed in any preceding claim and wherein said cathode member, or plurality of cathode members, is of Kovar.

56. Apparatus as claimed in any preceding claim and where said anode member, or plurality of anode members, is of Kovar.

57. Apparatus as claimed in any preceding claim, and wherein said envelope is of glass.

58. Apparatus as claimed in any preceding claim and wherein the said gas filling is helium.

59. Apparatus as claimed in any preceding claim and wherein said gas filling is at a pressure of between 0.5 and 2.5 mB.

60. Apparatus as claimed in any preceding claim and wherein the high voltage applied between the anode member and the cathode member is between 1 and 2.5 kV.

61. Apparatus as claimed in any preceding claim and wherein said cathode member is of thorated tungsten.

62. Apparatus substantially as illustrated in and described with reference to Fig. 1 of the accompanying drawings.

63. Apparatus substantially as illustrated in and described with reference to Fig. 2 of the accompanying drawings.

64. Apparatus substantially as illustrated in and described with reference to Fig. 3 of the accompanying drawings.

65. Apparatus substantially as illustrated in and described with reference to Fig. 6 of the accompanying drawings.

66. Apparatus substantially as illustrated in and described with reference to Figs. 7 to 12 of the accompanying drawings.

67. Apparatus substantially as illustrated in and described with reference to Figs. 13 to 15 of the accompanying drawings.

68. Apparatus substantially as illustrated in and described with reference to Fig. 16 of the accompanying drawings.

69. Apparatus substantially as illustrated in and described with reference to Fig. 17 of the accompanying drawings.

70. Apparatus substantially as illustrated in and described with reference to Figs. 18 and 19 of the accompanying drawings.

71. Apparatus substantially as illustrated in and described with reference to Fig. 20 of the accompanying drawings.

72. Apparatus substantially as illustrated in and described with reference to Fig. 21 of the accompanying drawings.

73. Apparatus substantially as illustrated in and described with reference to Fig. 22 of the accompanying drawings.

74. Apparatus substantially as illustrated in and described with reference to Fig. 23 of the accompanying drawings.

75. Apparatus substantially as illustrated in and described with reference to Figs. 24 of the accompanying drawings.

76. Apparatus substantially as illustrated in and described with reference to Fig. 25 of the accompanying drawings.

77. Apparatus substantially as illustrated in and described with reference to Fig. 26 of the accompanying drawings.

78. Apparatus substantially as illustrated in and described with reference to Fig. 27 of the accompanying drawings.

Printed in the United Kingdom for
Her Majesty's Stationery Office, Dd 8818935, 1985, 4235.
Published at The Patent Office, 25 Southampton Buildings,
London, WC2A 1AY, from which copies may be obtained.

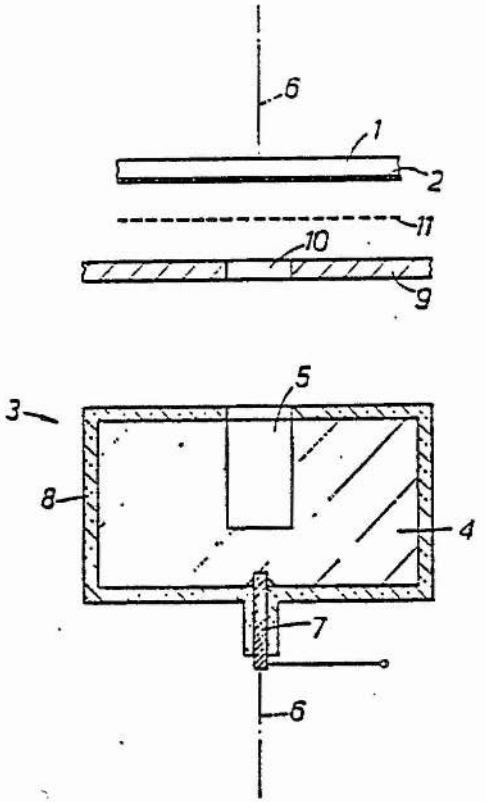

FIG. 1.

2153140

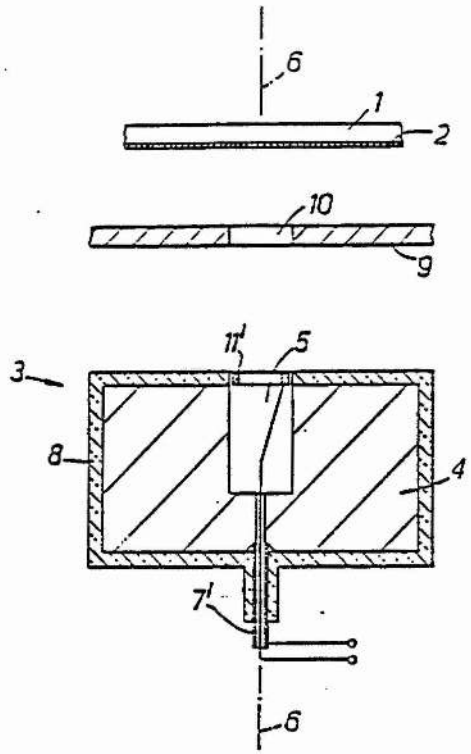

FIG. 2.

3/16

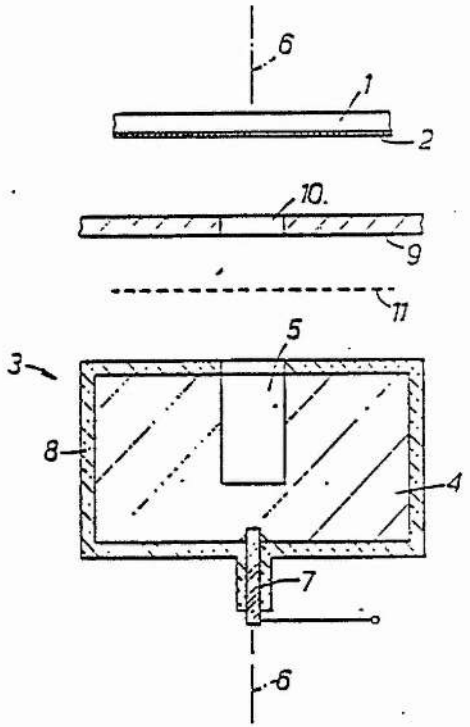

FIG. 3.

2153140

4/16

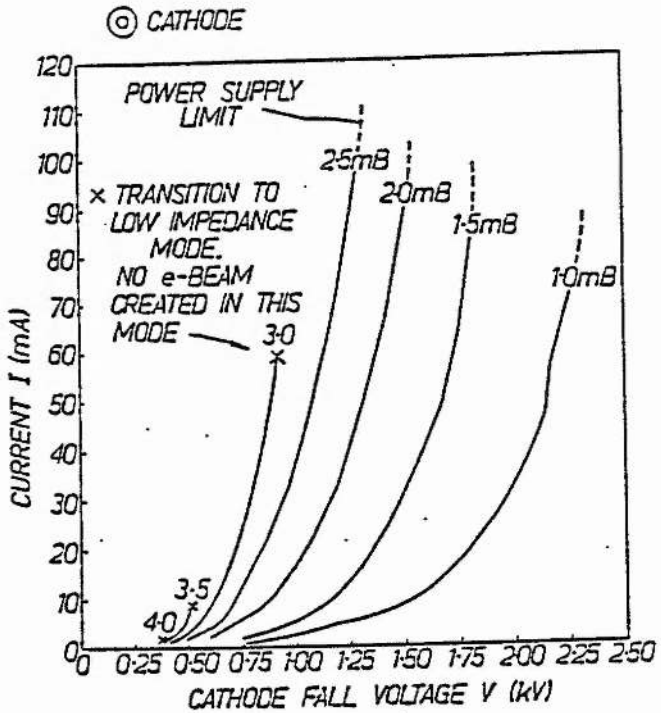

FIG. 4.

5/16

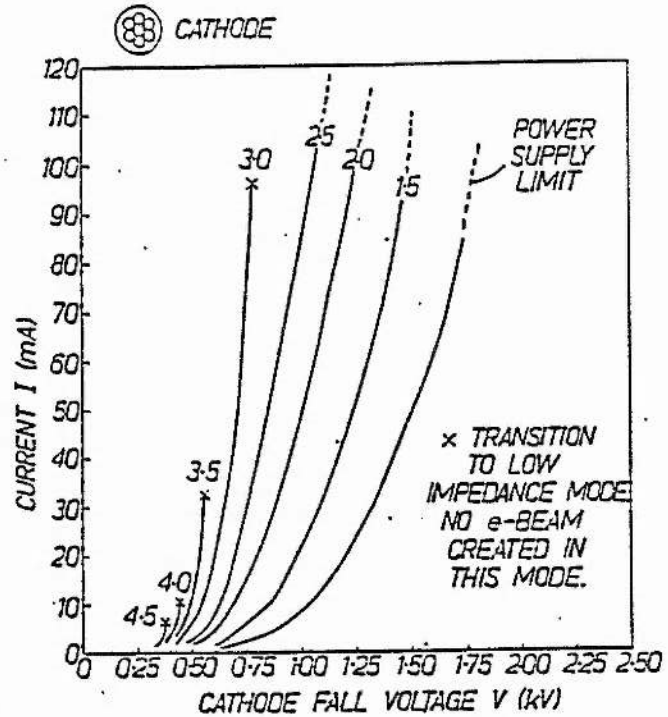

FIG. 5.

2153140

6/16

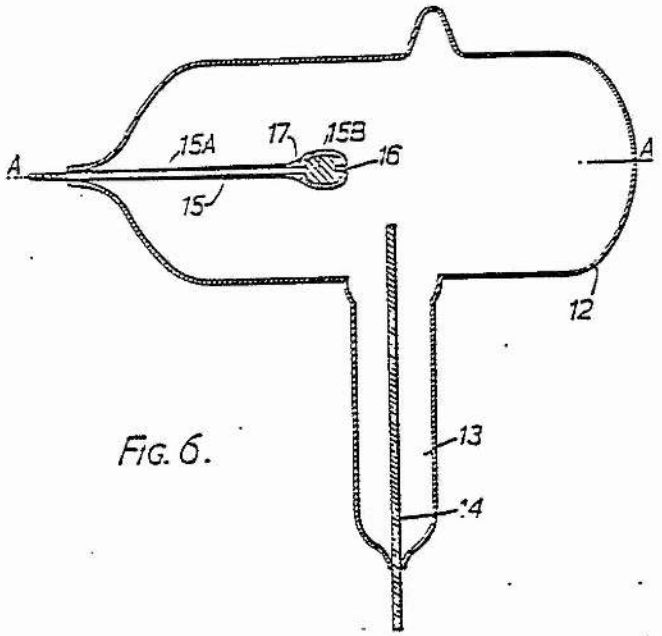

FIG. 6.

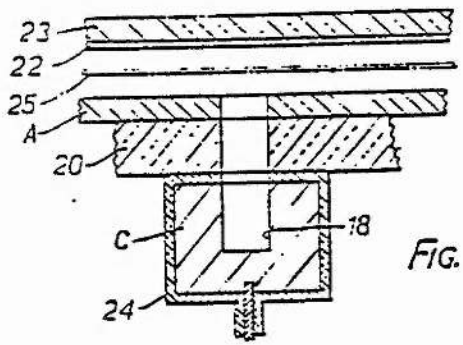

FIG. 7.

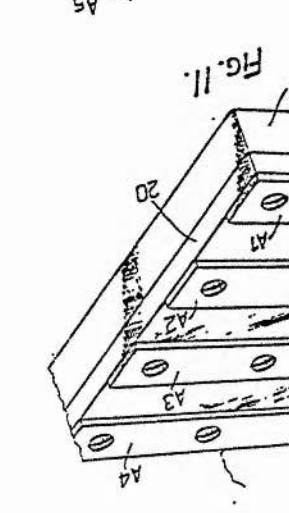

Fig. 12.

Fig. 11.

8/16

2153140

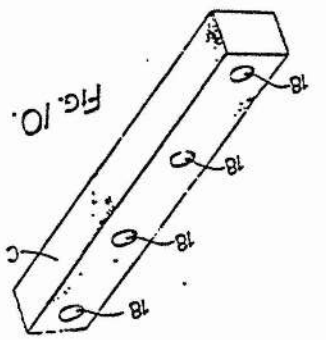

Fig. 10.

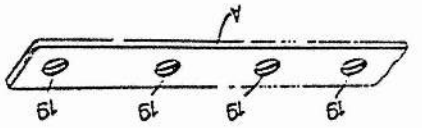

Fig. 9.

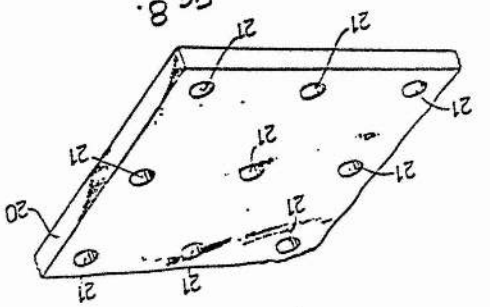

Fig. 8.

7/16

2153140

9/16

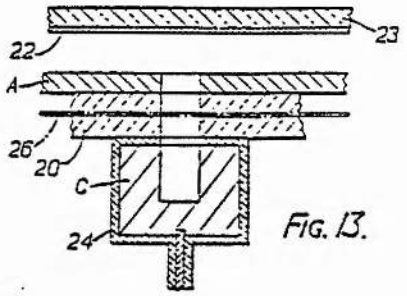

FIG. 13.

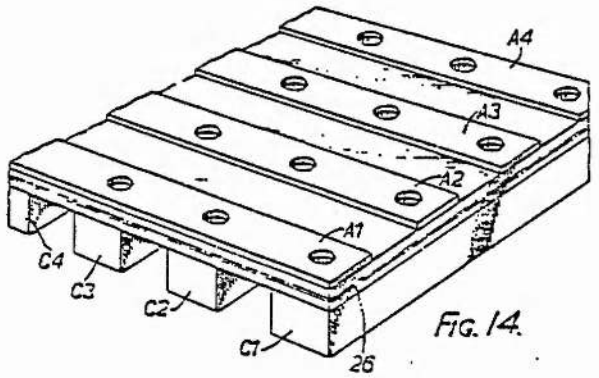

FIG. 14.

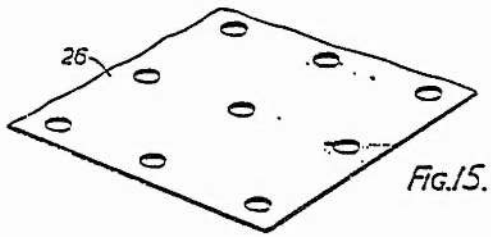

FIG. 15.

2153140

10/16

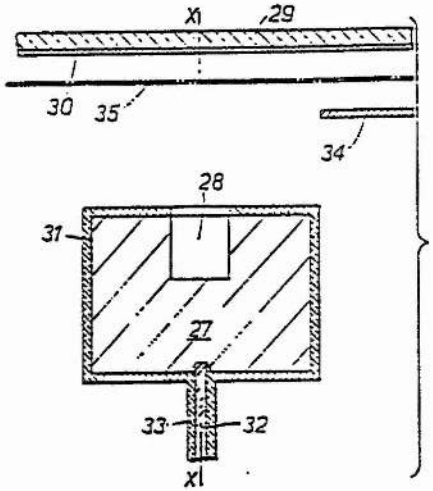

FIG. 16.

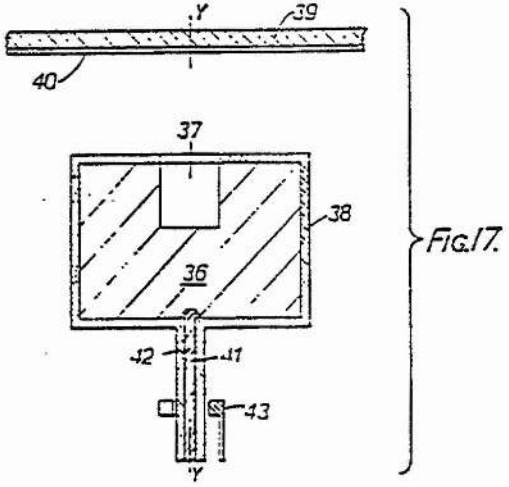

FIG. 17.

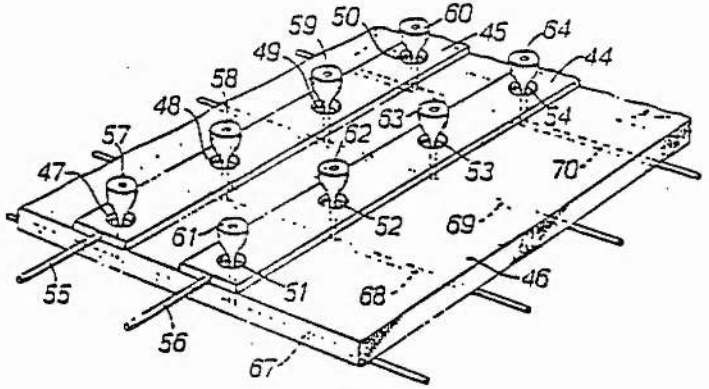

FIG.18.

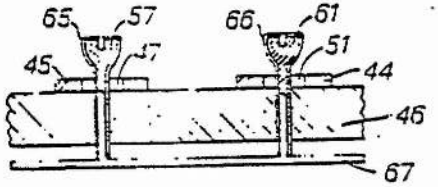

FIG.19.

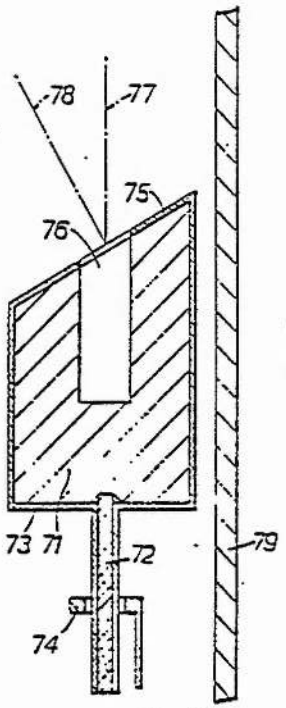

FIG. 20.

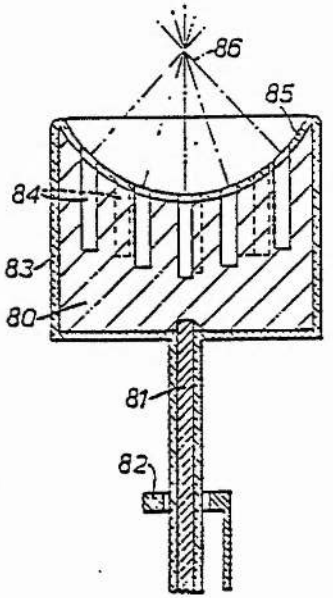

FIG.21.

13/16

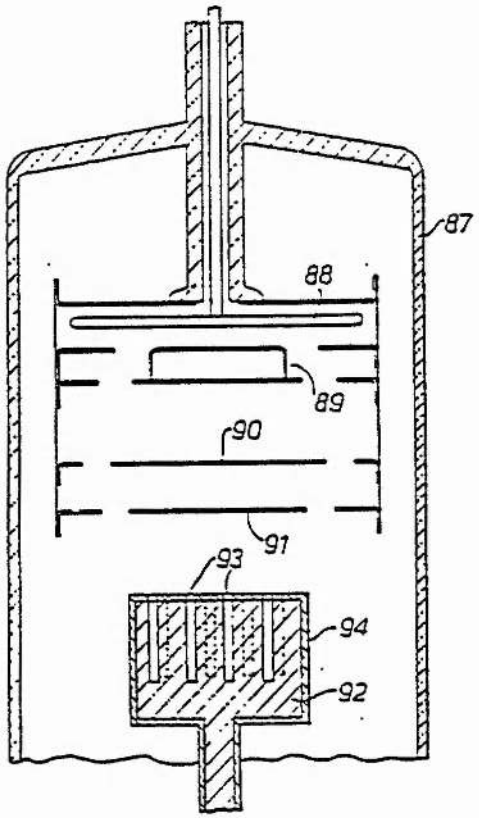

FIG. 22.

2153140

14/16

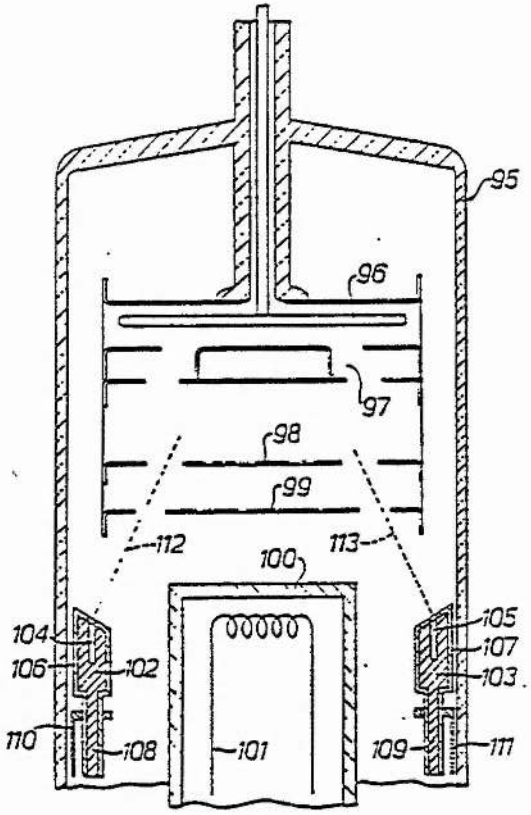

FIG. 23.

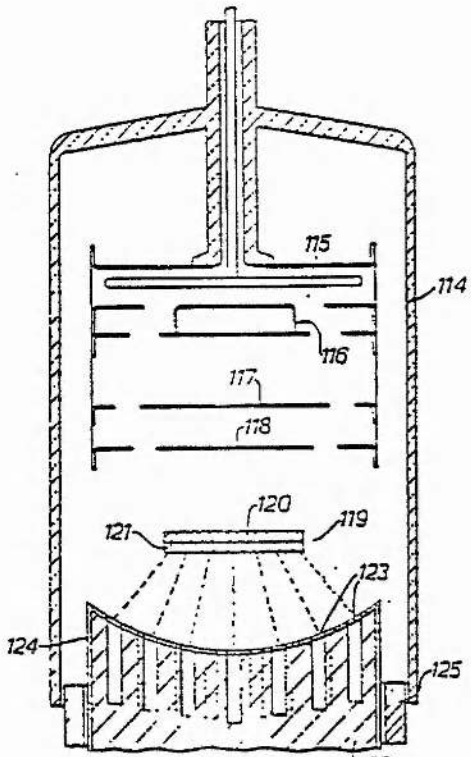

FIG. 24.

2153140

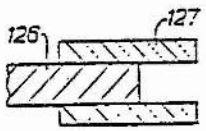

FIG. 25.

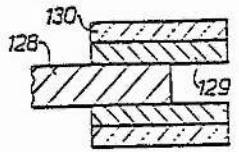

FIG. 26.

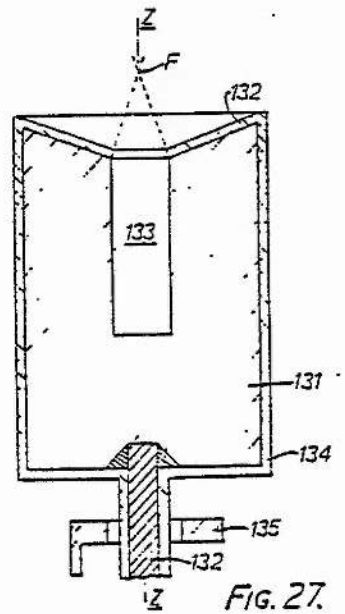

FIG. 27.